DIPARTIMENTO
DI SCIENZE DELLA TERRA
SAPIENZA
UNIVERSITÀ DI ROMA

DOTTORATO DI RICERCA
IN SCIENZE DELLA TERRA

Francesca Frasca

Ph.D. Thesis in Earth Sciences

Curriculum in Environment and Cultural Heritage

XXXI cycle (2015-2018)

Academic Discipline

FIS/06 and ING-IND/11

An effective strategy for preventive conservation in historic buildings coupling dynamic simulation and experimental data of indoor climate

Advisors:

Prof Anna Maria Siani
Department of Physics – Sapienza Università di Rome

Prof Cristina Cornaro
Department of Enterprise Engineering – Università degli Studi di Roma "Tor Vergata"

This page intentionally left blank

Preface

It is my hope that the results of the work presented in this doctoral thesis will contribute to further increase the awareness of the necessity to investigate the microclimate in buildings which preserve works of art. This is truly important in the field of preventive conservation, since the understanding of the interactions between indoor climate parameters and objects plays a fundamental role in order to avoid any kind of restoration and guarantee a longer and safer life to the objects. Indeed, it allows reducing the issues associated with degradation phenomena, leading to a better management of the indoor environment in relation with the conservation of artefacts and the wellbeing of the users of these buildings. Furthermore, I hope that the results will contribute to the definition of more sustainable buildings, both modern and historic, with due regard for cultural heritage conservation.

In 2015, I started my PhD research with the challenging task to combine the topics of microclimate and whole building dynamic simulation as an efficient approach in the field of preventive conservation. The possibility of investigating the microclimate within buildings which preserve cultural heritage, which was the main topic of my bachelor and master theses, encouraged me to decide to spend other three years on this research. I would also add that three years are not yet enough to have a complete overview and understanding of the topic.

During these three years, I have learnt how to be an independent young researcher. I set the on-site measurements of indoor climate at the "Museo Archelogico di Priverno" as scientific participant within the multidisciplinary project "Preservation, Conservation and valorisation of archaeological sites: the case of ancient site of Privernum" funded by Sapienza University of Rome in 2015. In addition, I supervised the microclimate monitoring systems installed at the "Museo delle Origini" belonging to the Sapienza "Polo museale" and at "Villa Blanc", one of headquarters of the LUISS Carlo Guidi University. My research activities were appreciated by Sapienza University of Rome, that funded my visiting stay at the Department Hygrothermics of the Fraunhofer Institute for Building Physics and my participation as speaker at the "7th International Building Physics Conference, Syracuse (NY, USA) September 23-26, 2018 (IBPC 2018)". Moreover, I was co-advisor of two bachelor theses and one master thesis concerning the data mining of indoor climate in different buildings which preserve works of art. In addition, I was also co-supervisor of two bachelor theses in Atmospheric Sciences within the Erasmus exchange with the Leibniz Universität Hannover.

It has been a great opportunity to conduct this research and I feel to dedicate some sincere words to whom smartly guided this last important academic path, always leaving me the full control of my research activities.

I would like to thank my advisor Dr Anna Maria Siani (my mentor), professor at Sapienza University of Rome – Department of Physics, who trusted in me from the first time and shared her working space and knowledges with me far beyond the microclimate topics. These few words will never be enough to express my gratitude.

I am grateful to my co-advisor Dr Cristina Cornaro, professor at the University of Rome "Tor Vergata" – Department of Enterprise Engineering, who believed both in this project and in me, even though my academic background was different from her expertise.

No words can describe how much I appreciate the truth placed in me. Thank you! Thank you all for your support and advice!

I would also like to thank PhD Massimiliano Pedone, PhD Giuseppe Rocco Casale, prof Alfredo Colosimo and prof Eugenio Fazio for sharing their expertise with me. Special thank goes to prof Dario Camuffo for the interesting and precious courses on microclimate in Milan, Padua, Venice and Rome (Italy). I express also my gratitude to Dr Florian Antretter and all the other colleagues at the Fraunhofer Institute for Building Physics, Holzikirchen (Germany), for their hospitality and fruitful discussions during my research stay in the spring of 2017. Thank you all.

Then, I would also like to thank the external reviewers, Prof. Targo Kalamees (Tallinn University of Technology, School of Engineering: Department of Civil Engineering and Architecture) and PhD Marcin Strojecki (Jerzy Haber Institute of Catalysis and Surface Chemistry, Polish Academy of Sciences), for their constructive comments and suggestions, that allowed improving the quality of my dissertation.

Finally, I would like to thank Prof. Giovanni Battista Andreozzi, coordinator of my Doctoral school (Scuola di dottorato "Vito Volterra" in Scienze Astronomiche, Chimiche, Fisiche, Matematiche e della Terra) and all the members of the Ph.D. committee for their constructive suggestions and for the several scientific activities planned over the year.

I grew up in a home filled with curiosity. My parents have always encouraged me to learn beyond the limits and to fix my problems with my own strength. Thank you, mom and dad, you supported me every time in your unique way.

Finally, my beloved Alex, thank you for being here and for making my life such fun and so complete! Thank you for your patience when I am discouraged, even pathetic, and when I am not able to fight my demons.

Francesca Frasca

Abstract

The preventive conservation consists in all activities that allow to mitigate the degradation of cultural heritage. Among these activities, the study of environmental conditions is crucial to assess the degradation process as well as to manage and preserve the cultural heritage. The ageing of an object and the alteration of chemical-physical properties are activated and controlled, directly and indirectly, by the microclimate and its fluctuations. Any departure from the microclimate, especially the relative humidity (RH), that has promoted the conservation of an object (historical climate) might be harmful to its future preservation. For this reason, conservation scientists focus on methodologies able to reduce, predict and prevent the degradation. Combining experimental and modelling approaches in studies of indoor climate proves to be effective (a) to diagnose key factors that determine the microclimate and (b) to predict its dynamic behaviour if boundary conditions change. However, the efficacy of the building dynamic simulation strongly depends on the accuracy of the building model, that should derive both short- and long-term fluctuations of the indoor climate variables, especially those concerning RH, which is, besides, complex to simulate due to its dependence on many factors. Consequently, the use of dynamic simulation can be effective only when the relative humidity is accurately measured, analysed and modelled.

This thesis addresses a very important timely topic in the preventive conservation providing a strategy in the control and management of the indoor climate within historic buildings which house permanent collections. To achieve this purpose, the research focused on combining experimental and dynamic simulation studies. Particular attention was paid to moisture modelling as well as to the moisture-induced damage in hygroscopic materials. There were four main reasons to have prompted this research: (1) providing an objective assessment about the quality of indoor climate measurements; (2) developing a damage function specific for mechanical degradation; (3) extending the features of a commercial building dynamic simulation software with a one-dimensional heat and moisture transfer model; (4) easing the set-up of the building model using hourly climate variables instead of energy data. The issues (3) and (4) were needed for using the dynamic simulation as a diagnostic tool. The issue (2) was needed for extending the use of simulation from a diagnostic tool to a predictive tool. The methodology proposed by this research consists of three steps: (i) microclimate monitoring and its characterization for conservation risk assessment based on dose-response model; (ii) creation of a building model and its calibration; (iii) use of calibrated building and dose-response models to predict the microclimate evolution after a new strategy of microclimate control. The specific purposes were achieved using different case studies and the whole strategy (i.e. the general purpose) was successfully exploited in the case of "Archaeological Museum of Priverno", which might be defined as the pilot case study.

The combination of indoor climate measurements jointly with the dynamic simulation has demonstrated to be a powerful tool to assess a climate control solution within

historic buildings. The proposed approach results to be completely non-invasive, non-destructive and with zero-costs in terms materials. Indeed, the conservative quality of the exhibition spaces after modification of the indoor climate is directly assessed in the simulation environment. In this way, outcomes can support advantageously decision-making for a better control and management of the exhibition environment.

Riassunto

La conservazione preventiva consiste in tutte quelle attività che consentono di mitigare il degrado dei Beni Culturali. Tra queste attività, lo studio delle condizioni ambientali è fondamentale per valutare il processo di degrado così come per gestire e tutelare il patrimonio culturale. L'invecchiamento di un oggetto e l'alterazione delle sue proprietà chimico-fisiche e strutturali sono processi innescati e regolati in modo diretto e indiretto dal microclima e dalle sue fluttuazioni. Qualsiasi allontanamento dalle condizioni ambientali, in particolar modo dall'umidità relativa (UR), che ha favorito la conservazione del manufatto fino a oggi (clima storico), potrebbe essere deleterio alla sua futura tutela. Per questo motivo, l'interesse dei conservatori scientifici è rivolto a trovare metodologie di studio che consentano di rallentare, prevedere e prevenire il degrado. La combinazione di misure sperimentali e simulazione dinamica del clima interno risulta efficace (a) a diagnosticare le cause che determinano il microclima e (B) a prevedere il suo comportamento in caso di modifiche delle condizioni a contorno. Tuttavia, l'efficacia della simulazione dinamica degli edifici dipende fortemente dall'accuratezza del modello di edificio, che dovrebbe esser in grado di derivare le fluttuazioni a medio e lungo termine, in particolar modo quelle di UR, che è complessa da simulare a causa della sua dipendenza da molti fattori. Di conseguenza, l'uso della simulazione dinamica può essere efficace solo quando l'umidità relativa è misurata, analizzata e modellata accuratamente.

Questa tesi affronta un argomento molto importante nel campo della conservazione preventiva, fornendo una strategia per il controllo e la gestione del microclima all'interno di edifici storici che ospitano collezioni permanenti. Per raggiungere questo obiettivo, la ricerca si è focalizzata sull'uso combinato di studi sperimentali e di simulazione dinamica. Particolare attenzione è stata indirizzata alla modellazione dell'umidità così come ai fenomeni di degrado meccanico indotti dall'umidità nei materiali igroscopici. Esistevano quattro ragioni per condurre questa ricercar: (1) fornire una valutazione oggettiva circa la qualità delle misure microclimatiche; (2) sviluppare una funzione di danno specifica per il degrado meccanico; (3) estendere le caratteristiche di una software commerciale di simulazione dinamica degli edifici con un modello monodimensionale di trasferimento simultaneo di calore e vapore attraverso le pareti; (4) facilitare il settaggio dei parametri necessari alla costruzione del modello di edificio a partire dai dati orari di temperatura e umidità relativa. I punti (3) e (4) erano necessaria per usare la simulazione dinamica come uno strumento diagnostico. Il punto (2) era necessario per estendere l'uso della simulazione anche a strumento prognostico. La

metodologia proposta da questa ricerca consiste di tre fasi: (i) monitoraggio microclimatico e sua caratterizzazione per la valutazione del rischio di degrado basata un modello dose-risposta; (ii) creazione del modello di edificio e sua taratura; (iii) uso dei modelli tarati di edificio e di degrado per prevedere l'evoluzione del microclima dopo una nuova strategia di controllo microclimatico. Gli obiettivi specifici precedentemente elencati sono stati raggiunti usando differenti casi studio, mentre l'intera metodologia è stata applicata con successo al Museo Archeologico di Priverno che potrebbe essere definito come caso studio pilota.

La combinazione di misure microclimatiche insieme alla simulazione dinamica si è dimostrata uno strumento potente and flessibile per la valutazione di una soluzione di controllo microclimatico in edifici storici. L'approccio proposto risulta essere completamente non invasivo, non distruttivo e con costo-zero in termini di materiali (se si esclude il costo del monitoraggio microclimatico). Infatti, le qualità conservative degli spazi da esposizione dopo la modifica del microclima sono direttamente valutate nell'ambiente di simulazione. In questo modo, i risultati possono sostenere vantaggiosamente i processi decisionali riguardanti il controllo e la gestione dell'ambiente espositivo.

List of publications

This thesis is based on the following papers (P), conference papers (CP) and pre-submitted papers (PP), which will be referred to by their appendix in the text.

Appendix A (P, Impact Factor: 2.8):

Frasca F., Siani A.M., Casale G.R., Pedone M., Strojecki M. and Mleczkowska A. (2017). Assessment of indoor climate of Mogiła Abbey in Kraków (Poland) and the application of the analogues method to predict microclimate indoor conditions. Environmental Science and Pollution Research, 24(16), 13895-13907.

My work input: main author, analysis and critical interpretation of data, methodology, investigation on meteorological approaches in preventive, conservation, critical review

Appendix B (P, Impact Factor: 2.8):

Siani A.M., **Frasca F.**, Di Michele M., Bonacquisti V. and Fazio E. (2018). Cluster analysis of microclimate data to optimize the number of sensors for the assessment of indoor environment within museums. Environmental Science and Pollution Research, 25(29), 28787-28797.

My work input: co-author, conceptualization, analysis and critical interpretation of data, drafting of the manuscript, critical review.

Appendix C (CP):

Frasca F., Lovati M., Cornaro C., Moser D. and Siani A.M. (2017) Use of photovoltaic modules as static solar shadings: Retrofit of a paleontological site in Rome. In 12th Conference on Advanced Building Skins, 2-3 October 2017, Bern, Switzerland. Proceedings book. pp. 1235-1245.

My work input: main author, study conception and design, analysis and critical interpretation of data, critical review.

Appendix D (CP):

Frasca F., Cornaro C. and Siani A.M. (2018, June). Performance assessment of a heat and moisture dynamic simulation model in IDA ICE by the comparison with WUFI Plus. In IOP Conference Series: Materials Science and Engineering (Vol. 364, No. 1, p. 012024). IOP Publishing.

My work input: main author, literature review, study conception and design, analysis and critical interpretation of data, drafting of the manuscript, critical review, oral contribution.

Appendix E (PP):

Frasca F., Cornaro C. and Siani A.M. (201?) Performance assessment of a heat and moisture dynamic simulation model in IDA ICE by comparison with WUFI Plus. Pre-submitted paper

My work input: main author, literature review, conception of the original methodology workflow, implementation of simulation code, analysis and critical interpretation of data, proofing outline.

Appendix F (CP):

Frasca F., Cornaro C. and Siani A.M. (2017) On-site measurements and whole-building thermal dynamic simulation of a semi-confined prefabricated building for heritage conservation. In Building Simulation Applications (BSA) 2017, 8-10 February 2017, Bolzano, Italy. Proceedings book ISBN 9788860461360 pp 185.-192.

My work input: main author, study conception and design, analysis and critical interpretation of data, development of a semi-automatic calibration program, oral contribution

Appendix G (PP):

Frasca F., Cornaro C. and Siani A.M. (2019) A method based on environmental monitoring and building dynamic simulation to assess indoor climate control strategies in the preventive conservation within historical buildings. Submitted in: Science and Technology for the Built Environment (STBE) "IBPC Topical Issue".

My work input: main author, literature review, conception of the original methodology workflow, implementation of simulation code, analysis and critical interpretation of data, proofing outline.

Other related publications by the author

The other publications are listed below in chronological order.

Frasca F., Siani A.M. and Cornaro C. (2016) Microclimatic measurements and whole-building dynamic simulation of a semi-confined paleontological site: La Polledrara di Cecanibbio (Rome). In CMA4CH - 6th International Meeting, Straighforward Approach in Cultural Heritage and Environment Studies - Multivariate Analysis and Chemometry, 18-19 December 2016, Rome, Italy. Proceedings book - ISBN:9788875474416 pp 18-19.

My work input: main author, study conception and design, analysis and critical interpretation of data, oral contribution.

Fazio E., Bonacquisti V., Di Michele M., **Frasca F.**, Chianese A. and Siani A.M. (2017) CleAir Monitoring System for Particulate Matter: A Case in the Napoleonic Museum in Rome. Sensors 17(9): 2076.

Impact Factor (5 years): 3.01

My work input: co-author, analysis and critical interpretation of data, proofing outline.

Frasca F., Caratelli A. and Siani A.M. (2018, June). The capability of capacitive sensors in the monitoring relative humidity in hypogeum environments. In IOP Conference Series: Materials Science and Engineering (Vol. 364, No. 1, p. 012093). IOP Publishing.

My work input: main author, study design, analysis and critical interpretation of data, drafting of the manuscript, critical review, oral contribution.

Siani A.M., **Frasca F.**, Scarlatti F., Religi A., Diémoz H., Casale G.R., Pedone M. and Savastiouk, V. (2018). Examination on total ozone column retrievals by Brewer spectrophotometry using different processing software. Atmospheric Measurement Techniques, 11(9), 5105-5123.

Impact Factor (5 years): 3.65

My work input: co-author, analysis and critical interpretation of data.

List of abbreviations and terminology

Roman symbol

Symbol	Description	Unit
A_w	water absorption coefficient	$kg/(m^2 \cdot s^{0.5})$
c_p	specific heat	J/(kg·K)
C	crack width	mm
CHOY	heating hours of the year	h
CO_2	carbon dioxide	ppm
D_φ	liquid conduction coefficient of water	kg·m/s
df	diffuse solar irradiance components	W/m^2
DP	dew point	°C
dr	direct solar irradiance components	W/m^2
D_w	liquid transport coefficient	m^2/s
D_{ws}	liquid transport coefficient for suction	m^2/s
G(HOY,c)	irradiance of the least irradiated string in a given HOY and c	W/m^2
G(HOY,p)	relative irradiance in a specific hour	W/m^2
GAIN	gain index	--
g_v	vapour diffusion flux	$kg/(m^2 \cdot s)$
g_w	capillary moisture flux	$kg/(m^2 \cdot s)$
H	enthalpy	J/m^3
HHOY	cooling hours of the year	h
h_v	evaporation enthalpy of water	J/kg
L	length	month
MC	moisture content	kg/m^3
MR	mixing ratio	g/kg
N(c)	number of strings that are not bypassed in the configuration	--
NBI	number of intervals	--
$N_{modules}$	number of modules in the solution	--
Nr	number of good measurements	--
p	measuring planes	m
P(HOY)	power in a specific hour	W
PI	Preservation Index	year
p_k	capillary pressure	kg/(m·s·Pa)
PR	Performance Ratio	--
p_{sat}	saturated vapour pressure of water	Pa
p_v	vapour partial pressure	Pa
RH	relative humidity	%
RH_s	relative humidity at the interface air-surface	%
s	thickness	m
T or ϑ	temperature	°C
TN	total number of values	--
Ts	surface temperature	°C
TWPI	Time Weighted Preservation Index	year

U-value	heat transmittance	$W/(m^2 \cdot K)$
w	water content	kg/m^3
w_{80}	Equilibrium water content at 80% rel hum	kg/m^3
W_d	Wind direction	°
w_f	Free water saturation	kg/m^3
W_s	Wind speed	m/s

Greek symbol

Symbol	Description	Unit
β_P	water vapour transfer coefficient	$kg/(m^2 \cdot s \cdot Pa)$
δ_a	water vapour permeability of air	$kg/(m \cdot s \cdot Pa)$
δ_p	water vapour permeability of material	$kg/(m \cdot s \cdot Pa)$
η	efficiency	%
ϑ	temperature	°C
λ	thermal conductance	$W/(m \cdot K)$
μ^*	absolute mean	--
μ_d	dry cup vapour diffusion resistance factor	--
μ_w	wet cup vapour diffusion resistance factor	--
ρ	density	kg/m^3
φ	relative humidity	--

Mathematical symbol

Symbol	Description
d	operator for total differential
∂	operator for partial differential
Δ	difference operator
∇	nabla operator

Abbreviations and acronyms

a, b, c, d	general coefficient (ambiguous)
A, B, C, D	instrumental category
AA, A, As, B, C, D	climate classes of control according to ASHRAE
ASHRAE	American Society of Heating, Air-Conditioning and Refrigerating Engineers
b_1, b_2, b_3	general coefficients (ambiguous)
BDFWall	Finite difference wall model using own THETA-method integrator

BIPV	Building Integrated PhotoVoltaic system
CA	Cluster Analysis
CCS	Convetional Capacitive Sensor
CE3	Common Exercise 3
CEC	Climate Evaluation Chart
CfC	Climate for Culture
CI	Continuity Index
CoI	Completeness Index
COMBO	Combination Optimized to Meet Building Objectives
CV-RMSE	Coefficient of Variation of Root-Mean-Square-Error
DBS	Dynamic Building Simulation
E'	centered root-mean-square-error
ECBCS	Energy Conservation in Buildings and Community Systems program
EDA	Exploratory Data Analysis
EEs	Elementary Effects
EN	European Norm
EU	European Union
FP	Framework Programme
GenOpt	Genetic Optimization
HAM tool	Heat air and Moisture tool
HCS	Heated Capacitive Sensor
HMWall	Heat air and Moisture Wall
HVAC	Heating Ventilating and Air Conditioning
IDA ICE	IDA Indoor Climate and Energy
IEA	International Energy Agency
in	indoor
IQR	Inter-Quartile Range
MAE	Mean Absolute Error
max	maximum
MBE	Mean Biased Error
min	minimum
MPPT	Maximum Power Point Tracking
MQI	Microclimate Quality Index
out	outdoor
PB	Percentage Bias
PSO-GPSHJ	Particle Swarm Optimization – General Pattern Search of Hooke-Jeeves
PV	PhotoVoltaic
PVC	PolyVinyl Chloride
r_s	Spearman's rank correlation coefficient
REMO	Regional Climate Modelling
RMSE	Root Mean Square Error
SA	Sensitivity Analysis
SAC	Semi-Automatic Calibration
S_i	Silhouette index
SD or σ	Standard Deviation

SSBAR	Soprintendenza Speciale per i Beni Archeologici di Roma
TB	Thermal Bridge
TRY	Test Reference Year-type
UNESCO	United Nations Educational, Scientific and Cultural Organization
UNI	Ente nazionale italiano di unificazione
UTC	Coordinated Universal Time
WP	Work Package
WUFI	Wärme Und Feuchte Instationär

List of contents

Chapter 1: Rationale

"For ethical reasons, the conservation of cultural heritage is a duty for all nations. Slowly, decision makers are beginning to understand that caring about cultural heritage and especially about museum, library and archival collection is a valuable long-term investment for their economy and in the interest of their citizens. The accessibility of movable heritage depends not only on its direct conservation but also on preventive conservation, because the quality of the indoor environment is crucial for the preservation of a collection."

Dario Camuffo, Vasco Fassina and John Havermans

Context of the study

In 1972, the General Conference of the UNESCO (United Nations Educational, Scientific and Cultural Organization), in the *"Convention concerning the protection of the world cultural and natural heritage"*, highlighted the importance of safeguarding the irreplaceable cultural and natural heritage. This meant that artefacts, that have artistic historic and cultural value, cannot be simply replaced, copied or reconstructed, but they must be preserved as far as possible in their original state and place.

In 2004, the Italian Republic published the Legislative Decree No 42 of 24 January 2004 (D. Lgs. 42/2004). Four articles point out the requirement on the authority on the conservation of cultural heritage.

Article 3[1]: Preventive conservation

The protection of cultural heritage consists in practice of the activities and in the discipline of the direct activities, on the basis of an adequate knowledge, to individuate

[1] The translation is provided by the author. The original text is reported. Articolo 3: La tutela consiste nell'esercizio delle funzioni e nella disciplina delle attività dirette, sulla base di un'adeguata attività conoscitiva, ad individuare i beni costituenti il patrimonio culturale ed a garantirne la protezione e la conservazione per fini di pubblica fruizione.

the cultural heritage and to guarantee the preservation and conservation aimed at public enjoyment purposes.

Article 20[2]: Forbidden intervention

The cultural heritage cannot be destroyed, damaged or unsuitable used or such as to be detrimental to their conservation.

Article 29[3]: Conservation

The conservation of cultural heritage is guaranteed by a coherent, coordinated and planned activity of study, prevention, maintenance and restoration.

Article 30[4]: Preservative obligations

The State, the Regions and the territorial public institutions are obligated to guarantee the security and conservation of their cultural heritage.

The awareness to preserve cultural heritage stands out both at national and international scale. Thus, the main objective of conservation scientists is to find solutions capable to reduce the degradation phenomenon as well as further damaging occurrences. This can be successfully achieved only through the knowledge of the chemical, physical and biological properties of material and its environment as well as their mutual interaction. Therefore, both the analysis of the problems related to conservation and the identification of the induced-degradation causes can be successfully conducted with a multidisciplinary approach, as also documented by several programmes regarding the conservation required and promoted by the European Community.

The study of environmental conditions is crucial to assess the degradation process as well as to manage and preserve the cultural heritage. The ageing of an object and the alteration of its chemical-physical properties are activated and controlled, directly and indirectly, by the indoor climate and its fluctuations, also called *microclimate*[5]. Recently, a new concept has been introduced: the *historical climate*, i.e. the climate in which an object has, always or for a long period of time, has been kept and to which it has acclimatized (acclimatisation concept). Any departure from the historical climate might be harmful to future preservation of cultural heritage, since it might not only cause the acceleration of existing degradation phenomena but also trigger new ones. In this

[2] The translation is provided by the author. The original text is reported. Articolo 20: I beni culturali non possono essere distrutti, danneggiati o adibiti ad usi non compatibili con il loro carattere storico o artistico oppure tali da recare pregiudizio alla loro conservazione.

[3] The translation is provided by the author. The original text is reported. Articolo 29: La conservazione del patrimonio culturale è assicurata mediante una coerente, coordinata e programmata attività di studio, prevenzione, manutenzione e restauro.

[4] The translation is provided by the author. The original text is reported. Articolo 30: Lo Stato, le regioni, gli altri enti pubblici territoriali nonché ogni altro ente ed istituto pubblico hanno l'obbligo di garantire la sicurezza e la conservazione dei beni culturali di loro appartenenza.

[5] The microclimate is the synthesis of the ambient physical conditions over a period representative of all natural and anthropic forcing factors

context, conservation scientists focus on developing methodologies within the microclimate analysis able to reduce, predict and prevent the main degradation processes. The microclimate analysis contributes to the preventive conservation only if it can individuate and assess all the ongoing climatic processes, that are strongly affected by the building's features. The building, indeed, plays a key role in the indoor energy and moisture balance since it is a buffer of the outdoor environmental conditions. Sometimes, it could be sufficient to ensure adequate microclimate and air quality. However, both the use of powerful HVAC (Heating Ventilating and Air Conditioning) system and the increase of cultural tourism can be additional disturbing factors, as internal heat and moisture sources, responsible for unstable microclimate.

So far, most of approaches in the microclimate study has been to analyse microclimate data or to use the building dynamic simulation. In the very last years, the increasing awareness on the interaction between climate and objects has led to explore more and more sophisticated methodologies, that combine indoor climate measurements with (a) the damage functions or (b) with the whole building dynamic simulation. The methodology (a) reveals to be effective in relating the degradation risk assessment with the microclimate, contributing to the preventive conservation activity for a better protection of movable and immovable works of art. The methodology (b), instead, mainly concerns the best performance of the HVAC system solution within a historic building in order to obtain the lowest aesthetic impact, the energy saving and the thermal comfort of users. However, little attention has been giving so far to the combination of long-term on-site measurements with the dynamic simulation, in terms of both damage functions and building modelling, as a synergic tool for preventive conservation. Moreover, even less attention has been paid to the modelling of the relative humidity, even though its influence on degradation phenomena has been widely demonstrated. Consequently, the use of dynamic simulation can be effective only when the relative humidity is accurately measured, analysed and modelled.

The high potentialities of the above methodologies can be combined in order to define a multidisciplinary strategy suitable for the preventive conservation and based on diagnosing the microclimate and prognosing its evolution whether boundary conditions change. In this research thesis, such a strategy was investigated and proposed.

Aim of the research

The objective of my research is to demonstrate that the multidisciplinary use of experimental data of indoor climate combined with the dynamic simulation is a thorough and meticulous strategy in the field of the preventive conservation within historic buildings.

Since any indoor environment behaves differently according to the features of the building envelope and its internal heat and moisture loads, a general approach would be desired in order to be successfully applied for a wide typology of buildings. For this reason, the multidisciplinary use of on-site measurements and of building dynamic simulation shows to be potentially an effective approach (a) to diagnose the actual

indoor climate and (b) to predict its evolution whether modifications in the boundary conditions occur.

In this study, the IDA Indoor Climate and Energy (IDA ICE) was chosen as whole-building dynamic simulation software because of its modular architecture. Indeed, it can be extended with the HMWall model, that allows modelling the one-dimensional heat air and moisture transfer through hygroscopic and porous materials, such as building materials.

The achievement of this general objective implies addressing the four following issues:

1. *Is it possible to objectively assess the quality of indoor climate time series to apply the recent standards and guidelines?*

   The recent standards and guidelines on the microclimate assessment are based on the acclimatisation concept. However, they can be applied, only when monitoring systems provide long-term historic climate data with specific requirements. This means that the time series of microclimate parameters (such as for example relative humidity and temperature) must have (1) the length and (2) the instrumental accuracy in accordance with the current European standards. If time series do not meet these characteristics, the data mining and its interpretation might provide erroneous information leading to ambiguous assessments.

2. *Can the observed degradation measurements be related to the indoor climate and used to predict the effect of new control climate strategy to control the degradation?*

   Measurements related to a specific degradation phenomenon, e.g. moisture-induced strain in hygroscopic materials, such as wood, paper, textile, etc., might be very useful to understand the interaction between indoor climate and material's response to dynamics of environmental variables. Such an interaction, indeed, would depend on the heat and moisture transfer at the interface between the air and the material surface. If a dose-response function is established between degradation process and climate, it can be used as a specific damage marker. Its integration in the simulation environment as a goodness target would allow predicting the effect of different indoor climate conditions.

3. *How can a hygrothermal model be fine-tuned and then used in the field of preventive conservation?*

   Some of commercial dynamic simulation software are extended with one- or two-dimensional hygrothermal models (hereafter called HAM tool) to calculate the heat air and moisture transfer through porous materials. In IDA Indoor Climate and Energy environment, the HMWall model was integrated but less used due to its weak robustness output. The assessment of the performance model should be conducted using several tests or exercises with the aim to pinpoint the most relevant issues. Adding the moisture flow through walls in the modelling of old buildings might play a key role to diagnose the processes responsible for a microclimate dynamic. Indeed, old masonries can be characterised by uncontrolled condensation

phenomena that might affect the durability of the cultural objects, both architectural elements and, if present, works of art preserved within the building, as well as the thermal comfort of users and the energy consumption within the building.

4. *Can a semi-automatic calibration of building model with indoor temperature and relative humidity measurements be implemented for historic buildings?*

   A building model can be representative of a real case and can be advantageously used, only if it is accurately calibrated with respect to the measurements. Most of calibration procedures are based on matching of measured and modelled energy consumptions within tolerable limits recommended by official documents. However, in the case of historic buildings, such data are not always available, because most of these buildings are not fitted with HVAC system. This means that the calibration should be conducted with other measurements data that are recorded in continue and do not entail destructive or invasive sampling of architectural elements, due to their cultural and historic value. In this context, hourly measured indoor microclimate data might be used, since the accurate modelling of these variables, especially relative humidity, is fundamental to the assessment of the preventive conservation. However, manual calibration procedure can be time consuming especially in the case of historic buildings, where materials are not precisely known and structures of different ages are superimposed. For this reason, automatic or semi-automatic calibration procedure is preferred.

Scope and limitations

This thesis describes an effective strategy in the field of the preventive conservation combining on-site measurements and dynamic simulation. It focuses on modelling accurately the relative humidity within historic buildings and its relationship with the stress-and-strain cycle, i.e. mechanical degradation in restrained wooden structures. The methodology is applied to suggest a new climate control in the selected case study. The new climate control strategy is specific for the conservation of wooden material and the comfort of users. The energy consumptions are not considered.

The results cannot be applied to the preventive conservation of outdoor building structures, e.g. façades, roofs etc., where the contributions from rainfall, wind and solar radiation etc. may affect in synergic way all the ongoing processes.

In addition to the mechanical degradation, chemical and biological degradation processes also contribute to the conservation of Cultural Heritage. However, these processes were not dealt with in this thesis, since they were negligible in the selected case study. Nevertheless, the strategy can be extended and applied to other specific degradation phenomena, rearranging the monitoring system, if needed, and identifying other specific dose-response functions to the damage.

Outline of the thesis

Chapter 2 provides the state-of-the-art about the main topics concerning my research. It is divided in two sections that separately deal with the evolution of methods used in microclimatic analysis and the novelty use of dynamic simulation to study the indoor climate within historic buildings.
Chapter 3 describes the methodology I developed, structured in two sections:

- the description of the pilot case study, i.e. the Archaeological Museum of Priverno;
- the general workflow, i.e. the preventive conservation strategy.

The latter section consists of three parts necessary in the proposed strategy: (a) the microclimate analysis, (b) the simulation environment and (c) the control climate strategy. This section also includes the procedures developed and used to solve the four specific issues listed in Chapter 1 and tested on different case studies. Questions 1 and 2 are included in (a), whereas questions 3 and 4 are described in (b). The preliminary results of such research activities are linked into the appendices as ancillary supports.
In Chapter 4, the most relevant outcomes derived from the proposed strategy on the Archaeological Museum of Priverno are shown and discussed.
Chapter 5 draws the general conclusion of my research, the answers to the research questions listed in Chapter 1 and, finally, suggests implications and future possible researches coming from my outcomes.
This manuscript also includes six appendices, listed from A to F, that present the preliminary outcomes from the four specific issues published or pre-submitted papers and conference papers. Finally, the Appendix G includes the manuscript related to the whole strategy developed in my research and applied in the case of the Archaeological Museum of Priverno.

- Appendix A:
  Frasca F., Siani A.M., Casale G.R., Pedone M., Bratasz Ł., Strojecki M., Mleczkowska, A. (2017) Assessment of indoor climate of Mogiła Abbey in Kraków (Poland) and the application of the analogues method to predict microclimate indoor conditions. Environmental Science and Pollution Research, 24(16): 13895–13907.

  My work input: main author, analysis and critical interpretation of data, methodology, investigation on meteorological approaches in preventive conservation, writing, critical review, creation of a partnership.

- Appendix B:
  Siani A.M., Frasca F., Di Michele M., Bonacquisti V. and Fazio E. (2018). Cluster analysis of microclimate data to optimize the number of sensors for the assessment of indoor environment within museums. Environmental Science and Pollution Research, 25(29), 28787-28797.

  My work input: co-author, conceptualization, analysis and critical interpretation of data, drafting of the manuscript, critical review.

- Appendix C:
  Frasca F., Lovati M., Cornaro C., Moser D. and Siani A.M. (2017) Use of photovoltaic modules as static solar shadings: Retrofit of a paleontological site in Rome. In 12th Conference on Advanced Building Skins, 2-3 October 2017, Bern, Switzerland. Proceedings book. pp. 1235-1245.

  My work input: main author, study conception and design, analysis and critical interpretation of data, critical review, creation of a partnership.

- Appendix D:
  Frasca F., Cornaro C. and Siani A. M. (2018, June). Performance assessment of a heat and moisture dynamic simulation model in IDA ICE by comparison with WUFI Plus. In IOP Conference Series: Materials Science and Engineering (Vol. 364, No. 1, p. 012024). IOP Publishing.

  My work input: main author, literature review, study conception and design, methodology, analysis and critical interpretation of data, writing, critical review, oral contribution, creation of a partnership.

- Appendix E:
  Frasca F., Cornaro C. and Siani A. M. (----). Performance assessment of a heat and moisture dynamic simulation model as an extension of IDA ICE.
  PRE-SUBMITTED

  My work input: main author, literature review, conception of the original methodology workflow, implementation of simulation code, analysis and critical interpretation of data, proofing outline.

- Appendix F:
  Frasca F., Siani A.M. and Cornaro C. (2017). On-site measurements and whole-building thermal dynamic simulation of a semi-confined prefabricated building for heritage conservation. In BSA 2017–Building Simulation Applications 3rd IBPSA-Italy Conference, 8.2. 2017–10.2. 2017. BU, press. Proceedings book ISBN 9788860461360 pp 185.-192.

  My work input: main author, study conception and design, analysis and critical interpretation of data, development of a semi-automatic calibration program, writing, critical review, oral contribution.

- Appendix G:
  Frasca F., Cornaro C. and Siani A.M. (2019) A method based on environmental monitoring and building dynamic simulation to assess indoor climate control strategies in the preventive conservation within historical buildings. Submitted in: Science and Technology for the Built Environment (STBE) "IBPC Topical Issue".

  My work input: main author, literature review, conception of the original methodology workflow, implementation of simulation code, analysis and critical interpretation of data, proofing outline.

Table 1 summarises a schematic outline of the appendices, identifying which one contributes to the formulated research questions.

Table 1 Research questions related to appendices.

Research questions	**Appendices**					
	A	B	C	D	E	F
1	x	x				
2			x			
3				x	x	
4						x

Chapter 2: Background and state-of-the-art

This chapter concerns the literature about the topic of my research: (a) Evolution of the methods used in microclimatic analysis and control and (b) Dynamic simulation of indoor climate. The former overviews the methods dealing with the microclimate from the end of 1970s to the present time. The latter describes the potential use of the whole building dynamic simulation, as an effective tool to support the microclimatic analysis and to predict the indoor climate conditions related to any change of the current state.

Evolution of the methods used in microclimatic analysis and control

The concept of preventive conservation consists in all measures and actions that aim at avoiding and minimizing future deterioration or loss in cultural property (ICOM-CC 2010). Every degradation phenomenon, including the natural cumulative and irreversible ageing of the objects, is strictly related to the direct and indirect interactions between the climate and materials both in indoor and outdoor environment. In historic buildings and more in general in exhibition spaces, the assessment of the indoor climate or microclimate, i.e. the synthesis of the ambient physical conditions over a period representative of all natural and anthropic forcing factors (Camuffo 2014), is fundamental to individuate and, if any, reduce the occurrences of damage.

The awareness of the influence of the microclimate, especially relative humidity (RH), on the conservation of artworks already emerged at the beginning of 20th century, as extensively described by Browne and Rose (1996) and by Erhartdt et al. (2007) in their overview on the development of climate control in historic buildings or museums in Europe and in USA.

Nevertheless, from the end of 1970s, an increasing interest in defining suitable indoor climate conditions can be inferred by the progressive evolution of the methodological approaches, the standards (or norms) and the guidelines, both at national and international level. As well, the main scientific research databases (Scopus, Web of Science, etc.) report more than four-hundred publications in the time range 1991-2017,

using the words *"indoor climate AND cultural heritage AND conservation"*, revealing an increasing trend for the topic year-by-year (Figure 1).

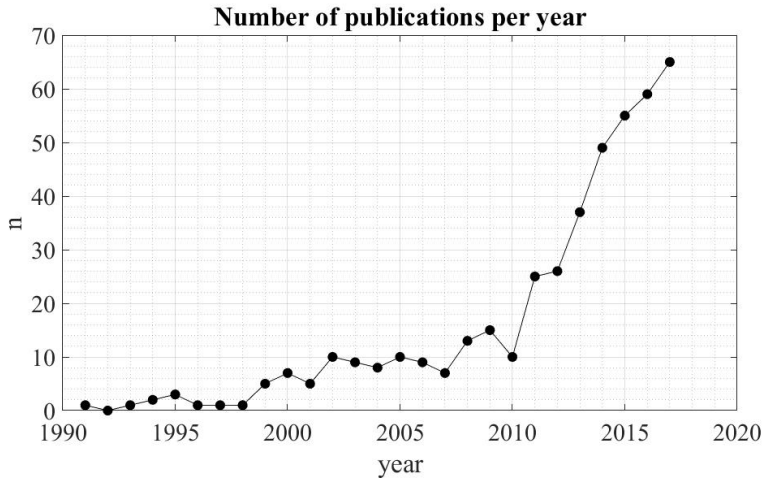

Figure 1 Number of publications per year. Data retrieved from Scopus (last access September 2018) by using the words: "indoor climate AND cultural heritage AND conservation".

The first approaches to control the indoor climate were to fix hygrothermal intervals with the aim to limit fluctuating conditions. For example, many recommendations based on "*The Museum Environment – 2nd edition*" (Thomson 1986) suggested to keep the relative humidity (RH) at 50% or 55 ± 5% and temperature (T) at 19°C or 24°C ± 1°C for winter and summer, respectively, in the new and "important" museums.

The study of the interaction between the microclimate and the artworks was pointed out in the 1980's (Camuffo 1983). However in the 1990's, the research was dedicated to analyse collection degradation processes, showing the importance of differentiating the allowable hygrothermal intervals according to material type, storage place and damage/deterioration risk. This derived from the awareness that degradation phenomena were mainly affected by (a) the sensitivity of the object at T and RH fluctuations and/or (b) the recent history of the object. The main consequence was that climate guidelines were considered too strict (Ashley-Smith et al. 1994; Michalski 1993; Michalski 1994; Michalski 1996) and maintaining such narrow ranges resulted expensive and, in some cases, impractical (Brown 1994).

a. The works of Mecklenburg (1991) and Tumosa (1991) and Erhardt (1998), followed by those of Jakieła et al. (2007) and Jakieła and Kozłowski (2008) showed crucial issues about the identification of climate specification based on the analysis of structural response, i.e. mechanical processes, of coatings, gilding, paint on canvas, wood and paint on wood. Mechanical degradation, indeed, is caused by stresses in the material due to strain of the artefact, i.e. its dimensional changes caused by fluctuating T and RH. Especially, RH strongly affects the absorption and desorption of moisture in material, provoking cracking when the stress exceeds the failure stress limit. The risk of cracking, indeed, depends on many aspects: the magnitude of the RH change, the rate of the RH change, the level of RH at which the RH change starts and the number of RH fluctuation cycles that the object has been subjected to in the past. These authors

prove that the range of 50% ± 15% of RH was tolerable and hence safe for such a material (Bratasz 2013).

The increase of laboratory and *in-situ* tests on different historical or aged materials led to individuate T and RH limits suitable on the basis of material category or risk of degradation. Thus, the first methods for the microclimate assessment were focused on analysing T and RH averages and their variability (Bernardi and Camuffo 1995; Camuffo and Bernardi 1996; Pavlogeorgatos 2003), as well as on investigating the impact of external climate conditions on indoors (Camuffo et al. 1999). Then, studies investigated the relationship between T-RH variables and other atmospheric variables, such as pollutants and light. The monitoring campaigns became more sophisticated aiming at analysing hygrothermal vertical profiles and spatial gradients, e.g. for detecting processes related to the vehiculation, diffusion and deposition of pollutants or for individuating sinks and sources of heat and moisture (Camuffo et al. 2001; Camuffo and Giorio 2003; Camuffo et al. 2004; Samek at al. 2007; Becherini et al. 2010; Cataldo et al. 2005). In the last years, the methodological approach has been also oriented to assess the climate risk analysis on artworks. Corgnati et al. (2010) developed an index to assess the percentage of time in which T-RH were in climate limits, as provided by standards or guidelines. Moreover, many damage functions were established to define the quality of environment with respect to chemical (Michalski 2002; Kruger and Diniz 2011), mechanical (Martens 2012) and biological (Adan 1994; Sedlbauer et al. 2001) degradation. This approach reveals to be effective for the decision-making process (Silva and Henriques 2015). It is worth to notice that the damage functions are material-specific and assess the indoor climate with respect to "ideal" or safe hygrothermal conditions. For this reason, they should be used as relative indicators. Moreover, some functions are based on indoor air T and RH, showing two issues: (1) the temperature of an object often differs from air temperature and (2) many degradation processes depend on moisture content (MC), that is difficult to measure and its relationship with RH is dynamic.

b. The attention was also paid to the recent history of the object, related to the so-called acclimatisation concept or historic climate, i.e. the climate to which the objects, especially those made of organic and hygroscopic materials suffering from shrinkage and swelling, have been acclimatized and adapted over their time life (Bratasz et al. 2007a; Bratasz et al. 2007b). It was assumed that the risk of further mechanical damage (beyond that already accumulated in the past) from fluctuations which do not go beyond the proofed pattern is extremely low. The proofed fluctuation concept (Michalski 2007) eliminates any need for elaborate mechanical response calculations and offers a risk assessment based just on past climate records. The studies prove that climate limits, especially RH limits, had to correspond to the T-RH variability that has been found satisfactory for conservation by qualified specialists. However, conservation treatments, changing the dimensional and mechanical properties of materials, and some fluctuations, even if not exceeding the historical levels, or their combination could increase the risk of damage, since physical damage can be

cumulative rather than catastrophic (Bratasz 2013). This approach has transformed the practices of microclimate investigations, since it has brought out the importance of long-term monitoring to detect all cycles (seasonal and daily) due to natural and anthropic factors.

In this context, new methodologies were developed to compare the historic climate (defined at present with measurements) with the reconstructions of past and future indoor climate. The aim was to investigate past climate-induced damage and to predict future climate-induced damage on artworks in order to plan suitable conservation strategies. The climate reconstructions can be performed by means of heat transfer functions (Lankester and Brimblecombe 2012; Bertolin et al. 2015) or with the use of more detailed models (see section

Dynamic simulation of indoor climate), starting from data of past (proxies for far past and instrumental observations for near part) and future (climate scenario models) outdoor climate (Camuffo et al. 2014).

The conventional practice in exhibition spaces (museums, galleries, archives, historic buildings, etc.) has always been to control T and RH of the rooms in which the most valuable artworks are preserved and to keep them at constant levels according to standards, guidelines or museums' procedure. This led to use increasing powerful HVAC (Heating Ventilating and Air Conditioning) systems, that have showed several weaknesses and disadvantages. Firstly, it was found that to guarantee strict limits the HVAC systems required lots of energy, whose consumption became an issue of relevant importance after the OPEC[6] crisis (Brown and Rose 1996) and for the latest directives on energy efficiency around the world. An example is given by Rota et al. (2015), that demonstrated the necessity of systematic approaches for actions oriented to investments for energy retrofitting, appropriated for the existing context and based on the real needs of museums. Secondly, the use of HVAC systems could not be justified, especially in historic buildings, if they compromised the acclimatisation of artworks in their environment. For example, the European project "*Friendly Heating: both comfortable for people and compatible with conservation of art works preserved in churches*" (2002-2005) demonstrated the potential impact of indoor heating on the conservation of organic-hygroscopic artworks, when the heating system were used to only satisfy thermal comfort of users (Bratasz et al. 2007; Camuffo and Della Valle 2007; Camuffo et al. 2010). The preliminary conclusion was that the environmental conditions, most suitable for historic churches and their contents, were less suitable in terms of the comfort of churchgoers. This outcome could apply to all historic buildings which preserve climate-sensitive artworks.

The requirement to provide documents that guide experts in the control of indoor climate and in the choice of the most suitable instruments for indoor climate monitoring campaigns led to the development of standards and guidelines. A review of the initial

[6] The acronym OPEC stands for (Organization of the Petroleum Exporting Countries).

use and development of recommendations can be found in Erhardt et al. (2007) and Bratasz (2012).

The European Committee for Standardization (CEN) has already published seven standards through the Technical Committee TC 346 (Fassina 2008; Johnsen 2012), as reported in Table 2. These standards aim at specifying methodologies, procedures and instruments for accurate measurement of the indoor climate and its interactions with materials constituting cultural heritage. They have to be accepted by each National Standardization Body, member of the CEN, with the duty to withdraw any existing national standard that conflicts with the new European Standard. For example, the Italian Body of Standardization (UNI) has withdrawn and replaced the standards reported in Table 3.

Table 2 Summary of the European standards published by the European Committee for Standardization (CEN) and developed by the Technical Committee 346 (TC 346) within the Working Group 4 "WG 4 – Environment" (until 2012), then become "WG 4 – Protection of collections" and the Working Group 7 "WG 7 – Specifying and measuring Indoor/outdoor climate". The standards published by the old WG 4 have an asterisk (*), those by the new WG4 have a circle (°) and those by the WG 7 have a dagger (†). The light-green-highlighted standards concern the specification of instruments and measuring methods.

Reference	Title
EN 15757:2010 (*)	Conservation of Cultural Property - Specifications for temperature and relative humidity to limit climate-induced mechanical damage in organic hygroscopic materials
EN 15758:2010 (*)	Conservation of Cultural Property - Procedures and instruments for measuring temperatures of the air and the surfaces of objects
EN 15759-1:2011 (*)	Conservation of cultural property - Indoor climate - Part 1: Guidelines for heating churches, chapels and other places of worship
EN 16242:2012 (†)	Conservation of cultural heritage - Procedures and instruments for measuring humidity in the air and moisture exchanges between air and cultural property
EN 16682:2017 (†)	Conservation of cultural heritage - Methods of measurement of moisture content, or water content, in materials constituting immovable cultural heritage
EN 15759-2:20018 (†)	Conservation of cultural heritage - Indoor climate - Part 2: Ventilation management for the protection of cultural heritage buildings and collections
EN 16893:2018 (°)	Conservation of Cultural Heritage - Specifications for location, construction and modification of buildings or rooms intended for the storage or use of heritage collections

Related to the Michalski expertise (2007), the Handbook of the American Society of Heating, Air-Conditioning and Refrigerating Engineers (ASHRAE) was integrated with the Chapter 23 dedicated to "Museums, Galleries, Archives and Libraries" (ASHRAE 2011). The chapter is a support design for HVAC systems related to the conservation of collections and to quantify the damage risks (biological, mechanical, and chemical) of

environments already active. It is worth to notice that the proofed band for relative humidity at 50±15%, based on the scientific evidence above mentioned, fits with the only possible moderate-cost strategy available to historic buildings and museums, i.e. Class of Climate Control B.

Table 3 Summary of the Italian standards withdrawn and replaced by the European ones.

Italy		Europe
UNI Reference	**Title**	**EN Reference**
UNI 10969:2002	Beni culturali - Principi generali per la scelta e il controllo del microclima per la conservazione dei beni culturali in ambienti interni	EN 15757:2010
UNI 11120:2004	Beni culturali - Misurazione in campo della temperatura dell'aria e della superficie dei manufatti	EN 15758:2010
UNI 11131:2005	Beni culturali - Misurazione in campo dell'umidità dell'aria	EN 16242:2012

Dynamic simulation of indoor climate

The dynamic simulation[7] has revealed an innovative approach for the preventive conservation in old buildings, because it is a flexible tool and can produce accurate results when joint with on-site measurements. It has been considered one of the best tools to approach the historic buildings' refurbishment in terms of sustainability and energy performance evaluation (Martínez-Molina et al. 2016).

A review of the existing simulation tools is not the aim of this thesis. However, it was already demonstrated that neither a simulation tool either a methodological approach is possible to recommend for the modelling of historic buildings (Widstrom 2012).

The first applications of dynamic simulation regarded the assessment of the thermal comfort of users (Cardinale et al. 2010) and the energy retrofitting solutions (Balocco and Grazzini 2007; Ferdyn-Grygierek 2014). The last topic mainly concerned the improvement of thermal insulation and the renovation of HVAC systems trying to minimize their impact in terms of consumption and costs of energy. This requirement was strongly related to the objectives of European Community, that aimed at reducing the greenhouse gas emissions (Directives 2002/91/CE and 2010/31/EU), at increasing the share of renewable sources (Directive 2009/28/CE) and at enhancing the energy performance of existing buildings, especially in the construction sector belonging to the public institutions (Directive 2012/27/EU). The Italian situation showed a peculiarity. It was estimated that about the 30% of public building stock was built before 1945, i.e. they are historical buildings, and that a 2% of these belongs to the cultural heritage according

[7] The simulation enables the realistic reproduction of a process by means of physical or mathematical models, in which boundary conditions and reliable input parameters are defined.

to the Legislative Decree No 42 of 24 January 2004 (D. Lgs. 42/2004), i.e. they are historic buildings (De Santoli 2015; Filippi 2015; Mazzarella 2015). Since the Italian Legislative Decree No 192 of 19 August 2005 (D. Lgs. 192/2005) claims that in the case of historic buildings the conservation requirements have priority with respect to the energy retrofit, some studies were focused on the use of simulation as an effective tool to know in advance the impact of the refurbishment on the esthetical and architectural features of such buildings. Thus, several approaches were proposed with the aim to balance architectural conservation and energy efficiency (Ascione et al. 2015; Bellia et al. 2015; De Berardinis et al. 2014; Cornaro et al. 2016; Franco et al. 2015; López and Frontini 2014; Tronchin and Fabbri 2017). The attention paid to this topic is also revealed by the several projects funded by the European programmes in the last two decades. The Intelligent Energy Europe (IEE) programme funded *New4Old* – New energy for old buildings (2007-2010) for integrating renewable energy and energy efficiency technologies into historic buildings protecting their values, and *SECHURBA* – Sustainable Energy Communities in Historic Urban Areas (2008-2011) so to encourage energy efficiency practices and renewable energy systems in historical buildings. Within the Baltic Sea Region Programme (2007-2013), the *Co2ol Bricks* – Climate Change, Cultural Heritage & Energy Efficient Monuments (2010-2013) was funded with the purpose to reduce the energy consumption of historical buildings without destroying their cultural value and identity. The 7th Framework Programme (EU FP7) funded *3ENcult* – Energy Efficiency for EU cultural heritage (2010-2014) in order to use energy efficient retrofit for structural protection as well as for comfort and conservation requirements, and the *EFFESUS* – Energy Efficiency for EU Historic Districts′ Sustainability (2012-2016), with the aim of developing technologies and systems for energy efficiency in European historic urban districts.

Even though the whole building dynamic simulation is mainly used for the energy performance evaluation, it can be used as a diagnostic tool for achieving a comprehensive assessment of the current indoor climate (Janssen and Christensen 2013). Another potential use is related to the assessment of the impact of climate change on the indoor climate, especially the global warming, as already demonstrated in the CIBSE TM 36:2005, in which a building of 19th century was simulated to suggest adaptation to avoid overheating. This is important since any change in the heat and moisture exchange between indoor and outdoor has a direct influence not only on the energy performance of the building but also on the conservation of artworks (Cassar and Pender 2003). Some relevant publications over the last 5 years demonstrated the potentiality of the dynamic simulation as a tool for conservation risk assessment (Huijbregts et al. 2012; Kompatscher et al. 2017; Kramer et al. 2013; Kramer et al. 2015; Muñoz-González et al. 2016; Sciurpi et al. 2015; Schito and Testi 2017).

This issue was the main topic of the European project *Climate for Culture* (CfC – 2009-2014) funded within the 7th Framework Programme (EU FP7). The project was based on a multidisciplinary research team with the aim to identify the damage potential of the cultural heritage at risk and to encourage the development of strategies to mitigate the effects of climate change. This project, indeed, reflected the interest of scientific

community to take advantages from the dynamic simulation (Leissner et al. 2013). It used high-resolution climate change evolution scenarios (derived by REMO simulations) with whole building simulation models to give the risk assessment on artworks at near future (2021–2050) and far future (2071–2100) with respect to the reference period (1961–1990). However, the prediction capability of such a method is particularly complex, since it should consider at least the uncertainty related to (1) the future outdoor climate, (2) the building model and (3) the damage functions (Leijonhufvud et al. 2012).

The uncertainty in the future outdoor climate depends on the climate models, that resolve in a simplified way all relevant processes.

The efficacy of the dynamic simulation strongly depends on the accuracy of the building model, that should be able to detect short- and long-term fluctuations of the indoor climate variables, especially the relative humidity (Bilchmair et al. 2012; Antretter et al. 2013; Kupczak et al. 2018). This variable is particularly complex to simulate, since many factors should be simultaneously considered. Most of simulation codes were developed to model moisture exchanges between indoor and outdoor environments setting a specific moisture storage capacity to the interior of the building (Holm et al. 2003) and not to model the moisture flow between the air and porous surfaces (Rode and Woloszyn 2007). For this reason, in the last 30 years, some dynamic simulation tools were developed to model moisture exchanges also through porous materials (Delgado et al. 2012), allowing to study issues related to uncontrolled condensation typical of old masonries (O'Leary et al. 2015). Furthermore, in the case of old buildings, the complexity in geometry and the heterogeneity in materials make extremely complicated and time consuming the model building setting (Coakley et al. 2014; Coelho et al. 2018). Thus, the calibration of the building model becomes of essential importance to solve such an issue. As opposed to manual calibration, Caucheteux et al. (2013) and O'Neill and Eisenhower (2013) demonstrated the effectiveness of the semi-automatic calibration by means of the Sensitivity Analysis for identifying the most influential input parameters to be considered in order to minimise the discrepancy between modelled and measured energy data. Indeed, most of the calibration procedures is based on matching of energy data at different time scale (Ascione et al. 2011) or indoor air/surface temperature at hourly scale (Pernetti et al. 2013; Roberti et al. 2015) and few studies use relative humidity data.

The efficacy of damage functions relies on three kind of uncertainty: epistemic, aleatory and ambiguous (Refsgaard et al. 2013). The first depends on the input data and the lack of knowledge about processes, especially those related to the hygroscopic materials subject to the moisture content exchange. The second regards the randomness of mechanisms and the synergetic effects that cannot be included in the functions. The third, finally, relates to the interpretation of the output, that must be used as a relative predictor.

Chapter 3: Methodology

This chapter concerns the description of the case study selected for testing the preventive conservation strategy developed within this research and the explanation of the general workflow. The general workflow includes three subsections that also describe the four specific tasks defined in Chapter 1.

The case study

The case study is the historic building "Valeriani-Guarini-Antonelli Palace", located at Priverno (Latina) in the central Italy at about 70 km SE far away from Rome (Lat. 41.5° and Long. 13.2°), which houses the Archaeological Museum of Privernum, hereafter called museum. The site currently is a three-storey building and constitutes an architectural complex with the cathedral (12th century) and the historic town hall (13th century) which all together enclose the town square.

The first construction of the palace dates back to Medieval age (13th century) as still evident by the double-arched windows at the first floor (Figure 2), by the will of the illustrious Valeriani family.
At the beginning of 15th century, the Guarini family – new owners – wanted to enlarge the palace adding the second floor and the lateral wings that led to the current size of the building, as documented on the architrave inscription (*Petrus Johannes Guarinus. 1514*).
In 1924, the palace was bought at auction by the Antonelli family, who commissioned the retrofit of the façade and the interiors' decoration. The restoration lasted two years. The façade was restored by the sculptor Angelo Domenico Cives in Renaissance style with an amaranth and lead-grey *graffito* decoration (Figure 2). Valuable ceilings were decorated in *late-Liberty* style by Giulio Sordoni and Pietro Campeggi. The former depicted the ceilings at the first floor with tempera on plaster with grotesque, zodiac allegories, herms and caryatids that support *neorococò* cornucopias filled with fruit and flowers or *clipei* with interesting urban views of the Priverno (Figure 3); whereas the latter painted the wooden ceilings at the second floor with oil paintings with geometric patterns typical from Viennese school (Figure 5).

In 2012, the building was bought and restored in order to house the Archaeological Museum of Priverno.

The palace is oriented in the SW-NE direction with respect to the main entrance and has an internal courtyard and a terrace in the north-west side. The courtyard is accessible from the corridor close to the room 4 whereas the terrace from the room 13. The west-side of the palace is contiguous with another historical building; whereas the east-side overlooks a narrow street.

At the ground floor, there are the ticket office, the bookshop and the restroom. The thirteen rooms of the museum are deployed between the first (from room 1 to room 7) and second floor (from room 8 to room 13) following a path according to the historical events, from the Bronze Age to the Roman Age, of the ancient Priverno. Each room exhibits the evidences from the near archaeological area. The collection mainly consists of sculptures, architectural elements, ceramics, inscriptions, etc. The most valuable artefacts, e.g. jewellery and pottery, are exhibited in black glass-and-metallic showcases arranged along walls. In the room 9 at the second floor, there is the most important evidence of the museum - *the Nilotic sill* or *Soglia Nilotica* - that is often loaned for temporary exhibition around the world.

The dark interior design allows standing out all the evidences (mainly white) thanks to a LED lighting system used inside and outside the showcases (Figure 3).

Figure 2 The Archaeological Museum of Privernum (Latina, Italy): the main entrance (second door from left at the ground floor), the double-arched windows (first floor) and the façade in Renaissance style with an amaranth and lead-grey *graffito* decoration.

All rooms are opened-adjoining and, except for the west-side ones, have one or more wooden-framed windows shaded by wooden shutters and black-roller blinds (Figure 3 and Figure 4).

A HVAC system connected to fan coils for the temperature control is turned on during the opening hours by staff both in cold season (from November to April) and in warm season (from June to August). All fan coils are installed under the windows and some devices are covered by black drilled-metallic panels (Figure 4). The system is set to 18°C and 26°C for heating and cooling hours, respectively. However, rigid internal temperatures in winter and warm temperatures in summer make the indoor climate unpleasant to visitors.

Figure 3 A detail of the exhibition's configuration in room 4 (first floor): a detail of the ceiling decorated with tempera on plaster by Giulio Sordoni (top-left side); the windows shaded by wooden shutters and black roller-blinds.

To preserve the works of art, the conservation staff carries out periodical surveys to check the conservation state of the objects, belonging to the collection, and to the wooden ceilings at the second floor. The wooden ceilings, indeed, were restored in 2012, since evident degradation phenomena were visible in terms of painted-layer detachments, panels' deformations and cracks along the tangential section of wood (Figure 5). After the restoration, no further damage was observed by the restorer.

Figure 4 Black drilled-metallic panels cover fan coil installed under a window shaded by wooden shutters and a black roller blind.

The museum was object of the research study - *"Preservation, conservation and valorisation of archaeological sites: the case of the ancient site of Privernum"* - funded by Sapienza Università di Roma in 2015 and coordinated by Prof Silvia Fedeli (Department of Economics and Law, Sapienza Università di Roma). The microclimate monitoring campaign, indeed, was inserted within this framework.

Figure 5 Details of the wooden ceilings decorated with oil paintings by Pietro Campeggi at the second floor. Cracks are visible along the tangential sections of wood.

The general workflow

The workflow methodology of the research is schematised in Figure 6. The four issues reported as specific questions in Chapter 1 are shown as background-coloured boxes in the figure. Each issue is separately described in the following subsections and has been distinctly analysed using different case studies, whose preliminary outcomes are reported as ancillary support at the end of this dissertation. Besides, Figure 6 identifies the main three subsections of the workflow as dashed boxes.

The first step of the methodology consists in collecting experimental data of the main indoor climate parameters, i.e. temperature (T) and relative humidity (RH) in the room, the surface temperature (T_s) and the crack-width (C) close to objects, if needed. The latter parameter, indeed, is used as a damage marker for the mechanical degradation of hygroscopic materials. The monitoring should last one year, at least, in order to significantly record short- and long-term variability of indoor climate over seasons.
Then, the quality and representativeness of collected data are evaluated before conducting any further investigation on the indoor climate and on the degradation risk assessment. Thereafter, climate and damage-marker data are investigated to find whether a strong relation exists between them. In such a case, a dose-response function of the damage-marker can be derived and calibrated with the measurements. It is

specific for the observed degradation, since it depends on the environmental conditions at which object has been kept, at least, over a whole year.

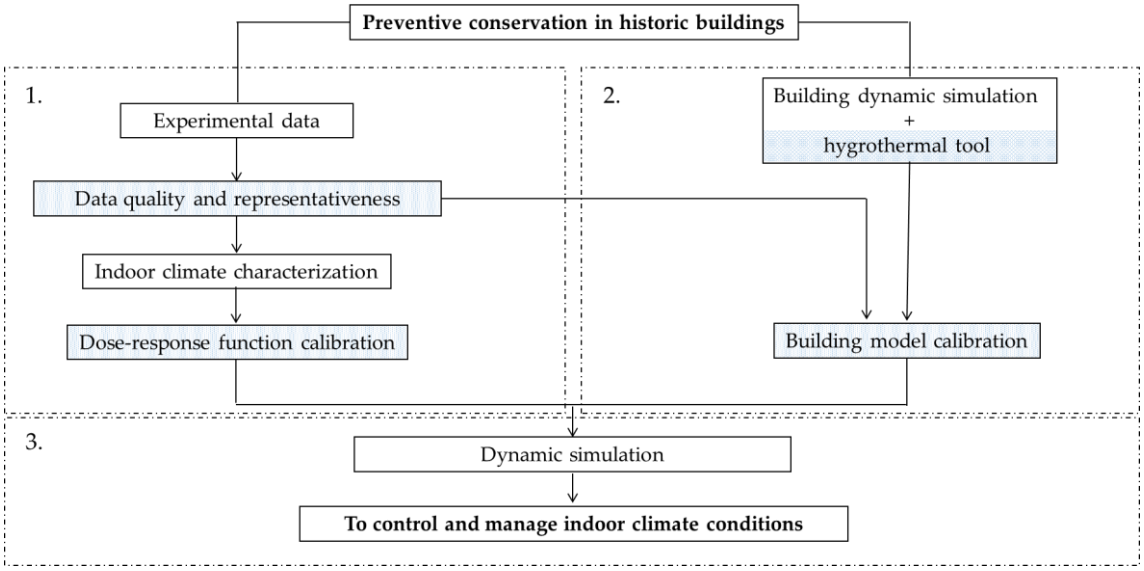

Figure 6 Schematic workflow methodology. Background-coloured boxes are the specific purposes of the dissertation. Dashed boxes correspond to the three subsections: 1. The microclimate analysis; 2. The simulation environment; 3. The control climate strategy.

In parallel, a building model is created based on geometric and stratigraphy features of the building envelope. In this research, the whole-building dynamic simulation is performed with IDA Indoor Climate and Energy (IDA ICE) software integrated with a one-dimensional heat and moisture transfer model, i.e. the HMWall model, with the aim to include the sorption effect of hygroscopic and porous materials. The last modelling is of crucial importance to accurately and thoroughly model the indoor moisture dynamic and behaviour. This aspect becomes decisive in the case of historic building, since old masonries might experience uncontrolled condensation phenomena that can negatively affect the duration of the building and the preservation of hygroscopic movable and immovable artworks.

Then, the building model calibration is carried out. In this project, a calibration procedure is developed using hourly indoor climate parameters, i.e. T and RH. This is a further reason to trigger the assessment of high-quality T-RH data. The calibration concerns those periods in which the indoor climate is exclusively affected by outdoor climate in order to skip the setting of HVAC system, if any, whose feature rarely are available in historic buildings.

After the calibration of the dose-response function and of the building model simulation, climate control strategies and/or retrofitting interventions can be modelled in the simulation environment and assessed with respect to the current conservation state of the object.

It is worth to notice that this general workflow has been tested for studying the mechanical degradation of restrained hygroscopic materials, i.e. the wooden ceiling at the second floor of the Archaeological Museum of Priverno. However, it can be extended and applied to other specific degradation phenomena. This implies the rearrangement

of the monitoring system, if needed, and the identification of another dose-response function specific to the damage.

The following three subsections describe in detail the strategy. The first section concerns the microclimate analysis and includes the description of the monitoring system, the microclimate assessment and the derivation of the dose-response function. The second section describes the setting of the building model within the dynamic simulation environment and is supported by the description of the HMWall model and the calibration procedure developed within this research. Finally, the third section provides a description of a climate control strategy defined to reduce stress-and-strain cycle in material also guaranteeing pleasant temperature for visitors

The microclimate analysis

This section describes in detail the on-site monitoring system, the analysis of microclimate data and the derivation of the dose-response function specific of the mechanical degradation in restrained wooden structures.

On-site monitoring system

The monitoring campaign lasted from August 2016 till November 2017.
Four indoor temperature (T) and relative humidity (RH) sensors were installed in three of the most representative rooms of the museum, coded as *4*, *9* and *10* and indicated by colours in Figure 7. Each location allowed characterizing a different partition typology of the building. All probes were supported by black stands in order to fit with the interior design and were protected with a polycarbonate plastic cage and a polyethylene dust filter. In room 9, indicated as yellow room in Figure 7, the two T-RH probes were positioned at 1 m and 2m, coded as 9d and 9u respectively, in order to individuate any vertical gradient responsible for unstable hygrothermal conditions. In the same room, a surface temperature sensor (T_s) and a crack-width meter (C) were installed on a crack of a wooden panel ceiling, as shown in Figure 7. The aim was to detect the evolution of the crack width related to the environmental conditions at the interface between air and surface layer. The T_s sensor was fixed on the wood via paraloid and lied on the crack-width meter support. The support, i.e. a parallelepiped of 15-by-15-by-10 mm, had a "L" clamp (size 15-by-15 mm) and was fixed on the wood with an epoxy on a substrate of gauze and paraloid.
A probe with T-RH sensor, coded as *out*, was also installed at the terrace to record the outdoor hygrothermal conditions (blue circle in Figure 7). The external probe was shaded from radiation and protected from ventilation.
The list of sensors and their technical features are reported in Table 4. The metrological features of T and RH sensors are in accordance with the highest accuracies suggested by the current European standards EN 15758:2010 and EN 16242:2012, respectively.
All the sensors were connected to four dataloggers "Grillo Bee", each corresponding to the three rooms and the outdoor spot, developed and distributed by Tecno.El S.r.l. (Italy), with a remote data transmission by GSM/GPRS technology (Global System for Mobile Communications/General Packet Radio System). Data were transmitted to the

server allowing their visualization and download via the web application "OLINDA". The acquisition time was set to 5 minutes and the processing time was set to 30 minutes, providing the average, minimum and maximum of the recorded parameters.

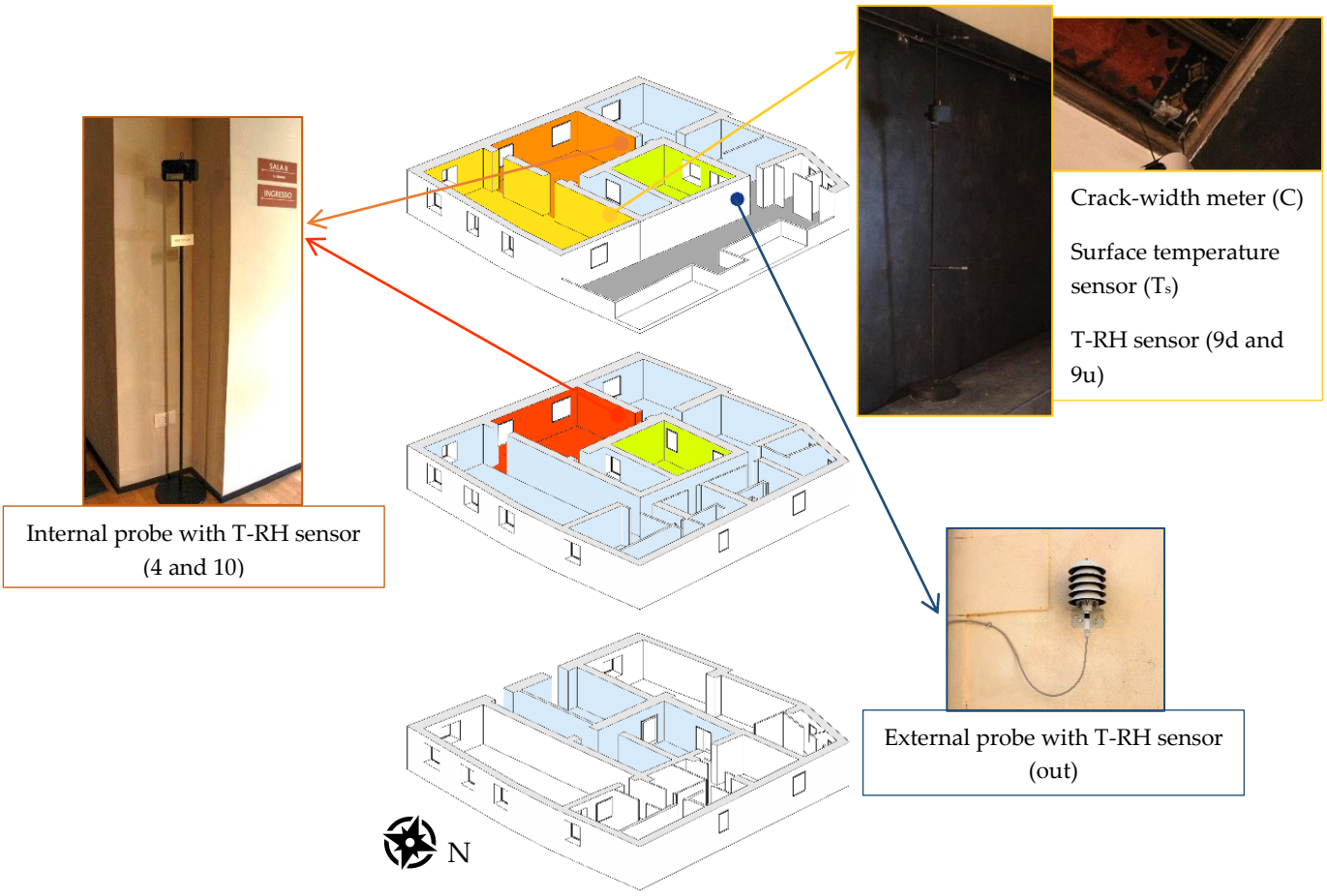

Figure 7 Exploded view of the "Valeriani-Guarini-Antonelli Palace". All coloured rooms belong to the Archaeological Museum of Priverno. The green area indicates the internal courtyard. Probes were installed in room *4* (red), *9* (yellow) and *10* (orange). Blue circle indicated the external probe.

Table 4 The technical features of sensors used within the monitoring campaign.

	T	**RH**	**T_s**	**C**
sensor	Pt100 1/3 DIN	film capacitor "Rotronic" C94	thermistor NTC	potentiometer in conductive plastic
operating range	-40°C to +60°C	0 – 100%	-30°C to +150°C	10 mm
accuracy	±0.3°C	+1.5%	±0.1°C	+0.025 mm

The mixing ratio of moist air (MR) and the dew point (DP), both indoors and outdoors, was calculated from T and RH readings, using the equation reported in the European standard EN 16242:2012 and taking into account the standard value of the atmospheric pressure (p = 1013 hPa).

$$MR = 38.015 \times \frac{10^{\frac{(7.65\times T)}{(243.12+T)}} \times RH}{p + \left(0.06112 \times 10^{\frac{(7.65\times T)}{(243.12+T)}} \times RH \right)} \quad (1)$$

$$DP = \frac{243.12 \times \ln\left(10^{\frac{7.65\times T}{243.12+T}} \times \frac{RH}{100} \right)}{17.62 - \ln\left(10^{\frac{7.65\times T}{243.12+T}} \times \frac{RH}{100} \right)} \quad (2)$$

For both derived variables, the maximum propagation of uncertainty was calculated. The uncertainty related to MR and DP was 0.3 g/kg and 0.6°C, respectively.

Analysis of microclimatic data series

The first step of the microclimate analysis was a synthetic visualization of the hygrothermal behaviour by means of box-and-whisker plots (McGill et al. 1978). The line inside the box is the median value; the top and bottom of each box are the 25th and 75th percentiles of the samples, respectively. The whiskers are lines extending above and below each box. Here, they were set as 1.7 times the interquartile range (IQR) away from the 75th and 25th percentiles, respectively, instead of the common value of 1.5×IQR. In this way, a 99.9% data coverage is considered. Data outside this range are defined outliers or suspected outliers and indicated as black circles in figures. Outliers can be rejected whether they are not within the sensor's operating range or are not physically consistent (data cleaning). As support of this analysis, the Wilcoxon test with a significance level of α=0.05 was performed to identify any significant difference on the basis of median among variables recorded in the same room (Gibbons and Chakraborti 2011).
Since data mining of data collections with several missing values might be little reliable, an objective quality assessment of time series plays a key role in providing a realistic data interpretation and, hence, a significant damage risk analysis. Three indexes were used before performing data mining and determining the historic climate: the Completeness Index (CoI); the Continuity Index (CI) and the Microclimatic Quality Index (MQI). The indexes range between zero and unity. The CoI and the CI should be used in complementary way. For values higher than 0.6, reliable and robust results can be provided by data mining. The MQI is specifically developed for the investigation on historic climate according to the EN 15757:2010, but it can be also extended for the application of the American guideline ASHRAE 2011. The MQI synthetises the information about the length of the time series, as required by climate documentations (at least 12 months), and the sensors' accuracy, as suggested by the current European standards, i.e. EN 15758:2010 for temperature sensors and EN 16242:2012 for relative humidity sensors. For the same length, the MQI is 0.7 or 1 if the sensor's accuracy is low or high, respectively. The indexes were tested for the first time with hygrothermal data collected for 24 months within the Mogiła Abbey, located in Krakow – Poland. The Appendix A provides a detail description of the indexes and their interpretation. The

indexes were also successfully used to identify the most proper period within a longer data collection (seven years), which had several missing intervals of values due to the malfunction of sensors over years (Appendix B).
The Spearman's rank correlation coefficient (r_s) with a significance level of α=0.05 was calculated by pairing T-RH variables in order to assess the relationship between two variables using a monotonic function, i.e. without any assumption on data distribution.
Thereafter, short-term variability of the indoor climate was investigated as daily span, i.e. the difference between the maximum and minimum value observed during each day. The analysis allowed to study both the variability of the hygrothermal parameters finding possible disturbing internal factors and the short-term stresses of environmental conditions experienced by the material.
Besides, to understand how the indoor climate is affected by external conditions both in terms of heat and vapor exchanges, the scatter plots of the indoor T and MR monthly means *vs* the corresponding outdoor monthly means were provided.
As the restorer claimed that no further damage was observed after the restoration, the historical climate was defined according to the EN 15757:2010. The procedure is based on the calculation of (1) the 30-day central moving average (MA) to define the seasonal cycle; (2) the deviation of raw data from MA to extract the short-term fluctuations; (3) the safe band of RH defined as the 7th and the 93rd percentiles of the short-term fluctuations.
Moreover, the ASHRAE 2011 was applied in order to couple a climate type, defined as Class of Climate Control, to the risks and benefits that this climate poses to mixed collections (Martens 2012), as reported in Table 5. The six classes, from AA (associated with no risk to most objects) to D (protection only from dampness), help to fit a proper climate into a building, that is classified according to a combination between various types of the building envelope and the climate control. The former considers the building construction, the type of building and the building use. The latter concerns the climate system in use and the limit of the practical limit of climate control according to the building type and the outdoor climate. In such a way, six building classes are identified and grouped in three categories of the climate control: uncontrolled, partial control, and climate controlled, as reported in Table 6. The Archaeological Museum of Priverno would belong to the class V within the controlled climate. It means that the climate classes of control AA, A, As and B would be sustainable in relation to the energy usage. Since no degradation phenomena of artworks occurred over the last years as claimed by the restorer and the HVAC system does not allow the RH control, a higher class of control, such as AA and A, would mean an excessive energy cost for the museum. Thus, the classes of control As and B were chosen in accordance with the characteristic of:

- the building envelope: heavy masonries and double glazing;
- the typical building use: gift shop, walk-through visitors only and education groups;
- the HVAC system: simple fan coils for heating and cooling.

Finally, T-MR data were plotted into a psychrometric chart in order to provide a synthetic visualization of data with respect to the short-term fluctuations' limits as defined by the chosen classes of climate control (Martens 2012).

Table 5 Museum climate guidelines according to ASHRAE (2011).

		Maximum Fluctuations and Gradients in Controlled Spaces			Collection Risks and Benefits
Type	et Point or annual average	Class of Control	hort fluctuations plus space gradients	Seasonal Adjustments in System Set Point	
General Museums, Art Galleries, Libraries, and Archives	50% RH (or historic annual average for permanent collections) Temperature set between 15 and 25°C	AA	±5% RH, ±2 K	RH no change Up 5 K; down 5 K	No risk of mechanical damage to most artefacts and paintings. Some metals and minerals may degrade if 50% rh exceeds a critical relative humidity. Chemically unstable objects unusable within decades.
		A As	±5% RH, ±2 K	Up 10%, down 10% RH Up 5 K; down 10 K	Small risk of mechanical damage to high vulnerability artefacts; no mechanical risk to most artefacts, paintings, photographs, and books. Chemically unstable objects unusable within decades.
		A A	±10% RH, ±2 K	RH no change Up 5 K; down 10 K	
		B	±10% RH, ±5 K	Up 10%, down 10% RH Up 10 K, but not above 30°C, down as low as necessary to maintain RH control	Moderate risk of mechanical damage to high vulnerability artefacts; tiny risk to most paintings, most photographs, some artefacts, some books; no risk to many artefacts and most books. Chemically unstable objects unusable within decades, less if routinely at 30°C, but cold winter periods double life.
		C	Within 25 to 75% RH year-round T rarely over 30°C, usually below 25°C		High risk of mechanical damage to high vulnerability artefacts; moderate risk to most paintings, most photographs, some artefacts, some books; tiny risk to many artefacts and most books. Chemically unstable objects unusable within decades, less if routinely at 30°C, but cold winter periods double life.
		D	Reliably below 75% RH		High risk of sudden or cumulative mechanical damage to most artefacts and paintings because of low-humidity fracture; but avoids high-humidity delamination and deformations, especially in veneers, paintings, paper, and photographs. Mould growth and rapid corrosion avoided. Chemically unstable objects unusable within decades, less if routinely at 30°C, but cold winter periods double life.

Table 6 Classification of Climate Control potential in buildings to ASHRAE (2011).

Category of control	Building class	Typical building construction	Typical type of building	Typical building use	System used	Practical Limit of Climate Control	Class of Control Possible
Uncontrolled	I	Open structure	Privy, stocks, bridge, sawmill, well	No occupancy, open to viewers	No system.	None	D (if benign climate)
	II	Sheathed post and beam	Cabins, barns, sheds, silos, icehouse	No occupancy. Special event access.	Exhaust fans, open windows, supply fans, attic venting. No heat.	Ventilation	C (if benign climate) D (unless damp climate)
Partial control	III	Uninsulated masonry, framed and sided walls, single-glazed windows	Boat, train, lighthouse, rough frame house, forge	Summer tour use. Closed to public in winter. No occupancy.	Low-level heat, summer exhaust ventilation, humid-static heating for winter control.	Heating, ventilating	C (if benign climate) D (unless hot, damp climate)
	IV	Heavy masonry or composite walls with plaster. Tight construction; storm windows	Finished house, church, meeting house, store, inn, some office buildings	Staff in isolated rooms, gift shop. Walk-through visitors only. Limited occupancy. No	Ducted low-level heat. Summer cooling, on/off control, DX cooling, some humidification. Reheat capability.	Basic HVAC	B (if benign climate) C (if mild winter) D
Climate controlled	V	Insulated structures, double glazing, vapor retardant, double doors	Purpose-built museums, research libraries, galleries, exhibits, storage rooms	Education groups. Good open public facility. Unlimited	Ducted heat, cooling, reheat, and humidification with control dead band.	Climate control, often with seasonal drift	AA (if mild winters) A B
	VI	Metal wall construction, interior rooms with sealed walls and controlled occupancy	Vaults, storage rooms, cases	No occupancy. Access by appointment.	Special heating, cooling, and humidity control with precision constant stability control.	Special constant environments	AA A Cool Cold Dry

The dose-response function

The wood, as a hygroscopic material, responds to variations in relative humidity (RH) by absorbing and desorbing moisture. This in turn results in dimensional changes, i.e. swelling and shrinkage of wooden fibres. Generally, the movement of wood is not the source of its damage when the element can move freely without any kind of restraint. On the contrary, restraint of movement, resulting from a rigid construction, can have damaging effect on objects such as components of furniture-doors, sides of cabinets and table tops, frames, or other types of wooden structures. Wooden materials can also experience internal restraint, as the moisture diffusion is not instantaneous and uneven moisture change induces uneven dimensional response. This occurs when a quick response to variations in ambient RH is experienced by the outer parts of wooden elements that are restrained by the core beneath. This is typical of bulky and massive objects, like sculptures. In this context, the monitoring of the crack width can be reasonably conceived as a marker-tracking of microdamage of wood structure at the crack tip due to stress concentration through the mechanism related to the fatigue process. Since the interaction between climate and object is dynamic and cumulative, the highest risk for the conservation of organic and hygroscopic material strongly depends on the extent and rapidity at which environmental conditions change. For this reason, the RH propagation within the material was investigated, starting from the estimation of hygrometric conditions (RH_s) at the surface-air layer (eq. 3) and supposing that the water vapour gradient (ΔMR) was constant from air ambient to the interface between air and wooden surface.

$$RH_s = \frac{MR \times p}{38.015 \times 10^{\frac{(7.65 \times T)}{(243.12+T)}} + 0.06112 \times 10^{\frac{(7.65 \times T)}{(243.12+T)}} \times MR} \qquad (3)$$

The central moving average (smoothed-RH_s) at 3h, 24h, 48h and 1 week were calculated from RH_s values with the aim to approximate the hygrometric gradient from superficial layer to the inner layers of panel. Then, the deviation of RH_s from smoothed-RH_s values was computed to extract the short-term fluctuations. The safe band variability was defined as the third step of the procedure suggested by the EN 15757:2010, i.e. the 7th and the 93rd percentiles of the short-term fluctuations. Finally, the hygrometric gradient was compared with the crack width evolution in order to pinpoint any physical relation between RH_s and C.

After that, a procedure was developed to define a dose-response function which related the strain of hygroscopic objects with the hygrothermal variables. It is schematised in Figure 8 and can be summarised in the following steps:

1. computation of air mixing ratio (MR) or dew point (DP) from indoor air temperature (T) and relative humidity (RH) according to the equation provided by the EN 16242:2012;
2. computation of the relative humidity at the interface between the surface and the air layer (RH_s) from MR or DP and the surface temperature (T_s) with the inverse formula;

3. investigation on the monotonic correlation of the measured crack width (C) with T_s and RH_s, using the Spearman's rank correlation coefficient (r_s) and assuming any distribution of data. The procedure continues, if the modulus of r_s is higher than 0.6, i.e. the paired variables are highly correlated.
4. calculation of the crack width (C_m) from T_s and RH_s using the non-linear multiple regression reported in eq. 4:

$$C_m = a \times RH_s^{\ b} \times T_s^{\ c} \qquad (4)$$

where a, b and c are coefficients;

5. comparison between C and C_m using the root-mean-square-error (RMSE) as target function. If RMSE is close to the accuracy of the crack-width meter, the empirical model can be successful exploited.

The empirical model was applied for the first time to the soil which supports faunal fossils in the palaeontological excavation of La Polledrara di Cecanibbio (Appendix C).

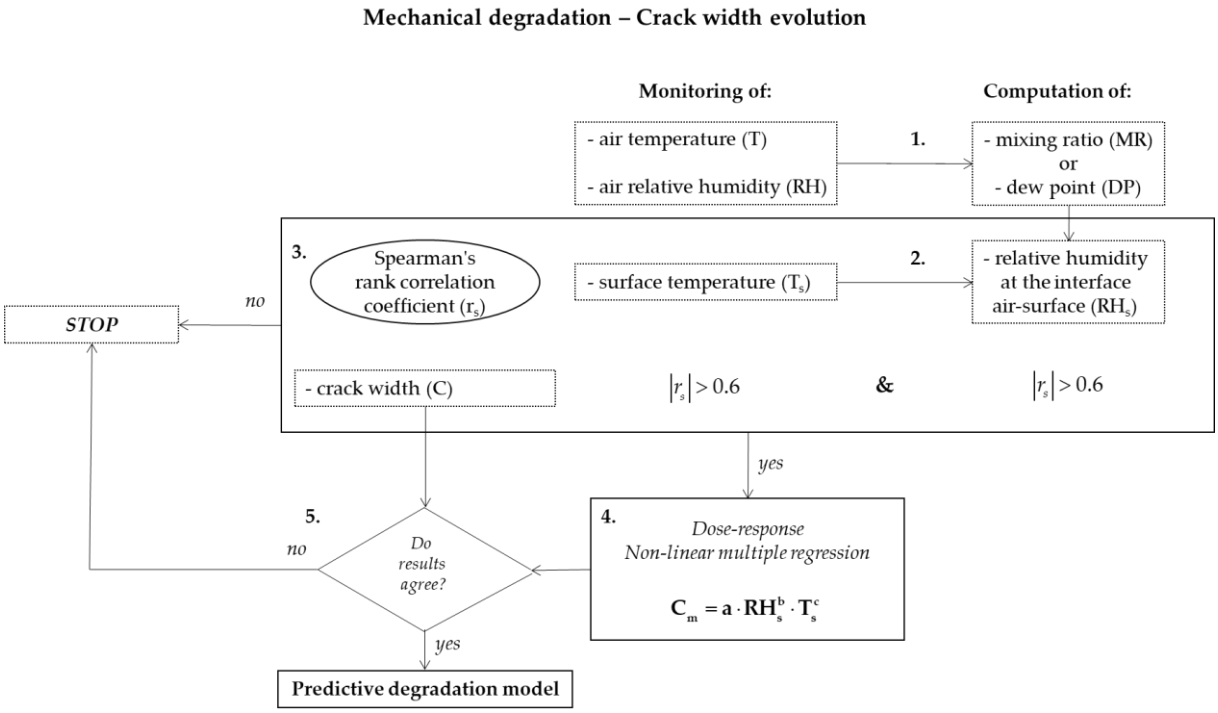

Figure 8 The workflow for the identification of a dose-response function of cracks in restrained wooden material. Formulas for the computation of missing ratio (MR), dew point (DP) and relative humidity at the interface air-surface (RHs) are reported in equations (1), (2) and (3), respectively.

The simulation environment

Dynamic building simulation for indoor climate analysis was performed using the IDA Indoor Climate and Energy (IDA ICE) 4.8 developed and distributed by EQUA simulation AB. The IDA ICE software was chosen in this research as it has a modular architecture, that allows extending his features at advanced level with an object that implements a one-dimensional heat and moisture transfer model, i.e. the HMWall model. The extension with the HMWall model allows including the vapour sorption effect of opaque components, made of porous and hygroscopic materials, in the relative humidity modelling. In this dissertation, IDA ICE was extended with the HMWall model

only for the modelling of monitored rooms (4, 9 and 10). The performance assessment and the validation of the HMWall model is described in (Appendix E). Four exercises at increasing complexity were used in order to fulfil the three requirements suggested by Judkoff and Neymark (1995) for validation procedure: analytical verification, empirical validation and comparative test.

The following subsections are focused on the descriptions of *The hygrothermal model* and *The building model calibration*. The reader, if wish, can directly skip to *The museum model construction and calibration*, in which the modelling of the museum is provided.

The hygrothermal model

The hygrothermal assessment concerns the analysis of temperature (T or ϑ), relative humidity (RH or φ) and moisture content (w) within buildings. This assessment is of crucial importance, because an accumulation of indoor RH due to uncontrolled condensation in the wall can strongly affect the human comfort and the energy savings as well as the durability of materials sensitive to moisture-induced damage. To cite as a few, the moisture in building elements, such as solid walls, strongly affects the heat transfer of the building envelope (Barclay et al. 2014). For this reason, at the end of fifties, the research was focused on the simulation of the heat, air and moisture transport through the opaque components.

Since the heat and moisture flows are transient, sophisticated one- and two-dimensional dynamic models were implemented with the aim to give more detailed and accurate information than the *Glaser method*[8] (Glaser 1958). The one- or two-dimensional dynamic modelling is generally performed with the so-called HAM model, i.e. Heat Air and Moisture model, that combines the equations of heat and moisture flows with the energy and mass balances.

In this context, the whole moisture exchange in a building can be mainly modelled using the co-simulation or extending the dynamic building simulation (DBS) software architecture. The co-simulation is one of the most advanced and versatile method (Nicolai et al. 2007; Steeman et al. 2010; Tariku et al. 2010; Djedjig et al. 2012; Spitz et al. 2013; Ferroukhi et al. 2016), since it consists in combining two existing software (Gomes et al. 2018), one for whole building dynamic simulation and the other one for the

[8] The most common method used in the hygrothermal assessment was, for long time, the *Glaser method*, which provides an assessment of critical interstitial condensation and considers only steady-state conditions of heat and vapour diffusion in light-weight buildings. The method, standardized in the EN ISO 13788:2002, consists in a simplified calculation procedure based on monthly average of temperature and vapour pressure and steady-state conduction of heat. The moisture transfer is calculated as pure water vapour diffusion. The method assumes that the built-in water has dried out and no effect of moisture content on material intrinsic properties. This means that it can be applied only in those cases where these effects are negligible (Hagentoft et al. 2004). The Glaser method is mainly used when an approximation of reality is enough for understanding the building issues, as demonstrated in Ramos et al. (2009) and Magrini et al. (2017).

hygrothermal transfer modelling (Ferroukhi et al. 2015). On the contrary, the DBS extension has the main advantage to use a single simulation tool. As far as reported by Delgado et al. (2012), nine software are available as commercial programs (1D-HAM, BSim2000, Delphin, GLASTA, hygIRC-1D, IDA-ICE extended with HMWall, MATCH, MOISTURE-EXPERT and WUFI); whereas five are available as freeware software (EMPITIED, HAMLab, HAM-Tools, MOIST and HUMIDUS).

The HMWall model

The HMWall model belongs to the family of HAM tools (heat air and moisture model). In IDA ICE, it can be used either as a single independent wall-object or as a component of a larger system, by simply replacing the default thermal wall selected by the program. It is not available in the release of IDA ICE, but it can be integrated on request.
The first version of the HMWall model, the so-called HAMWall model, was developed in 1999 by Kurnistki and Voulle (2000). The moisture transfer was modelled by one moisture-transfer potential, i.e. the humidity by volume (ν), neglecting the temperature dependence; whereas the liquid water transport and the hysteresis of moisture transport were not considered. This version, coupled with IDA ICE 3.0, was used within the IEA Annex 41 (Kalamees, report meeting) and reported in the review of the whole building dynamic simulation software given by Woloszyn and Rode (2008). It was also used to model the hygrothermal behaviour inside three historical buildings located in Estonia after the refurbishment of the HVAC system (Napp et al. 2015; Napp et al. 2016a; Napp et al. 2016b). In 2011, the HMWall code was edited according to the balance heat and moisture equations and the driving potentials given by Hartwing Künzel and used in WUFI family tools (Künzel 1995). The previous code, indeed, could be run only with hygrometric properties of materials that were mostly unknown in literature. WUFI was chosen because it was validated by means of comparative test and analytical verification more than other hygrothermal simulation tools demonstrating its high quality and robustness (Holm 2003; Karagiozis 2010). The main differences between the IDA ICE extended with the HMWall object and WUFI as well as the basic governing equations are reported in Appendix D. Currently, a correct implementation of wind driven rain and its impact on the building envelope remains a weakness as well as any liquid moisture source within the wall layer.

The basic governing equations

The HMWall model used in this research was updated according to the results reported in Appendix E.
The total enthalpy ($\partial H/\partial t$) through the building component consists of the enthalpy of the dry building material, i.e. the Fourier's law, and the latent heat related to the phase transition of moisture as water vapour diffusion.

$$\frac{\partial H}{\partial t} = -\left(\nabla\left(\lambda \times \nabla\vartheta\right) + h_v \times \nabla g_v\right) \qquad (5)$$

where λ is the thermal conductivity, h_v is the evaporation enthalpy of water and g_v is the vapour diffusion flux.

Figure 9 shows the difference in λ when w is modelled through the wall (dashed line) and when not (solid line). Indeed, there is a relation between λ and w, that can be calculated as follows:

$$\lambda(w) = \lambda_0 + \left(1 + b \times \frac{w}{\rho_s}\right) \qquad (6)$$

where λ_0 is the thermal conductivity of material in dry condition, b is the thermal conductivity supplement and ρ_s is the bulk density of material in dry condition. This means that λ in (5) should be replaced λ calculated in (6).

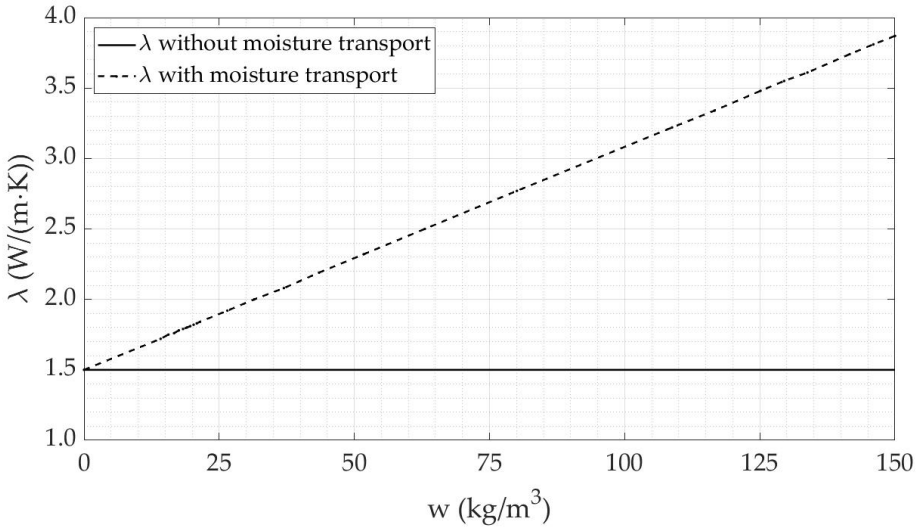

Figure 9 Thermal conductivity (λ) *vs* water content (w), when w is modelled through the wall (dashed line) and when not, i.e. the λ of material in dry condition (solid line).

The moisture transfer ($\partial w/\partial t$), instead, includes the vapour diffusion flux density (g_v) and the liquid transport flux density (g_w) and is calculated as follows:

$$\frac{\partial w}{\partial t} = -\nabla\left(g_w + g_v\right) \qquad (7)$$

The driving potentials for vapour and liquid flux density are the vapour partial pressure (p_v) and the relative humidity (φ)[9], respectively.

[9] Based on the Darcy formula (Janssen 2014), the liquid flux density is driven by the capillary suction pressure (p_k), that strongly depends on the water content (w) within the material. Substituting p_k with the Kelvin's equation (Skinner and Sambles 1972) and considering negligible the temperature gradient, the relative humidity (φ) can be used as driving potential in liquid flux density. This variable is preferred, because it is a material-independent moisture transport potential that is continuous also at the boundary layers.

$$g_v = -\left(\delta_p \times \nabla p_v\right) = -\left(\delta_p \times \nabla\left(\varphi \times p_{sat}\right)\right) \qquad (8)$$

where δ_p is the water vapour permeability of the material calculated as the ratio between the water vapour permeability of air (δ_0), derived from the Schmirer's equation (Slanina and Šilarová 2009), and the water vapour diffusion resistance factor (μ). p_{sat} is the saturated vapour pressure of water.

$$g_w = -\left(D_\varphi \times \nabla\varphi\right) \qquad (9)$$

where D_φ is the liquid conduction coefficient. The calculation of D_φ is executed starting from the liquid transport coefficient for suction (D_{ws}) and assuming no difference between suction and redistribution processes, i.e. no difference between absorption and desorption as below explained.

$$D_{ws}\left(w\right) = 3.8 \cdot \left(\frac{A_w}{w_f}\right)^2 \cdot 1000^{\frac{w}{w_f}-1} \qquad (10)$$

where A_w is the water penetration coefficient. D_φ and D_{ws} are related each other as reported in Künzel (1995):

$$D_\varphi = D_{ws} \cdot \frac{dw}{d\varphi} \qquad (11)$$

where $dw/d\varphi$ is the derivative of moisture storage curve. The moisture storage curve, i.e. the dependence between moisture in material and environmental conditions (Künzel 1995), is calculated as a function of φ:

$$w\left(\varphi\right) = w_f \cdot \frac{\left(b-1\right)\cdot\varphi}{b-\varphi} \qquad (12)$$

where w_f is the free water saturation, φ is the relative humidity and b is the approximation factor (Torres and de Freitas 2003). b must always be greater than one and it is calculated from the equilibrium water content at 80% of relative humidity (w_{80}) (Künzel 1995).

In this context, the effect of the temperature can be disregarded, so the moisture storage curve can be described as sorption isotherms. Besides, the hysteresis between absorption and desorption isotherms is not very distinct in most building material, therefore the absorption isotherm is enough to characterise the moisture storage of a building material.

The equations for the heat balance (5) and the moisture balance (7) are closely coupled and can be solved when the number of variables is limited to two: temperature (ϑ) and relative humidity (φ).

$$\frac{dH}{d\vartheta}\times\frac{\partial\vartheta}{\partial t}=\nabla\left(\lambda\times\nabla\vartheta\right)-h_v\times\nabla\left(\delta_v\times\nabla\left(\varphi\times p_{sat}\right)\right) \quad (13)$$

$$\frac{dw}{d\varphi}\times\frac{\partial\varphi}{\partial t}=\nabla\left(D_\varphi\times\nabla\varphi+\delta_v\times\nabla\left(\varphi\times p_{sat}\right)\right) \quad (14)$$

Indeed, the heat balance closely depends on the water content (w) at the first term and on the vapour diffusion flux (g_v) at the second term of the equation. Moreover, the saturated vapour pressure of water (p_{sat}) in the moisture balance equation exponentially depends on the temperature.
The effect of the heat transfer on the water vapour transfer (g_v) between the wall surface and the boundary air layer close to it is not considered, since its contribution is negligible as demonstrated in Appendix D.
To be run, the HMWall model needs for the hygrothermal properties listed below:

- thermal conductivity (λ)
- density (ρ)
- specific heat (c_P)
- free water saturation (w_f)
- equilibrium water content at 80% of relative humidity (w_{80})
- thermal conductivity supplement (b)
- vapour diffusion resistance factor (μ)
- water absorption coefficient (A_w)

All these properties, collected by seven research institutes, are available in the *MASEA geprüfte DatenBank* web site for most of building materials (https://www.masea-ensan.de/). The web site is written in German.

The building model calibration

For historic buildings, the manual calibration can be time consuming especially when building materials are not precisely known and structures of different ages are superimposed. As opposed to manual calibration, the semi-automatic calibration (SAC) might widely boost this phase in the building modelling. Figure 10 shows the workflow proposed for the SAC of historic building model by using hourly temperature (T) and relative humidity (RH) data. The SAC has the main advantage to control step-by-step if input parameters are consistent with the real conditions. The procedure can be summarised in five steps:

1. architectural surveys and microclimate analysis for identifying the potential input parameters that should be adjusted and the period of calibration;
2. creation of a building model, the so-called *first guess model*, using as input parameters the data provided by standards or database;
3. selection of the most influencing input parameters along with uncertainty ranges through the Sensitivity Analysis (SA). The SA is based on the Elementary Effects method (EEs). Here, IDA ICE is communicated with the MATLAB environment, that iteratively run the building model after elaborating the setting of the input parameters using the Morris sampling matrix (Morris 1991). The experimental plan

is built considering the number of EEs (r) for each parameter and the number of levels (p) in which parameters range. The total number of simulations (N) is calculated as follows:

$$N = k \times (r + 1) \qquad (15)$$

Thus, the input set parameter matrix given by Morris sampling is N-by-k. The mean absolute error (MAE) is used as target function for the calculation of the EEs from T and RH data. The EEs ascribed to each parameter are defined as the difference in the output between two following simulations divided by the variation of the input parameter (Saltelli et al. 2004). The EEs are computed as follows:

$$EEs(x) = \frac{y(x_1, x_2, ..., x_i + \Delta x_1, ..., x_k) - y(x)}{\Delta x} \qquad (16)$$

where x is the set of parameters, $y(x_i)$ is the target function for the n-model, y(x) is the target function for the first guest model and Δx is the variation of the input parameter. Finally, the absolute values (μ^*) of the mean of the EEs (μ) associated with each parameter, the standard deviation (σ) and the ratio σ/μ^* are calculated. μ^* provides a measure of the parameter relevance and the effect on the response y (Campolongo et al. 2011): higher μ^*, more relevant is the input parameter and monotonic is its effect. σ estimates the dependence on the effect of x_k of the values taken by the other factors (Saltelli et al. 2004). The ratio σ/μ^* is an indicator of the linearity of each parameter effect with respect to other parameters and to whole modelled building. It assumes that the EEs are normally distributed and, hence, 95% of EEs are within $\mu^* \pm 1.96\,\sigma$ for $\mu^* \approx \mu$. As a consequence, if $\sigma/\mu^* < 0.1$, 95% of EEs is in a range of ± 20% around μ^* (Sanchez et al. 2014). In the EEs scatter plot (σ *vs* μ^*), four areas delimited by $\sigma/\mu^* < 0.1$ (linear), $0.1 \leq \sigma/\mu^* < 0.5$ (monotonic), $0.5 \leq \sigma/\mu^* < 1$ (almost monotonic) and $\sigma/\mu^* \geq 1$ (non-monotonic) allows highlighting whether outcomes from SA are physically consistent.

4. model calibration:
   - manual calibration: the input parameter setting is defined by the user after each simulation run. The minimization of the discrepancy between measured and modelled data can be evaluated with the Taylor Diagram (Taylor 2001), as applied in Appendix F.
   - automatic calibration: IDA ICE is communicated with GenOpt® by means of a module called *Parametric Run*, which is already integrated in the simulation software. The calibration of the building model is performed with the Particle Swarm Optimization – General Pattern Search of Hooke-Jeeves (PSO-GPSHJ) genetic algorithm, which is a hybrid algorithm. The mean absolute error (MAE) and the root mean square error (RMSE) are used as objective targets. Finally, the coefficient of variation of RMSE (CV-RMSE) is calculated: the lower is the CV, the smaller is the residuals relative to the predicted value, i.e. a good model fit.
5. model validation comparing modelled and measured T-RH data in a period not included in the calibration. Target functions are calculated again.

The procedure succeeds if the target functions achieved in the calibration and the validation steps are comparable. Since threshold limits of statistical criteria for

calibration with hourly T and RH data are not available in the literature or standards, a general criterion can refer to the accuracy of hygrothermal sensors. More the targets are close to sensor accuracy, more the building model fits the actual building.

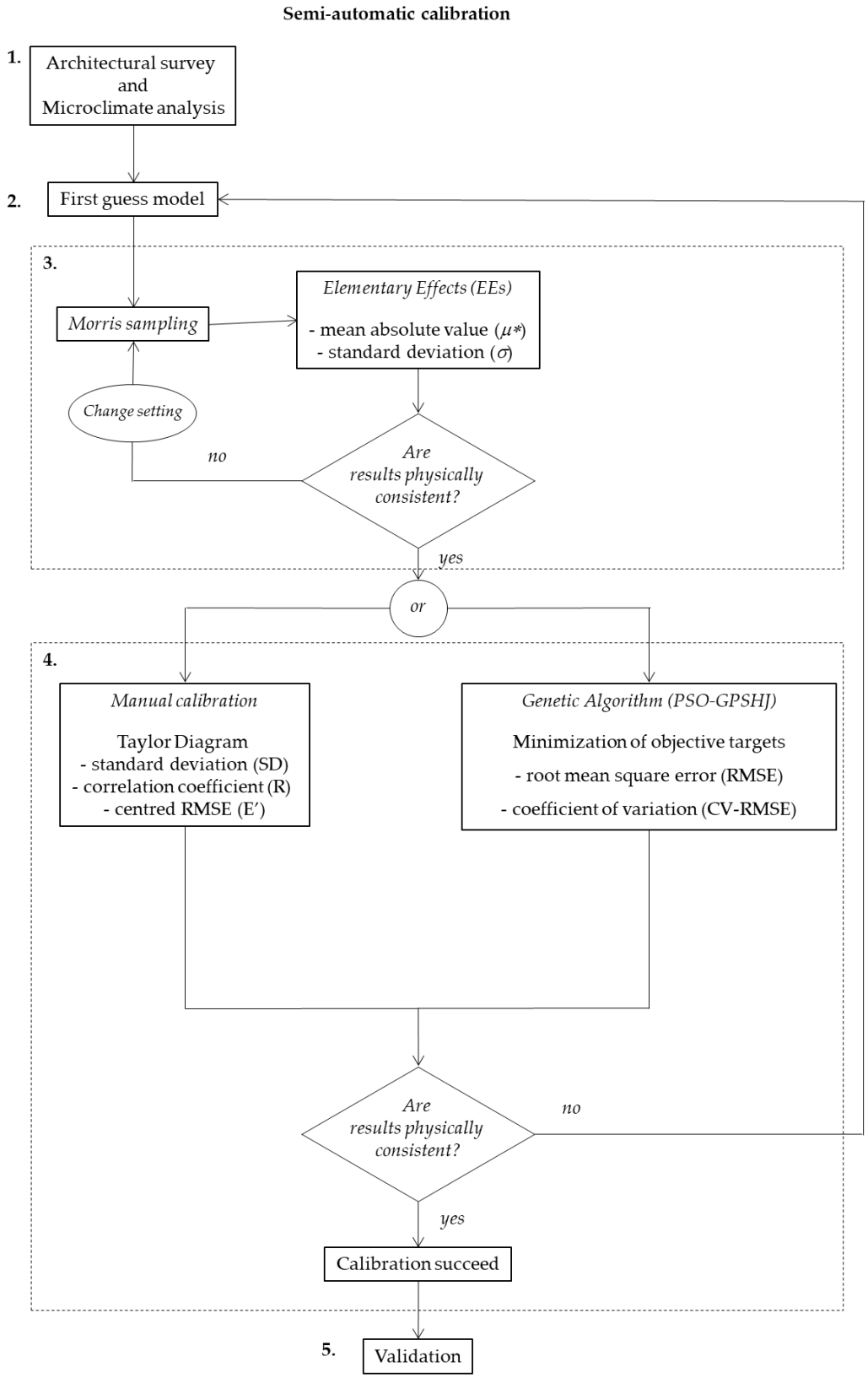

Figure 10 The workflow of the calibration procedure. The third point of the procedure was developed by communicating IDA ICE with the MatLab environment.

The equation of the statistical parameters mentioned in the procedure and used in this thesis are reported below:

$$MAE = \frac{\sum_{i=1}^{N} |y_i - x_i|}{N} \quad (17)$$

$$RMSE = \sqrt{\frac{\sum_{i=1}^{N} (y_i - x_i)^2}{N}} \quad (18)$$

$$CV - RMSE = \frac{RMSE}{\langle x \rangle} \quad (19)$$

where y_i is the i-th modelled data, x_i is the i-th measured data, N is the number of all the possible data pairs analysed and <x> is the average of measured data.

The museum model construction and calibration

The geometry of the building model was created starting from the architectural survey provided by Arch. Lucia Di Noto. The building model, sketched by the dynamic building simulation (DBS) tool and shown in Figure 11, consisted of sixteen zones included the stairwell, the crawl space under the roof and the spaces at the ground floor. It was oriented in the SW-NE direction with respect to the main entrance (indicated by a black arrow in figure). In Figure 11, rooms with measurements were shown by different colours: room 4 as red, room 10 as orange and room 9 as yellow.

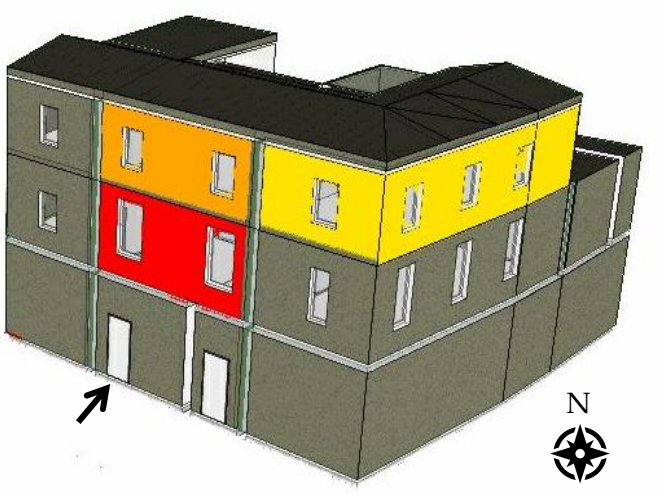

Figure 11 3D model of the museum obtained with the dynamic building simulation tool. Rooms 4, 9 and 10 are indicated with different colours, i.e. red, orange and yellow, respectively, according to Figure 7. The black arrow indicates the main entrance of the building

The default thermal model (BDFWall) used by the DBS tool for wall modelling was replaced by the HMWall model only in the case of room 9. This room was chosen as the pilot room, for testing the climate control strategy described in the following section.

The wall stratigraphy was retrieved from literature referred to construction techniques in lower Latium in the Middle Age and was assumed to be unchanged over time except for ceilings, which were rebuilt after the restoration in 1924-26. The hygrothermal properties of opaque components were gathered from the MASEA Datenbank and reported in Table 7. In Table 8, the stratigraphy of opaque components is discretised as in the HMWall model. These values were used in the initial model. It is worth to notice

that only the first three columns of Table 7 were needed for the default thermal wall modelling.

On the contrary, glazing system parameters were retrieved during the preliminary survey conducted to design the microclimate monitoring system. They consisted of wooden frames with low-emitted double pane glazing filled with air (6mm - 12mm - 6mm). The internal and external emissivity were 0.04 and 0.84, respectively. The glazing system parameters were set with a U-value of 1.59 W/m²·K and solar heat gain coefficient (SHGC) value of 0.38 for the glazing and U-value of 1.0 W/m²·K for the frame. All windows were shaded with black interior roller shades in PVC.

The infiltrations were set fixed at 0.09 ACH and the wind profile was defined as in the case of urban centre, due to the position of the building.

The ground floor properties were left by default according to the standard ISO 13370:2007, since they only affected the basement of the building.

Table 7 The hygrothermal properties of building materials for opaque components gathered from MASEA Datenbank both for the default thermal model (BDFWall) and for the HMWall model. For the BDFWall, only the first three columns were needed.

Material	Hygrothermal properties						
	ρ	c_p	λ	μ	w_{80}	w_f	A_w
	kg/m³	J/(kg·K)	W/(m·K)	-	kg/m³	kg/m³	kg/(m²·h$^{0.5}$)
brick	1900.0	1000.0	1.07	28.0	24.9	250.0	2.70
concrete	2104.0	776.0	1.94	76.1	101.0	144.0	0.75
lime plaster	1600.0	850.0	0.70	7.0	30.0	250.0	3.00
lime-cement render	1900.0	850.0	0.90	19.0	45.0	210.0	2.00
restoration plaster	590.0	1000.0	0.17	8.6	11.9	500.0	0.24
floor brick	1952.0	863.0	0.96	19.4	123.0	161.0	8.51
light mortar	830.0	1000.0	0.21	13.2	26.3	423.0	1.63
wood	740.0	1400.0	0.81	223.0	104.0	349.0	0.10

Table 8 Stratigraphy of opaque components used in the HMWall model. Cell numbers and thickness of each layer of the material (m) are summarised; the internal surface is at the left side (+ in, – out).

		external wall																		
Cell №	+	1	2	3	4	5	6	7	8	9	10	11	12	13	14	15	16	17	18	-
Thickness, m	+	0.01	0.01	0.01	0.03	0.03	0.04	0.05	0.05	0.06	0.07	0.05	0.05	0.04	0.03	0.03	0.01	0.01	0.02	-

		internal wall																		
Cell №	+	1	2	3	4	5	6	7	8	9	10	11	12	13	14	15	16	17	18	-
Thickness, m	+	0.015	0.01	0.01	0.03	0.03	0.04	0.05	0.05	0.06	0.07	0.05	0.05	0.04	0.03	0.03	0.01	0.01	0.015	-

		floor									
Cell №	+	1	2	3	4	5	6	7	8	9	-
Thickness, m	+	0.02	0.02	0.02	0.02	0.03	0.03	0.02	0.01	0.03	-

		wooden slab		
Cell №	+	1	2-9	-
Thickness, m	+	0.03	0.05	-

The weather file used to run the model was determined from T_{out} and RH_{out} measurements. Wind variables (direction and speed) and global horizontal solar irradiance, measured at Maenza station (Lat. 41.5° and Long. 13.2°) belonging to the ARSIAL (Agenzia Regionale per lo Sviluppo e l'Innovazione dell'Agricoltura del Lazio),

were also included in the weather file. The global horizontal solar irradiance (GHI) was split in the direct (dr) and diffuse (df) solar irradiance components. The former was derived with the Maxwell model (Ineichen et al. 1992); whereas the latter was derived as follows:

$$df = GHI - \left(dr \times \cos\left(ZA\right)\right) \qquad (20)$$

where ZA is the solar zenith angle.

The calibration was carried out using data collected from May 15th, 2017 till May 31st, 2017, with an initialization period from February 1st, 2017 till May 14th, 2017 due to the high inertia of historic buildings. In this period, it was sure that no internal gain was present. First, the model was calibrated referring to the T-RH measurements taken in all the three monitored rooms, according to the procedure described in The building model calibration. The error procedure was carried on finding the best hourly T and RH trends match, simultaneously for data gathered at the three measurement points. Thus, the Sensitivity Analysis (SA), based on the Elementary Effects method (EEs), was carried out for identifying the most effective input parameters of the building model, which were mostly unknown, such as thermal bridges and infiltrations. The EEs was applied using hourly indoor T and RH. The Morris matrix (N-by-k) was defined considering 18 input parameters (k), listed in Table 9. The experimental plan was built so that the number of EEs (r) was 10 for each parameter and the number of discretized levels (p) was 4. According to eq. (15), the resulting computational effort (N) was of 198 simulation runs.

Table 9 Parameters used for the initial model and parameter ranges used for the sensitivity analysis. Each parameter is identified by a code. Parameters' abbreviation: λ = thermal conductivity, s = thickness, TB = thermal bridge, EXT-WALL tot = external walls envelope, EXTWL-SLAB = external wall-slab, EXTW-INTW = external-internal wall, EXTW-CORN = external wall-inner corner, WIN = windows, ROOF = roof, INTW-ROOF = internal wall-roof, EXTW-INC = external slab and wall-inner corner, ROOF-INC = roof-inner corner, SLAB-INC = slab-inner corner, INFILT = infiltration.

cod.	Parameter	Unit	Initial model value	Range for SA
X1	λ brick	W/(m·K)	1.00	0.80 – 1.20
X2	λ concrete	W/(m·K)	1.94	1.55 – 2.33
X3	λ lime plaster	W/(m·K)	0.70	0.56 – 0.84
X4	λ lime plaster	W/(m·K)	0.17	0.14 – 0.20
X5	λ light concrete	W/(m·K)	0.21	0.17 – 0.25
X6	λ wood	W/(m·K)	0.81	0.65 – 0.97
X7	s wooden slab	m	0.20	0.16 – 0.24
X8	TB EXT-WALL tot	W/(m²·K)	0	0.00 – 0.90
X9	TB EXTW-SLAB	W/(m·K)	0	0.00 – 1.05
X10	TB EXTW-INTW	W/(m·K)	0	0.00 – 1.00
X11	TB EXTW-CORN	W/(m·K)	0	0.00 – 0.40
X12	TB WIN	W/(m·K)	0	0.00 – 1.00
X13	TB ROOF	W/(m·K)	0	0.00 – 0.85
X14	TB INTW-ROOF	W/(m·K)	0	0.00 – 0.40
X15	TB EXTW-INC	W/(m·K)	0	-0.21 – 0.00
X16	TB ROOF-INC	W/(m·K)	0	-0.10 – 0.00
X17	TB SLAB-INC	W/(m·K)	0	-0.18 – 0.00
X18	INFILT	ACH	0.09	0.01 – 0.20

Then, an automatic calibration was performed on the basis of the most influential parameters resulted from the SA. It was performed using the Particle Swarm Optimization – General Pattern Search of Hooke-Jeeves (PSO-GPSHJ) genetic algorithm, implemented in GenOpt®. The aim was to minimize the discrepancy between modelled and measured T-RH data, calculated as the root mean square error (RMSE) and the coefficient of variation of RMSE (CV-RMSE) with respect to the average of measured data. In this way, the building model was calibrated taking into account its thermal behaviour. At this step, the opaque building components of room 9 were update with the HMWall model in order to consider the simultaneous heat and moisture transfer through building materials, that are porous and hygroscopic. The effect of moisture transfer on the heat transfer was clear, therefore a further calibration of the room was carried out. It is worth to notice that the HMWall model is still in implementing phase and it is not possible to perform an automatic calibration. For this reason, room 9 and the above crawl space of roof were cloned in a new file as shown in Figure 12 and manually calibrated. Here, the internal wall and floor were defined as adiabatic components and, for this reason, layers from + to 9 (internal walls) and from + to 5 (internal floor) reported in Table 8 were considered. They were connected to a RH value of 50%, since it corresponded to the monthly averages of room 10 (close to the internal wall) and room 4 (close to the internal floor). The internal wooden ceiling was thermally connected with the crawl space and with a RH value of 55%. The wooden ceiling was not connected with the RH modelled in the crawl space, due to the high uncertainty on RH modelling in historic building explained and integrated in Appendix E. The manual calibration concerned the setting of the hygrothermal properties of the wooden ceiling, since it was mostly affected by the crawl space and, hence, by outdoor conditions. As well, the thermal properties of external walls were adjusted.
In this case, the calibration procedure can be defined as mixed, since it consists in an automatic (first phase) and manual (second phase) calibration. It should be added that for the manual calibration the Taylor diagram was not exploited to visualize modelled data, since few modifications were done on the building model.

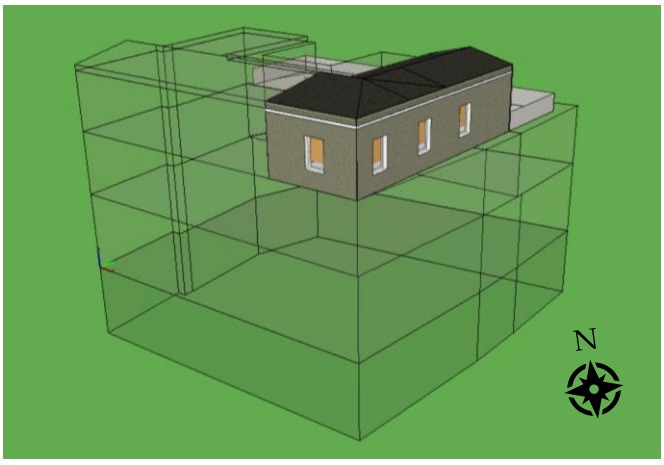

Figure 12 3D model of the room 9 and the above crawl space obtained with the dynamic building simulation tool after the cloning of the whole building.

After that, the building model, both the whole building and the single room 9, was validated using data collected from September 24th, 2017 till October 8th, 2017. In the case of room 9, the RH above the ceiling was set to 50%, since the validation was performed after a warm period where RH was, on average, less than 50% in the other rooms of the building.
The calibration and validation periods were selected so that no occupancy and internal gains were present. In this way, any misleading related both to the set-up of the HVAC system and to the schedule and features of occupants, i.e. the metabolic rate (MET) and the clothing factor, was not included in the simulation. Moreover, both periods were representative of two different outdoor conditions, since they came after a cold and a warm season, respectively.
Finally, the calibrated room 9 model was used to carefully assess the impact of a new control climate strategy suitable for the conservation of the wooden ceiling integrating the thermal comfort requirements.

The control climate strategy

The optimization of the indoor climate control strategy was addressed to update the set-point controller of the existing HVAC system without any modification of the plant. The HVAC was designed in the simulation environment as simple fan coils. The fan coils were set to a maximum heating power of 3500.0 W and a maximum cooling power of 3000.0 W. In this step, only room 9 was evaluated, since it was calibrated and validated using the HMWall model. The simulations were run over a whole year using the same weather file of Priverno described in the previous section.
The new control strategy of the indoor climate was tested using a dynamic set-point for temperature (T), as suggested in Kramer et al. (2017). The indoor relative humidity (RH) was evaluated a-posteriori and left in free-floating. The new climate control aimed at assessing the effect of a rational use of the HVAC system taking into account both the conservation of wooden ceilings and the thermal comfort of users.
The workflow consists in three steps as schematised in Figure 13 and described below:

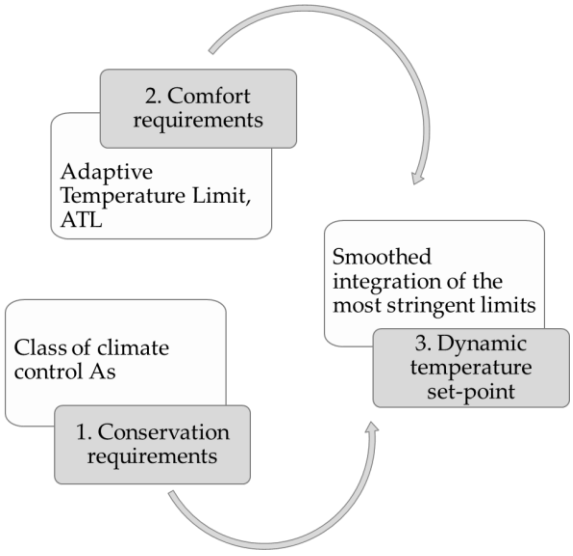

Figure 13 Workflow to calculate the dynamic temperature setpoints.

1. *Conservation T set-point safe band.* To assess mechanical conservation risk, T set-point is computed from the class of climate control As, as recommended in ASHRAE (2011) and reported in Table 5. The class As was chosen because it fitted for the building features of museum (building type V) and provided less mechanical degradation risk than the class of climate control B. The set-point was derived as follows. From indoor air T measurements, the 90-days centred moving average is calculated and seasonally adjusted with respect to the annual average according to +5/-10 K (T_{seas}). The upper ($T_{As\_up\_lmt}$) and lower ($T_{As\_lo\_lmt}$) limits are defined as ±2 K of T_{seas} and shown in Figure 14 (upper panel).

$$T_{As\_up\_lmt} = T_{seas} + 2 \quad (21)$$

$$T_{As\_lo\_lmt} = T_{seas} - 2 \quad (22)$$

2. *Comfort T set-point safe band.* The Adaptive Temperature Limits (ATL) were chosen as T set-point limits for the thermal comfort requirement (Nicol and Humphreys 2002). The T set-point is dynamic because it depends on the phenomena of adaptation and expectation of people with respect to the outdoor temperature (T_{out}) (Van der Linden et al. 2006). The ATL is calculated on the basis of procedure suggested by Kramer et al. (2018) for temperate climates. The thermal sensation and clothing level of users are related to the reference outdoor temperature ($T_{out,ref}$) and calculated as follows:

$$T_{out,ref} = \frac{T_{out,i} + 0.8 \times T_{out,i-1} + 0.4 \times T_{out,i-2} + 0.2 \times T_{out,i-3}}{2.4} \quad (23)$$

where $T_{out,i}$ is the average T_{out} on the survey day and $T_{out,i-x}$ is the average T_{out} of x-days before. T set-point is related to the $T_{out,ref}$ for defining upper ($T_{ATL\_up\_lmt}$) and lower ($T_{ATL\_lo\_lmt}$) limits. The limits are shown in Figure 14 (mid panel).

$$T_{ATL\_up\_lmt} = 20.7 + 0.175 \times T_{out,ref} \quad (24)$$

$$T_{ATL\_lo\_lmt} = 18.3 + 0.175 \times T_{out,ref} \quad (25)$$

3. *T set-point safe band.* T set-point, both for upper and lower limit, is determined comparing for each hourly value the most stringent limits according to the collection safe band and the comfort safe band. After that, T limits are smoothed out as shown in Figure 14 (lower panel).

After simulation, the modelled RH values were compared with limits recommended in the ASHRAE (2011) to check if the system also indirectly guarantees the RH control. The RH limits according to Class of Climate Control As are defined as for T limits. From indoor air RH measurements, the 90-days centred moving average is calculated and seasonally adjusted with respect to the annual average according to ±10% (RH_{seas}). The upper ($RH_{As\_up\_lmt}$) and lower ($RH_{As\_lo\_lmt}$) limits are defined as ±5% of RH_{seas} and shown in Figure 15.

$$RH_{As\_up\_lmt} = RH_{seas} + 5 \quad (26)$$

$$RH_{As\_lo\_lmt} = RH_{seas} - 5 \quad (27)$$

The estimated indoor variables were replaced in the equation (4) to analyse the effect of the new control strategy on the crack width with respect to no control strategy, i.e. the free-floating indoor climate.

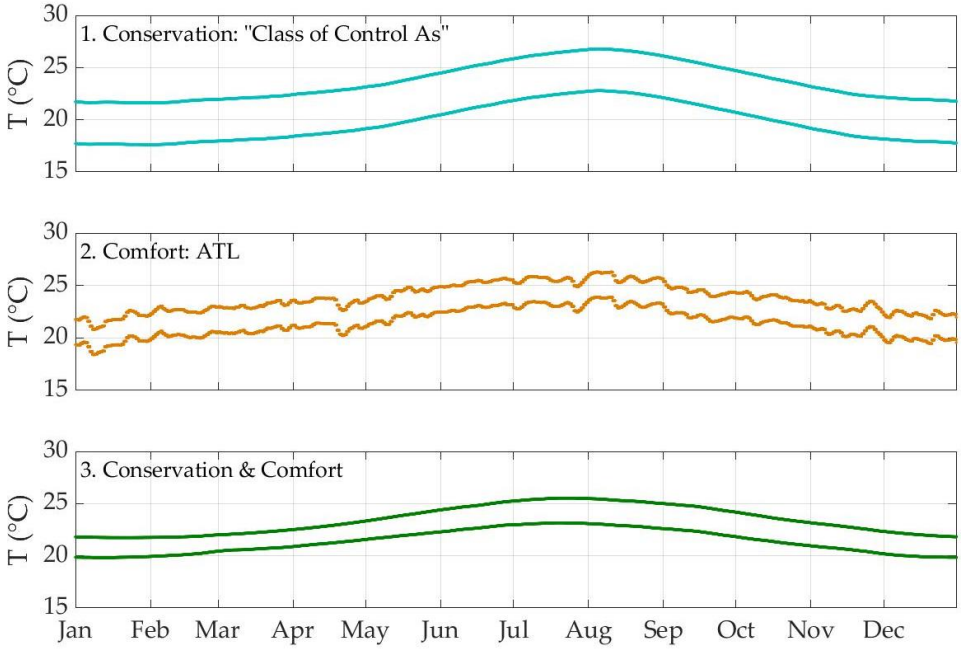

Figure 14 The three steps used for defining the dynamic temperature set-point: 1. Conservation requirements as Class of Climate Control As; 2. Comfort requirements as Adaptive Temperature Limits (ATL) and 3. Smoothed-integration of conservation and comfort requirements.

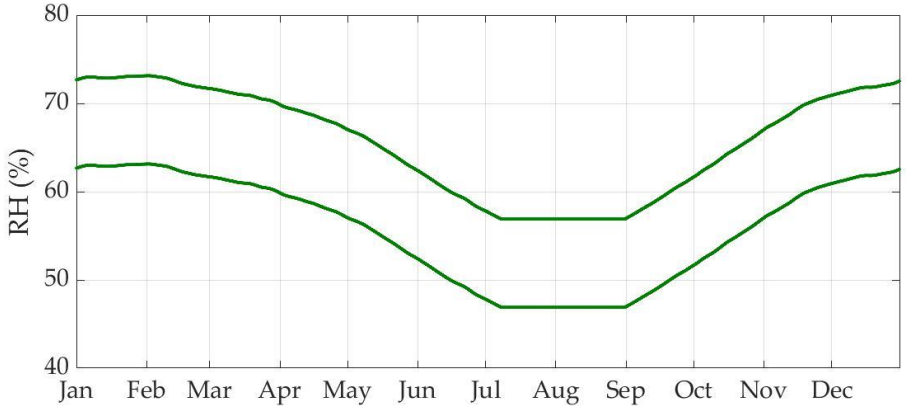

Figure 15 RH dynamic set-point defined according to the Class of Climate Control As.

This page intentionally left blank

Chapter 4: Results and discussion

This chapter shows the most relevant outcomes following the strategy proposed by this thesis. It contains the three sections that follow the structure used in The general workflow described in the previous chapter.

The microclimate analysis

The first screening of recorded data of temperature (T) and relative humidity (RH), both inside and outside, has shown that all probes properly worked in their operating range.

Quality of time series

Table 10 reports the Completeness Index (CoI) and the Continuity Index (CI) values for each internal and external probe, since the indexes both for T and RH are the same. In the case of room 9, the indexes also summarise the time series of surface temperature (T_s) and crack-width (C). The MQI was determined only for the RH time series. All the time series resulted to be of high quality (> 0.993) and, hence, suitable for the exploratory data analysis and to define the historical climate in the case of organic and hygroscopic materials. The lower values of the CoI and the MQI (= 0.938) achieved in room 9 are due to an erroneous transmission of data by the data logger in January 2017.

Table 10 Summary of the results of the Completeness Index (CoI), the Continuity Index (CI) and the Microclimate Quality Index (MQI) for each of probes inside the museum (room 4, 9 and 10) and for that outdoors (out)

Probe	CoI	CI	MQI
room 4	0.984	0.999	0.984
room 9	0.938	0.999	0.938
room 10	0.993	0.994	0.993
out	0.998	0.999	--

Box-and-whiskers plots

Figure 16 and Figure 17 show the box-and-whiskers plot grouped by season for T and RH, respectively. Figures are supported by Table 11 for T and Table 12 for RH, that provide a synthetic summary of the main statistics over the whole period. Outliers were

identified both for T and RH. However, since they are not due to instrumental problems but to the climate evolution, they were included in the following analysis.

Temperature (T)

On average, T values recorded in room 4 are significantly different from the other rooms, especially in winter. Moreover, during this season, some outliers were detected in room 9 and 10, that can be related to the use of the heating system. The annual T4 mean is 22.6°C, whereas T means in other rooms are, on average, lower than 21.3°C. On the contrary, the maximum annual variability (Δx, i.e. max - min) in room 4 is the lowest and corresponds to 18.1°C; whereas the highest Δx has been found in room 9u (Δx = 24.9°C). It is worth to notice that this behaviour is strongly related to the rooms' position with respect to the building orientation. Room 4 is at the first floor and has only one external wall and two windows, meaning that it is more protected than room 9, that is in the south corner of the building at the second floor and has three external walls and five windows. Even though boxes related to room 9 overlap in all season (Figure 16), the Wilcoxon test has shown that T9d and T9u are significantly different with a p-value of 10^{-4}. This means that a stratification of the air might occur.

Considering the whole period, the mean value of internal T medians is 20.5°C, ranging between 17.1°C (the mean of the 25th percentile) and 27.1°C (the mean of the 75th percentile), whereas Tout has a lower median (17.1°C) and a greater variability, as expected (25th percentile = 11.4 °C and 75th percentile = 23.8 °C).

Table 11 Summary the statistics of outdoor and indoor temperature (T) within the three rooms, coded as out, 4, 9d, 9u and 10, respectively (min: minimum; 25th per: 25th percentile or first quantile; 75th per: 75th percentile or third quantile; max: maximum; IQR: inter-quantile range (75th per - 25th per); Δx: max - min).

	Tout (°C)	T4 (°C)	T9d (°C)	T9u (°C)	T10 (°C)
min	-4.4	13.2	8.6	8.5	8.9
25th per	11.4	19.0	16.4	16.5	16.6
median	17.1	21.4	20.1	20.2	20.2
mean	17.8	22.6	21.1	21.3	21.3
75th per	23.8	27.2	26.9	27.2	27.1
max	39.3	31.3	32.8	33.4	32.6
IQR	12.4	8.3	10.5	10.7	10.5
Δx	43.6	18.1	24.2	24.9	23.8

Over seasons (Figure 16), it was found as follows:

- winter: the mean value of internal T medians is 15.2°C, ranging between 13.7°C and 16.5°C with room 4 warmer than the others, whereas Tout has a lower median (8.8°C) ranging between 4.5°C and 11.7°C;
- spring: the mean value of internal T medians is 20.1°C, ranging between 18.4°C and 21.8°C, whereas Tout has a lower median (16.3°C) ranging between 12.7°C and 20.7°C;
- summer: the mean value of internal T medians is 29.4°C, ranging between 28.5°C and 30.2°C, whereas Tout has a lower median (27.4°C) ranging between 23.7°C and 31.7°C;

- autumn: the mean value of internal T medians is 20.6°C, ranging between 18.6°C and 23.8°C, whereas Tout has a lower median (17.6°C) ranging between 14.2°C and 21.2°C.

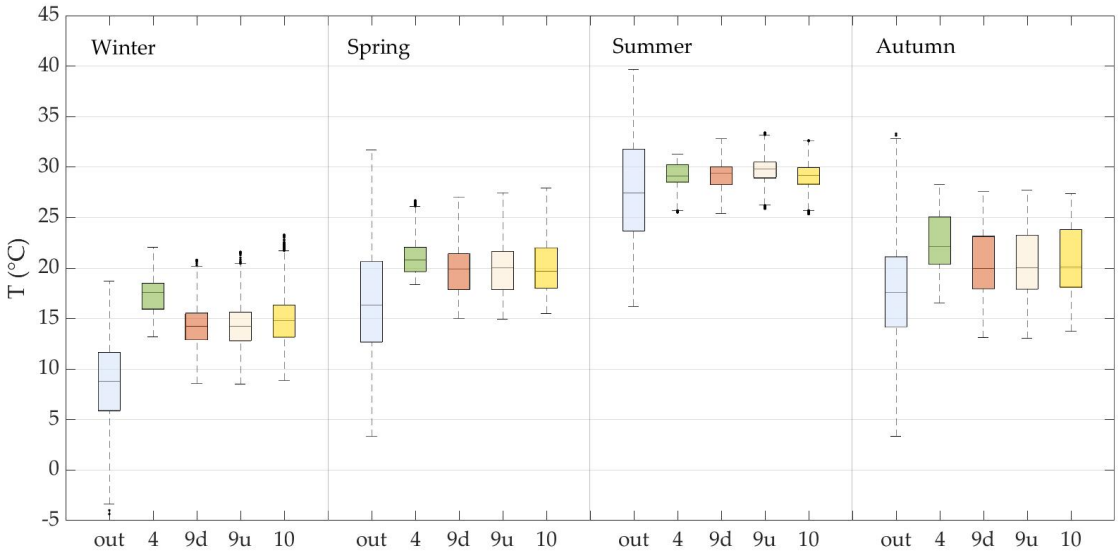

Figure 16 Box-and-whiskers plot of temperature (T) for each room grouped by season over the whole monitoring period.

Relative humidity (RH)

RH values are significantly different among rooms in all season except in summer. In addition, the Wilcoxon test has shown that no significant difference is between RH9d and RH9u (p-value = 0.65). The maximum annual variability (Δx) is 53.7% in room 10 and lower than 36.4% in room 9.

Considering the whole period, the mean value of internal RH medians is 50.7%, ranging between 46.3% (the mean of the 25th percentile) and 54.2% (the mean of the 75th percentile), whereas RHout has a higher median (63.7%) and a greater variability (25th percentile = 48.7% and 75th percentile = 77.2%).

Over seasons, it was found as follows:

- winter: the mean value of internal RH medians is 51.2%, ranging between 46.7% and 53.2% with room 4 and room 10 drier than room 9, whereas RHout has a higher median (69.2%) ranging between 57.3% and 79.2%;
- spring: the mean value of internal RH medians is 51.3%, ranging between 49.0% and 52.8% with room 4 and room 10 drier than room 9, whereas RHout has a higher median (60.9%) ranging between 45.6% and 74.9%;
- summer: the boxes of internal RH overlap with a median of 45.2%, ranging between 43.4% and 47.1%, whereas RHout has a slightly higher median (48.9%) ranging between 37.5% and 61.7%;
- autumn: the mean value of internal RH medians is 56.2%, ranging between 53.8% and 58.9% with room 4 and room 10 drier than room 9, whereas RHout has a higher median (75.0%) ranging between 61.7% and 83.8%.

Table 12 Summary the statistics of outdoor and indoor relative humidity (RH) within the three rooms, coded as out, 4, 9d, 9u and 10, respectively (min: minimum; 25th per: 25th percentile or first quantile; 75th per: 75th percentile or third quantile; max: maximum; IQR: inter-quantile range (75th per - 25th per); Δx: max - min).

	RHout (%)	RH4 (%)	RH9d (%)	RH9u (%)	RH10 (%)
min	18.0	21.9	37.2	35.3	20.3
25th per	48.7	45.0	47.9	47.5	44.8
median	63.7	47.8	52.9	53.0	49.3
mean	62.4	47.7	52.3	52.3	48.9
75th per	77.2	50.8	56.3	56.7	53.0
max	98.8	69.6	71.3	71.6	74.0
IQR	28.5	5.8	8.5	9.2	8.2
Δx	80.8	47.7	34.1	36.4	53.7

In all seasons except for summer, RH values in room 4 as well as room 10 show to be drier than those recorded in room 9, even though room 9 and 10 are open-adjoining. This is probably due to the combined effect of ventilation, coming from the hallway close to room 4 and 10 and connected to the stairwell, and of the efficacy of the heating system in winter time. The former allows moisture removal and depends on the MR of the air mass; on the contrary, the latter affects the saturated pressure of water vapour in the air.

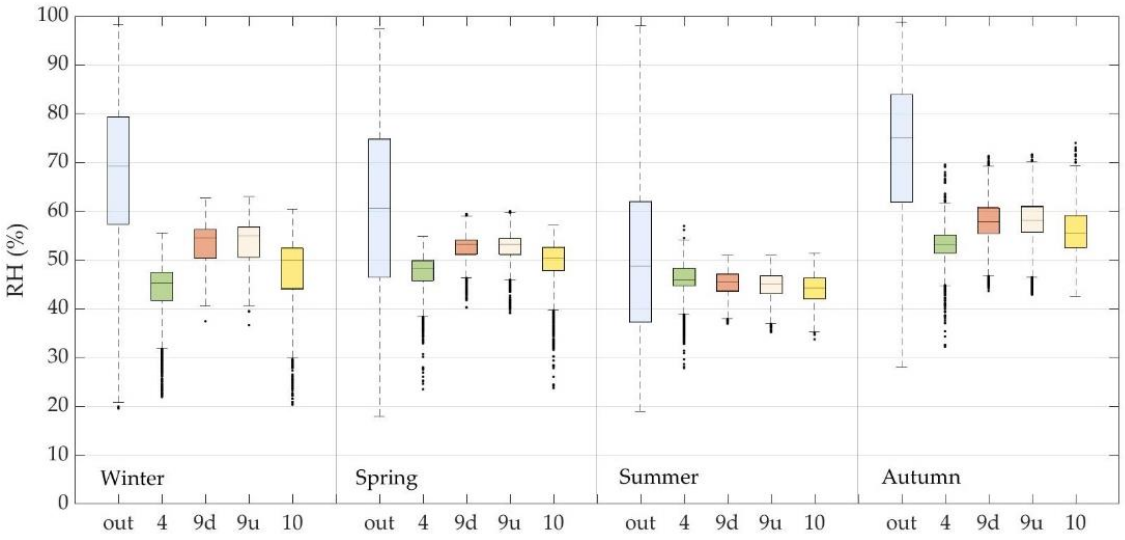

Figure 17 Box-and-whiskers plot of relative humidity (RH) for each room grouped by season over the whole monitoring period.

To understand if RH values mainly depended from T, the Spearman's rank correlation coefficient (r_s) was calculated. It was found that T and RH data were not correlated each other inside room 4 ($r_s = 0.01$), meaning that RH is governed by source or sink of water vapour. On the contrary, r_s between T and RH were -0.51 and -0.68 inside room 10 and 9, respectively. In general, the thermal and moisture behaviour among rooms were highly correlated ($r_s > 0.98$).

Daily span

Figure 18 shows the RH daily span (ΔRH) *versus* the T daily span (ΔT) calculated as the difference between the maximum and minimum value observed during each day for the

three rooms. In room 4 (upper-left panel), ΔT never is higher than 4°C, whereas ΔRH generally is lower than 20%. Moreover, in summer time (red dots) ΔRH has more occurrences above 10% with respect to the other rooms. The data from room 10 (upper-right panel) show larger daily cycles than those from the other three rooms, especially in winter. The maximum of ΔT and ΔRH is 8°C and 28%, respectively, and mainly occurs in winter time or when the heating system is on (late autumn and early spring). In room 9 (lower panels), ΔRH is always lower than 20%, whereas ΔT overcomes 7°C in some winter days. In all the rooms, winter data (blue dots) assemble a distinct area with respect to the other season, standing out the effect of the heating system on the indoor climate. Large ΔRH could induce mechanical damage in hygroscopic materials.

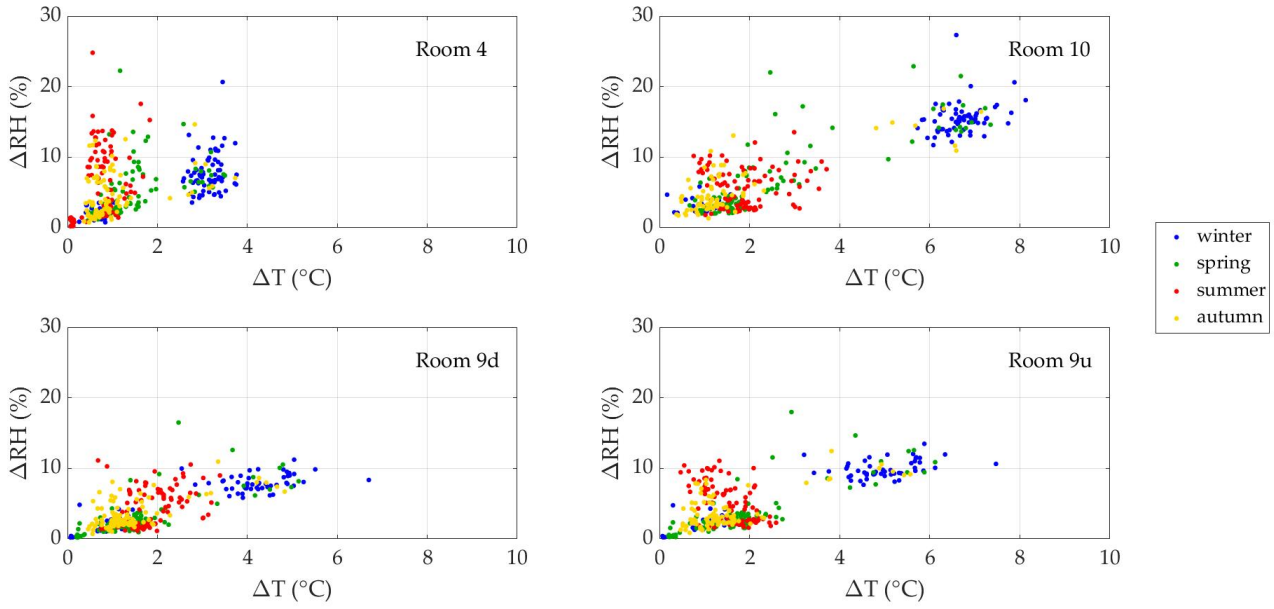

Figure 18 Scatter diagram of daily RH span (ΔRH) *vs* daily T span (ΔT) for room 4 (upper-left panel), 10 (upper-right panel), and 9d-9u (lower panels). The daily span is calculated as the difference between the maximum and minimum values. Blue, green, red and orange dots indicate winter, spring, summer and autumn, respectively.

Outdoor climate influence

The scatter plots of the indoor temperature (T) and mixing ratio (MR) monthly means as a function of the corresponding outdoor monthly means are shown in Figure 19 and Figure 20.

Looking at the temperature scatter plots (Figure 19), T_{in} values are always above the bisector, i.e. internal thermal conditions are warmer than outdoors as already shown in Figure 16. In winter time, the difference with respect to outdoors is from 6°C (room 9 and 10) up to 10°C (room 4), whereas in summer time, internal thermal conditions are, on average, 2°C warmer. Even though the heating system was switched on during cold days from November to April, its effect is slightly visible in room 9 (lower panels) and 10 (upper-right panel), probably due to the effect of the roof, which is not insulated. Instead, in room 4 (upper-left panel), T_{in} was, on average, 2°C higher than T_{in} of other rooms, showing a pattern closer to heated buildings.

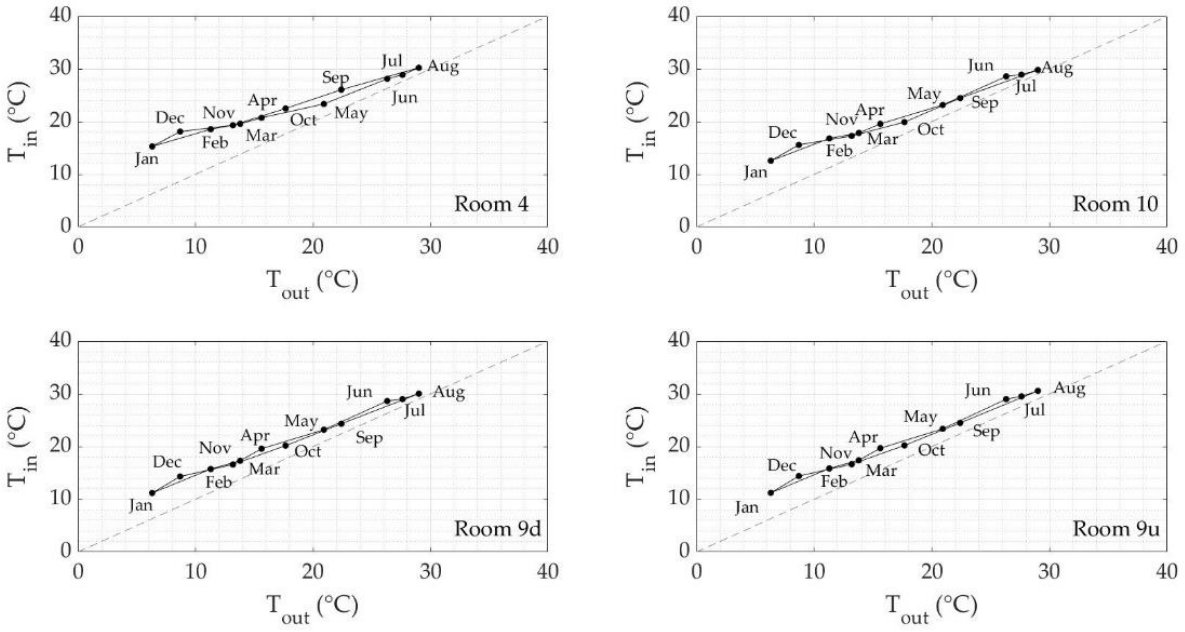

Figure 19 Indoor *vs* outdoor monthly averages of temperature data (T_{in} *vs* T_{out}) for room 4 (upper-left panel), 10 (upper-right panel) and 9 (lower panels). The averages were calculated from September 1st, 2016 to August 31st, 2017.

The monthly indoor MRs do not differ largely from the external variations (Figure 20) as shown by the values which are placed close to the bisector. On September-October in room 9 (lower panels) and 10 (upper-right panel), the smaller internal MR values, with respect to external ones, could be due to the ventilation responsible for the water vapour removal.

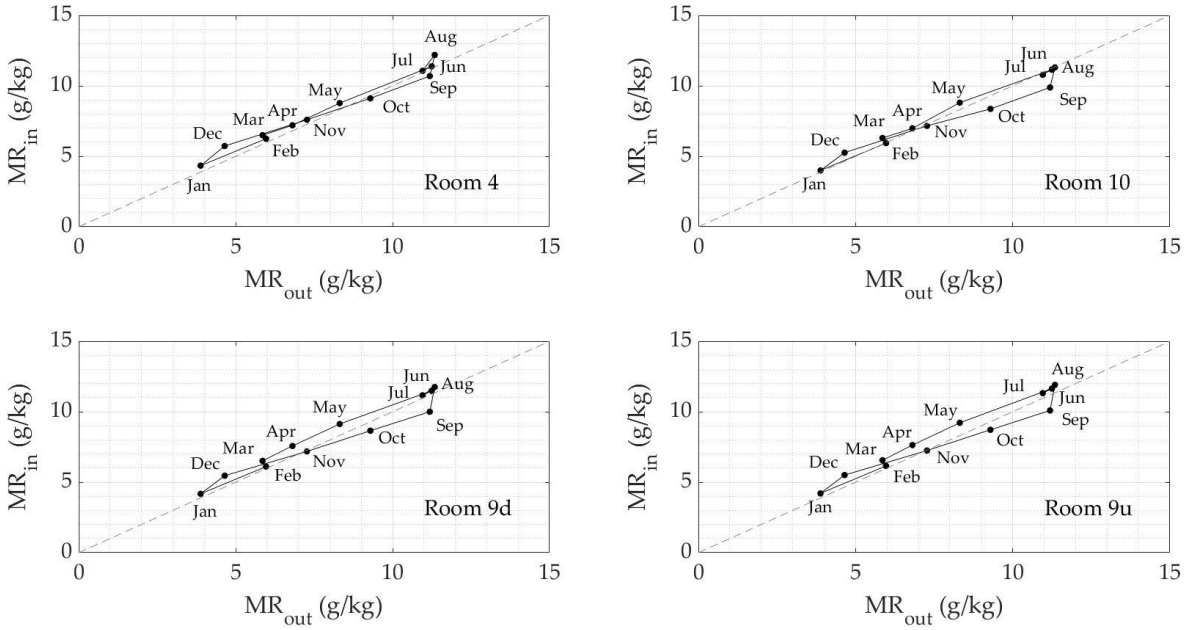

Figure 20 Indoor *vs* outdoor monthly averages of mixing ratio data (MR_{in} *vs* MR_{out}) for room 4 (upper-left panel), 10 (upper-right panel) and 9 (lower panels). The averages were calculated from September 1st, 2016 to August 31st, 2017.

The application of EN 15757:2010

The use of the standard EN 15757:2010 requires that the objects stored have no recent damages. After the restoration in 2012, the restorer claimed that the wooden ceilings have not suffered from further degradation phenomena. This means that the 7th and the 93rd percentiles of deviations from the 30-days centred-moving-average (MAC) with respect to RH readings delimit the safe band of allowable RH fluctuations, i.e. the historical climate at which the wooden ceiling has been acclimatised. RH measured from September 2016 till August 2017 together with the historic climate expressed in terms of the annual mean, the 30-day MAC and the safe band (the 7th and the 93rd percentiles of deviations from the MAC) are shown in Figure 21 and Figure 22 for room 9 and 10, respectively. These rooms were chosen because located at the second floor where there are the wooden ceilings.

Looking at Figure 21, the seasonal increase of RH, with respect to the annual average, is 9.3% and occur in November; on the contrary, the seasonal decrease, with respect to the annual mean, is 9.1% and occur in August.

Looking at Figure 22, the seasonal increase of RH, with respect to the annual average, is 10.4% and occur in October; on the contrary, the seasonal decrease, with respect to the annual mean, is 5.9% and occur in January. Most of occurrences below the lower limit is from November till May and probably are due to the effect of the heating system that is switched on during the opening hours.

Data below the lower limit (too dry environment) can be related either to the heating episodes, as they mainly occur between December and April, or to summer temperature peaks, as it is visible between June and August, combined with moisture removal, as already shown in Figure 20. These occurrences might cause risky shrinkage of wooden fibres. RH values higher than the upper limit can be correlated with additional indoor sources of moisture.

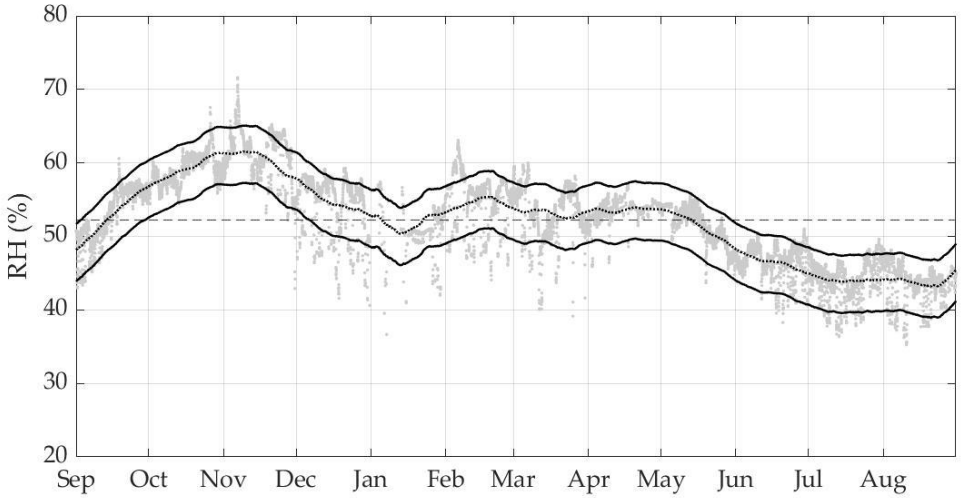

Figure 21 RH data (grey dots) measured from September 2016 till August 2017 at room 9 (upper level); the seasonal RH cycle (black line) determined as the 30-day central moving average of the readings; the lower and upper limits ("safe band") correspond to 7th and the 93rd percentiles of the short fluctuations (dotted lines). The yearly RH average is marked by a horizontal dashed-line.

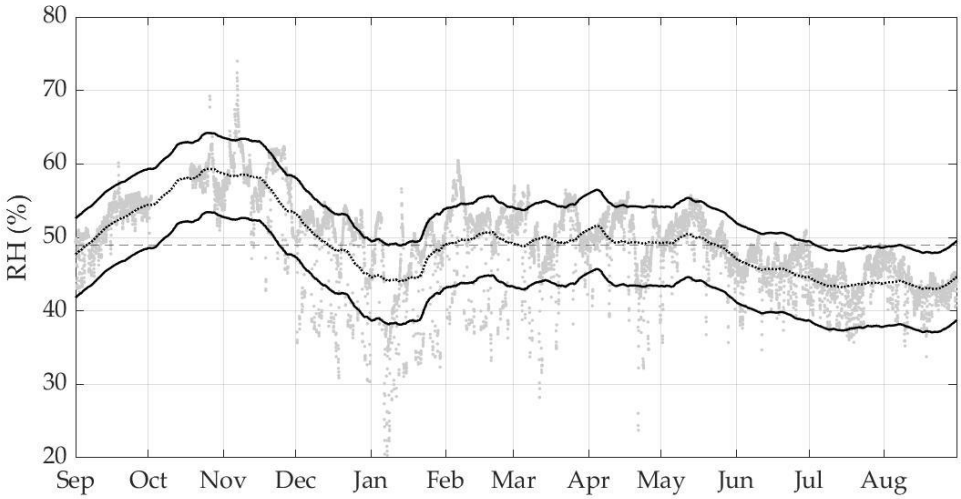

Figure 22 RH data (grey dots) measured from September 2016 till August 2017 at room 10; the seasonal RH cycle (black line) determined as the 30-day central moving average of the readings; the lower and upper limits ("safe band") correspond to 7th and the 93rd percentiles of the short fluctuations (dotted lines). The yearly RH average is marked by a horizontal dashed-line.

The application of ASHRAE 2011

Figure 23 shows the comparison of the T-RH data, measured in room 9 from September 2016 till August 2017, within the class of climate control, from AA to B, suggested by ASHRAE 2011 and described in Table 5.

In this research, a particular attention was paid to the class of climate control As and B, since no degradation phenomena of artworks occurred over the last years as well the HVAC system does not allow the RH control. T-RH data fit the class of climate control As in 60.0% of time and the class of climate control B in more than 90% of the time. This means that a moderate risk of mechanical damage may occur to highly vulnerable artworks in less than 10% of time.

To provide a thorough comprehension of indoor climate with respect to the classes of climate control, Table 13 summarises the percentage of data in which the T-RH measured in all the three rooms fits into the classes from AA to D. The difference between room 9d and 9u is mainly related to T readings, since no significant difference was individuated in RH data.

Table 13 Summary of the percentage of data in which the climate fits into the classes of climate control, from AA to D, as suggested by the ASHRAE 2011 and reported in Table 5.

Class of Climate Control	Room 4	Room 9d	Room 9u	Room 10
AA	58.2	42.3	37.8	36.9
A	77.7	63.0	59.9	56.0
AS	70.3	60.0	57.2	51.2
B	90.3	92.5	87.8	86.5
C	92.9	93.1	88.9	93.9
D	92.9	93.1	88.9	93.9

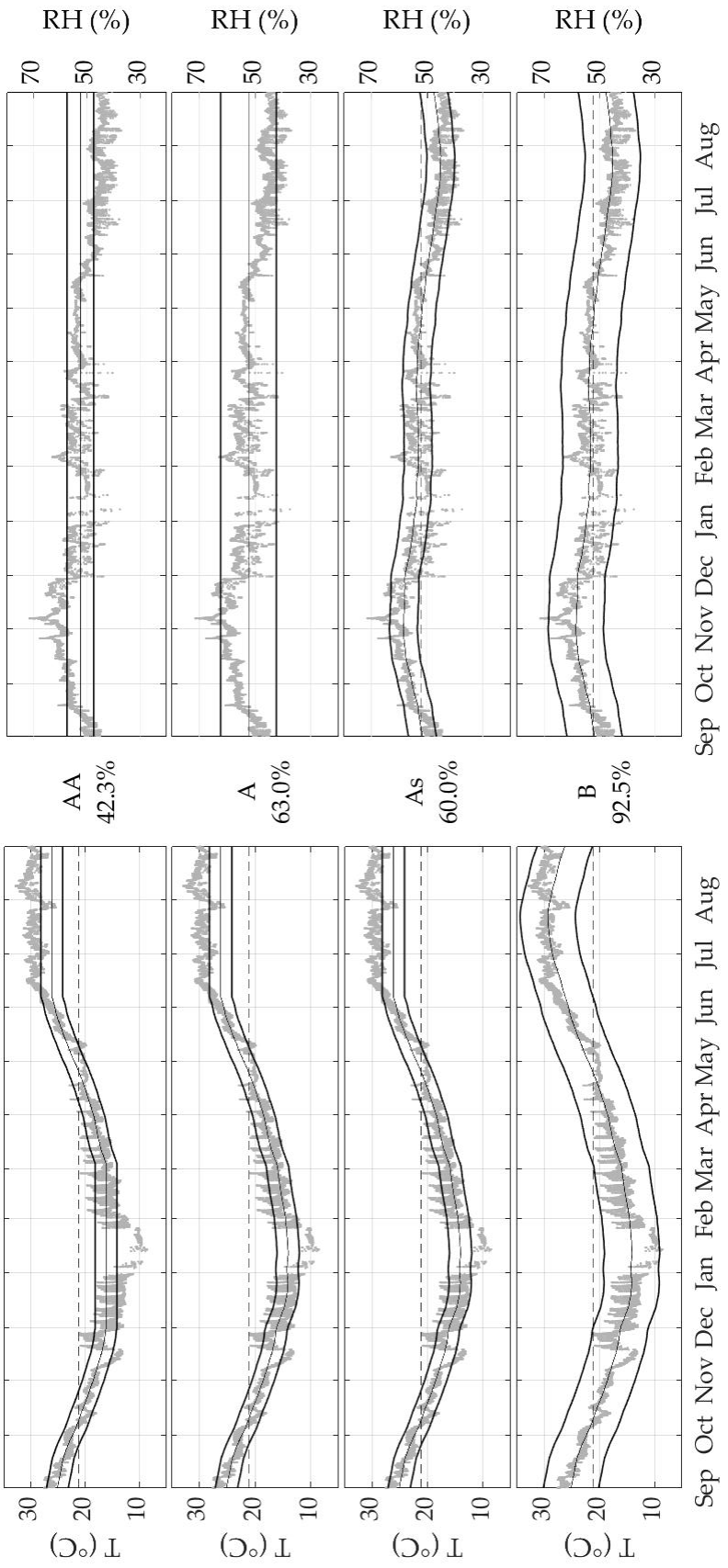

Figure 23 Comparison of temperature (T) and relative humidity (RH) data, measured in room 9 (upper level), with the ASHRAE climate classes from AA to B. T plots are on left, whereas RH plots are on right. In the middle, the summary of the percentage of data in which the climate fits into the climate classes is reported.

The psychrometric charts with T and RH data measured in room 9 (upper level) were seasonally plotted and compared with the short-fluctuations calculated from the annual average of T and RH, as suggested by the ASHRAE 2011 in the case of the class of climate control As (Figure 24) and B (Figure 25).
The allowable limits are indicated in figures as an area delimited by blue lines (T limits) and blue curves (RH limits). Temperature limits are defined as the annual average 21.3°C ranging between 2°C for class As and 5°C for class B. Relative humidity limits are defined as the annual average 52.3% ranging between 5% for class As and 10% for class B. The intensity of the colour in each season is related to the percentage of cases characterized by similar hygrothermal values. It follows that more data are scattered and more indoor climate is fluctuating. Seasonal monthly averages are also displayed. Each psychrometric chart includes a 3-by-3 matrix at the right that reports, on yearly and seasonal basis, the percentage of time that indoor conditions are within the guidelines (second row and column), above the T and RH maxima (first row (too warm) and third column (too humid), respectively) and below the T and RH minima (third row (too cold) and first column (too dry), respectively).
It was found that the percentage of total data within the guideline' limits is 13.1% for the class As (Figure 24) and 41.8% for the class B (Figure 25).
Following the seasonal interpretation, it was found that:

- in winter (blue data), T values are lower than limit in 98% and 82.6% of time, respectively, with January as the coldest month.
- In spring (green data), T limits imposed by class As (Figure 24) show that the environment is too cold and too warm in 35.7% and 16.9% of time, i.e. in March and May, respectively. On the contrary, more than 88.0% of time T-RH data are within limits of class B (Figure 25).
- In summer (red data), the environment is too warm for both classes (100.0% and 99.0%, respectively) and alsotoo dry for class As (81% of time).
- In autumn (orange data), looking at Figure 24, the environment is too warm in September in 19.8% of time and too humid in 57.4% of time (October and November). Instead in Figure 25, the environment results to be too humid only in 15.7% of time.

The dose response function for crack-width

The hygrothermal conditions at the interface air-surface (T_s – RH_s) were compared with the crack-width (C), as shown in Figure 26. The RH_s was derived from equation (3) and its uncertainty (4.5%) was calculated starting from T and MR uncertainties. It was found that an increase of ΔT_s = 10.0°C and a decrease of ΔRH_s = 10.0% over the year with respect to the annual averages (upper panel in Figure 26) cause an increase of C equal to 0.12 mm (lower panel in Figure 26). This confirms that too dry environmental conditions (= stress), mainly related to too warm thermal conditions, could be responsible for C widening (= strain) and, hence, risky for conservation requirements. Besides, C was compared with T_s RH_s by using the Spearman's rank correlation coefficient (r_s). It resulted that $r_s(C, T_s)$ = 0.67 and $r_s(C, RH_s)$ = -0.91, showing that C is highly correlated with both hygrothermal variables, as expected.

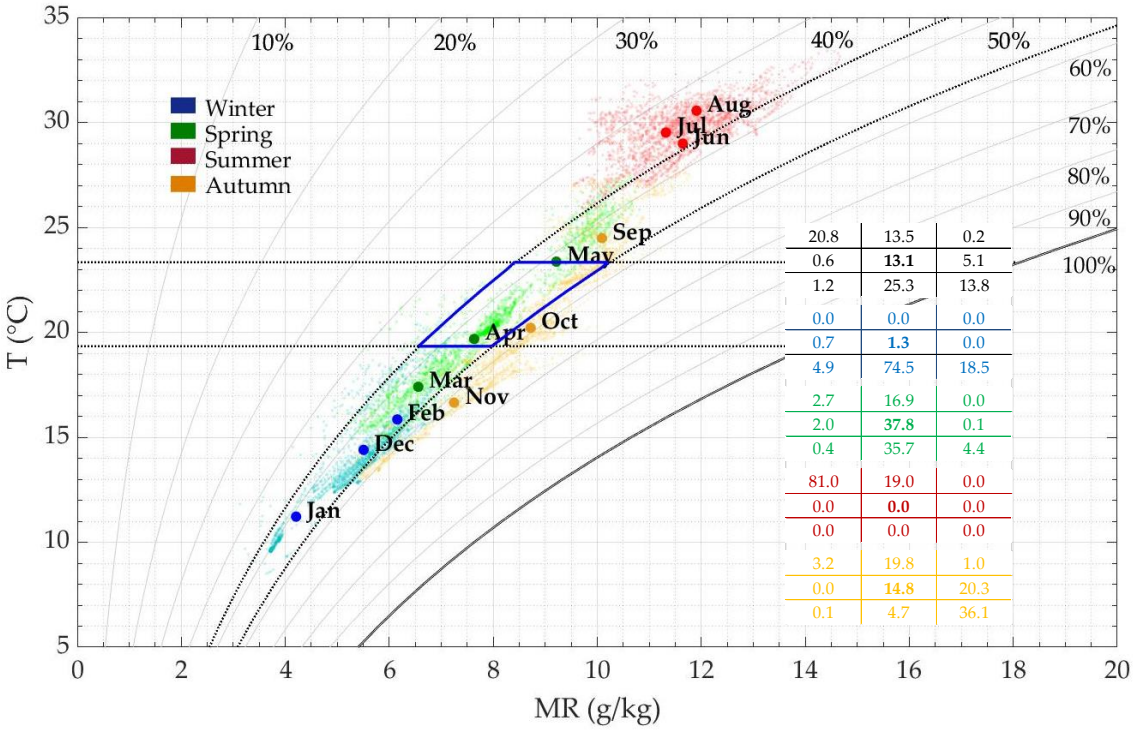

Figure 24 Psychrometric chart. Indoor climate within room 9 is seasonally represented: blue (winter), green (spring), red (summer), and orange (autumn). Seasonal monthly averages are also displayed. The Class of Climate Control As area is delimited by two horizontal blue lines (T = 21.3 ± 2°C) and two blue curves (RH = 52.3 ± 5%). The T and RH limits divide the chart into nine parts and the percentage of data within limits is represented by the 3-by-3 matrixes on the right.

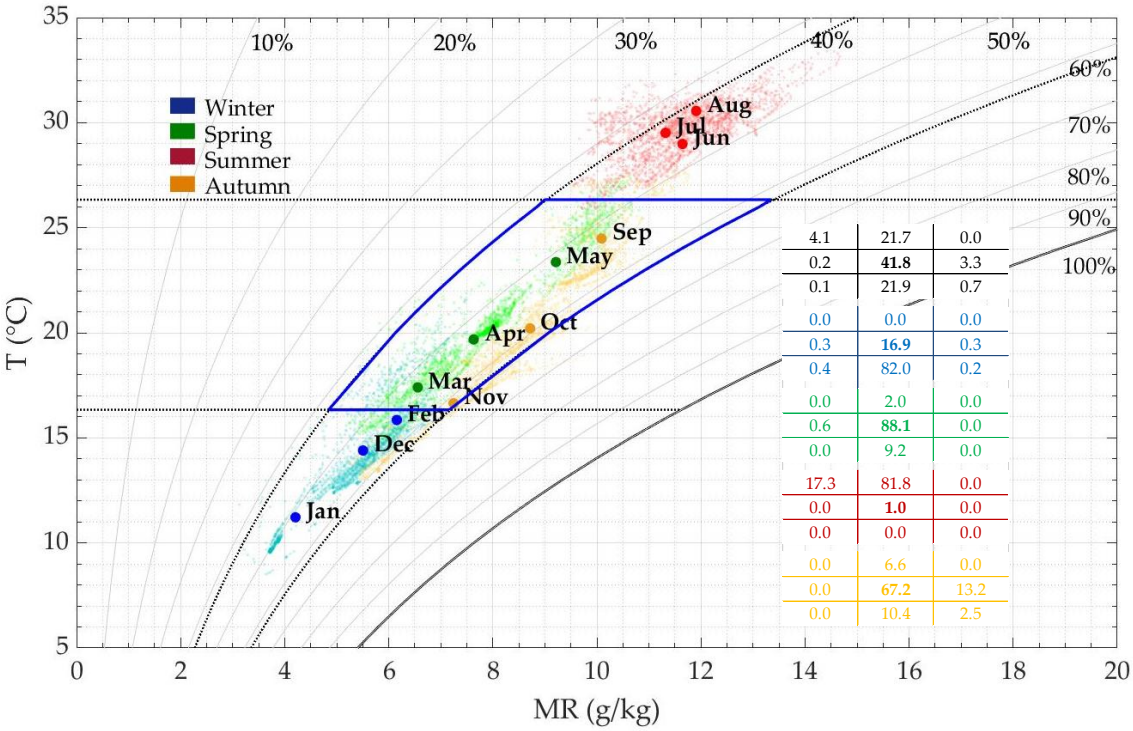

Figure 25 Psychrometric chart. Indoor climate within room 9 is seasonally represented: blue (winter), green (spring), red (summer), and orange (autumn). Seasonal monthly averages are also displayed. The Class of Climate Control B area is delimited by two horizontal blue lines (T = 21.3 ± 5°C) and two blue curves (RH = 52.3 ± 10%). The T and RH limits divide the chart into nine parts and the percentage of data within limits is represented by the 3-by-3 matrixes on the right.

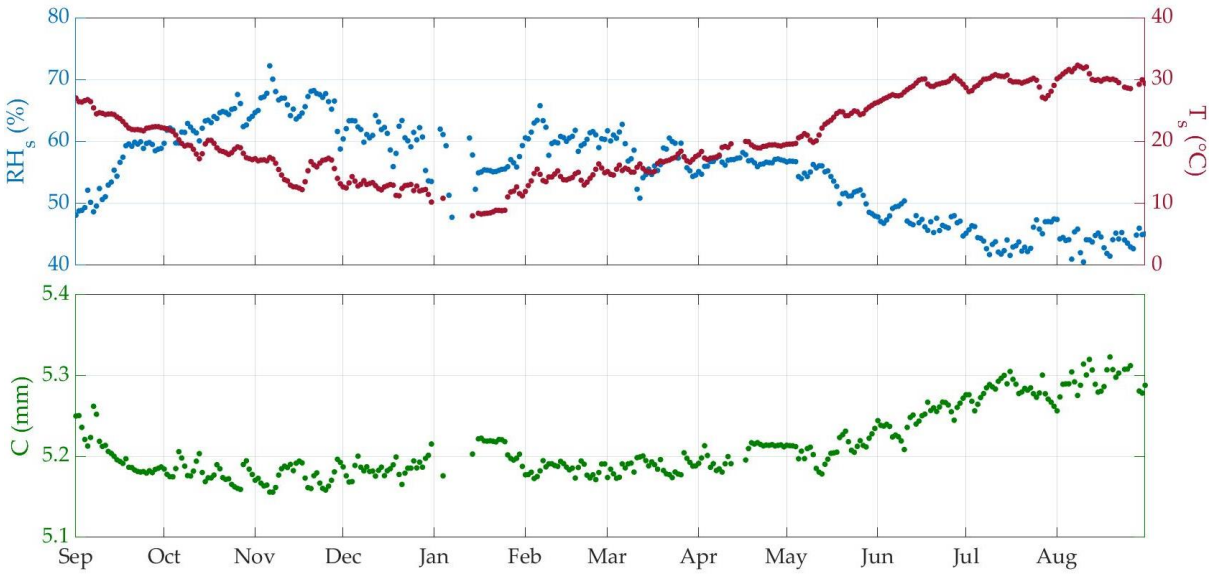

Figure 26 Upper panel. Relative humidity (blues dots) and temperature (red dots) evolution at the interface air-surface (Ts – RHs) over the whole year. Lower panel. Crack width (C) evolution over the whole year.

To pinpoint the RH_s gradient within the monitored wooden panel, the difference (ΔRH_s) between RH_s at the surface and RH_s smoothed at 3h, 24h, 48h and 1w was calculated and displayed in Figure 27 along with the safe band calculated as the 7th and 93rd percentile of ΔRH_s. In this way, the 14% of occurrences represents the riskiest hygrometric conditions for the stress-and-strain cycle of wooden material. Positive values correspond to drier conditions of inner layer than those in surface; whereas negative values indicate drier conditions at the surface than those in inner layers. Greater is ΔRH_s, i.e. the moisture gradient, higher will be the internal stress. Here, negative values are more frequent from June till August and from December till April.

Looking at the daily span of T_s – RH_s shown in Figure 28, in the former period (red dots), the large daily ΔRH_s (up to 10.0%) are probably due to moisture removal from the environment jointly with a high thermal level of the ambient air. The RH_s daily span is probably governed by the daily-night cycle buffered by the building envelope. This causes that the difference with the inner RH_s may be large. Indeed, ΔT_s never exceeds 2°C. On the contrary, in the latter period (blue dots), the intermittent use of the heating system provokes large daily fluctuations of T_s (up to 6°C), that indirectly affect daily fluctuations of RH_s. In this way, drops in RH_s values are suddenly replaced by RH_s peaks.

Once again it is clear how microclimate variables and their mutual relations are of crucial importance in interpreting the damage process.

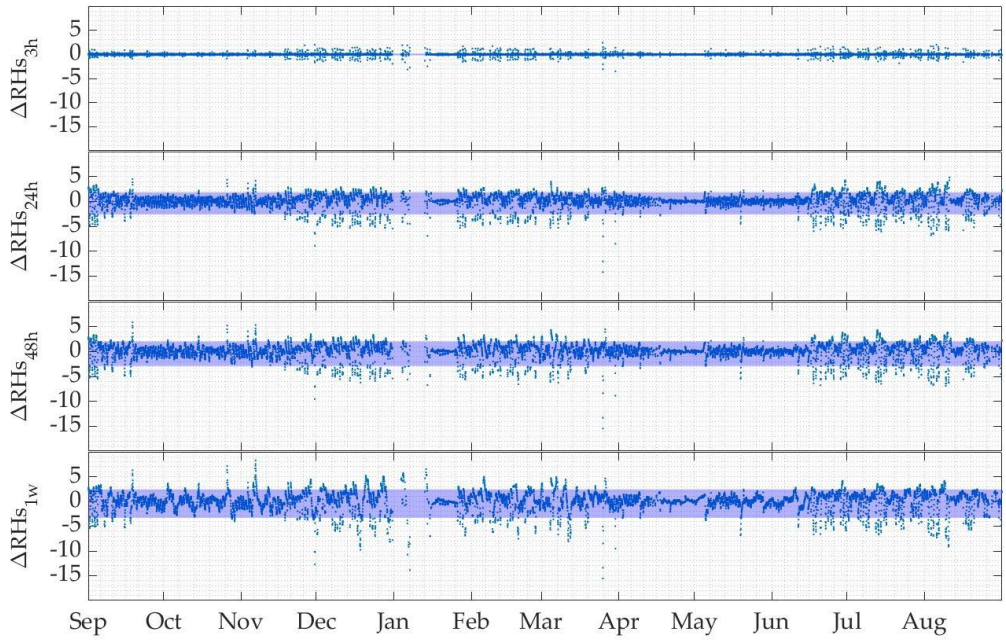

Figure 27 Relative humidity gradient (ΔRH_s) through the wooden panel (from surface to inner layers) calculated as the difference between RH_s at the superficial layer and RH_s smoothed at 3h, 24h, 48h and 1w. Blue bands are the allowable limits defined as the 7th and 93rd percentile of ΔRH_s.

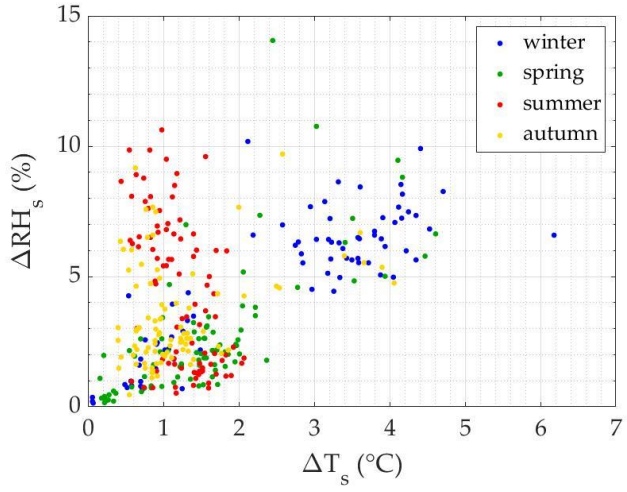

Figure 28 Scatter diagram of daily RH_s span (ΔRH_s) vs daily T_s span (ΔT_s). The daily span is calculated as the difference between the maximum and minimum values. Blue, green, red and orange dots indicate winter, spring, summer and autumn, respectively.

As above described, the riskiest periods for conservation of wooden ceilings seem to be when the heating system is on and during summer time. Figure 29 shows the ΔRH_s calculated with a time lag of one-week and the crack width evolution over the whole year. It is clear that, when the heating system is on, the moisture-induced strain is closely related to the daily fluctuations of hygrothermal conditions; whereas, in summer time, it is strongly affected by the moisture gradient within the material, since the inner layers are more humid than the surface layer. On the other hand, when ΔRH_s is within the safe band, C is stable as occurred in September-October and in April-May.

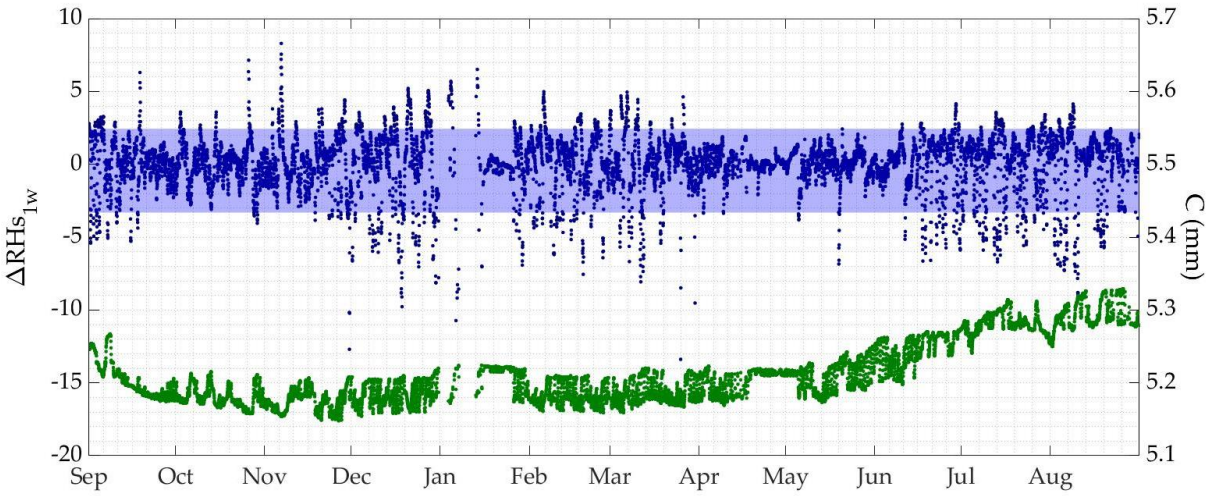

Figure 29 ΔRH_s calculated as RH_s smoothed at 1w (inner layer of wooden panel) and crack width evolution.

The high relation between C and T_s-RH_s allowed deriving the dose-response function by minimising the coefficients of the equation (4). The coefficients are reported in Table 14. Figure 30 shows the measured C and the C modelled (C_m) starting from T_s-RH_s. The discrepancy between C and C_m, expressed as RMSE, is 0.014 mm, i.e. lower than the crack-width meter's accuracy (Table 4), as well the coefficient of determination (R^2) is 0.86 (Figure 31), meaning that the model well replicates the observed outcomes. The dose response function, indeed, is well calibrated and can be used for the following purposes.

Table 14 Equation coefficients calculated by a non-linear multiple regression.

a	b	c
6.4790	-0.0542	-0.0004

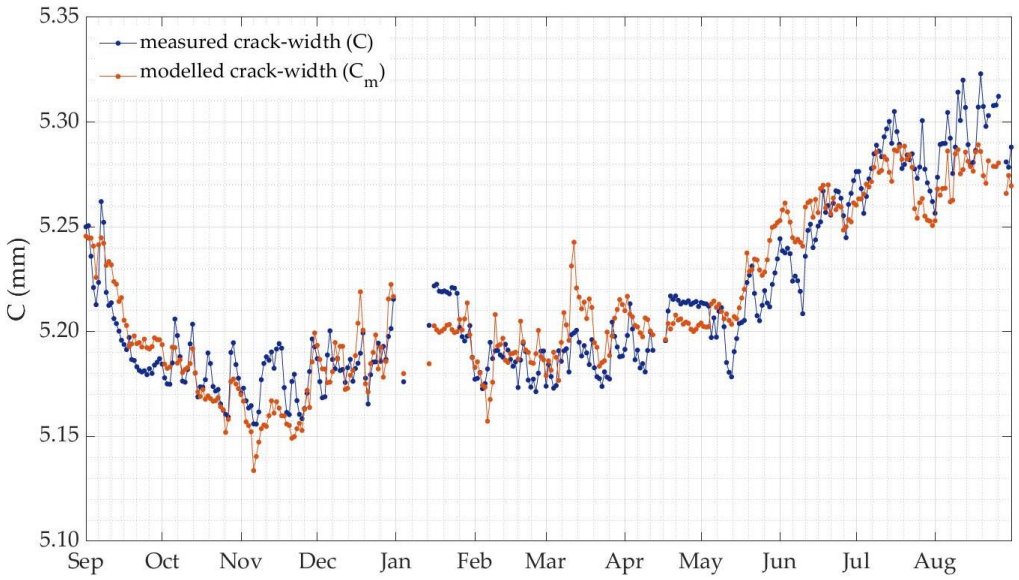

Figure 30 Measured crack width (C) and modelled crack width (C_m) from September 2016 to August 2017 are plotted as blue and orange lines, respectively. The uncertainty related to C_m is 0.008 mm.

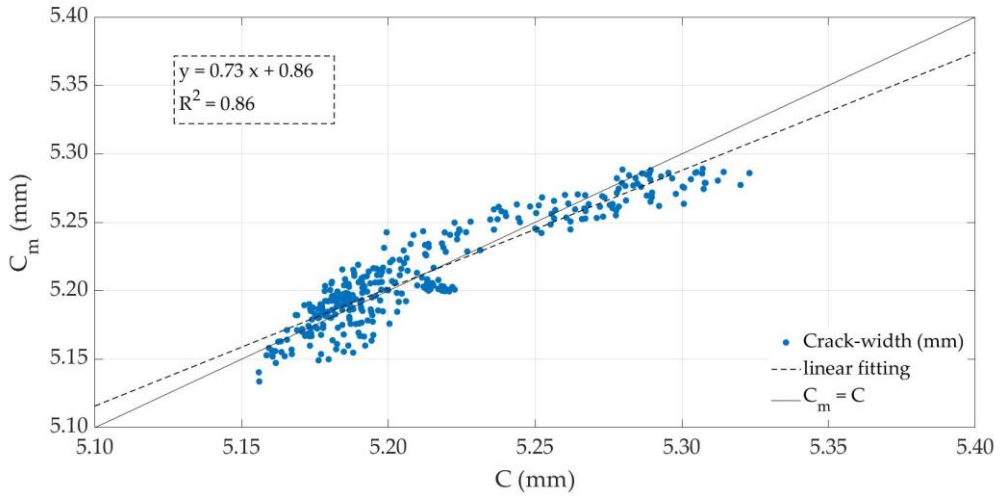

Figure 31 Scatter diagram of modelled crack width (C_m) *vs* measured crack width (C). Dashed line is the linear fitting, whose equation is reported on the top right. Solid line is the bisector.

The simulation environment

The results from the Sensitivity Analysis (SA) by means of the Elementary Effects method (EEs) was carried out using the eighteen general input parameters reported in Table 9. Figure 32 shows that the indoor T is strongly affected by the thermal bridge of external walls envelope (X8) and external wall-slab (X9) in all the three rooms. The effect is monotonic – almost monotonic, since σ/ μ* is lower than 0.5. This means that most of EEs, i.e. 95% with the assumption of normal distribution, has the same sign and the model response can be considered as monotonic with respect to the input factor (X_i).

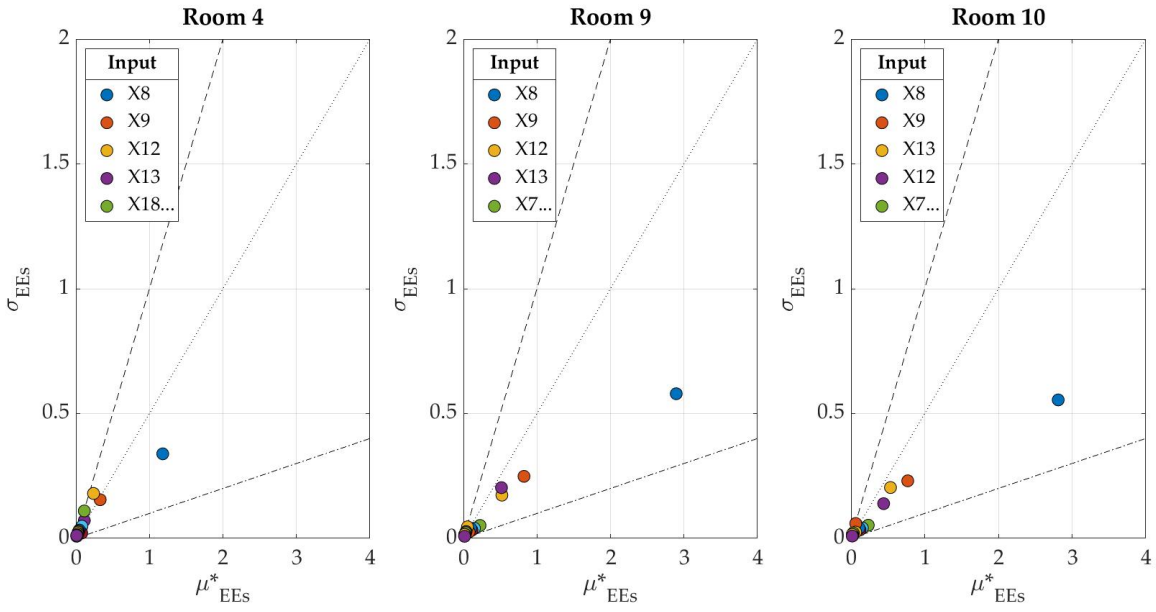

Figure 32 Scatter plot (σ *vs* μ*) of Elementary Effects method performed using the Mean Absolute Error (MAE) from hourly temperature data as target function. The eighteen input parameters are indicated as coloured dots and labelled as in Table 9. Four areas delimited by the ratio σ/μ* indicate the effect of parameter on model: dash-dotted line is σ/μ* = 0.1 (linear effect), dotted line is σ/μ* = 0.5 (monotonic effect), dashed line is σ/μ* = 1 (almost monotonic effect). The area above σ/μ* = 1 represents a non-linear and/or a non-monotonic effect.

Figure 33 shows that the indoor RH of building model is strongly affected by the infiltration rate (X18), especially in the case of room 9 (mid panel) and 10 (right panel), and on average from the thermal bridges (X8 and X9) as in the case of EEs calculated for temperature. The effect of the infiltration rate is clearly non-linear and non-monotonic, since the absolute average μ* is very different from the absolute average (μ_i) and the input parameter's effect is more influenced by σ.

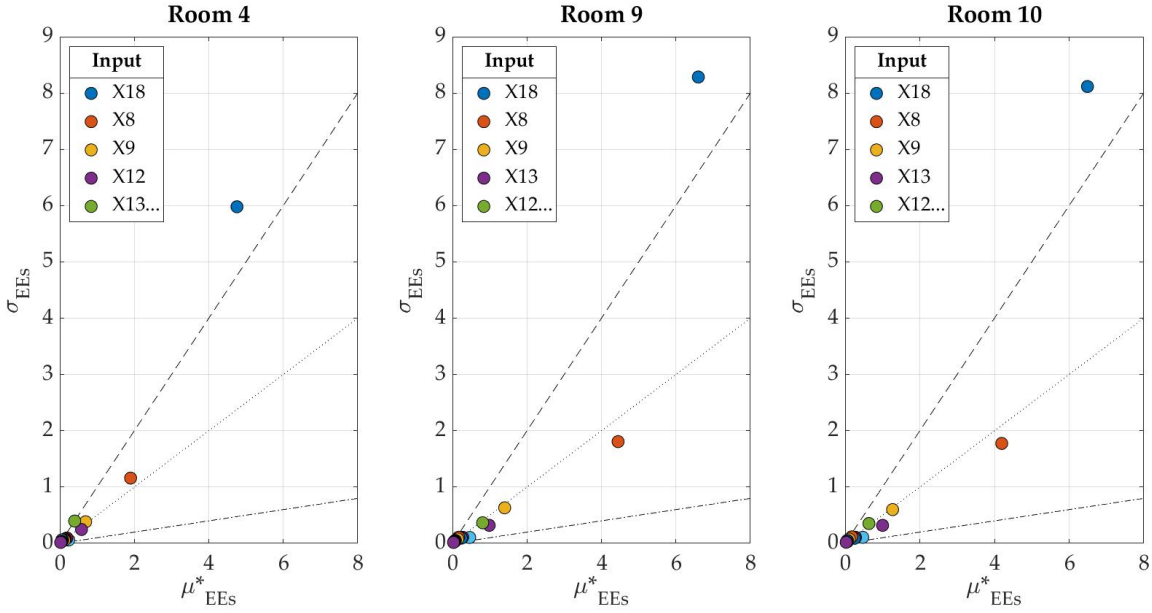

Figure 33 Scatter plot (σ *vs* μ*) of Elementary Effects method performed using the Mean Absolute Error (MAE) from hourly relative humidity data as target function. The eighteen input parameters are indicated as coloured dots and labelled as in Table 9. Four areas delimited by the ratio σ/μ* indicate the effect of parameter on model: dash-dotted line is σ/μ* = 0.1 (linear effect), dotted line is σ/μ* = 0.5 (monotonic effect), dashed line is σ/μ* = 1 (almost monotonic effect). The area above σ/μ* = 1 represents a non-linear and/or a non-monotonic effect.

Starting from the outcomes of SA, the building model was calibrated using the most influential input parameters by means of the PSO-GPSHJ genetic algorithm. In this step, the thermal properties of wooden slabs were added in order to furtherly include the surface temperature (T_s) of the wooden ceiling in the calibration of room 9. The automatic calibration lasted about 3 hours and consisted of 225 simulation runs.

Table 15 reports the statistics about the automatic calibration for the three rooms. The MAE is, on average, 0.3°C for T, 1.6% for RH and 0.2°C for T_s. The RMSE is, on average, 0.4°C for T, 2.1% for RH and 0.2 for T_s. The CV-RMSE is less than 2.0% for T, less than 1.0% for T_s and less than 5.0% for RH. The building model is well calibrated, since the discrepancy between modelled and measured data is close to the instrumental accuracy as reported in Table 4. Finally, the correlation between modelled and measured data is $r_s > 0.9$ for T, $r_s > 0.6$ for RH and $r_s = 0.9$ for T_s.

Then, the building model was run in the validation period (from September 24th, 2017 till October 8th, 2017). It was found that the discrepancy between modelled and measured data increases. Indeed, the RMSE is, on average, 0.6°C for T, 3.2% for RH and 0.5 for T_s; as well as the CV-RMSE is less than 3.0% for T, less than 3.0% for T_s and less than 8.0% for RH. The correlation between modelled and measured data decreases for all

parameters. The decrease of statistics during the validation might be due to the effect of the summer cooling, i.e. the building is still not acclimatised with the outdoor climate.

Table 15 Summary of the calibration statistics of air temperature (T) and relative humidity (RH) in rooms 4, 9 and 10, and the surface temperature (T_s) in room 9 (MAE: mean absolute error; RMSE: root mean square error; CV-RMSE: coefficient of variation of RMSE; r_s: Spearman's rank correlation coefficient).

Statistics	**T**	**RH**	**T_s**
		Room 4	
MAE	0.4°C	1.5%	
RMSE	0.5°C	2.1%	
CV-RMSE	1.8%	4.3%	
r_s	0.8	0.6	
		Room 9	
MAE	0.4°C	1.6%	0.2°C
RMSE	0.4°C	2.0%	0.2°C
CV-RMSE	1.7%	3.9%	1.0%
r_s	1.0	0.7	0.9
		Room 10	
MAE	0.3°C	1.6%	
RMSE	0.4°C	2.2%	
CV-RMSE	1.6%	4.6%	
r_s	1.0	0.7	

Table 16 reports the statistics about the manual calibration performed for room 9 modelled with the HMWall model. It is clear that the use of the HMWall model allows better simulate the relative humidity inside the room, halving the error between modelled and measured RH and increasing their correlation from 0.7 to 0.9. As well, indoor temperature is better modelled. This outcome encourages the use of hygrothermal tool for historic building modelling. Figure 34 shows measured and modelled T (upper panel) and RH (lower panel) trends taking into account the instrumental uncertainty of T-RH sensors (shaded area).

Table 16 Summary of the calibration statistics of air temperature (T), relative humidity (RH) and the surface temperature (T_s) in room 9 modelled extending IDA ICE with the HMWall model (MAE: mean absolute error; RMSE: root mean square error; CV-RMSE: coefficient of variation of RMSE; r_s: Spearman's rank correlation coefficient).

Statistics	**T**	**RH**	**T_s**
		Room 9 (HMWall model)	
MAE	0.2°C	0.8%	0.4°C
RMSE	0.3°C	1.0%	0.5°C
CV-RMSE	1.2%	2.0%	2.1%
r_s	1.0	0.9	0.9

In the validation period, the discrepancy between modelled and measured T does not change. On the contrary, it was found for RH: MAE = 1.0%, RMSE = 1.2%, CV-RMSE = 2.4% and r_s = 0.7.

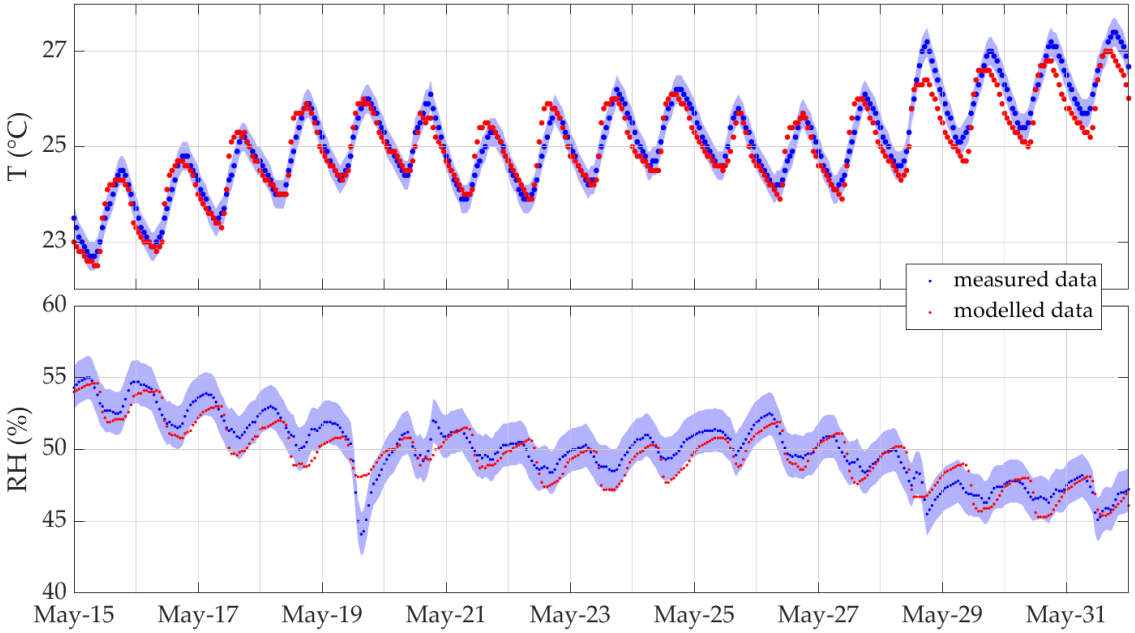

Figure 34 Measured (blue dots) and modelled (red dots) temperature (T) and relative humidity (RH) trends inside room 9. The shaded area represents the measurement uncertainties: ±0.3°C and ±1.5%, respectively.

The calibrated room 9 model is characterised by the hygrothermal properties reported in Table 17; whereas the infiltration and the thermal bridges were summarised in Table 18. A summary of the main features of room 9 is listed below:

- a floor area of 62 m^2 and a volume area of 185 m^3;
- three external walls of 0.6 m a thermal transmittance (U-value) of 1.4 W m^{-2} K^{-1} (material properties in Table 17);
- an adiabatic internal wall of 0.6 m with a U-value of 1.1 W m^{-2} K^{-1} and connected to a RH value of 50% (material properties in Table 17);
- an adiabatic floor with a U-value of 2.7 W m^{-2} K^{-1} and connected to a RH value of 50% (material properties in Table 17);
- an internal wooden ceiling of 0.08 m with a U-value of 3.5 W m^{-2} K^{-1} and connected to a RH value of 55% with the above crawl space (material properties in Table 17);
- poor thermal bridges (Table 18);
- a fixed infiltration at 0.02 ACH (Table 18);
- a glazing system with wooden-framed low-emission double panes (6-12-6 mm filled with air) characterised by a U-value of 1.6 W m^{-2} K^{-1} and a solar heat gain coefficient (SHGC) of 0.4. All windows have an area of 1.5 m^2 and are covered by black interior roller shades.

Table 17 The list of building materials and the changed hygrothermal properties (as bold) of building materials obtain from the calibration of room 9.

Material	Hygrothermal properties						
	ρ	**c_p**	**λ**	**μ**	**w_{80}**	**w_f**	**A_w**
	kg/m³	J/(kg·K)	W/(m·K)	-	kg/m³	kg/m³	kg/(m²·h$^{0.5}$)
brick	1900.0	1000.0	**1.06**	28.0	24.9	250.0	2.70
concrete	2104.0	776.0	**1.81**	76.1	101.0	144.0	0.75
lime plaster	1600.0	850.0	**0.65**	7.0	30.0	250.0	3.00
light mortar	830.0	1000.0	**1.20**	13.2	26.3	423.0	1.63
wood	740.0	**740.0**	0.81	223.0	**155.0**	349.0	**15.00**

Table 18 Parameters update with respect to the initial building model and used in the calibrated building model. Each parameter is identified by a code as in Table 9. Parameters' abbreviation: TB = thermal bridge, EXTW-INTW = external-internal wall, EXTW-CORN = external wall-inner corner, WIN = windows, ROOF = roof, INTW-ROOF = internal wall-roof, INFILT = infiltration.

cod.	Parameter	Unit	Calibrated model value
X10	TB EXTW-INTW	W/(m·K)	0.6667
X11	TB EXTW-CORN	W/(m·K)	-0.07
X12	TB WIN	W/(m·K)	1.0
X13	TB ROOF	W/(m·K)	0.85
X14	TB INTW-ROOF	W/(m·K)	0.40
X18	INFILT	ACH	0.02

The control climate strategy

The calibrated room model was used to estimate the effect of the dynamic temperature control strategy on the conservation of wooden ceilings, by replacing the estimated T-RH into equation 1. The conservation needs and the thermal comfort requirements were both considered.

For the above control strategies inside room 9, the peak demand is 2.6 kW during heating hours and 1.6 kW during cooling hours; whereas the annual energy consumption is 4532 kWh and 1877 kWh, respectively.

Figure 35 shows the psychrometric chart of the estimated T-RH data related to the new climate control configuration. The annual averages of T and RH are 22.3°C and 54.9%, respectively. The hygrothermal data are less scattered with respect to the actual environmental conditions (T ranges between 19.8°C and 25.8°C and RH ranges between 47.7% and 65.4%). T-RH data are within the allowable limits in 41.5% of time. Specifically, in Winter, T is 91% of time below the lower T limit (20.3°C); whereas RH is 56% of time above the RH upper limit (59.9%), never exceeding the value of 64.5%. In Spring, T-RH data are within the allowable area in more than 85% of time, even though RH is below the lower limit and above the upper limit in 5% and 8% of time, respectively. In Summer, T is always above the upper limit (24.3°C), however it never exceeds 25.8°C; whereas RH is below the lower limit (49.9%) in 18% of time. Finally, in Autumn, warmer

episodes than the upper T limit (on average 15%) are related to September; whereas RH is lower than 49.9% in 5% of time. Moreover, the daily spans are less than 2.5°C for T and less than 4.0% for RH.

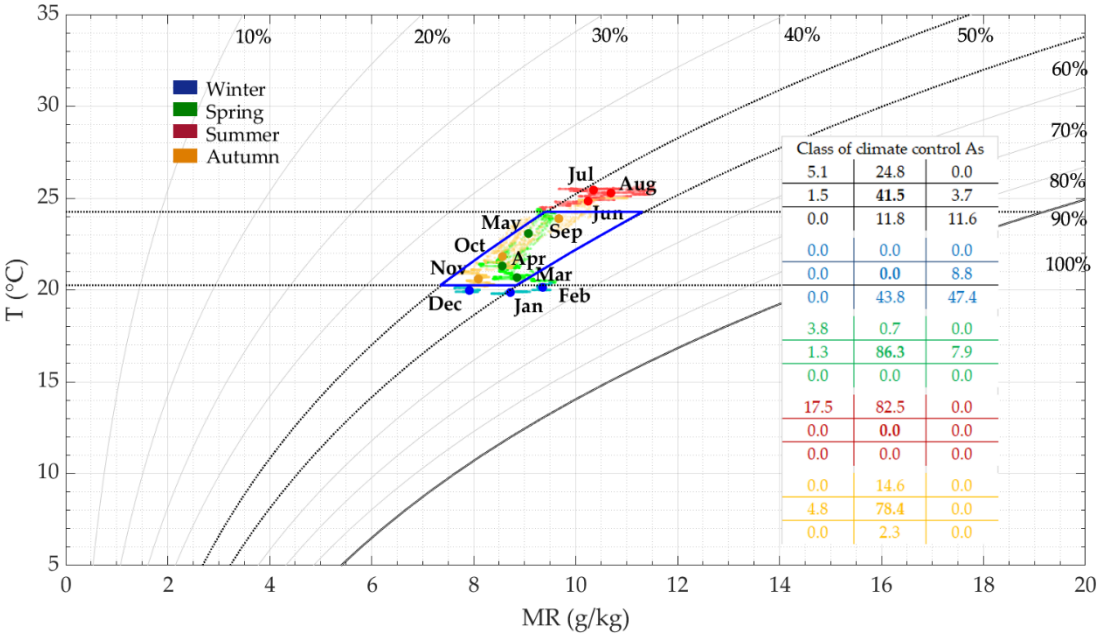

Figure 35 Psychrometric chart. Indoor climate within room 9 with the new climate control strategy is seasonally grouped: blue (winter), green (spring), red (summer), and orange (autumn). Seasonal monthly averages are also displayed. The class of climate control As area is delimited by two horizontal blue lines (T = 22.3 ± 2°C) and two blue curves (RH = 54.9 ± 5%). The T and RH limits divide the chart into nine parts and the percentage of data within limits is represented by the 3-by-3 matrixes on the right.

Figure 36 shows the histogram with the percentage of occurrences of C in: i) current climate conditions (black-white bins); ii) the free-floating (red bins) and iii) the new climate control strategy (blue bins). Cm is calculated from the equation 1 in ii) and iii) by replacing Ts and RHs with those retrieved as output from the simulation file.

In i) case, the observed cracks range between 5.15 mm and 5.35 mm and, among those, about 20% is above 5.25 mm, corresponding to the Summer.

In ii) case, the T-RH conditions allow to meet the conservation requirements in 22% of time, since T is below the lower limit in 47% of time and above the upper limit in 32% of time. The thermal comfort requirement of visitors, instead, is reached only in 10% of time, since T is below the ATL lower limit in 58% of time in cold season and above the ATL upper limit in 32% of time in warm season. Finally, RH is about 51% of time below the RH lower limit in the warm season. In these climate conditions, as shown in Figure 11a, about 15% of data is within the range of 5.00-5.05 mm, when, in cold period, T is <15°C and RH is >60%. Instead, about 27% of data is within the range of 5.25-5.35 mm, when, in warm period, T increases up to 31°C and RH decreases below 40%.

On the contrary, in iii) case, the new control of the indoor climate determines a reduced annual variation between minimum and maximum width of wooden cracks, since it is 0.10 mm instead of 0.20 mm in current conditions and 0.25 mm in free-floating. This

means that, when both thermal comfort and conservation needs are satisfied, wooden panels would experience less stresses and, consequently, less strains.

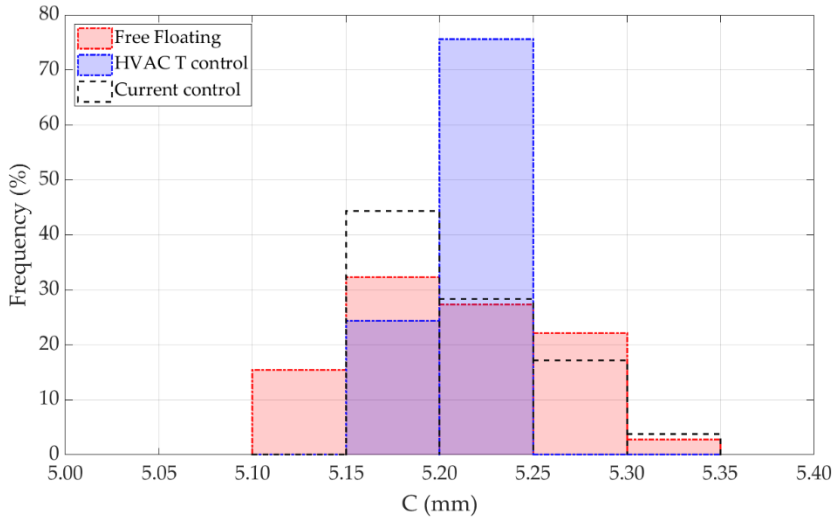

Figure 36 Histogram plot with the percentage of occurrences (%) of crack width (C) observations (black-and-white bins), when the indoor climate is free-floating (red bins) and when it is controlled by a dynamic T safe-band (blue bins).

Looking at Figure 36, i.e. the histograms of daily span of Cm (ΔCm), the current conditions is characterised by daily stresses up to 0.06 mm. On the contrary, the free-floating strategy might induce daily stress up to 0.03 mm per day. If a control of indoor climate is considered, the daily span is less than 0.01 mm in more than 80% of the occurrences.

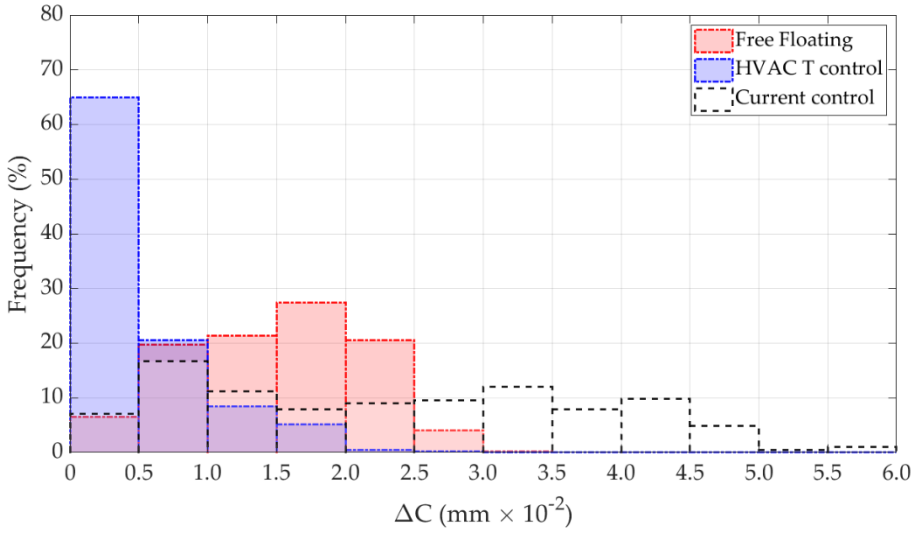

Figure 37 Histogram plot with the percentage of daily span (ΔC) of crack width observations (black-and-white bins), when the indoor climate is free-floating (red bins) and when it is controlled by a dynamic T safe-band (blue bins).

It results that a dynamic temperature control is more effective to reduce the stress-and-strain cycle in wooden ceilings, since it reduces both the annual spread of cracks and, especially, their daily spans. It is worth to notice that the T control, so as that designed,

can guarantee the control of RH as recommended by the class of climate control As in more than 70% of time. Nevertheless, this implies that a new climate control strategy cannot be designed only with the temperature control, because the HVAC system should be integrated with a de/humidifying device in order to guarantee the RH control, as well.

Chapter 5: Conclusions

This final chapter describes the general conclusions and the answers to the research questions, reported in Chapter 1. Finally, some suggestions are proposed for further researches.

General conclusions

My thesis addresses a very important timely topic in the preventive conservation providing a strategy in the control and management of the indoor climate within historic buildings which house permanent collections. To achieve this purpose, my research focused on combining experimental data and dynamic simulation approach. Particular attention was paid to the simultaneous modelling of heat and moisture through the walls of the building as well as to the stress-and-strain cycle in hygroscopic materials related to moisture-induced dynamics. There were four main reasons which have prompted this research: (1) providing a robust quality assessment of the microclimate measurements; (2) developing a specific dose response function for mechanical degradation of restrained hygroscopic materials; (3) extending the features of a commercial whole building dynamic simulation software, the IDA Indoor Climate and Energy, with a one-dimensional heat and moisture transfer model (the HMWall model); (4) easing the set-up of the building model for historic buildings using hourly temperature and relative humidity data. The issues (3) and (4) were needed for using the dynamic simulation as a diagnostic tool. The issue (2) was needed to exploit the simulation as a predictive tool. The dynamic simulation, as a diagnostic tool, allows to identify sources or sinks of heat and moisture that determine and affect the dynamic behaviour of environmental conditions. The dynamic simulation, as a predictive tool, provides useful data on the indoor climate within the building as the result of changes in boundary conditions or air-conditioning systems. Empirical and specific degradation model, i.e. a dose-response function, allows to know how the estimated indoor conditions affect the conservation state of the artworks.

The specific purposes were achieved using different case studies and the whole methodology (i.e. the general objective of my research) was successfully exploited in the

case of the Archaeological Museum of Priverno, which might be defined as the pilot case study in the developed preventive conservation strategy.

The application of the method to the case study of the Archaeological Museum of Priverno has proved that the building model which more accurately simulates the indoor temperature and relative humidity dynamics is that in which a hygrothermal transfer model of opaque building components is included in the dynamic simulation software. Furthermore, the semi-automatization of calibration method using hourly measurements of climate variables is effective to design a building model as representative as possible of the actual case.

In addition, the study has demonstrated that long-term indoor climate observations coupled with the monitoring of the crack width of wood can be effectively used to investigate on the indoor climate aimed at reducing the stress-and-strain cycle of valuable wooden ceilings, and improving the thermal comfort. The new climate control strategy has the main advantage to consider the historical climate at which wooden ceilings have been kept over the last years. This means that the application of the dynamic temperature safe-band does not imply any abrupt changes in the indoors, highly reducing further triggers of degradation.

It is worth to notice that this methodology takes advantages only if a thorough knowledge of the indoor climate and its interaction with the objects is reached. Even if the method has been applied to a particular case study, the Archaeological Museum of Priverno (Italy), it can be potentially exploited for other cases in which also other types of degradation are present, providing that a degradation response function or its empirical evaluation of object is available.

The proposed approach results to be completely non-invasive, non-destructive and with zero-costs in terms materials. Indeed, the conservative quality of the exhibition spaces after modification of the indoor climate is directly assessed in the simulation environment. In this way, outcomes can support advantageously decision-making for a better control and management of the exhibition environment.

To sum up, a thorough and meticulous assessment of the microclimate, given by the combination of on-site measurements and dynamic simulation, plays a crucial role in investigating the interaction between hygrothermal variables and the degradation process, estimated by means of degradation markers. Besides as emerged in the literature review and in this thesis, the relative humidity strongly affects the degradation processes of hygroscopic materials and, for this reason, it must be measured, modelled and predicted as accurately as possible. Only when this is achieved, it is possible to use consciously the dynamic simulation tools in the field of the preventive conservation.

Answers to research questions

In this section, the answers to research questions are listed:

1. *Is it possible to objectively assess the quality of indoor climate time series to apply the recent standards and guidelines?*

   Yes, it is possible to objectively assess the quality of temperature and relative humidity time series. Three indexes have been proposed to objectively assess the quality of time series: the Completeness Index (CoI), the Continuity Index (CI) and the Microclimate Quality Index (MQI). The indexes range between zero and unity. The CoI and the CI should be used in complementary way. It was found that for CoI and CI values > 0.6 reliable and robust results are provided by data mining. The MQI was specifically defined for the analysis of historic climate. The MQI synthetises the information about the length of the time series, as required by climate records (at least 12 months), and the sensors' accuracy, as suggested by the current European standards. For the same length, the MQI ranges between 0.7, if the sensor's accuracy is low, and 1.0, if it is high. The indexes were tested for the first time in the Mogiła Abbey – Krakow, Poland (Appendix A). The indexes were also successfully used to identify the most proper period within a longer data collection (seven years), which had several missing intervals of values due to the malfunction of sensors over years (Museo Napoleonico – Rome, Italy) (Appendix B). In the case of the Archaeological Museum of Priverno, the indices were used to assess the robustness of the monitoring system in gathering and recording data.

2. *Can the observed degradation measurements be related to the indoor climate and used to predict the effect of new control climate strategy on degradation?*

   Yes, it can. The shrinkage-swelling of organic-hygroscopic materials (wood, textile, paper, etc.) due to indoor climate is not the source of its damage unless the object is restrained. In such a case, a relationship can be found between the T-RH variables and the strain of material measured as crack width (C). A dose-response function of C can be derived using a no-linear multiple regression. The dose-response function was applied to two different hygroscopic materials: the faunal remains (La Polledrara di Cecanibbio – Rome, Italy) and the wooden ceilings of a historic building (the Archaeological Museum of Priverno –Italy). The dose-response function proved to be effective as a damage tracking, when it is used to assess a retrofitting solution or a new climate control strategy in the environment simulation. In both cases, the estimated T-RH data can be inserted in the dose-response function to pinpoint the extent of the crack width behaviour. In the case of La Polledrara di Cecanibbio (Appendix C), a retrofitting strategy was evaluated based on the use of building integrated photovoltaics (BIPVs) as shading elements and ancillary source of electrical power. The dose-response function allowed to evaluate the dynamic behaviour of C both in passive (air-conditioning system is off) and active control (air-conditioning system is on) of indoor climate. It was found that the only control of temperature in winter might induce a C widening with respect to the initial conditions due to drops in RH values. In the case of the Archaeological Museum of Priverno, the estimated hygrothermal variable from the novel control strategy, which

considers the historical climate at which the wooden ceiling has been kept over the last years, has demonstrated to be effective in reducing the annual variability of crack-width and the maximum daily fluctuations with respect to the current hygrothermal conditions.

3. *How can a hygrothermal model be validated and then used in the field of preventive conservation?*

   The performance of the HMWall model, as an extension of the IDA Indoor Climate and Energy (IDA ICE) software, was carried out and assessed using exercises at the increasing complexity: i) a semi-infinite wall, ii) an adiabatic building envelope, iii) a modern building and iv) a historic building.
   The validation was based on: a) the general standard procedure (analytical verification) for exercise i; b) output provided by another simulation code (comparative test) for exercise ii; c) experimental data collected during field campaigns (empirical validation) for exercise iii and iv. The general standard procedure showed that the HMWall code properly calculated the heat transfer and underestimated the moisture transfer. The comparative test, indeed, has revealed that the code did not properly calculate the saturated pressure of water vapour (p_{sat}) and did not include the water vapour transfer (g_v) between the wall surface and the boundary air layer close to it. However, the latter parameter showed to be not relevant and not affecting the moisture flow (Appendix D). I improved the HMWall code concerning p_{sat} and the liquid transfer coefficient (D_φ). The modified HMWall code revealed to be more performing with respect to the original code, providing more realistic results in all exercises (Appendix E). It is worth to notice in the exercise iv (Chiesa di Santa Rosalia – Palestrina, Italy) that the integration of the IDA ICE with the updated HMWall model improves the simulation of the moisture behaviour with respect to the IDA ICE as it is, halving the discrepancy between the measured and modelled relative humidity. Moreover, good results were achieved in the case of the Archaeological Museum of Priverno, since a better modelling of indoor temperature and relative humidity was performed. These outcomes encourage the use of the building dynamic simulation tool integrated with a hygrothermal code in modelling those buildings where the moisture plays a key role in degradation phenomena.

4. *Can a semi-automatic calibration of building model with indoor temperature and relative humidity measurements be implemented for historic buildings?*

   Yes, it can. To better calibrate the building model of a historic building, the existing calibration procedure was integrated with the Sensitivity Analysis (SA) by using the Elementary Effects (EEs) method. This step is fundamental to find the most relevant input parameters of the building model before of reducing the discrepancy between modelled and measured data by means of a manual calibration, i.e. input parameters have changed step-by-step by the user, or of genetic algorithms, i.e. input parameters automatically change to achieve the minimisation. The integration was performed coupling IDA ICE with the MatLab environment. The MatLab code was programmed

to iteratively: set the input parameters, initialize IDA ICE, run simulations and execute the EEs. The output of SA provides the principal statistic outcomes and visualizes the scatter plot of EEs. This allows busting the choice of input parameters to use in the Genetic Optimization (GenOpt®, already implemented in IDA ICE library). GenOpt uses a hybrid approach coupling the Particle Swarm Optimization with the General Pattern Search of Hooke-Jeeves (PSO-GPSHJ) to minimize the discrepancy between modelled and measured hourly data. The whole calibration procedure lasts about 24-36 hours, depending on the complexity of the building model. In the calibration procedure hourly indoor climate data (T and RH) were used as target variables. Since no recommendation exists on the acceptable tolerance of the calibration using hourly indoor climate data, it has been estimated that the discrepancies between measured and modelled data must be close to the instrumental accuracies. This is a further reason to trigger the assessment of high-quality T-RH data. The procedure has been tested for the calibration of a modern building (La Polledrara di Cecanibbio – Rome, Italy) (Appendix F). It has also revealed to be successfully exploited for the calibration of historic buildings, as demonstrated in the case of the Archaeological Museum of Priverno (Latina, Italy).

Future researches

The achieved outcomes are encouraging for the integration of other crucial elements in the preventive conservation activities.

The potential use of empirical dose-response functions as a damage target for assessing the environmental quality of the exhibition space leads to develop sustainable conservation strategy based on multi-objective optimization. In this way, the climate control or the retrofitting solution can be addressed in order to simultaneously consider the conservation of artworks, the thermal comfort of users, the energy and costs savings.

Most of the research was dedicated to investigating the performance of the HMWall model as an extension of the IDA ICE software for modelling the heat air and moisture transfer through walls. Even though the main errors in the code was solved, some crucial elements should be still integrated. The first is the implementation of a library with the hygrothermal properties of the most common building materials. This would ease the use of the modelling object that has to be filled in and used at advanced level. The second is the optimization of liquid water loads at wall level that poses new interesting research goals. This is very important to study the effect of precipitation on the heat and moisture balance of the building envelope and to assess the presence of liquid water in damp sites, such as hypogea, crypts, cellars and underground storage spaces. The latter aspect is a topic very little explored till now and suggests the potential use of such a dynamic model in other fields, such as food and drink storage and conservation.

This page intentionally left blank

References

Adan, O.C.G. (1994). On the fungal defacement of interior finishes. Doctoral dissertation, Eindhoven University of Technology, Eindhoven, the Netherlands.

Antretter, F., Kosmann, S., Kilian, R., Holm, A., Ritter, F., & Wehle, B. (2013). Controlled Ventilation of Historic Buildings: Assessment of Impact on the Indoor Environment via Hygrothermal Building Simulation. In Hygrothermal Behavior, Building Pathology and Durability (pp. 93-111). Springer, Berlin, Heidelberg.

Ascione, F., De Rossi, F., & Vanoli, G. P. (2011). Energy retrofit of historical buildings: theoretical and experimental investigations for the modelling of reliable performance scenarios. Energy and buildings, 43(8), 1925-1936.

Ascione, F., Bianco, N., De Masi, R. F., de'Rossi, F., & Vanoli, G. P. (2015). Energy retrofit of an educational building in the ancient center of Benevento. Feasibility study of energy savings and respect of the historical value. Energy and Buildings, 95, 172-183.

Ashley-Smith, J., Umney, N., & Ford, D. (1994). Let's be honest—realistic environmental parameters for loaned objects. Studies in Conservation, 39(sup2), 28-31.

Balocco, C., & Grazzini, G. (2007). Plant refurbishment in historical buildings turned into museum. Energy and buildings, 39(6), 693-701.

Barclay, M., Holcroft, N., & Shea, A. D. (2014). Methods to determine whole building hygrothermal performance of hemp–lime buildings. Building and environment, 80, 204-212.

Becherini, F., Bernardi, A., & Frassoldati, E. (2010). Microclimate inside a semi-confined environment: Valuation of suitability for the conservation of heritage materials. Journal of Cultural Heritage, 11(4), 471-476.

Bellia, L., Alfano, F. R. D. A., Giordano, J., Ianniello, E., & Riccio, G. (2015). Energy requalification of a historical building: A case study. Energy and Buildings, 95, 184-189.

Bernardi, A., & Camuffo, D. (1995). Microclimate in the chiericati palace municipal museum, Vicenza. Museum Management and Curatorship, 14(1), 5-18.

Bertolin, C., Camuffo, D., & Bighignoli, I. (2015). Past reconstruction and future forecast of domains of indoor relative humidity fluctuations calculated according to EN 15757: 2010. Energy and Buildings, 102, 197-206.

Bichlmair, S., Krus, M., Kilan, R., & Sedlbauer, K. (2012). Building simulation modelling of the historic building Linderhof Palace taking account visitors. In 7th IBPSA Conference (pp. 296-309).

Bratasz, L., Camuffo, D., & Kozłowski, R. (2007a). Target microclimate for preservation derived from past indoor conditions. In T. Padfield, K. Borchersen (Eds.), Contributions to the museum microclimates conference, The National Museum of Denmark, Copenhagen (2007), pp. 129-134.

Bratasz Ł., Kozłowski R., Camuffo D. & Pagan E. (2007b) Impact of Indoor Heating on Painted Wood - Monitoring the Altarpiece in the Church of Santa Maria Maddalena in Rocca Pietore, Italy. Studies in Conservation, 52(3), 199-210.

Bratasz Ł. (2012) Allowable microclimatic variations in museums and historic buildings: reviewing the guidelines, in: J. Ashley-Smith, A. Burmester, M. Eibl (Eds.), Climate for

Collections—Standards and Uncertainties, Postprints of the Munich Climate Conference, London, 2012, pp. 11–19.

Bratasz, Ł. (2013). Allowable microclimatic variations for painted wood. Studies in Conservation, 58(2), 65-79.

Brown, J. P., & Rose, W. B. (1996). Humidity and moisture in historic buildings: the origins of building and object conservation. APT bulletin, 27(3), 12-23.

Brown, J. P. (1994). Hygrometric measurement in museums: calibration, accuracy, and the specification of relative humidity. Studies in Conservation, 39(sup2), 39-43.

Campolongo, F., Saltelli, A., & Cariboni, J. (2011). From screening to quantitative sensitivity analysis. A unified approach. Computer Physics Communications, 182(4), 978-988.

Camuffo, D. (1983). Indoor dynamic climatology: investigations on the interactions between walls and indoor environment. Atmospheric Environment (1967), 17(9), 1803-1809.

Camuffo, D., & Bernardi, A. (1996). Controlling the microclimate and particulate matter inside the historic anatomy theatre, Padua. Museum Management and Curatorship, 15(3), 285-298.

Camuffo, D., Sturaro, G., & Valentino, A. (1999). Thermodynamic exchanges between the external boundary layer and the indoor microclimate at the Basilica of Santa Maria Maggiore, Rome, Italy: the problem of conservation of ancient works of art. Boundary-Layer Meteorology, 92(2), 243-262.

Camuffo, D., Van Grieken, R., Busse, H. J., Sturaro, G., Valentino, A., Bernardi, A., ... & Wieser, M. (2001). Environmental monitoring in four European museums. Atmospheric Environment, 35, S127-S140.

Camuffo, D., & Giorio, R. (2003). Quantitative evaluation of water deposited by dew on monuments. Boundary-layer meteorology, 107(3), 655-672.

Camuffo, D., Pagan, E., Bernardi, A., & Becherini, F. (2004). The impact of heating, lighting and people in re-using historical buildings: a case study. Journal of Cultural Heritage, 5(4), 409-416.

Camuffo, D., & Della Valle, A. (2007). Church heating: a balance between conservation and thermal comfort. Contribution to the Experts' Roundtable on Sustainable Climate Management Strategies, Tenerife, Spain.

Camuffo, D., Pagan, E., Rissanen, S., Bratasz, Ł., Kozłowski, R., Camuffo, M., & della Valle, A. (2010). An advanced church heating system favourable to artworks: A contribution to European standardisation. Journal of Cultural Heritage, 11(2), 205-219.

Camuffo, D., Bertolin, C., Bonazzi, A., Campana, F., & Merlo, C. (2014). Past, present and future effects of climate change on a wooden inlay bookcase cabinet: a new methodology inspired by the novel European Standard EN 15757: 2010. Journal of Cultural Heritage, 15(1), 26-35.

Camuffo D (2014) Microclimate for cultural heritage (second edition) conservation, restoration, and maintenance of indoor and outdoor monuments. Elsevier, Amsterdam.

Cardinale N., Rospi G. and Stazi A. (2010) Energy and microclimatic performance of restored hypogeous buildings in south Italy: The "Sassi" district of Matera. Building and Environment. 45(1), 94-106

Cassar, M., & Pender, R. (2003). Climate change and the historic environment. ISBN: 0-9544830-6-5

Cataldo, R., De Donno, A., De Nunzio, G., Leucci, G., Nuzzo, L., & Siviero, S. (2005). Integrated methods for analysis of deterioration of cultural heritage: the Crypt of "Cattedrale di Otranto". Journal of cultural heritage, 6(1), 29-38.

Caucheteux, A., Stephan, E., & Ouest, C. (2013). Transient simulation calibration of an old building using an experimental design: evaluating uncertainty results. In 13th Conf. Int. Build. Perform. Simul. Assoc., Chambery, France (pp. 677-684).

Coakley, D., Raftery, P., & Keane, M. (2014). A review of methods to match building energy simulation models to measured data. Renewable and sustainable energy reviews, 37, 123-141.

Coelho, G. A., Silva, H., & Henriques, F. A. (2018). Hygrothermal simulation models optimization for historic buildings. Building and Environment. 142, 439-450

Corgnati, S. P., & Filippi, M. (2010). Assessment of thermo-hygrometric quality in museums: Method and in-field application to the "Duccio di Buoninsegna" exhibition at Santa Maria della Scala (Siena, Italy). Journal of Cultural Heritage, 11(3), 345-349.

Cornaro, C., Puggioni, V. A., & Strollo, R. M. (2016). Dynamic simulation and on-site measurements for energy retrofit of complex historic buildings: Villa Mondragone case study. Journal of Building Engineering, 6, 17-28.

De Berardinis, P., Rotilio, M., Marchionni, C., & Friedman, A. (2014). Improving the energy-efficiency of historic masonry buildings. A case study: A minor centre in the Abruzzo region, Italy. Energy and Buildings, 80, 415-423.

De Santoli, L. (2015). Reprint of "guidelines on energy efficiency of cultural heritage". Energy and Buildings, 95, 2-8.

Delgado, J. M., Barreira, E., Ramos, N. M., & de Freitas, V. P. (2012). Hygrothermal numerical simulation tools applied to building physics. Springer Science & Business Media.

Djedjig R, Ouldboukhitine SE, Belarbi R, Bozonnet E (2012). Development and validation of a coupled heat and mass transfer model for green roofs. International Communication of Heat and Mass Transfer, 39: 752–761.

Erhardt, D., Tumosa, C. S., & Mecklenburg, M. F. (2007). Applying science to the question of museum climate. In Museum Microclimates Conference. National Museum of Denmark.

Fassina, V. (2008, May). European Technical Committee 346: Conservation of cultural property: Updating of the activity after a three-year period. In 9th International Conference on Non-Destructive Investigations and Microanalysis for the Diagnostics and Conservation of Cultural and Environmental Heritage: Art 2008, Jerusalem, May 25–30.

Ferdyn-Grygierek, J. (2014). Indoor environment quality in the museum building and its effect on heating and cooling demand. Energy and Buildings, 85, 32-44.

Ferroukhi, M. Y., Djedjig, R., Belarbi, R., Limam, K., & Abahri, K. (2015). Effect of coupled heat, air and moisture transfers modeling in the wall on the hygrothermal behavior of buildings. Energy Procedia, 78, 2584-2589.

Ferroukhi, M. Y., Djedjig, R., Limam, K., & Belarbi, R. (2016). Hygrothermal behavior modeling of the hygroscopic envelopes of buildings: A dynamic co-simulation approach. Building Simulation, 9:5, 501-512.

Filippi, M. (2015). Remarks on the green retrofitting of historic buildings in Italy. Energy and Buildings, 95, 15-22.

Franco, G., Magrini, A., Cartesegna, M., & Guerrini, M. (2015). Towards a systematic approach for energy refurbishment of historical buildings. The case study of Albergo dei Poveri in Genoa, Italy. Energy and buildings, 95, 153-159.

Gibbons, J. D., and S. Chakraborti. Nonparametric Statistical Inference, 5th Ed., Boca Raton, FL: Chapman & Hall/CRC Press, Taylor & Francis Group, 2011.

Glaser, H. (1958). Temperatur und Dampfdruckverlauf in einer homogene Wand bei Feuchteausscheidung. Kältetechnik, 6, 174-181.

Hagentoft, C. E., Kalagasidis, A. S., Adl-Zarrabi, B., Roels, S., Carmeliet, J., Hens, H., and Adan, O. (2004). Assessment method of numerical prediction models for combined heat, air and moisture transfer in building components: benchmarks for one-dimensional cases. Journal of thermal envelope and building science, 27(4), 327-352.

Holm, A., Kuenzel, H. M., & Sedlbauer, K. (2003). The hygrothermal behaviour of rooms: combining thermal building simulation and hygrothermal envelope calculation. IBPSA Proceedings Building Simulation Einhoven.

Huijbregts, Z., Kramer, R. P., Martens, M. H. J., Van Schijndel, A. W. M., & Schellen, H. L. (2012). A proposed method to assess the damage risk of future climate change to museum objects in historic buildings. Building and Environment, 55, 43-56.

Ineichen, P., Perez, R. R., Seal, R. D., Maxwell, E. L., & Zalenka, A. (1992). Dynamic global-to-direct irradiance conversion models. Ashrae Transactions, 98(1), 354-369.

Jakieła, S., & Kozłowski, R. (2008). Numerical modelling of moisture movement and related stress field in lime wood subjected to changing climate conditions. Wood Science and Technology, 42(1), 21-37.

Jakieła, S., Bratasz, U., & Kozłowski, R. (2007). Acoustic emission for tracing the evolution of damage in wooden objects. Studies in conservation, 52(2), 101-109.

Janssen, H., & Christensen, J. E. (2013). Hygrothermal optimisation of museum storage spaces. Energy and Buildings, 56, 169-178.

Janssen, H. (2014). Simulation efficiency and accuracy of different moisture transfer potentials. Journal of Building Performance Simulation, 7(5), 379-389.

Johnsen, J. S. Conservation of cultural heritage—European standards on the environment in: J. Ashley-Smith, A. Burmester, M. Eibl (Eds.), Climate for Collections—Standards and Uncertainties, Postprints of the Munich Climate Conference, London, 2012, pp. 35-44.

Judkoff, R., & Neymark, J. (1995). International Energy Agency building energy simulation test (BESTEST) and diagnostic method (No. NREL/TP-472-6231). National Renewable Energy Lab., Golden, CO (US).

Karagiozis, A., Desjarlais, A., Künzel, H. M., & Holm, A. (2010). The evolution of hygrothermal design: WUFI to WUFI Plus. Journal of Building Enclosure Design, 24-9.

Kompatscher, K., Seuren, S., Kramer, R., van Schijndel, J., & Schellen, H. (2017). Energy efficient HVAC control in historical buildings: a case study for the Amsterdam Museum. Energy Procedia, 132, 891-896.

Kramer, R., van Schijndel, J., & Schellen, H. (2013). Inverse modeling of simplified hygrothermal building models to predict and characterize indoor climates. Building and Environment, 68, 87-99.

Kramer, R., Schellen, H., & van Schijndel, J. (2015). Energy impact of ASHRAE's museum climate classes: a simulation study on four museums with different quality of envelopes. Energy Procedia, 78, 1317-1322.

Kramer, R., van Schijndel, J., & Schellen, H. (2017). Dynamic setpoint control for museum indoor climate conditioning integrating collection and comfort requirements: Development and energy impact for Europe. Building and Environment, 118, 14-31.

Kramer, R., Schellen, L., & Schellen, H. (2018). Adaptive temperature limits for air-conditioned museums in temperate climates. Building Research & Information, 46(6), 686-697.

Krüger, E. L., & Diniz, W. (2011). Relationship between indoor thermal comfort conditions and the Time Weighted Preservation Index (TWPI) in three Brazilian archives. Applied energy, 88(3), 712-723.

Kupczak, A., Sadłowska-Sałęga, A., Krzemień, L., Sobczyk, J., Radoń, J., & Kozłowski, R. (2018). Impact of paper and wooden collections on humidity stability and energy consumption in museums and libraries. Energy and Buildings, 158, 77-85.

Kurnitski, J., & Vuolle, M. (2000, March). Simultaneous calculation of heat, moisture, and air transport in a modular simulation environment. In Proceedings of the Estonian academy of sciences engineering (Vol. 6, No. 1, pp. 25-47).

Künzel, H. M. (1995). Simultaneous heat and moisture transport in building components. One-and two-dimensional calculation using simple parameters. IRB-Verlag Stuttgart.

Lankester, P., & Brimblecombe, P. (2012). Future thermohygrometric climate within historic houses. Journal of Cultural Heritage, 13(1), 1-6.

Leijonhufvud, G., Kjellstrom, E., Brostom T., Ashley-Smith J. and Camuffo D. Uncentainties in damage assessment of future indoor climates. In: J. Ashley-Smith, A. Burmester, M. Eibl (Eds.), Climate for Collections—Standards and Uncertainties, Postprints of the Munich Climate Conference, London, 2012, pp. 11–19.

Leissner, J., Kilian, R., Antretter, F., Huijbregts, Z., Schellen, H. L., & Schijndel, van, A. W. M. (2013). Impact of climate change on historic buildings and future energy demand by using whole building simulation tools. In Implementing Sustainability - Barriers and Chances: Proceedings of SB13, 24-26 April 2013, Munich, Germany (pp. 1-10)

López, C. S. P., & Frontini, F. (2014). Energy efficiency and renewable solar energy integration in heritage historic buildings. Energy Procedia, 48, 1493-1502.

Magrini, A., Lazzari, S., & Marenco, L. (2017). Energy retrofitting of buildings and hygrothermal performance of building components: Application of the assessment

methodology to a case study of social housing. International Journal of Heat and Technology, 35(S1), S205-13.

Martens MHJ (2012) Climate risk assessment in museums: degradation risks determined from temperature and relative humidity data. Doctoral dissertation, Technische Universiteit Eindhoven.

Martínez-Molina, A., Tort-Ausina, I., Cho, S., & Vivancos, J. L. (2016). Energy efficiency and thermal comfort in historic buildings: A review. Renewable and Sustainable Energy Reviews, 61, 70-85.

Mazzarella, L. (2015). Energy retrofit of historic and existing buildings. The legislative and regulatory point of view. Energy and Buildings, 95, 23-31.

McGill, R., Tukey, J. W., & Larsen, W. A. (1978). Variations of box plots. The American Statistician, 32(1), 12-16.

Mecklenburg, M. F. (1991). Some mechanical and physical properties of gilding gesso. InGilded wood: Conservation and history (Doctoral dissertation, ed. D. Bigelow et al. Madison, Conn. Sound View Press. 163-70).

Mecklenburg, M. F., & Tumosa, C. S. (1991). Mechanical behavior of paintings subjected to changes in temperature and relative humidity. Art in transit: studies in the transport of paintings, 173-216.

Mecklenburg, M. F., Tumosa, C. S., & Erhardt, D. (1998). Structural response of painted wood surfaces to changes in ambient relative humidity (pp. 464-483). The Getty Conservation Institute.

Michalski S. (1993) Relative humidity: a discussion of correct / incorrect values. ICOM Committee for Conservation, 2:624–9.

Michalski, S. (1994). A systematic approach to preservation: description and integration with other museum activities. Studies in Conservation, 39(sup2), 8-11.

Michalski, S. (1996). Quantified risk reduction in the humidity dilemma. APT bulletin, 27(3), 25-29.

Michalski, S. (2002, September). Double the life for each five-degree drop, more than double the life for each halving of relative humidity. In Preprints of 13th Meeting of ICOM-CC (pp. 66-72).

Michalski, S. (2007). The ideal climate, risk management, the ASHRAE chapter, proofed fluctuations, and towards a full risk analysis model. Experts roundtable on sustainable climate management strategies, 1-19.

Morris, M. D. (1991). Factorial sampling plans for preliminary computational experiments. Technometrics, 33(2), 161-174.

Muñoz-González, C. M., León-Rodríguez, A. L., & Navarro-Casas, J. (2016). Air conditioning and passive environmental techniques in historic churches in Mediterranean climate. A proposed method to assess damage risk and thermal comfort pre-intervention, simulation-based. Energy and Buildings, 130, 567-577.

Napp, M., & Kalamees, T. (2015). Energy use and indoor climate of conservation heating, dehumidification and adaptive ventilation for the climate control of a mediaeval church in a cold climate. Energy and Buildings, 108, 61-71.

Napp, M., Kalamees, T., Tark, T., & Arumägi, E. (2016a). Integrated Design of Museum's Indoor Climate in Medieval Episcopal Castle of Haapsalu. Energy Procedia, 96, 592-600.

Napp, M., Wessberg, M., Kalamees, T., & Broström, T. (2016b). Adaptive ventilation for climate control in a medieval church in cold climate. International Journal of Ventilation, 15(1), 1-14.

Nicol, J. F., & Humphreys, M. A. (2002). Adaptive thermal comfort and sustainable thermal standards for buildings. Energy and buildings, 34(6), 563-572.

Nicolai, A., Zhang, J., & Grunewald, J. (2007). Coupling strategies for combined simulation using multizone and building envelope models. In Proc. of Building Simulation.

O'Leary, T. P., Menzies, G., & Duffy, A. (2015). The Design of a Modelling, Monitoring and Validation Method for a Solid Wall Structure. Energy Procedia, 78, 243-248.

O'Neill, Z., & Eisenhower, B. (2013, December). Leveraging the analysis of parametric uncertainty for building energy model calibration. In Building simulation (Vol. 6, No. 4, pp. 365-377). Springer Berlin Heidelberg.

Pavlogeorgatos, G. (2003). Environmental parameters in museums. Building and Environment, 38(12), 1457-1462.

Pernetti, R., Prada, A., & Biggio, P. (2013). On the influence of several parameters in energy model calibration: the case of a historical building. In 1st IBPSA Italy conference BSA.

Ramos, N. M., Delgado, J. Q., Barreira, E., & De Freitas, V. P. (2009). Hygrothermal properties applied in numerical simulation: Interstitial condensation analysis. Journal of Building Appraisal, 5(2), 161-170.

Refsgaard, J. C., Arnbjerg-Nielsen, K., Drews, M., Halsnæs, K., Jeppesen, E., Madsen, H., ... & Christensen, J. H. (2013). The role of uncertainty in climate change adaptation strategies—A Danish water management example. Mitigation and Adaptation Strategies for Global Change, 18(3), 337-359.

Roberti, F., Oberegger, U. F., & Gasparella, A. (2015). Calibrating historic building energy models to hourly indoor air and surface temperatures: Methodology and case study. Energy and Buildings, 108, 236-243.

Rode, C., & Woloszyn, M. (2007). Whole-building hygrothermal modeling in IEA Annex 41. In Thermal Performance of the Exterior Envelopes of Whole Buildings: Buildings X (pp. 1-15). American Society of Heating, Refrigerating and Air-Conditioning Engineers.

Rota, M., Corgnati, S. P., & Di Corato, L. (2015). The museum in historical buildings: Energy and systems. The project of the Fondazione Musei Senesi. Energy and Buildings, 95, 138-143.

Saltelli, A., Tarantola, S., Campolongo, F., & Ratto, M. (2004). Sensitivity analysis in practice: a guide to assessing scientific models. John Wiley & Sons.

Samek, L., De Maeyer-Worobiec, A., Spolnik, Z., Bencs, L., Kontozova, V., Bratasz, Ł., ... & Van Grieken, R. (2007). The impact of electric overhead radiant heating on the indoor environment of historic churches. Journal of Cultural Heritage, 8(4), 361-369.

Sanchez, D. G., Lacarrière, B., Musy, M., & Bourges, B. (2014). Application of sensitivity analysis in building energy simulations: Combining first-and second-order elementary effects methods. Energy and Buildings, 68, 741-750.

Schito, E., & Testi, D. (2017). Integrated maps of risk assessment and minimization of multiple risks for artworks in museum environments based on microclimate control. Building and Environment, 123, 585-600.

Sciurpi, F., Carletti, C., Cellai, G., & Pierangioli, L. (2015). Environmental monitoring and microclimatic control strategies in "La Specola" museum of Florence. Energy and Buildings, 95, 190-201.

Sedlbauer, K., Krus, M., Zillig, W., & Kunzel, H. M. (2001). Mold growth prediction by computational simulation. Fraunhofer Institute for Building Physics.

Silva, H. E., & Henriques, F. M. (2015). Preventive conservation of historic buildings in temperate climates. The importance of a risk-based analysis on the decision-making process. Energy and Buildings, 107, 26-36.

Skinner, L. M., & Sambles, J. R. (1972). The Kelvin equation—a review. Journal of Aerosol Science, 3(3), 199-210.

Slanina, P., & Šilarová, Š. (2009). Moisture transport through perforated vapour retarders. Building and Environment, 44(8), 1617-1626.

Spitz C, Woloszyn M, Buhe C, Labat M (2013). Simulating combined heat and moisture transfer with EnergyPlus: An uncertainty study and comparison with experimental data. In: Proceedings of International IBPSA Building Simulation Conference, Chambery, France.

Steeman M, Janssens A, Steeman HJ, Van Belleghem M, De Paepe M (2010). On coupling 1D non-isothermal heat and mass transfer in porous materials with a multizone building energy simulation model. Building and. Environment, 45: 865–877.

Tariku F, Kumaran K, Fazio P (2010). Integrated analysis of whole building heat, air and moisture transfer. International Journal of Heat and Mass Transfer, 53: 3111–3120.

Taylor, K. E. (2001). Summarizing multiple aspects of model performance in a single diagram. Journal of Geophysical Research: Atmospheres, 106(D7), 7183-7192.

Thomson G. 1986. The Museum Environment – 2nd edition, London (1986).

Torres, M. I. M., & de Freitas, V. P. (2003). Rising damp in historical buildings. In Research in Building Physics: Proceedings of the Second International Conference on Building Physics, Leuven, Belgium, 14-18 September 2003 (p. 369). CRC Press.

Tronchin, L., & Fabbri, K. (2017). Energy and Microclimate Simulation in a Heritage Building: Further Studies on the Malatestiana Library. Energies, 10(10), 1621.

Van der Linden, A. C., Boerstra, A. C., Raue, A. K., Kurvers, S. R., & De Dear, R. J. (2006). Adaptive temperature limits: A new guideline in The Netherlands: A new approach for the assessment of building performance with respect to thermal indoor climate. Energy and buildings, 38(1), 8-17.

Widström, T. (2012). Enhanced Energy Efficiency and Preservation of Historic Buildings: Methods and Tools for Modeling (Doctoral dissertation, KTH Royal Institute of Technology).

Woloszyn, M. and Rode, C. (2008, March). Tools for performance simulation of heat, air and moisture conditions of whole buildings. In Building Simulation (Vol. 1, No. 1, pp. 5-24). Springer-Verlag.

Online resources

3ENCULT Energy Efficiency for EU cultural heritage, EU FP7 project. Accessed August 2018. http://www.3encult.eu

CfC Climate for Culture, EU FP7 project. Accessed August 2018. https://www.climateforculture.eu/

Co2ol Bricks, Climate Change, Cultural Heritage and Energy Efficient Monuments, Baltic Sea Region Programme. Accessed August 2018. http://www.co2olbricks.eu

EFFESUS Energy Efficiency for EU Historic Districts´ Sustainability, EU FP7 project. Accessed August 2018. http://www.effesus.eu

ICOM-CC (2010) Terminology to characterize the conservation of tangible cultural heritage. Accessed September 2018 http://www.icom-cc.org/54/document/terminology-to-characterize-the-conservation-of-tangible-culturalheritage-english/?id=368

New4Old, New energy for old buildings, IEE project. Accessed August 2018. http://www.new4old.eu

SECHURBA Sustainable Energy Communities in Historic Urban Areas, IEE project. Accessed August 2018. http://www.sechurba.eu

Standards and Guidelines resources

ASHRAE (2011) ASHRAE handbook—HVAC applications. Chapter 23: Museums, galleries, archives, and libraries. American Society of Heating, Refrigerating and Air-Conditioning Engineers, Inc., Atlanta

CIBSE TM36: 2005, Climate change and the indoor environment: impacts and adaptation.

EN ISO 13788 (2002) Hygrothermal performance of building components and building elements—internal surface temperature to avoid critical surface humidity and interstitial condensation—calculation methods. International Standards Organization, Geneva.

EN 15757:2010. Conservation of cultural property—Specifications for temperature and relative humidity to limit climate-induced mechanical damage in organic hygroscopic materials. European Committee for Standardization, Brussels

EN 15758:2010. Conservation of cultural property—Procedures and instruments for measuring temperatures of the air and the surfaces of objects. European Committee for Standardization, Brussels

EN 15759–1:2011. Conservation of cultural property—Indoor climate— Part 1: guidelines for heating churches, chapels and other places of worship. European Committee for Standardization, Brussels

EN 16242:2012. Conservation of cultural property—Procedures and instruments for measuring humidity in the air and moisture exchanges between air and cultural property. European Committee for Standardization, Brussels

EN 16682:2017. Conservation of cultural heritage—Methods of measurement of moisture content, or water content, in materials constituting immovable cultural heritage. European Committee for Standardization, Brussels

EN 15759-2:20018. Conservation of cultural heritage—Indoor climate—Part 2: Ventilation management for the protection of cultural heritage buildings and collections. European Committee for Standardization, Brussels

EN 16893:2018. Conservation of cultural heritage—Specification for location construction and modification of buildings or rooms intended for the storage or use of heritage collection. European Committee for Standardization, Brussels

ISO 13370:2007. Thermal performance of buildings – Heat transfer via the ground – Calculation methods. International Organization for Standardization

UNI 10829:1999. Beni di interesse storico e artistico—Condizioni ambientali di conservazione—Misurazione ed analisi. Ente Nazionale Italiano di Normazione

UNI 10969:2002. Beni culturali - Principi generali per la scelta e il controllo del microclima per la conservazione dei beni culturali in ambienti interni. Ente Nazionale Italiano di Normazione

UNI 11120:2004. Beni culturali - Misurazione in campo della temperatura dell'aria e della superficie dei manufatti. Ente Nazionale Italiano di Normazione

UNI 11131:2005. Beni culturali - Misurazione in campo dell'umidità dell'aria. Ente Nazionale Italiano di Normazione

European directives

Directive 2002/91/EC of the European Parliament and of the Council of 16 December 2002 on the energy performance of buildings

Directive 2009/28/EC of the European Parliament and of the Council of 23 April 2009 on the promotion of the use of energy from renewable sources and amending and subsequently repealing Directives 2001/77/EC and 2003/30/EC (Text with EEA relevance)

Directive 2010/31/EU of The European Parliament and of the Council of 19 May 2010 on the energy performance of buildings (recast)

Directive 2012/27/EU of the European Parliament and of the Council of 25 October 2012 on energy efficiency, amending Directives 2009/125/EC and 2010/30/EU and repealing Directives 2004/8/EC and 2006/32/EC (Text with EEA relevance)

Italian Legislative Decrees

Decreto Legislativo 22 gennaio 2004, n. 42. "Codice dei beni culturali e del paesaggio", ai sensi dell'articolo 10 della legge 6 luglio 2002, n. 137 pubblicato nella Gazzetta Ufficiale n. 45 del 24 febbraio 2004 - Supplemento Ordinario n. 28

Decreto Legislativo 19 agosto 2005, n. 192. "Attuazione della direttiva 2002/91/CE relativa al rendimento energetico nell'edilizia" pubblicato nella Gazzetta Ufficiale n. 222 del 23 settembre 2005 - Supplemento Ordinario n. 158

This page intentionally left blank

Appendix A

Assessment of indoor climate of Mogiła Abbey in Kraków (Poland) and the application of the analogues method to predict microclimate indoor conditions

Frasca F., Siani A.M., Casale G.R., Pedone M., Bratasz Ł., Strojecki M., Mleczkowska, A.

Environmental Science and Pollution Research, 24(16): 13895–13907. (2017).

Appendix A

Environ Sci Pollut Res (2017) 24:13895–13907
DOI 10.1007/s11356-016-6504-9

Assessment of indoor climate of Mogiła Abbey in Kraków (Poland) and the application of the analogues method to predict microclimate indoor conditions

F. Frasca[1] · A. M. Siani[2] · G. R. Casale[2] · M. Pedone[3] · Ł. Bratasz[4] · M. Strojecki[5] · A. Mleczkowska[5]

Received: 27 October 2015 / Accepted: 17 March 2016 / Published online: 4 April 2016

Abstract The microclimatic monitoring of the historic church of Mogiła Abbey (Kraków, Poland) was carried out to study the impact of the environmental parameters on the organic and hygroscopic artworks. Specific indexes were proposed to objectively assess the quality of time series of temperature (T), relative humidity (RH), and carbon dioxide (CO_2) before applying the exploratory data analysis. The series were used to define the historic environmental conditions as stated in the European Standard EN 15757:2010 and with the use of the climate evaluation chart (CEC). It was found that the percentage of time in which T and RH values are within the allowable limits of the ASHRAE (2011) Class B is more than 85 %. This means that, for about 15 % of the time, there is a high risk of mechanical damage to highly vulnerable objects mainly due to the RH variability. The environment at the chancel resulted moister than that at the cornice, and the fungal growth is possible. In addition, the time-weighted preservation index (TWPI) is computed to evaluate the life expectancy of the objects, taking into account the environmental conditions of the site under study. The method of analogues, developed to predict the evolution of a system given observations of the past and without the knowledge of any equation among variables, was proposed and applied to the time series of temperature, relative humidity, and carbon dioxide with a 1-h sampling time to avoid the influence of the autocorrelation.

Keywords Temperature · Relative humidity · Carbon dioxide concentration · Historic climate · Organic hygroscopic objects · Analogues method

Responsible editor: Gerhard Lammel

✉ A. M. Siani
annamaria.siani@uniroma1.it

[1] Department of Earth Sciences, Sapienza Università di Roma, P.le A. Moro 2, 00185 Rome, Italy

[2] Department of Physics, Sapienza Università di Roma, P.le A. Moro 2, 00185 Rome, Italy

[3] Centro InfoSapienza, Sapienza Università di Roma, P.le A. Moro 2, 00185 Rome, Italy

[4] Institute for the Preservation of Cultural Heritage, Yale University, PO Box 27395, West Haven, CT 06516, USA

[5] The Jerzy Haber Institute of Catalysis and Surface Chemistry, Polish Academy of Sciences, ul. Niezapominajek 8, 30239 Kraków, Poland

Introduction

Historic churches store valuable liturgical and decorative objects (sculptures, frescoes, wooden artworks); however, microclimatic conditions are often not beneficial for their preservation. Most historical buildings and churches are unheated (Camuffo et al. 2010a), and for centuries, indoor environmental conditions have been mainly affected by the outdoor climate. In these buildings, the internal climate is quite stable because of thick walls which attenuate both daily and seasonal cycles of temperature and relative humidity and of relatively small windows which reduce the ventilation. In cold seasons, churches can be heated during liturgical services to improve the thermal comfort of churchgoers (Samek et al. 2007). According to ASHRAE 2009, thermal comfort is defined as "that condition of mind that expresses satisfaction with the thermal environment," but such a definition is a cognitive process which involves many physical, physiological, and psychological processes and other factors. In the case of conservation of artworks, the current approach is to define the "historic climate" to which an object has resisted for a long

period under reasonably acceptable conditions and to which it has acclimatized (Camuffo et al. 2014). This means that an object has a memory of the past microclimate and large variations of thermo-hygrometric values with respect to the historic climate can be responsible for climate-induced mechanical damages (Bratasz et al. 2007; Camuffo et al. 2014). The European Standard EN 15759–1:2011 suggests that, in places of worship, a compromise solution between conservation and comfort needs should be satisfied, but, in the case of conflict, the priority should be given to the conservation.

Many studies have reviewed the pros and cons of heating systems on the conservation of cultural objects in churches and ancient buildings. A heating system is generally switched on only during liturgical services due to the necessity to have mild temperatures in a short time and at low cost (Camuffo et al. 2010a). This may generate fast temperature and relative humidity changes which can be very deleterious over long periods. The Friendly Heating Project (Samek et al. 2007; Camuffo et al. 2010a; Camuffo 2011) aimed at studying carefully the features of all heating systems and their impact on cultural artifacts and at suggesting the most appropriate heating strategy. In most cases, when a heating system is installed, the conservation requirements and the thermal features of architectural elements are rarely taken into account. Two heating solutions were identified (Camuffo and della Valle 2007): (1) the central heating, which uses traditional techniques where heat tends to rise and the upper layers are warmer than lower ones; and (2) the local heating, which optimizes the thermal comfort and reduces heating dissipation and the hygrothermal response of materials. Any heating strategy may have adverse effects on cultural objects because natural or historical indoor conditions are altered. Schellen (2002) found that during winter, if air is heated without moisture control, the absolute humidity may be very low and the relative humidity may decrease to values that could be dangerous for organic artworks. As a result, at certain height, the air temperature can be higher than the set up temperature at the comfort level for churchgoers and visitors and the relative humidity drops to more damaging values (Schellen 2002). In such cases, wooden materials (painting on wood, wooden decorative objects) are the most vulnerable materials to deterioration (Bratasz et al. 2005; Samek et al. 2007).

This study aimed at characterizing the microclimatic conditions of the Basilica of the Holy Cross, in which wooden artworks (a crucifix and a triptych) are preserved and where a central heating system is in operation from November till April. For this purpose, a monitoring campaign of temperature (T), relative humidity (RH), and carbon dioxide (CO_2) was carried out from March 2012 to April 2014.

First, the paper proposes three indexes to assess the quality of time series before applying exploratory data analysis. Second, the Climate Evaluation Chart and the General Risk Analysis (Martens et al. 2006) are carried out to show the impact of environmental parameters on the conservation of organic and hygroscopic cultural artworks. Afterwards, the analysis of the historic climate is performed using the classes of control given by ASHRAE (2011) and the RH "safe bands" as suggested by EN 15757:2010. The results derived by the above two methods are compared. Then, the time-weighted preservation index (TWPI) is computed to evaluate the life expectancy of the objects taking into account the environmental conditions of the site under study. Moreover, the analogues method is applied to the time series of T, RH, and CO_2 as an operative tool for predicting microclimatic patterns, even for CO_2 above the threshold of 1000 ppm (Bencs et al. 2007).

The case study: the Basilica of the Holy Cross in Mogiła Abbey

The Mogiła Abbey is a Cistercian monastery (Fig. 1a, b—left side) located in the Nowa Huta District of Kraków (Poland). The Basilica, a three-nave church closed by a chancel (Fig. 1b—right panel), is an architectural palimpsest, where several wooden artworks, Renaissance frescoes, and wall decorations are stored. The Basilica covers an area of about 1500 m^2 and, in the chancel, it reaches the maximum height of 15.5 m. The church is orientated along the east–west axis with the high altar in the eastern side (Opactwo Cystersów Kraków Mogiła 2014).

The church was built in the early thirteenth century and maintained its original configuration until the fifteenth century, when it was badly damaged by a fire: the chancel, the transept, and the chapels close to the sacristy still are in the

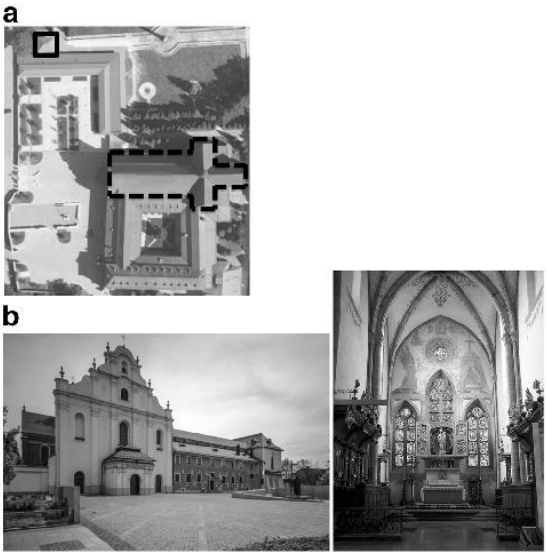

Fig. 1 **a** Top view of the Mogiła Abbey: the Basilica of the Holy Cross highlighted by *dashed line* and the bell tower (where the outdoor thermo-hygrometer was installed) by *bold line*. **b** The Basilica of the Holy Cross in Mogiła Abbey: outside (*left panel*) and inside (*right panel*)

Appendix A

original style. Over the high altar, a late-Gothic carved triptych represents a statue of the Madonna and Child in the middle and the life of Holy Family and the Passion of Christ on both wings. The wooden sculpture of Miraculous Christ, dated back to the twelfth century, is stored upon the Baroque altar in the Holy Cross Chapel.

The Mogiła Abbey is very popular among catholic Polish believers and also attracts many tourists. The church is open for visitors every day not only for liturgical services, and it is heated during the night (from midnight till 6:00 a.m. local time) with warm-air blow systems from November till April. The setting of heatings is shown in Fig. 2 by rectangles. The air velocity of warm air is generally in the range 0.05–0.4 m/s.

Instruments and methods

Measuring indoor and outdoor climate

The time series of T and RH values from April 2012 till January 2014 and of CO_2 concentration (limited to the period from December 2012 till January 2014) were analyzed. The mixing ratios of moist air (MR), both indoors and outdoors, were calculated from T and RH readings, using the equation reported in the EN 16242:2012, taking into account the standard value of the atmospheric pressure ($p = 1013$ hPa).

The measuring system consists of three thermo-hygrometric sensors S-THB-M002 (Onset Computer Corporation, USA) and one CO_2 concentration sensor GMM222 (Vaisala Inc., Finland). All thermo-hygrometric sensors were connected to the HOBO Micro Station Data Logger (H21-002, Onset Computer Corporation, USA). One thermo-hygrometric probe (coded as # 1) was placed in the chancel and the other two probes (coded as # 2 and # 3) were installed on the cornice at the height of 11 m with respect to the ground. The instrumental setting is shown in Fig. 2, and their technical features are reported in Table 1. The choice of sites, where the sensors were installed, allows to evaluate the difference, if any, between the lower layers of the church affected by heating systems and upper layers (Samek et al. 2007). The technical features of the T and RH sensors are in accordance with the metrological characteristics issued by EN 15758:2010 and EN 16242:2012, respectively.

At the cornice, the carbon dioxide concentration is also measured. The CO_2 parameter is a useful indicator related to the presence of visitors, candle burning, and air exchange (Bencs et al. 2007). The background CO_2 level in the suburb area of Kraków is 408 ppm (Jasek et al. 2014), while in winter in Kraków, the CO_2 background is higher up to 500 ppm (Mleczkowska et al. 2015).

The CO_2 instrument uses a technology, which measures at the absorption wavelength of 4.26 μm and at a reference wavelength where no absorption occurs. The reference is measured by placing an electrically tunable Fabry–Perot interferometer (FPI) filter in front of the detector.

Acquisition and recording time were set to 5 min to record short heating episodes and to retrieve reliable information when the church is heated and crowded (Samek et al. 2007; Camuffo et al. 2010b).

The outdoor air temperature and relative humidity were measured (every 15 min) by Pro v2 U23-002 (Onset Computer Corporation, USA) installed in the bell tower located next to the church (Fig. 1a).

Indexes to assess the quality control of microclimate data series

In general, data collections with several missing values are not allowed a reliable data analysis.

Three indexes were proposed before performing exploratory data analysis and determining the historic climate: the Completeness Index (CoI); the Continuity Index (CI), and the Microclimatic Quality Index (MQI).

The CoI (Eq. 1) was defined as the ratio between the number of good measurements (Nr) (i.e., not affected by poor instrumental performance) and the total numbers of the series (TN) over the selected time period, also including the missing values (Braca et al. 2013). The CoI is equal to 1 (no missing data) and tends to zero in the case of several missing data in the series.

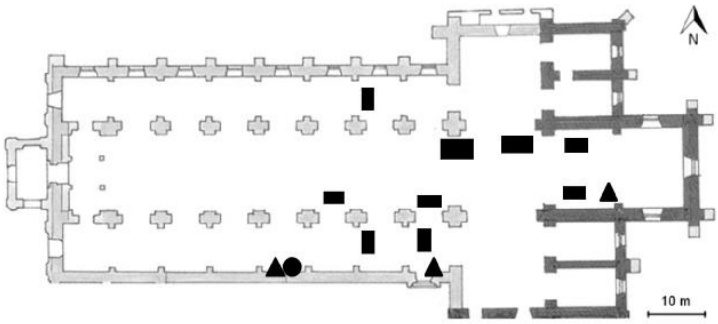

Fig. 2 The instrumental setting: the thermo-hygrometers (*triangle*), CO_2 sensor (*circle*), and warm-air blow systems (*rectangle*)

Appendix A

Table 1 Summary of technical specifications (measurement range, accuracy, and resolution) of T and RH sensors inside and outdoors, and CO_2 sensor

		Measurement range	Accuracy	Resolution
Indoor	T	−40 °C to 75 °C	±0.21 °C from 0 to 50 °C	0.02 °C at 25 °C
	RH	0–100 %	±2.5 % from 10 to 90 % RH, to a maximum of ±3.5 % including hysteresis	0.1 % RH at 25 °C
Outdoor	T	−40 to 70 °C	±0.21 °C from 0 to 50 °C	0.02 °C at 25 °C
	RH	0–100 %	±2.5 % from 10 to 90 % RH, to a maximum of ±3.5 % including hysteresis	0.03 %
Indoor	CO_2	0–7000 ppm	±(1.5 % of range + 2 % of reading)	12 bits

The CI (Eq. 2) provides the reliability of a series taking into account the number of intervals (NBI) with missing data respect to the TN value (Braca et al. 2013).The CI ranges between the unity (i.e., data set does not include unusual data called "outliers," due to instrumental errors or anomalous behavior of the parameter) and zero (i.e., NBI is maximum when it is approximately about the half of TN value).

$$CoI = \frac{Nr}{TN} \tag{1}$$

$$CI = 1-2\frac{NBI}{TN} \tag{2}$$

Furthermore, the MQI was introduced to assess the quality of the RH time series before determining the historic climate suitable for the preservation of organic hygroscopic objects as recommended by EN 15757:2010.

The MQI (Eq. 3) was defined as a linear combination of the ratios between the number of observations within the series measured by the instrument classified on the basis of its accuracy (hereafter called Nr_A, Nr_B, and Nr_C) and the total length (TN) of the series.

$$MQI = a_L\frac{Nr_A}{TN} + b_L\frac{Nr_B}{TN} + c_L\frac{Nr_C}{TN} + d_L\frac{Nr_D}{TN} \tag{3}$$

Four instrumental categories were proposed: category A (high accuracy), category B (medium accuracy), category C (low accuracy), and category D, in which Nr_D was associated to the interval with missing values. Six time lengths of the series were considered with the assumption that at least 1 year of data (L >12) is needed to characterize indoor climates in terms of the seasonal variability and short-term fluctuations (Table 2).

The weights a_L, b_L, c_L, and d_L, reported in Table 2, were obtained setting the higher limit to 1, when data are collected with an instrument of category A and for at least a 12-month monitoring period; the lower limit was set to 0, when data are missing and/or the monitoring period is below 3 months with an instrument belonging to category C. The remaining coefficients were downscaled.

The MQI can range from 0 (poor quality) to 1 (high quality).

Thereafter, exploratory data analysis was applied to microclimatic parameters.

The Evaluation Chart

Martens et al. (2006) proposed the Climate Evaluation Chart (CEC) to visualize the seasonal indoor T and RH behavior with the use of a psychrometric chart. The CEC has the advantage to provide an overall view of the internal climate simplifying the comparison among different climates both on seasonal and daily scales. The indoor microclimatic assessment is based on the use of ASHRAE climate classes guidelines (2011). The six classes (Martens 2012), reliant on the damage risk of biological, mechanical, and chemical degradation to the collections, are reported in Appendix. For historic buildings such as churches with heavy masonry and basic HVAC systems, the ASHRAE guideline suggests the following classes of climate control:

- Class B: RH fluctuations of ±10 % both on seasonal and short-term scales are allowable if climate is benign; ±5 °C in T is acceptable for the short-term fluctuations and up to 10 °C for seasonal variations.
- Class C: RH can range between 25 % and 75 % year-round and T never should exceed 30 °C, if winter is mild.
- Class D: allowed T fluctuations, RH below 75 %.

The CEC for the Basilica of the Holy Cross was created by the online application of the Physics of Monuments (Smulders and Martens 2014). Furthermore, the general risk assessment for T and RH, which provides the percentage of time in which T and RH values fit into the ASHRAE climate classes, was also provided by the online application.

The assessment of historic conditions

The ASHRAE (2011) recommends to keep constant the RH levels at the set point of 50 % or at the annual average (taken as the historic reference value), and, depending on the class of control, specific seasonal and short-term variations are allowable. The Standard EN 15757:2010 recommends the priority of the historic climate (expressed in terms of seasonal behavior and short-term fluctuations) to which old hygroscopic objects have acclimatized; i.e., objects have adapted over its lifespan to a specific RH variability, reaching an equilibrium

Appendix A

Table 2 The weights a_L,b_L,c_L, and d_L of Eq. 3 as a function of the instrumental category (A, B, C, D) and the length of the time series (L)

		L (month)					
		L > 12	9 ≤ L ≤ 12	6 ≤ L < 9	3 ≤ L < 6	1 ≤ L < 3	0.5 ≤ L < 1
Category	A	1.00	0.75	0.60	0.30	0.15	0.08
	B	0.90	0.65	0.45	0.20	0.10	0
	C	0.70	0.50	0.25	0.15	0	0
	D	0	0	0	0	0	0

0.5 ≤ L < 1 indicates the range between 15 days and 1 month

with the historic environmental conditions even if this has implied permanent deformation (Camuffo 2014; Caratelli et al. 2013). Then, it may be risky to modify these conditions and it is preferable to monitor the microclimatic parameters to avoid unexpected occurrences. The procedure is based on the calculation of (1) the 30-day central moving average (MA) to define the seasonal cycle; (2) the deviation of raw data from MA to extract the short-term fluctuations; and (3) the safe band of RH defined as the 7th and the 93rd percentiles of the short-term fluctuations.

The time-weighted preservation index

The preservation index (PI) and the TWPI were originally derived by a detailed study of the hydrolysis of cellulose acetate and later applied to other types of organic and hygroscopic cultural objects (Krüger and Diniz 2011). These indexes combine the effect of the T and RH values on the decay rate of vulnerable carbon-containing materials providing a tool to compare the quality of different environments where chemically unstable objects are stored.

The PI gives an awareness of how long it would take for organic materials to occur a significant deterioration, assuming that T and RH do not change from the time of measurement onward (Nishimura 2009).

The TWPI provides the cumulative effect of the PI values over a period; it indicates the damaging effectiveness of indoor climate and provides the quality of the environment (not air conditioned) for the preservation needs. The main advantage of TWPI is its capability to condense an entire period of thermo-hygrometric changes into a single value by weighting at each time interval contributing to the decay rate overall (Nishimura 2009). T and RH series were used to evaluate TWPI at the chosen sites in the Basilica.

The analogues method

In 1969, Lorenz introduced a mathematical formulation of the physical axiom "*that from like antecedents follow like* consequents" in the field of weather forecasting (Cecconi et al. 2012): the analogues method. This method, taking into account data from the past, can be used as an operative tool to predict future tendency, even without the knowledge of any equation among variables. The method can be synthesized as follows.

When a time series, x(t), sampled at given times ($t_k = k\Delta t$), is available, the evolution of the present state (x_M) can be predicted, searching the most similar state x_k in the past (analogue state). One or more analogs may be found for the same present state x_M. Then, we can use the analogue's following states as proxies for the future evolution of the present state. If the analogues were ideal (i.e., the difference between analogue and present state tends to zero), the behavior of the system would be periodic and the prediction would be trivial. In this case, the evolution of the present state is equivalent to the evolution of a past state. Zorita and Von Storch (1999) showed that a relevant problem associated with this method is the necessity of having a sufficiently long time series of observations so that a realistic analogue may be found.

Here, the method was applied to time series collected over the period under study, choosing a time step of 1 h because it resulted to be more effective than sampling frequency of 5 min; otherwise, the method could only have recognized the persistence of the time series (autocorrelation of the time series). First, we analyzed the thermo-hygrometric series (T and RH) in which the present state and the analogue state differ at most by 1 % (below the instrumental uncertainty). Then, the CO_2 concentrations were included taking into account a difference between the present state and the analogue state at most by 10 %. The use of CO_2 could have the effect of including a signal that is not physically related to the microclimatic parameters. In fact, CO_2 can be used as a predicted parameter to identify peculiar conditions exceeding 1000 ppm (crowded place and/or candle burning).

Results and discussion

Exploratory data analysis

Table 3 reports the CoI (Eq. 1) and CI (Eq. 2) values for each sensor (the indexes both for T and RH are the same). MQI was determined only for the RH series (Eq. 3). Both the T and RH series resulted to be of high quality and hence suitable for

Table 3 Summary of the results of the CI, the CoI, and the MQI for each of three sensors inside the church and for that outdoors (Out)

Sensor	CoI	CI	MQI
# 1	0.89	1.00	0.89
# 2	0.90	1.00	0.89
# 3	0.90	1.00	0.89
Out	0.95	1.00	
CO_2	0.55	1.00	

exploratory data analysis and to define the historical climate in the case of organic and hygroscopic materials. The lower value of CoI for the CO_2 series can be probably due to the shorter length of the series with respect to those of T and RH.

Box-and-whisker plots are used in non-parametric statistics for a synthetic visualization of data without making any assumption of data distribution. Figure 3 shows the box plots for the T (left panel) and RH (right panel) data, respectively. The line inside the box is the median value, with the 25th and 75th percentiles (lower and upper sides of the box), respectively. The upper and the lower extremes of the data set are plotted as whiskers (drawn at 1.5*IQR with respect to the 25th and 75th percentiles, IQR = interquartile range) providing 99.3 % data coverage (McGill et al. 1978). Data outside this range are called outliers (indicated as circles). Outliers were found only for the RH and CO_2 data. However, since they are not due to instrumental problems but to the climate evolution, they were included in the analysis. It can be noticed that the box plots of internal T overlap since there is no significant difference among data provided by the three sensors. The mean value of internal T medians is 17.3 °C, ranging between 13.3 °C (the mean of the 25th percentile) and 21.0 °C (the mean of the 75th percentile), whereas outdoor T has a lower median (12.1 °C) and a greater variability, as expected (25th percentile = 2.9 °C and 75th percentile = 18.8 °C). The box plot of RHs of sensor # 1 partially overlaps those recorded by sensors # 2 and # 3; there is likely a difference between the former and the latter data set. The RH median related to sensor # 1 is 66.2 % (25th percentile = 60.5 % and 75th percentile = 72.6 %); the mean value of RH medians of the two other sensors is 60.3 % ranging between 55.0 % and 66.0 %. A possible interpretation of the above difference, even small, could be attributed to the different placing of the sensors (Fig. 2).

Figure 4 shows the box plot for the CO_2 concentrations. The median is 886 ppm (25th percentile = 604 ppm; 75th percentile = 893 ppm). Outliers (indicated as circle in Fig. 4) were found when CO_2 concentration exceeded 1326 ppm. These values were observed during the liturgical services; however, CO_2 concentrations had never reached the dangerous level for human health (5000 ppm).

Figure 5 shows the RH daily span (difference between the maximum and minimum value observed during each day) versus the T daily span for the three sensors. The daily span behavior allows to study the variability of the parameters and the sustainability of the material with regard to the environment conditions. Two different periods can be distinguished: May–October when heating system is switched off (black dots) and November–April when it is switched on (gray dots). The data from the sensor # 1 (upper panel) show larger daily cycles than those from the other two sensors (mid and lower panel). The maximum of T and RH daily span is 6 °C and 32 %, respectively. The area of the scatter diagram with the largest daily spans is related to the late winter and early spring weeks when Easter ceremonies took place. These large variations could induce mechanical damage in organic hygroscopic materials.

To study the influence of the external conditions, the scatter plots of the indoor T and MR monthly means as a function of the corresponding outdoor monthly means are analyzed (Camuffo et al. 1999). In Fig. 6, the monthly means related only to the chancel (sensor # 1) are plotted since the monthly behavior of the other two sensors is similar. Looking at the temperature scatter plot (Fig. 6—upper panel), a typical pattern of heated buildings can be noticed in which, on average, winter monthly values are always above the bisectrix. In spring and early summer, the external temperature variations are smoothed out because of thick walls of the church which

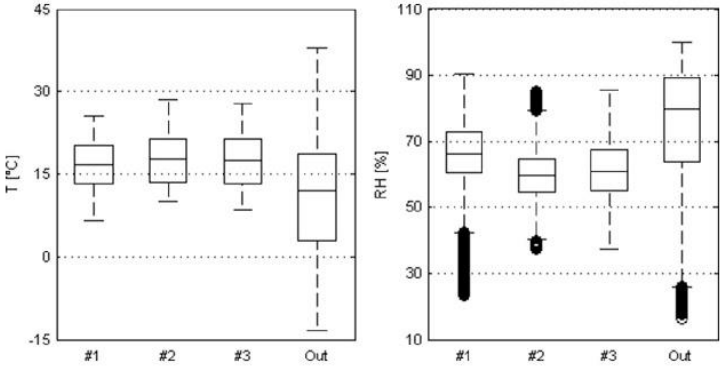

Fig. 3 Box-and-whisker plots of indoor T (*left panel*) and RH (*right panel*) for each internal sensor and outdoor (out). The line inside the box is the median value, with the 25th and 75th percentiles as lower and upper sides of the box, respectively. The lowest and the highest value of the data set are plotted as whiskers when they are not outliers, indicated as the *circle* (i.e., above or below 1.5*IQR, IQR interquartile range)

Appendix A

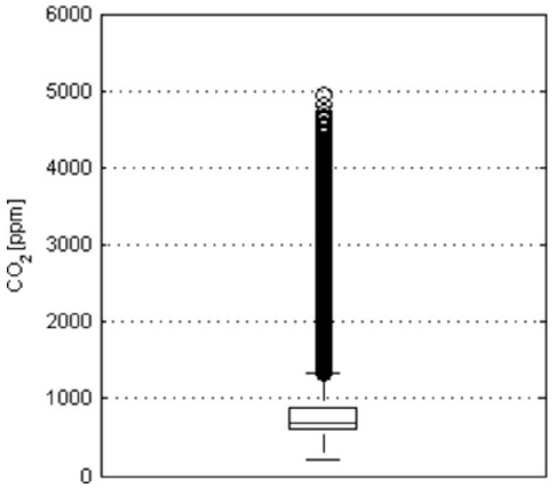

Fig. 4 Box-and-whisker plots of indoor CO_2 concentration. The line inside the box is the median value, with the 25th and 75th percentiles as lower and upper sides of the box, respectively. The lowest and the highest value of the data set are plotted as whiskers when they are not outliers, indicated as the *circle* (i.e., above or below 1.5*IQR, IQR interquartile range)

reduce the propagation of thermal gradient. In August and September, the church keeps some of the heat accumulated during the warmest months.

The winter difference with respect to outdoors is 10 °C, whereas in summer, internal thermal conditions are 2 °C cooler.

The monthly indoor MRs do not differ largely from the external variations (Fig. 6—lower panel) as shown by the values which are placed close to the bisectrix. This could depend on water absorbed by walls which migrates and diffuses inside during precipitation events and moisture transported inside during rainy days.

The Climate Evaluation Chart

Climate classes (AA, As, A, B, C, and D) with set points of 50 % for RH and T between 15 °C and 25 °C were taken into account. Table 4 summarizes the percentage of data in which the climate at both sites fits into the classes. It was found that the occurrences of class of control B are higher at the chancel, with respect to other classes, whereas classes of controls D and C are marginally prevailing at the cornice. These findings on the microclimatic conditions agree with the classes suggested by the ASHRAE (2011) for a church and indicate that a moderate risk of mechanical damage to high vulnerability artworks may occur.

Figure 7 shows the CEC for the chancel (upper panel) and for the cornice (lower panel) taking into account the control class B (the area delimited by blue lines and blue curves which indicate the climate limits of B class). The intensity of the

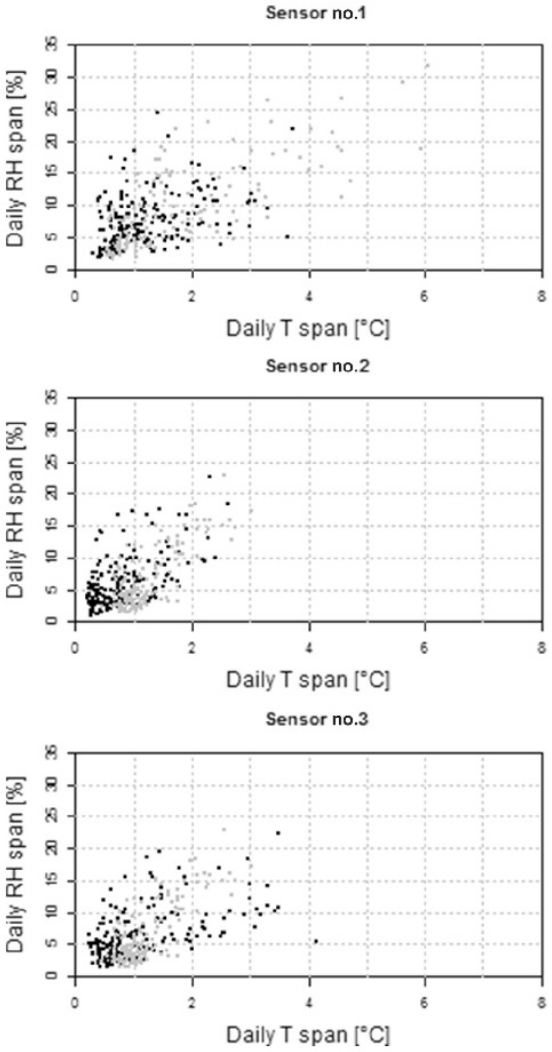

Fig. 5 Scatter diagram of daily RH span versus daily T span for the sensors # 1 (*upper panel*), # 2 (*mid panel*), and # 3 (*lower panel*). The daily span is calculated as the difference between the maximum and minimum values. *Gray dots* indicate days when the heating system is switched on, and *black dots* when the heating system is off

color in each season is connected to the percentage of cases characterized by similar thermo-hygrometric values. On the contrary, more data are scattered and more indoor climate is fluctuating.

At the chancel, RH drops down to too low values (about 20 %), mainly in winter and spring at $T < 15$ °C, because no humidification control is used. On the other hand, in spring and in summer at $T > 15$ °C, RH reaches values over 80 %, so the environmental conditions may be favorable to fungal growth (gray line), although this phenomenon has never been observed. T is generally higher at the cornice (Fig. 7—lower

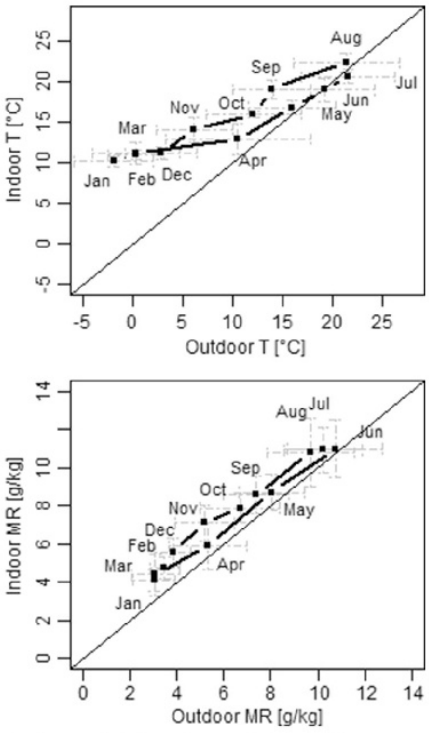

Fig. 6 Outdoor and indoor (sensor # 1) monthly averages of air temperature (*upper panel*) and mixing ratio (*lower panel*). The averages were calculated from January 2013 to December 2013. Horizontal and vertical bars are the standard deviations for internal and external values

panel) than at the chancel, and yet, at this site, RH never decreases below 40 %, even at lower T.

The area delimited by blue lines and blue curves indicates the climate limits of T and RH values in the class of control B (indicated on the bottom of both panels in Fig. 7). By using these limits, the chart is divided into nine parts and the 3×3 matrixes at the right report the percentage of time (on yearly and seasonal basis) that indoor conditions are within the guidelines (second row and column), above the T and RH maxima (first row and third column, respectively), and below the T and RH minima (third row and first column, respectively). It was found that the percentage of total data within the guidelines is 7 % for the chancel and 16 % for the cornice. In autumn and winter, the RH in chancel is higher than specified in class B (44 % and 45 %, respectively). The four histograms show the percentage of time in which hourly and daily changes in T and RH (ΔT/h and ΔT/day and ΔRH/h and ΔRH/day, respectively) are out of the allowable variations of class of control B (vertical blue line). It can be noticed that both ΔT/h and ΔT/day never exceed 5 °C in each season. At both sites, the values of ΔRH/day exceed 10 % in winter, in spring, and in summer.

Table 4 Summary of the percentage of data in which the climate fits into the climate classes

Site (sensor)	ASHRAE climate class					
	AA (%)	As (%)	A (%)	**B (%)**	**C (%)**	**D (%)**
chancel (# 1)	34.4	45.9	65.9	**86.3**	**81.8**	**81.8**
cornice(# 2)	46.0	60.4	74.5	**93.7**	**97.6**	**97.6**

In bold are the classes suggested by the ASHRAE (2011) for a church (B, C, and D)

Figure 8 shows the time plot of T readings at the chancel (upper panel) and at the cornice (lower panel) with the seasonal cycle (black line) and the annual mean (dotted line). It can be noticed that the maximum T occurs in August, whereas the higher outdoor T are observed in previous months (Fig. 6—upper panel). This is due to the thermal inertia of the building which releases slowly the heat accumulated previously. The seasonal increase of T, with respect to the annual average, is 7.0 °C and 7.4 °C at the chancel and the cornice, respectively. The seasonal decrease with respect to the annual average is 5.5 °C and 4.8 °C at the chancel and the cornice, respectively. These findings are consistent with the allowable variations of T according to class B.

Application of EN 15757:2010

The use of the standard EN 15757:2010 requires that the objects stored have no recent damages. Therefore, the 7th and the 93rd percentiles of deviations from the MA delimit the safe band of allowable RH fluctuations. In the application of this standard, we have assumed that physical damages, induced by stress–strain cycles due to RH fluctuations, did not occur on the organic and hygroscopic works of art stored in the church, since no investigation on the material conditions was performed. However, conservation surveys performed periodically by the regional conservator also involved in the project (Grant 2011/01/D/HS2/02604 from the Polish National Research Centre) did not reveal new damages on the stored object. RH measurements together with the historic climate expressed in terms of the annual mean, the 30-day MA, and the safe band (the 7th and the 93rd percentiles of deviations from the MA) are shown in Fig. 9. The seasonal increase of RH, with respect to the annual average, is 14.3 % and 12.4 % at the chancel and the cornice, respectively. The seasonal decrease, with respect to the annual mean, is 15.2 % and 8.4 % at the chancel and the cornice, respectively. Data below the lower limit (too dry environment) can be related to the heating episodes which can cause mechanical damages in hygroscopic artifacts. RH values higher than the upper limit can be correlated with additional indoor sources of moisture such as in crowded conditions or in months with high humidity (Fig. 6—lower panel).

Appendix A

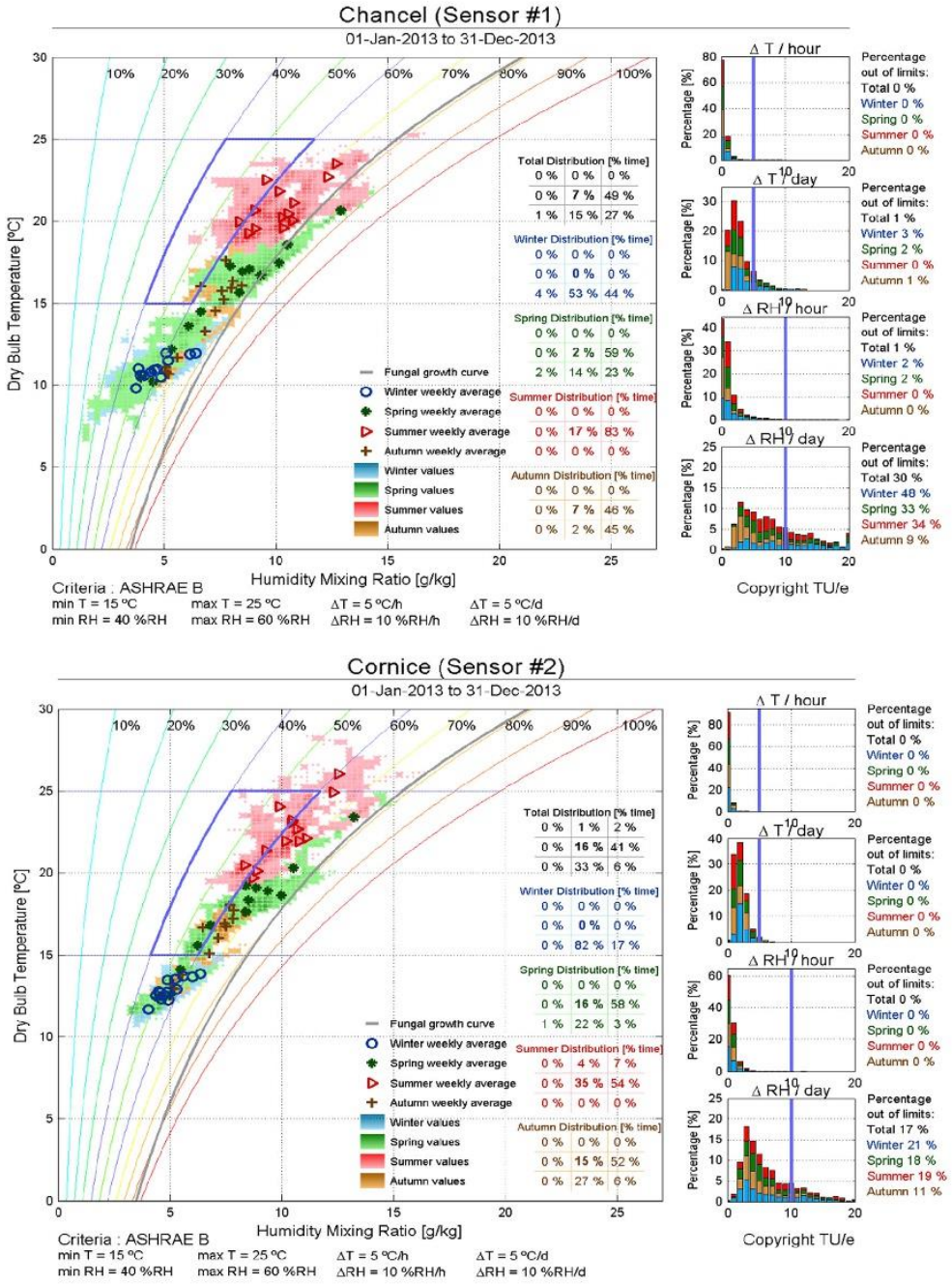

Fig. 7 Climate evaluation chart of the Basilica of the Holy Cross in Mogiła Abbey. The *upper panel* shows the chart for the chancel (sensor # 1), the *lower panel* for the cornice (sensor # 2). Indoor climate is seasonally represented: *blue* (winter), *green* (spring), *red* (summer), and *brown* (autumn). Seasonal weekly averages are also displayed with the following symbols: 'o' (winter), '*' (spring), '▷' (summer) and '+' (autumn). The Class B (its values are reported on the bottom of each CEC) area is delimited by two *horizontal blue lines* (the T limits) and *two blue curves* (the RH limits). The T and RH limits divide the chart into nine parts (which is represented by the 3 × 3 matrixes on the *right*). The four histograms show the percentage of time in which hourly and daily changes of T and RH (ΔT/h and ΔT/day and ΔRH/h and ΔRH/day, respectively) are out of the limits of Class B (*vertical blue line*)

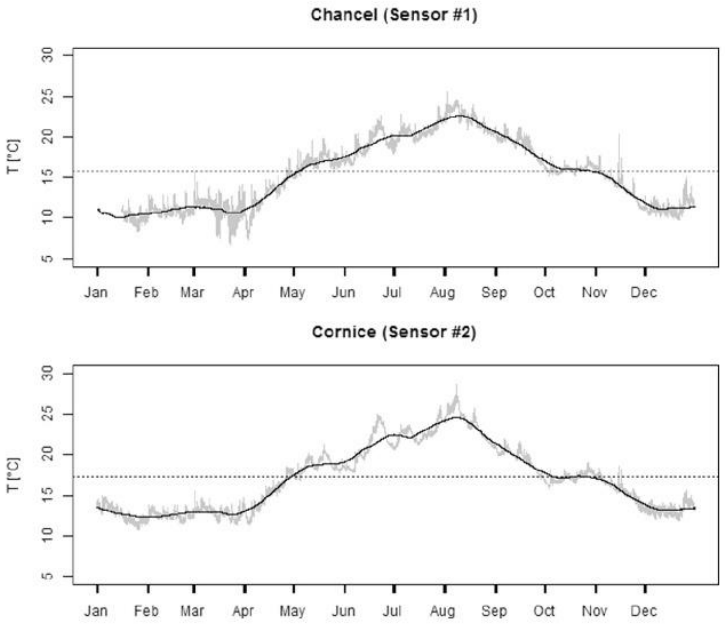

Fig. 8 T data (*gray line*) measured during 2013 at the chancel (*upper panel*) and at the cornice (*lower panel*); the seasonal T cycle (*black line*) determined as the 30-day moving average of the readings and the yearly T average (*horizontal dotted line*)

The time-weighted preservation index

Table 5 summarizes the results of the TWPI in unit of years. The results are below the reference TWPI (45 years) for an "average" aggressiveness of the environment on the preservation of organic and hygroscopic artworks. The Basilica presents poor environmental conditions because the thermo-hygrometric fluctuations are fast, and so an ideal environment in the church will not be reached.

The analogue method

Several analogues were identified when only T and RH series were used, and the present and the analogue states differ at most

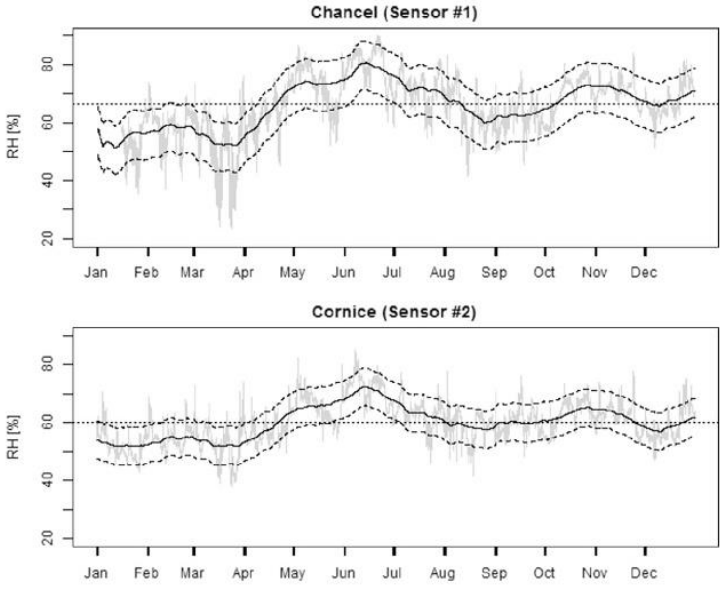

Fig. 9 RH data (*gray line*) measured during 2013 at the chancel (*upper panel*) and at the cornice (*lower panel*); the seasonal RH cycle (*black line*) determined as the 30-day central moving average of the readings; the *lower* and *upper limits* ("safe band") correspond to 7th and the 93rd percentiles of the short fluctuations (*dashed lines*) for the chancel (*upper panel*) and the cornice (*lower panels*). The yearly RH average is marked by a *horizontal dot-line*

Appendix A

Table 5 TWPI and the interpretation based on Nishimura (2009), for each thermo-hygrometric time series

Sensor	TWPI [years]	Interpretation
# 1	38	Poor environment; fast changes.
# 2	39	
# 3	38	

by 1 %. With the above criterion, most of analogues correspond to states at the earlier 1–2 h. This means that the method catches the persistence between the present state and its analogue.

Adding the criterion to CO_2 (the difference between the present and past state is ≤10 %), 3087 present states with corresponding analogues were found keeping out those at time lag less than 1 h.

To verify the capability of the analogue method as a predictive tool, the CO_2 value at each hour after the first analogue (i.e., from h = +1 h to h = +24 h) was compared with the corresponding actual value at the same time lag from the present state. Figure 10 shows the plots of predicted versus observed values from h = +1 h to h = +6 h. It can be noticed that the scatter of data increases with the time lag. In fact, it was found that the value of the correlation coefficient is above 0.6 till h = +6 h, whereas it becomes lower at longer time intervals.

Conclusions

A key role for conservation purposes is that the indoor climate to which the objects have been acclimatized and adapted (historic climate) is maintained as stable as possible. The first issue of this study was to propose indexes to evaluate the quality of indoor environmental parameters before performing any further analysis. With this approach, it was found that in the case of the church in Mogiła Abbey, collected data of T, RH, and CO_2 are of high quality and are adequate to apply exploratory data analysis and to determine the historic climate.

No significant T differences were found between the lower part of the church (chancel) and the upper part (cornice), whereas RH is higher in the chancel than in the cornice.

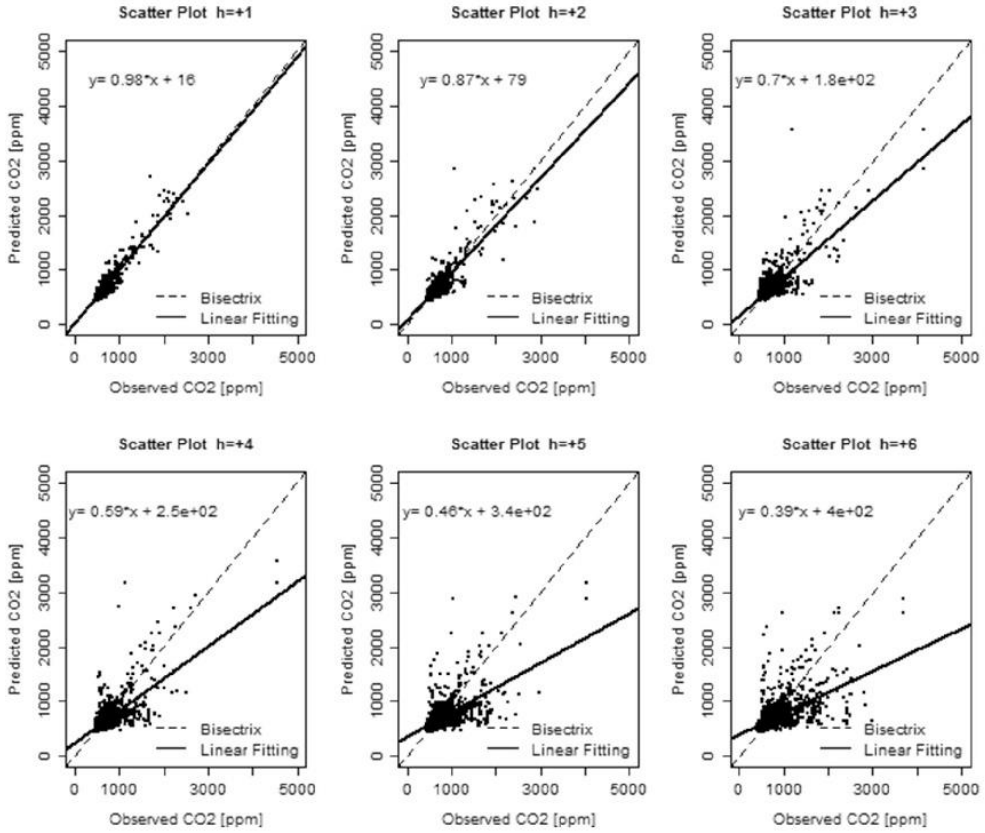

Fig. 10 Scatter diagrams of predicted CO_2 [ppm] versus observed CO_2 [ppm], from time lag h = +1 to h = +6. The *dashed line* is the bisectrix, whereas the *black line* is the linear regression fitting (equation is displayed in the *top left part* of each plot)

Furthermore, large daily changes in the thermo-hygrometric parameters can be observed ($\Delta T_{MAX\text{-}MIN}$ >6 °C, $\Delta RH_{MAX\text{-}MIN}$ >30 %) when the heating system is switched on during the nighttime. The response of the organic and hygroscopic materials to fast RH and T changes could cause internal stress and result in deterioration.

The upper levels of the church are less affected by daily thermo-hygrometric cycles, and the behavior in the two periods (heating system on and off) is quite similar. The fast daily changes which occurred in the late winter and early spring of 2013 can be risky for organic and hygroscopic artworks.

The microclimate in the church gains benefits from the thermal inertia of the thick walls which smooth out the seasonal variations of outdoor T. In fact, the structure of historical buildings typically allows to buffer the outdoor variations of T (Camuffo 2011).

The use of the CEC assessed that the percentage of data, in which T and RH values are within the allowable limits of the ASHRAE Class B, is more than 85 %. This means that, for about 15 % of the time, there is a high risk of mechanical damage to highly vulnerable objects mainly due to the RH variability. However, the environment at the chancel resulted to be moister than that at the cornice, and fungal growth is possible.

Historic climate was evaluated taking into account the Standard EN 15757:2010. It was found that liturgical services are the main responsible of RH levels out of the safe band.

Although the TWPI has indicated poor environment conditions (below 45 years), the ambient conditions in the church are similar (for 20 °C and 50 % TWPI is 47 years) to those for typical museums where thermal comfort of visitors and employees is a priority. The result on TWPI can be used to compare the quality of different environments where chemically unstable objects are stored.

The practical relevance of the analogue method is its capability to infer peculiar conditions when past analogue states are known. In the present study, the method was used to estimate the conditions which drive the CO_2 concentrations above 1000 ppm, with a probable impact on cultural objects when this threshold is exceeded (i.e., when the combined effect of crowded church as well as candle and incense burning may occur). The rapid increase of CO_2 in a confined environment neither is easily predicted by the forecasting models in use nor is represented by the climatic history of the place under study. The analogue method, which needs long and stable data series, does not require any "a priori" hypothesis and can be applied without a full comprehension of the physical laws underlying a given experimental evidence. The approach followed in this paper aims at showing that conservation scientists could take advantage of the analogue method: if it is applied to the variables such as CO_2, operators could better manage risk situations (e.g., CO_2 above the threshold of 1000 ppm) with the implementation of proper warning systems. It must be noticed that the application shown here is just the first attempt in this direction and needs more experimental verifications.

Notwithstanding that in our study, a detailed investigation on the preservation state of the objects stored in the church was not performed, the extensive analysis of a long-term series of environmental variables has allowed to better understand the hygrothermal response of the church to outdoor input and to disturbing factors such as human presence and heating systems. Our results on indoor climate can be used as basis for comparison of future microclimate campaigns, to identify solutions for the energy retrofit in order to reduce the large observed fluctuations. For the latter, issue building simulation is necessary and microclimatic measurements play a key role to obtain an accurate calibration of the building simulation.

Acknowledgments This research was supported by the Grant 2011/01/D/HS2/02604 from the Polish National Research Centre. Francesca Frasca thanks Sapienza Università di Roma for the internship mobility grant. The authors also wish to acknowledge the staff of the 5th CMA4CH Mediterraneum Meeting (held on 14–17 December 2014 in Rome), for the opportunity to present their study at the meeting. The authors thank all the anonymous reviewers for their precious contribution to improve the manuscript.

Appendix

Table 6 ASHRAE (2011) climate classes (Martens 2012)

Type	Set point or annual average	Maximum fluctuations and gradients in controlled spaces		
		Class of control	Short fluctuations plus space gradients	Seasonal adjustments in system set point
General museums, art galleries, libraries, and archives	50 % RH (or historic annual average for permanent collections) with temperature set between 15 and 25 °C	AA	±5 % RH, ±2 K	RH no change Up 5 K; down 5 K
		A As	±5 % RH, ±2 K	Up 10 % RH, down 10 % RH Up 5 K; down 10 K
		A	±10 % RH, ±2 K	RH no change Up 5 K; down 10 K
		B	±10 % RH, ±2 K	Up 10 %, down 10 % RH Up 10 K, but not above 30 °C
		C	Within 25 to 75 % RH year-round T rarely over 30 °C, usually below 25 °C	
		D	Reliably below 75 % RH	

Appendix A

References

ASHRAE (2009) ASHRAE handbook—fundamentals. Chapter 9: thermal comfort. American Society of Heating, Refrigerating and Air-Conditioning Engineers, Inc., Atlanta

ASHRAE (2011) ASHRAE handbook—HVAC applications. Chapter 23: museums, galleries, archives, and libraries. American Society of Heating, Refrigerating and Air-Conditioning Engineers, Inc., Atlanta

Bencs L, Spolnik Z, Limpens-Neilen D, Schellen HL, Jütte BA, Van Grieken R (2007) Comparison of hot-air and low-radiant pew heating systems on the distribution and transport of gaseous air pollutants in the mountain church of Rocca Pietore from artwork conservation points of view. J Cult Herit 8(3):264–271

Braca G, Bussettini M, Lastoria B, Mariani S (2013) Statistical characterization of time series (Caratterizzazione statistica di una serie storica). In: Linee guida per l'analisi e l'elaborazione statistica di base delle serie storiche di dati idrologici. ISPRA, Manuali e Linee Guida, Roma, pp 22–32 (in Italian)

Bratasz L, Jakiela S, Kozlowski R (2005) Allowable thresholds in dynamic changes of microclimate for wooden cultural objects: monitoring in situ and modelling. In: Bridgland J (ed) ICOM Committee for Conservation 14th Triennial Meeting, The Hague, 12–16 September 2005, vol 2. James & James, London, pp 582–589

Bratasz L, Camuffo D, Kozłowski R (2007) Target microclimate for preservation derived from past indoor conditions. In: Padfield T, Borchersen K (eds) Museum Microclimates Contributions to the Copenhagen conference 19–23 November 2007, Copenhagen, 2007. The National Museum of Denmark, Copenhagen, pp 129–134

Camuffo D (2011) The Friendly Heating Project and the conservation of the cultural heritage preserved in churches. In: Kilian R, Vyhlídal T, Broström T (eds) Developments in Climate Control of Historic Buildings. Proceedings from the International Conference "Climatization of Historic Buildings, State of the Art", Linderhof Palace, 2nd December 2010. Fraunhofer IRB Verlag, Stuttgart, pp 7–12

Camuffo D (2014) Microclimate for cultural heritage (second edition) conservation, restoration, and maintenance of indoor and outdoor monuments. Elsevier, Amsterdam

Camuffo D, della Valle A (2007) Church heating: a balance between conservation and thermal comfort. Paper presented at the Experts' Roundtable on Sustainable Climate Management Strategies, Tenerife, April 2007

Camuffo D, Sturaro G, Valentino A (1999) Thermodynamic exchanges between the external boundary layer and the indoor microclimate at the Basilica of Santa Maria Maggiore, Rome, Italy: the problem of conservation of ancient works of art. Bound-Layer Meteorol 92(2): 243–262

Camuffo D, Pagan E, Rissanen S, Bratasz L, Kozłowski R, Camuffo M, della Valle A (2010a) An advanced church heating system favourable to artworks: a contribution to European standardisation. J Cult Herit 11(2):205–219

Camuffo D, Bertolin C, Fassina V (2010b) Microclimate monitoring in a church. In: Camuffo D, Fassina V and Havermans J (eds) Basic environmental mechanisms affecting cultural heritage – understanding deterioration mechanisms for conservation purposes. COST Action D42 "Enviart", Kermes Quaderni. Nardini Editore, Firenze, pp 43–47

Camuffo D, Bertolin C, Bonazzi A, Campana F, Merlo C (2014) Past, present and future effects of climate change on a wooden inlay bookcase cabinet: a new methodology inspired by the novel European Standard EN 15757: 2010. J Cult Herit 15(1):26–35

Caratelli A, Siani AM, Casale GR, Paravicini A, Hermann Fiore C, Camuffo D (2013) Stucco panels of Room VI in the Galleria Borghese (Rome): physical–chemical analysis and microclimate characterization. Energy Build 61:133–139

Cecconi F, Cencini M, Falcioni M, Vulpiani A (2012) Predicting the future from the past: an old problem from a modern perspective. Am J Phys 80(11):1001–1008

EN 15757:2010. Conservation of cultural property—specifications for temperature and relative humidity to limit climate-induced mechanical damage in organic hygroscopic materials. European Committee for Standardization, Brussels

EN 15758:2010. Conservation of cultural property—procedures and instruments for measuring temperatures of the air and the surfaces of objects. European Committee for Standardization, Brussels

EN 15759–1:2011. Conservation of cultural property—indoor climate—part 1: guidelines for heating churches, chapels and other places of worship. European Committee for Standardization, Brussels

EN 16242:2012. Conservation of cultural property—procedures and instruments for measuring humidity in the air and moisture exchanges between air and cultural property. European Committee for Standardization, Brussels.

Jasek A, Zimnoch M, Gorczyca Z, Smula E, Rozanski K (2014) Seasonal variability of soil CO_2 flux and its carbon isotope composition in Krakow urban area, Southern Poland. Isot Environ Health Stud 50(2):143–155

Krüger EL, Diniz W (2011) Relationship between indoor thermal comfort conditions and the time weighted preservation index (TWPI) in three Brazilian archives. Appl Energy 88(3):712–723

Martens MHJ (2012) Climate risk assessment in museums: degradation risks determined from temperature and relative humidity data. Doctoral dissertation, Technische Universiteit Eindhoven

Martens MHJ, van Schijndel AV, Schellen HL (2006) Evaluation of indoor climates using the 'climate evaluation chart'. In: Guarracino G (ed) 27th AIVC and 4th Epic Conference "Technologies & sustainable policies for a radical decrease of the energy consumption in buildings", Lyon, 20–22 November 2006. EPIC 2006 AVIC: proceedings—actes, vol 4. Ecole Nationale des Travaux Publics de l'Etat, Vaulx-en-Velin, pp 523–528

McGill R, Tukey JW, Larsen WA (1978) Variations of boxplots. Am Stat 32(1):12–16

Mleczkowska A, Strojecki M, Bratasz Ł, Kozłowski R (2015) Particle penetration and deposition inside historical churches. Build Environ. doi:10.1016/j.buildenv.2015.09.017

Nishimura DW (2009) Understanding preservation metrics. Image Permanence Institute. https://www.imagepermanenceinstitute.org/environmental/research/preservation-metrics. Last accessed 20 Oct 2013

Opactwo Cystersów Kraków Mogiła (2014) The Sanctuary of the Holy Cross of the Cistercian Abbey. In: Mogiła. http://www.mogila.cystersi.pl. Last accessed 15 Sept 2014

Samek L, De Maeyer-Worobiec A, Spolnik Z, Bencs L, Kontozova V, Bratasz Ł, Van Grieken R (2007) The impact of electric overhead radiant heating on the indoor environment of historic churches. J Cult Herit 8(4):361–369

Schellen HL (2002) Heating monumental churches: indoor climate and preservation of cultural heritage. Doctoral dissertation, Technische Universiteit Eindhoven

Smulders H, Martens M (2014) Physics of monuments. http://www.monumenten.bwk.tue.nl. Last accessed 28 Jan 2015

Zorita E, Von Storch H (1999) The analog method as a simple statistical downscaling technique: comparison with more complicated methods. J Clim 12(8):2474–2489

Appendix B

Cluster analysis of microclimate data to optimize the number of sensors for the assessment of indoor environment within museums

Siani A.M., **Frasca F.**, Di Michele M., Bonacquisti V. and Fazio E.

Environmental Science and Pollution Research, 25(29), 28787-28797. (2018).

Appendix B

Environmental Science and Pollution Research (2018) 25:28787–28797
https://doi.org/10.1007/s11356-018-2021-3

STRAIGHTFORWARD APPROACH IN CULTURAL HERITAGE AND ENVIRONMENT STUDIES - MULTIVARIATE ANALYSIS AND CHEMOMETRY

Cluster analysis of microclimate data to optimize the number of sensors for the assessment of indoor environment within museums

Anna Maria Siani[1] · Francesca Frasca[2] · Marta Di Michele[1] · Valerio Bonacquisti[3] · Eugenio Fazio[3]

Received: 23 November 2017 / Accepted: 11 April 2018 / Published online: 27 April 2018

Abstract
For the first time, the cluster analysis (*k*-means) has been applied on long time series of temperature and relative humidity measurements to identify the thermo-hygrometric features in a museum. Based on ASHRAE (2011) classification, 84% of time all rooms in the Napoleonic Museum in Rome (case study) were found in the class of control *B*. This result was obtained by analyzing all recorded data in 10 rooms of the museum as well as using the cluster aggregation. The use of objective-oriented methodology allows to achieve an acceptable knowledge of the microclimate in case of multi-room buildings, reducing computations with large amounts of collected data and time-consuming in redundant elaborations. The cluster analysis enables to reduce the number of the sensors in microclimate monitoring programs within museums, provided that the representativeness of the instrument location is known, and professional conservators have assessed that the artifacts are well preserved.

Keywords Data quality assessment · Cluster analysis · Temperature · Relative humidity · Museum

Introduction

The conservation of artworks and collections is strongly affected by environmental conditions, which may be directly and indirectly responsible for their deterioration processes. In the last 30 years, a growing number of studies has been conducted with the aim at defining the adequate microclimate to better preserve the cultural heritage.

The first works (Bernardi and Camuffo 1995; Camuffo and Bernardi 1996; Pavlogeorgatos 2003) were focused on characterizing the indoor climate in terms of temperature and relative humidity averages and their variability, as well as on investigating the impact of external climate conditions on indoors (Camuffo et al. 1999). The recent methodological approach is instead oriented to determine the historic climate (i.e., the climate to which the object has been acclimatized and satisfactorily been preserved for a long time). In the case of objects sensitive to climate-induced damage, the approach is to apply the European Norm EN 15757 (2010), which recommends establishing the safety range of relative humidity if this climate has been proved to be beneficial for the conservation of preserved objects by qualified specialists (Camuffo 2014; Bertolin et al. 2015). In the last decade, more attention has been also paid to understand the causes of damage in the artwork triggered by climate conditions (Bratasz et al. 2007).

In case of multi-room buildings, the assessment of indoor climate is performed analyzing thermo-hygrometric data recorded in one or more rooms in which the most valuable artworks are preserved. This is for two main reasons: (1) it is not possible to install instruments in each room due to cost sustainability and (2) indoor climates of contiguous rooms may be similar, and consequently, several sensors might be useless.

However, when several sensors are placed in the same room or in every room on the same floor, a reduction of the same could be strategic in terms of maintenance and calibration costs. Consequently, it is possible to optimize the site configuration setting using a minor number of sensors whose

Responsible editor: Constantini Samara

✉ Anna Maria Siani
annamaria.siani@uniroma1.it

[1] Department of Physics, Sapienza Università di Roma, P.le A. Moro 2, 00185 Rome, Italy

[2] Department of Earth Sciences, Sapienza Università di Roma, P.le A. Moro 2, 00185 Rome, Italy

[3] Department of Fundamental and Applied Science for Engineering, Sapienza Università di Roma, P.le A. Moro 2, 00185 Rome, Italy

measurements are still representative of the general indoor climate. However, the priority of climate control should be given when deterioration processes of artifacts are observed; in that case, it is necessary to have the sensor.

In this paper, we used the cluster analysis to identify the thermo-hygrometric features of the Napoleonic Museum in Rome. To date, this method has never been applied in a museum. The novelty of this study is the use of objective methodology to achieve an acceptable knowledge of the microclimate in case of multi-room buildings allowing therefore to reduce computations with large amounts of collected data and time-consuming in redundant data analyses.

Material and method

The case study

The Napoleonic Museum is located in the ground floor of Palazzo Primoli— a historic building dating back to the sixteenth century—in the center of Rome (latitude 41.9°N and longitude 12.5°E)—between Lungotevere Tor di Nona and Via Giuseppe Zanardelli (Fig. 1).

The Palazzo Primoli is also the official location of the photographic archives of the Primoli Foundation and of the Primoli Library. This later owns over 30,000 volumes on the topics of history, literature, and art.

From June 1, 1995, the Mario Praz Museum, part of the National Gallery of Modern Art, has been functioning in the third floor. These three institutions, together in one building, are a valuable resource for the study of art, literature, and history of the nineteenth century.

The Napoleonic Museum—which consists of 12 rooms (hereafter coded by numbers as indicated in Fig. 1), preserves a significant collection of paintings, original manuscripts, Napoleonic relics, and family mementos. Count Giuseppe Primoli, a descendant of the Bonaparte family, has donated it to the city of Rome.

The orientation of the main axis of the building is north-east (Fig. 1). Most of the rooms are on the east side and are therefore exposed to the sun only in the early hours of the day. Only two rooms on the opposite side are exposed to the sun during the afternoon. One of the streets on which the Museum opens, leads to a restricted traffic zone. As a consequence of this, the other street in front of the building, on the Lungotevere, carries a heavy flow of traffic during the day, thus adding considerable smog to the environment surrounding the museum. The visits to the museum by groups of students are usually scheduled in advance in order to control the number of visitors. As a result of this provision, the total visitors sum up to a few hundred units per hour. Temporary exhibitions are occasionally organized during the year. The museum is equipped with a central heating system consisting of cast iron radiators in each room. These radiators are turned on 24 h daily from November to March. The windows are usually open early morning for cleaning.

To preserve the works of art, the conservation staff carries out periodical condition surveys of the objects in the collection. The main problem of this place has been the relative low humidity which is responsible for some cracks which appeared over the surface of several gilded frames and furniture, tenting of the paint layer of some paintings exhibited. These unfavorable dry conditions cause alterations in the structure of those works of art most sensitive to environmental conditions. This is particular true for wood, but it also holds true for other hygroscopic materials.

After the restoration of the damaged objects, a microclimate monitoring has been started in November 2008. It controls the thermo-hygrometer behavior and it is still in operation.

Besides, in the same year, humidification systems were installed in each room (except for rooms 2, 8, and 12) to secure relative humidity levels ranging from 40 to 60% and to avoid inadequate low levels of humidity during the cold season when the heating system is on. Humidifiers are turned off at the same time as the heating system. As a result of these

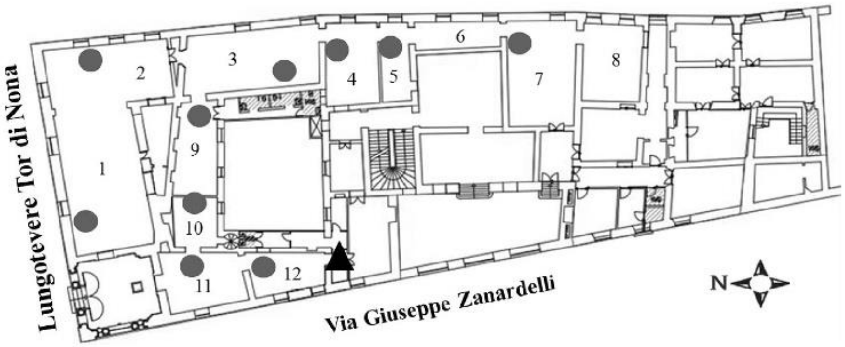

Fig. 1 Plan of the Napoleonic Museum with the instrumental setting: thermo-hygrometric sensors represented as gray circles. Numbers from 1 to 12 identify the 12 rooms of the Museum. Rooms 2, 8, and 12 do not have a humidification system

Appendix B

measures, no further deterioration processes of artworks in the collection have been observed by the conservation staff.

Monitoring campaign

Temperature (T) and relative humidity (RH) have been monitored since November 2008 using data loggers with internal thermistor and capacity sensors (model Fourier Microlog EC650 distributed by Fourtec-Fourier Technologies), installed in each of the ten rooms, as shown in Fig. 1. Acquisition and recording time are set to 1 h. The uncertainty on the temperature measurement (0.6 °C) exceeds the minimum requirement recommended by EN 15758 (2010), whereas RH uncertainty (3%) is in accordance with the metrological characteristic issued by EN 16242 (2012).

To study the influence of outdoor thermo-hygrometer conditions, T and RH data, provided by the meteorological station at Physics Department of Sapienza Università di Roma belonging to the ClimateNetwork of Climate Consulting S.r.l., were used. Sapienza Università is about 3 km far from the museum and hence has the same environmental characteristics of the area surrounding the case study.

Finally, both indoor and outdoor mixing ratios (MR) of moist air (i.e., the number of grams of vapor mixed with 1 kg of dry air) have been computed by measured data using the mathematical relation reported in the European Standard EN 16242 (2012). The MR is very useful parameter for diagnostic purposes because it gives the total amount of vapor water present. In this sense, it is different from RH which instead provides information how far or close to the saturation the vapor is. An increase of vapor in the air may or may not vary RH if the saturation point varies as well. In fact, the saturation point nonlinearly depends on temperature. Consequently, it would be of great importance to monitor contemporarily both RH and T, in order to discriminate the real evolution of local hygrometric conditions which means to resolve variations in vapor content with respect to the vapor saturation and temperature fluctuations. For these reasons, the correct approach to compute the RH averages is to use the equation which links RH with T and MR (EN 16242 (2012)) after having averaged MR and T on the same time slots (Camuffo 2014).

Data analysis of thermo-hygrometric parameters

The common approach in the museum microclimate evaluation is by visualizing all recorded T and RH data and performing exploratory data analysis. A more complete assessment can be provided by the use of the ASHRAE (2011) climate classification guidelines or by the "Climate Evaluation Chart" (Martens et al. 2006). All the above methods can become complex and time consuming when involving a large amount of data.

The well-known statistical cluster analysis (CA) technique allows to organize data in separate ensembles (clusters) according to their characteristics. In the present study, we have applied the "*k*-means" CA method with the aim to aggregate T, RH, and MR of the rooms in the museum. The data are distributed in the different clusters by an iterative algorithm in a way to minimize the variance within each cluster and maximize it between each individual cluster (Warren 2003). Mean values and the Euclidean distance are the output elements useful for the interpretation of results. Means identify the centroid of each cluster, whereas the Euclidean distance identifies objects with respect to each cluster centroid. The number of clusters was determined in according to the maximum value of the Silhouette index (*S*) that evaluates the within-cluster consistency of *i*th room with respect to the other clusters. *S* is defined for the *i*th room as

$$S(i) = \frac{b(i) - a(i)}{\max\{a(i),\ b(i)\}} \quad (1)$$

where $a(i)$ is the average distance of *i*th room to other rooms in the same cluster and $b(i)$ is the minimum average distance of *i*th room from other rooms in the different clusters, of which *i*th room is not a member. *S* index ranges between − 1 (i.e., *i*th room does not belong to that cluster) and + 1 (data are well clustered) (Rousseeuw 1987). $S(i)$ was calculated with a confidence level of 95%.

The following data mining was carried out both taking into account all rooms of the museum and the representative room of each cluster (i.e., the room at the smallest distance from the centroid) to fathom the CA capability as a tool to reduce the number of sensors guaranteeing the climate representativeness of the museum.

The first step of the analysis was a synthetic visualization of thermo-hygrometric behavior provided by box-and-whisker plots. The line inside the box is the median value; the top and bottom of each box are the 25th and 75th percentiles of the samples, respectively. The whiskers are lines extending above and below each box. Here, they were set as 1.7 times the interquartile range (IQR) away from the 75th and 25th percentiles, respectively, so that to consider 99.9% data coverage (instead of the common value of 1.5 × IQR). Data outside this range are defined outliers or suspected outliers and indicated as black circles in the figures.

Three indexes were calculated (Frasca et al. 2017) in order to assess the quality of each T and RH series: the Completeness Index (CoI), the Continuity Index (CI), and the Microclimatic Quality Index (MQI) to better identify the proper time intervals for the following analysis on the thermo-hygrometric time series.

CoI provides information on how many missing data are in the series, CI indicates the reliability of a series taking into account the number of intervals with missing data respect to

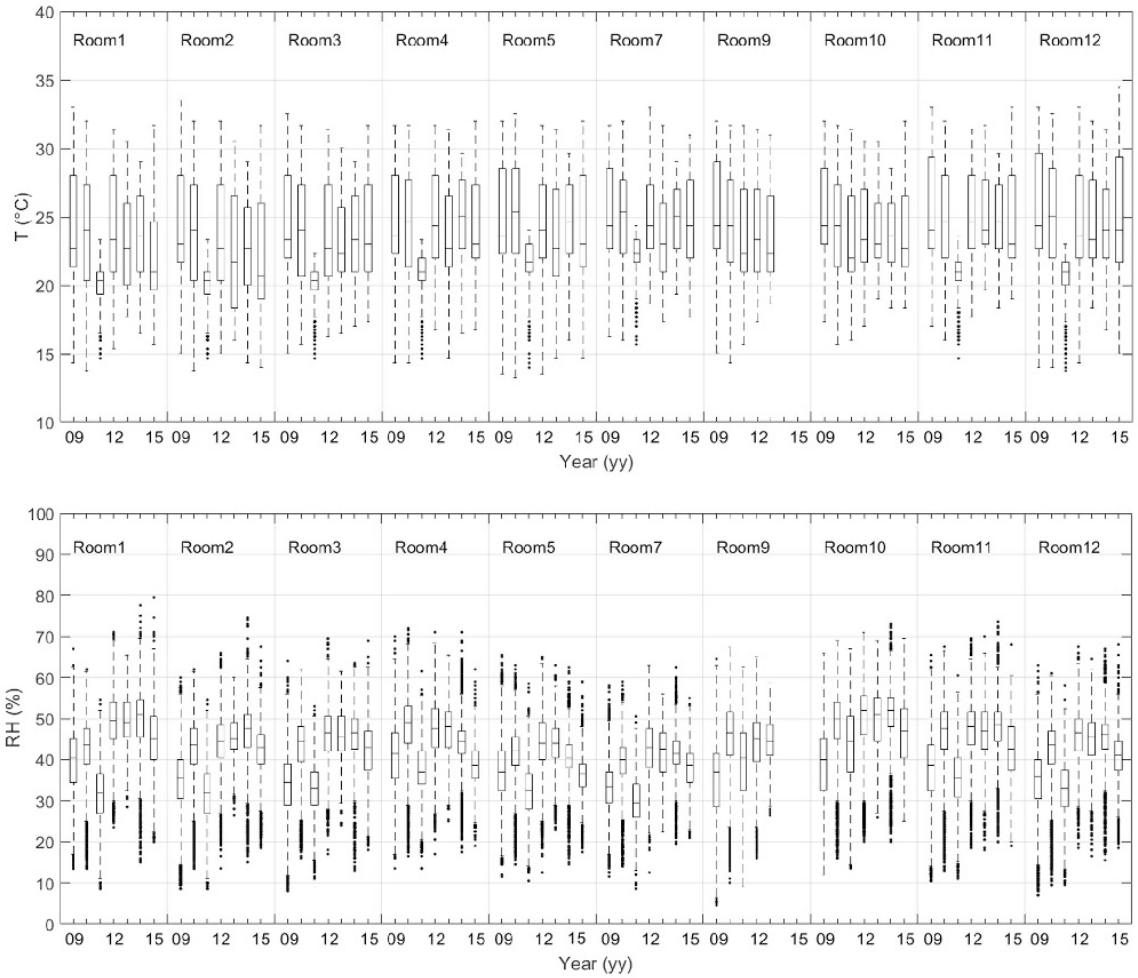

Fig. 2 Box-and-whisker plots of indoor T (upper panel) and RH (lower panel) for each room over the whole monitoring period

the total number of data, and MQI allows to assess the quality of T and RH time series considering both missing values and the accuracy of the sensor. All indexes range between 0 (poor quality) and unity (high quality, i.e., no missing values).

To understand how the indoor climate is influenced by external conditions both in terms of heat and vapor exchanges, the scatter plots of the indoor T and MR monthly means vs the corresponding outdoor monthly means were considered (Camuffo et al. 1999).

The ASHRAE (2011) climate classes and the Climate Evaluation Chart were then applied to assess the historic microclimate conditions of the site under study. The ASHRAE recommends keeping T between 15 and 25 °C and constant RH values at the set point of 50% or at the annual average corresponding to the historic reference values. Specific seasonal and short-term fluctuations are set based on six classes of control (AA, As, A, B, C, and D as described by Martens (2012)). The possible risks for collections increase gradually from class AA, associated with no risk to most objects, to class D, that protects only from dampness. Moreover, this guideline classifies buildings according to a combination between various types of the building envelope and the climate control. The former takes into account the building construction (open structure, heavy masonry, insulated structure, etc.), the type of building (house, museum, storage rooms, etc.), and the building use (no occupancy, limited occupancy, walk-through visitors, etc.). The latter considers the climate system in use (no system, no heating, summer cooling, etc.) and the limit of the practical limit of climate control (none, ventilation, basic heating and ventilation air conditioning (HVAC), special constant environment, etc.) according to the building type and the outdoor climate. In a such way, seven building classes are identified and grouped in three categories of the climate control (uncontrolled, partial control, and climate controlled).

Appendix B

Table 1 Results of minimum and maximum CI

	CI	CoI	MQI_T	MQI_RH
Minimum	0.999	0.62	0.44	0.56
Maximum	0.999	0.79	0.55	0.71

CoI and MQI_T (MQI for temperature series) and MQ_RH (MQI for RH series) over the whole monitoring period (from November 4, 2008 to October 6, 2015)

The Napoleonic Museum would belong to the class IV with the partial climate control, since it is a historical building with heavy masonry, basic HVAC used in winter, and walk-through visits. For this reason, the climate classes of control B, C, and D are sustainable in relation to the energy usage. The class of control B was chosen in accordance with the characteristic of building envelope and HVAC system used within the museum. Moreover, since no degradation phenomena of artworks has occurred over the last 8 years, a higher class of control, such as AA and A, would mean an excessive energy cost for the museum.

Then, the class of control B was used to assess at which extent both T and RH of the representative room can describe the behavior of rooms belonging to the same cluster.

Thereafter, another evaluation of the indoor climate has been done by using the Climate Evaluation Chart (hereafter called CEC) proposed by Martens et al. (2006). CEC is a psychrometric chart where T and RH behavior is displayed on both seasonal and monthly scales taking into account the allowable thresholds of the class of control (in this study, the class of control B).

Exploratory data analysis, cluster analysis, and climate classifications were carried out using MATLAB software (version 2017b). The scripts to calculate the quality indexes as well as the climate classifications were created by the authors in the same computing environment.

Results and discussion

Exploratory data analysis

Figure 2 shows box-and-whisker plots of T (upper panel) and RH (lower panel) data in each room over the whole monitoring period (January 2009 to October 2015). Looking at *T* box plots, it can be noticed that 2011 box in all rooms (except for the rooms 9 and 10) does not overlap those of other years; it means that there is significant difference among this year and the other years. This is due to several intervals without data. The same is for RH in 2011. Consequently, that year was not taken into account in the following analysis. Yet, RH boxes in 2009 show in general a median value lower in respect to other years. In addition, several RH outliers (very dry conditions) can be noticed. As they cannot be associated to instrumental problems, they were included in the analysis because they were related to the indoor climate evolution.

Table 2 Results of minimum and maximum CI, CoI and MQI_T (MQI for T series) and MQ_RH (MQI for RH series) over the selected monitoring period (from April 1, 2012 to June 30, 2013)

	CI	CoI	MQI_T	MQI_RH
Minimum	0.999	0.88	0.60	0.77
Maximum	0.999	0.92	0.64	0.82

Table 3 The average of Silhouette score

	$k=3$	$k=4$
T	0.57	0.52
RH	0.58	0.50
MR	0.68	0.64

k is the number of clusters

To better identify the proper time intervals for the following analysis, the three indexes described in the previous section were calculated. Table 1 summarizes the results of minimum and maximum values of CI, CoI, and MQI for the whole monitoring period (January 2009 to October 2015). The CI and CoI for T and RH are the same over the whole period because the sensors recorded contemporary both parameters; MQI was separately determined since T and RH sensors have different metrological characteristics, and hence, they can be classified in different categories. CI is very close to the unity, whereas CoI ranges from 0.62 to 0.79. MQI for T and RH series ranges from 0.44 to 0.55 and from 0.56 to 0.71, respectively. This means that both T and RH time series are continuous, incomplete due to several missing data, and of poor quality. Thus, we have searched continuous periods in which the indexes reached the highest values in all rooms. We found that the period from April 1, 2012 to June 30, 2013 is that appropriate (Table 2) for the analysis of indoor climate. The mean value of T and RH medians of all rooms is 22.8 °C (ranging from 21.7 to 26.6 °C) and 46.1% (ranging from 41.3 to 50.4%), respectively.

Cluster analysis on a single microclimate parameter

The CA was applied individually to indoor T, RH, and MR data set considering three and four clusters, because in case of

Table 4 The centroid values for T/RH/MR and the representative room (at the smallest distance from the centroid) for each cluster

	T (°C)	Room	RH (%)	Room	MR (g/kg)	Room
Cluster 1	22.5	2	42.4	7	7.7	2
Cluster 2	23.7	5	45.1	9	8.3	5
Cluster 3	24.4	12	48.8	1	9.2	11

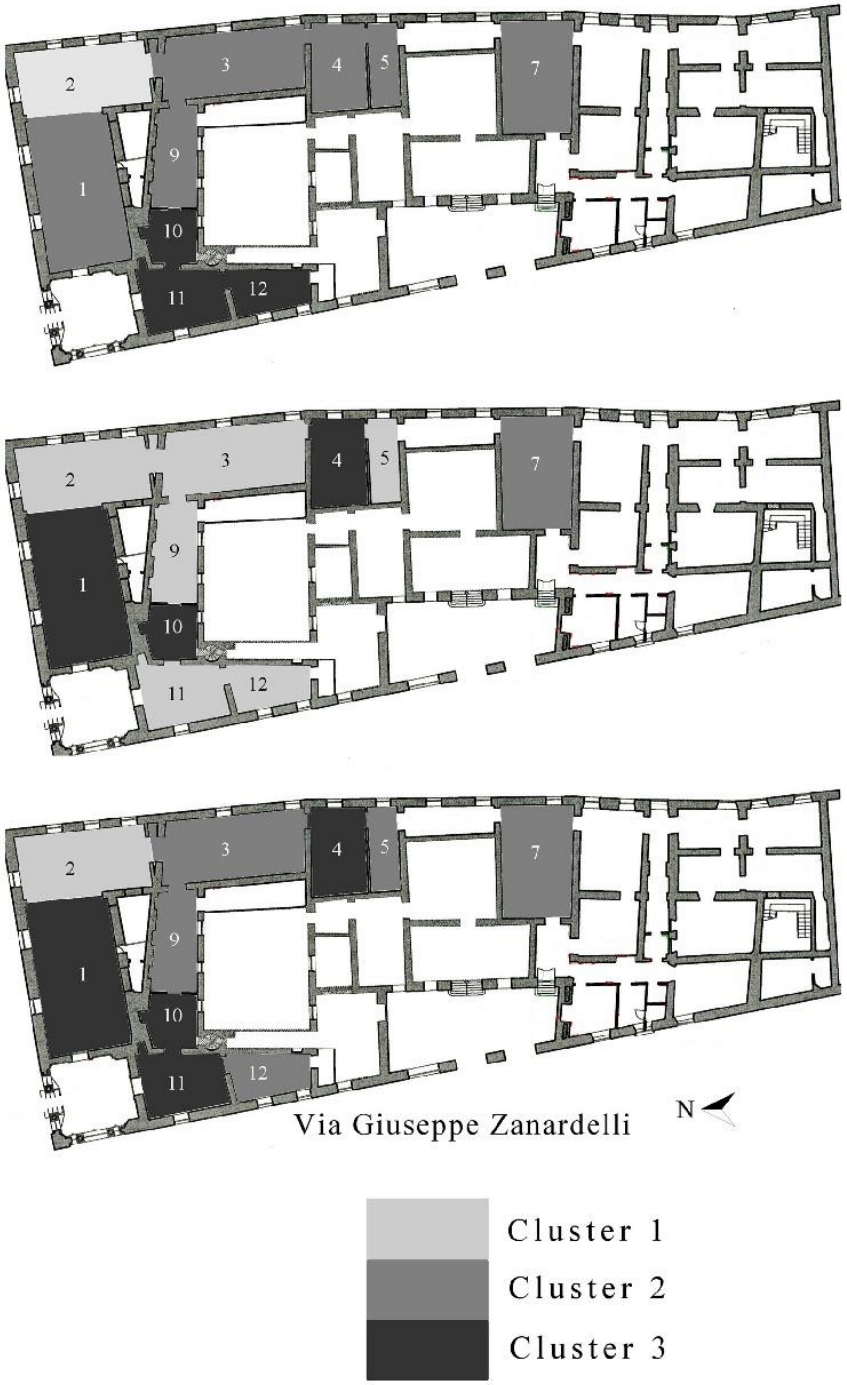

Fig. 3 Plan of the museum after the application of CA to each parameter: temperature clustering (the upper panel), relative humidity (the middle panel), and mixing ratio (the lower panel)

only two clusters, some rooms were assigned to the wrong cluster (negative *S*). Table 3 shows the averages of the *S* score. In general, the results on the Silhouette index indicate a moderate/high similarity among the rooms within their cluster. The number of the clusters was chosen equal to 3, taking into account the highest average value of the Silhouette index.

Appendix B

Each cluster was identified by a virtual center (centroid) characterized by the mean of T/RH/MR of the involved cases. The room at the minimum Euclidean distance from the virtual center was regarded as the most representative element of the whole cluster. The representative elements of each microclimatic parameter (virtual center and the room at the minimum distance for all clusters) are reported in Table 4. Looking at the temperature CA (Fig. 3, upper panel), cluster 1, composed only by room 2, is characterized by the lowest T (22.5 °C) with respect to both cluster 2 (rooms 1, 3, 4, 5, 7, 9; the representative is room 5) with T = 23.7 °C and cluster 3 (rooms 10, 11, 12; the representative is room 12) with T = 24.4 °C. This clustering could be associated to a temperature gradient from the northeast side of the building orientation towards west-south side.

Looking at the relative humidity CA output (Fig. 3, middle panel), cluster 1, composed by room 7, has RH = 42.4%, cluster 2 (rooms 2, 3, 5, 9, 11, 12; the representative is room 9) is associated to RH = 45.1%, whereas cluster 3 (rooms 1, 4, 10; the representative is room 1) is characterized by RH = 48.8%. Concerning the mixing ratio CA output (Fig. 3, lower panel), cluster 1 (room 2) is characterized by MR = 7.7 g/kg, cluster 2 (rooms 3, 5, 7, 9, 12; the representative is room 5) by MR = 8.3 g/kg, and finally, cluster 3 (rooms 1, 4, 10, 11, the representative is room 11) has MR = 9.2 g/kg. The MR clustering distribution seems largely to depend on the mass of vapor supplied by humidifiers which result to be more effective when the room size is small (for example, rooms 4 and 10).

Nevertheless, the above general considerations on the CA results do not physically well explain the different behavior between room 1 and the contiguous room 2, which are not divided by any architectural structure. To understand if there were real differences between the two rooms, ad hoc field campaign was performed in January 2018 by the authors measuring temperature and relative humidity at the same horizontal level (1.5 m above the floor). The results of the field campaign is that room 1 and 2 were thermal-hygrometric homogeneous. It was found that the thermo-hygrometer sensor of room 1 was placed behind a showcase in a corner; hence, likely, it is not quite representative of the real microclimate condition in the room 1. In this case, the CA has provided useful elements to identify measurements which may induce misleading interpretation of the ambient conditions.

The CA was then applied without T and RH data of room 1; i.e., rooms 1 and 2 were considered a unique area. The representative elements of this further analysis are identical to that reported in Table 4 for T and MR. Concerning RH, it was found that room 4 represents the cluster 3 (composed by rooms 4, 10, 11), with higher RH = 48.0%. The averages of the *S* score become 0.58 (T), 0.53 (RH), and 0.72 (MR).

Cluster analysis and outdoor conditions

To test the CA capability in studying the influence of external conditions by scatter plots, the representative room of the coldest/warmest cluster was plotted together with a room (taken as case-control) belonging to the same cluster as a function of the outdoor temperatures. The same was done for the clusters having the largest difference in moisture content.

Figure 4 shows T monthly means scatter plot taking into account the representative rooms 2 (the coldest cluster) and 12 (the warmest cluster) and room 10 as the case-control. For MR (Fig. 5), the representative rooms were 2 (the driest cluster) and 11 (the highest moisture content), and room 10 as the case-control.

Looking at the scatter plot in Fig. 4, a typical temperature pattern of heated buildings can be noticed, where on average, winter values are always above the bisectrix, as experienced in these rooms. However, room 2, due to its larger size and its placing towards north, seems also to be affected by the external temperature variations with lower temperatures in December, January, and February with respect to rooms 12 and 10. From spring to autumn, the internal temperature in these rooms follows the outdoor temperature trend.

The monthly indoor MRs (Fig. 5) differ among the rooms: room 2 is almost always placed below the bisectrix (small vapor exchange with outdoor), whereas rooms 11 and 10 identically well follow the external variations except in winter because the humidifier is in operation. In June–July, the larger internal MR values, with respect to external ones, could be due to the scarce ventilation responsible of the vapor accumulation.

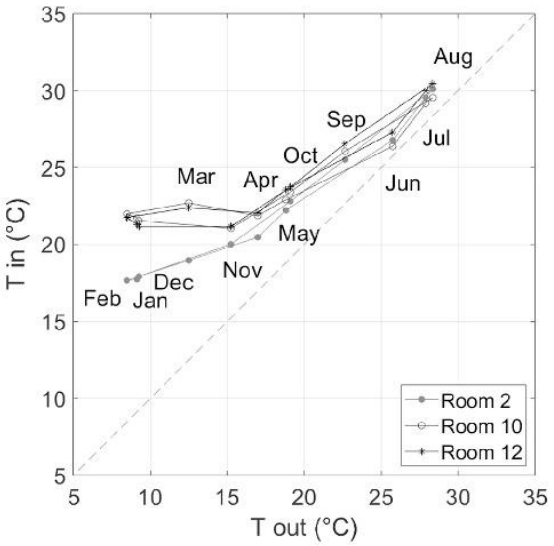

Fig. 4 Indoor vs outdoor monthly averages of temperature data (rooms 2, 10, and 12). The averages were calculated from June 1, 2012 to May 31, 2013

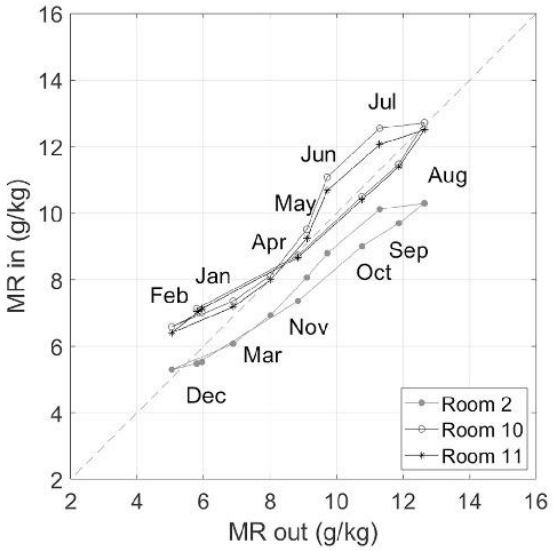

Fig. 5 Indoor vs outdoor monthly averages of mixing ratio values (rooms 2, 10, and 11). The averages were calculated June 1, 2012 to May 31, 2013

Based on the above results, the CA was further applied including also outdoor data with the purpose to better investigate the influence of external environmental conditions on the indoor clustering. Four clusters were taken into account. The CA identified a unique cluster associated only to external conditions (regardless of the considered microclimatic parameter), whereas the other clusters resulted identical to those described above. These CA results are not in contradiction with the scatter plots since the effects of heating and humidifier systems likely mitigate the natural response of the rooms to the external climate when the analysis is performed on the annual scale.

Table 5 The centroid values for T/RH/MR and the representative room (at the smallest distance from the centroid) for each cluster

	T (°C)	RH (%)	MR (g/kg)	Room
Cluster 1	23.5	44.9	8.2	9
Cluster 2	24.2	42.4	8.2	7
Cluster 3	24.4	48.0	9.3	4

Cluster analysis on all microclimatic parameters

The CA was applied to classify the rooms taking into account all internal microclimatic parameters. Also in this case, the number of the clusters is 3 (the average of *S* score is 0.52 higher than that of 4 clusters (0.46)).

Figure 6 shows the thermo-hygrometric clustering of the museum, and in Table 5, the mean values of the fields which define the centroid for each cluster are reported.

It is worth noticing that the cluster classification based on temperature with humidity variables might be different from the one based on just one single variable. In fact, while T and MR can change coherently from lower to higher levels or vice versa, RH can mainly drive the room clustering because of its nonlinear dependence from T and MR.

In Fig. 7, box-and-whisker plots of T (upper panel) and RH (lower panel) data for each cluster are displayed, showing that the use of representative room (filled box) of each cluster can replace the exploratory analysis performed on the other rooms (overlapping of the box belonging to the same cluster).

Cluster analysis and climate classification

The percentage of data in which the indoor climate of each room fits the class of control B (ASHARE 2011) is

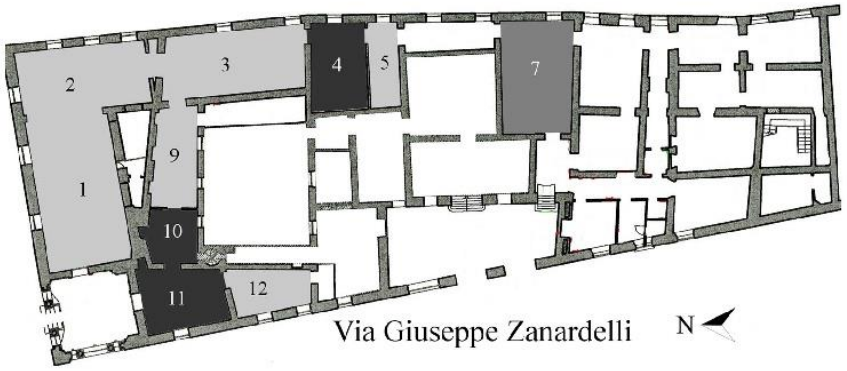

Fig. 6 Plan of the museum after the application of CA taking into account all three parameters

Appendix B

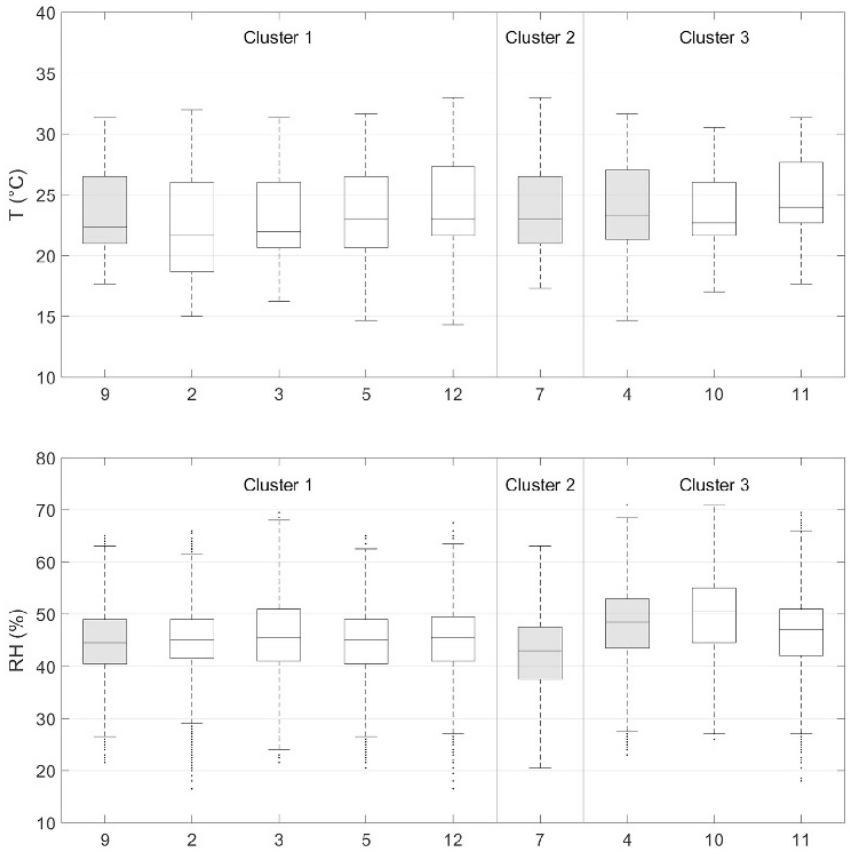

Fig. 7 Box-and-whisker plots of indoor T (upper panel) and RH (lower panel) for each cluster (the representative room is displayed as filled box)

reported in Table 6. The occurrences of the class B in all rooms are on average higher than 84%, indicating that a moderate risk of mechanical damage may occur to high vulnerable artworks (about 16% of cases).

According to the outcomes of the CA on T, MR, and RH data, the rooms which belong to cluster 1 differ from the representative room with a bias from 2 to 7%, while those of cluster 2 from 0 to 12%.

A further exercise on the application of CA in the microclimate assessment was by creating the CEC for each cluster in order to visualize the seasonal behavior of the representative room with respect to the other rooms of same cluster. Figures 8 and 9 show the CECs of clusters 1 and 3, respectively. Cluster 2 is not shown since it includes only one room. The climate *T* and RH limits (the area delimited by blue lines and blue curves) were determined from the dataset of the representative room of each cluster, i.e., room 9 for cluster 1 and room 4 for cluster 2 (both identified by filled circles). The colors visualize the seasonal distribution. Also, for this purpose, the CA can be used for the evaluation of indoor climate performances. Both representative rooms well explain the T-RH monthly variability of other rooms belonging to the same cluster. Both the representative rooms and the rooms of the respective cluster are within the RH thresholds. Concerning temperature, all rooms are above the T thresholds only in summer (mainly in July and August). Only room 2 (indicated as asterisk in Fig. 8) are below the T threshold of the representative room, showing that the heating system is not as effective as in

Table 6 Summary of the percentage of data which fit into the climate class of control B (ASHRAE 2011)

Room	Percentage of data (%)
2	89
3	90
4	84
5	84
7	88
9	91
10	94
11	84
12	84

The rooms 9, 7, and 4 are the representative of clusters 1, 2, and 3, respectively

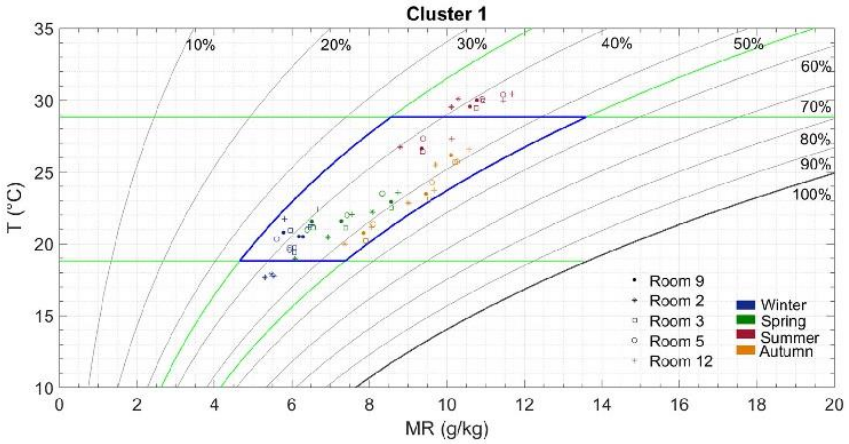

Fig. 8 The psychrometric chart of the cluster 1. Indoor climate is seasonally represented: blue (winter), green (spring), red (summer), and orange (autumn). The class B area is delimited by two horizontal blue lines (the T limits between 19 and 29 °C) and two blue curves (the RH limits ± 10% with respect to the historical annual average of the representative room of the cluster). The room are identified by the following symbols: circle (the representative room of the cluster, room 9), asterisk (room 2), square (room 3), circle (room 5), and cross (room 12)

other rooms, and in addition, it can be affected by the external temperature as already observed by scatter plots.

Conclusions

In this paper, we have demonstrated that the cluster analysis allows to assess the indoor climate conditions with the use of the exploratory data analysis and the ASHRAE climate classification. Indeed, the study has revealed that the museum fits the class of control B (84% on average), analyzing both all data recorded in each room and data from the most representative room from the cluster analysis application. As a result, a moderate risk for highly vulnerable object and a tiny risk for most objects might occur only on the 16% of occurrences.

The study has demonstrated that several sensors for the monitoring of temperature and relative humidity can be redundant at assessing the indoor climate in multi-room museum located in the same floor. Indeed, the cluster analysis by *k*-means algorithm can be considered an effective procedure to group climate physically consistent rooms, once the conservation surveys do not reveal damages on the stored objects. When the clusters are defined, indoor conditions can be monitored and analyzed even in the case the sensor in a room does not properly work or has been removed due to the lack of calibration or for damages.

Finally, the cluster analysis has proven to be effective in identifying sensor space-setting which was not adequate for an acceptable knowledge of the microclimate within a room.

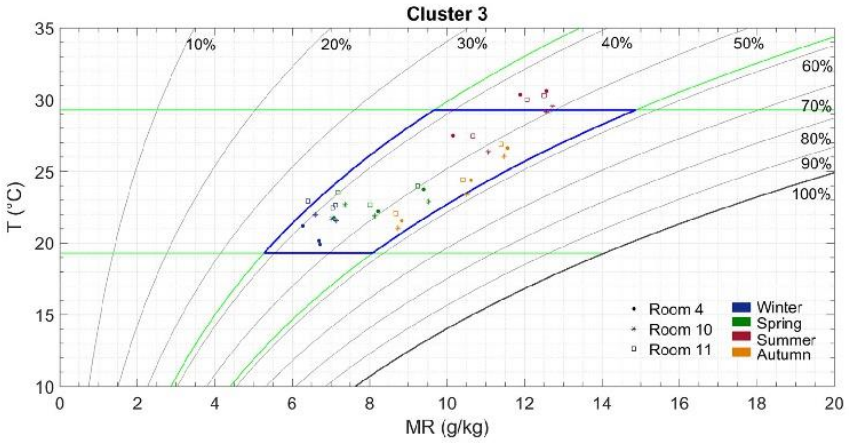

Fig. 9 The psychrometric chart of the cluster 3. Indoor climate is seasonally represented: blue (winter), green (spring), red (summer), and orange (autumn). The class B area is delimited by two horizontal blue lines (the T limits between 19 and 29 °C) and two blue curves (the RH limits ± 10% with respect to the historical annual average of the representative room of the cluster). The room are identified by the following symbols: circle (the representative room of the cluster, room 4), asterisk (room 10), and square (room 11)

Appendix B

Acknowledgments The authors are grateful to the Museo Napoleonico staff for their assistance and, in particular, to Dr. Fabio Benedettucci for his valuable support. We also thank Climate Consulting S.r.l. for providing the meteorological data.

Author contributions All authors have helped to develop the paper. A.M.S. has played the major role supervising and coordinating the whole work, A.M.S. and F.F. have equally contributed in the conceptualization and writing the paper, M.D.M. and V.B. have performed the measuring campaigns in the museums, A.M.S. has supervised the statistical elaboration of climatic data, F.F. and M.D.M. have equally contributed in the statistical elaboration of the experimental data, and E.F. has contributed in the statistical elaboration of the data and coordinated the manuscript preparation.

References

ASHRAE (2011) ASHRAE handbook—HVAC applications. Chapter 23: museums, galleries, archives, and libraries. American Society of Heating, Refrigerating and Air-Conditioning Engineers, Inc., Atlanta

Bernardi A, Camuffo D (1995) Microclimate in the Chiericati palace municipal museum, Vicenza. Museum Management and Curatorship 14(1):5–18

Bertolin C, Camuffo D, Bighignoli I (2015) Past reconstruction and future forecast of domains of indoor relative humidity fluctuations calculated according to EN 15757:2010. Energ Build 102:197–206

Bratasz L, Camuffo D, Kozłowski R (2007) Target microclimate for preservation derived from past indoor conditions. In: Padfield T, Borchersen K (eds) Museum microclimates contributions to the Copenhagen conference 19–23 November 2007, Copenhagen, 2007. The National Museum of Denmark, Copenhagen, pp 129–134

Camuffo D (2014) Microclimate for cultural heritage:- conservation, restoration and maintenance of indoor and outdoor monuments, Second Edition. Elsevier, New York, p 560

Camuffo D, Bernardi A (1996) Controlling the microclimate and particulate matter inside the historic anatomy theatre Padua. Museum Manag Curatorship 15:285–298. https://doi.org/10.1016/S0260-4779(96)00046-5

Camuffo D, Sturaro G, Valentino A (1999) Thermodynamic exchanges between the external boundary layer and the indoor microclimate at the basilica of Santa Maria Maggiore, Roma, Italy: the problem of conservation of ancient works of art. Bound-Layer Meteorol 92(2): 243–262

EN 15757 (2010) Conservation of cultural property—specifications for temperature and relative humidity to limit climate-induced mechanical damage in organic hygroscopic materials. European Committee for Standardization, Brussels

EN 15758 (2010) Conservation of cultural property—procedures and instruments for measuring temperatures of the air and the surfaces of objects. European Committee for Standardization, Brussels

EN 16242 (2012) Conservation of cultural property—procedures and instruments for measuring humidity in the air and moisture exchanges between air and cultural property. European Committee for Standardization, Brussels

Frasca F, Siani AM, Casale GR, Pedone M, Bratasz Ł, Strojecki M, Mleczkowska A (2017) Assessment of indoor climate of Mogiła Abbey in Kraków (Poland) and the application of the analogues method to predict microclimate indoor conditions. Environ Sci Pollut Res 24(16):13895–13907. https://doi.org/10.1007/s11356-016-6504-9

Martens MHJ (2012) Climate risk assessment in museums: degradation risks determined from temperature and relative humidity data. Doctoral dissertation, Technische Universiteit Eindhoven

Martens MHJ, van Schijndel AV, Schellen HL (2006) Evaluation of indoor climates using the ' climate evaluation chart'. In: Guarracino G (ed) 27th AIVC and 4th Epic Conference B Technologies & sustainable policies for a radical decrease of the energy consumption in buildings, Lyon, 20–22 November 2006. EPIC 2006 AVIC: proceedings — actes, vol 4. Ecole Nationale des Travaux Publics del' Etat, Vaulx-en-Velin, pp 523–528

Pavlogeorgatos G (2003) Environmental parameters in museums. Build Environ 38:1457–1462. https://doi.org/10.1016/S0360-1323(03)00113-6

Rousseeuw PJ (1987) Silhouettes: a graphical aid to the interpretation and validation of cluster analysis. J Comput Appl Math 20:53–65. https://doi.org/10.1016/0377-0427(87)90125-7

Warren LT (2003) Clustering of time series data—a survey. Pattern Recogn 38(11):1857–1874. https://doi.org/10.1016/j.patcog.2005.01.025

Appendix C

Use of photovoltaic modules as static solar shadings: Retrofit of a paleontological site in Rome

Frasca F., Lovati M., Cornaro C., Moser D. and Siani A.M.

In 12th Conference on Advanced Building Skins, 2-3 October 2017, Bern, Switzerland. Proceedings book. pp. 1235-1245. (2017).

Use of photovoltaic modules as static solar shadings: retrofit of a paleontological site in Rome

[1]Francesca Frasca, [2]Marco Lovati*, [3]Cristina Cornaro, [2]David Moser, [4]Anna Maria Siani

[1]Department of Earth Sciences, Sapienza Università di Roma, Italy, f.frasca@uniroma1.it

[2]EURAC Institute for Renewable Energy, Bozen, Itay, marco.lovati@eurac.edu

[3]Dep. of Enterprise Engineering, Università degli Studi di Roma "Tor Vergata", Italy cornaro@uniroma2.it

[4]Dep. of Physics, Sapienza Università di Roma, Italy, annamaria.siani@uniroma1.it

Abstract

An innovative approach for the design of a Building Integrated PhotoVoltaic system (BIPV) is tested in a prefabricated building with a glass façade on the southern side. The aim is to reduce the occurrences of excess heat in Summer using photovoltaic (PV) system as static shadings. Standard "off the shelf" photovoltaic modules set along the southern façade are used for the static shadings. The optimization involves the tilt angle and the distance of the PV arrays in a parametric design environment and aims at reaching the Combination Optimized to Meet Building Objectives (COMBO). The effect of PV shading on indoor microclimate and energy consumption of the building was evaluated by means of whole building dynamic simulation. The proposed design, as a passive control of indoor climate, achieves a decrease of 0.4°C in the yearly mean temperature and a reduction of 0.5°C of the maximum daily fluctuation with respect to the geometry without it. As for the energy consumption (active control), there is a reduction of 27.6% in the cooling hours even if the total energy over the period increases of about 1.18 kWh/m^2. The methodology features two main innovations which improve speed and versatility in the definition of a potential refurbishment by means of the dual approach given by the whole-building dynamic simulation and the BIPV system.

Keywords: BIPV, indoor climate, optimization, energy, whole-building dynamic simulation, conservation.

1. Introduction

This paper describes an innovative approach and workflow for the design of a Building Integrated PhotoVoltaics (BIPV) system in case of retrofit of an existing building. The technology consists in standard "off the shelf" photovoltaic modules to be used as static shadings, recently explored in terms of thermal and electrical performance evaluation [1, 2, 3]. BIPV systems are mainly used in the construction of new buildings, but they should be considered for the retrofitting projects of existing buildings as well. The advantage of using photovoltaic modules as building material is that they can replace conventional materials and systems (e.g. the static shading system considered in this study). The solution combines both active and passive properties, since it provides selective solar shading and produces clean electricity on site [4]. This methodology agrees with one of the strategic targets set by the European Union for 2020 *in the Energy Performance of Buildings Directive (E.P.B.D.)* [5], i.e. the achievement of energy efficiency in retrofitting interventions of existing buildings which belong to the public institutions.

Nowadays, both climate behaviour and energy performance inside a building can be accurately assessed by means of a whole-building dynamic simulation software. More reliable results are provided using simulation tools in conjunction with on-site ambient measurements, which allow the calibration and validation of the building model and then the representation of the actual case as accurately as possible [6]. A reliable simulation model is needed to retrieve meaningful retrofitting solutions. However, dynamic simulation

software need more detailed input data for climatic conditions and building properties with respect to static and semi-dynamic simulation software.

Recently, the use of BIPV system in combination with dynamic simulation software has gained commensurable interest in the scientific community for the possibility to assess in advance the impact of the retrofitting solutions in existing buildings in terms of energy consumption and thermal comfort of people. This approach has been used especially in the case of post Second World War period buildings, but in the latest years attention has been paid to historical buildings as well [7]. In the latter study, the aim was the definition of a retrofitting solution with the reduction of energy consumption and the respect of the historical-cultural values of the building. However, as yet, no study has been conducted with the aim at analysing the impact of the BIPV system using whole dynamic simulation in the case of buildings which preserve palaeontological remains.

This study addresses very important, timely topics:

1) the use of energy demand outputs from dynamic simulation as the basis for a purely geometrical optimization of BIPV system. This is relevant for the performance of the chosen solution without running a dynamic simulation for each combination.
2) the risk analysis of mechanical degradation of artefacts in the estimated thermo-hygrometric conditions by means of simulation after the retrofitting solution.

The approach is applied in the case of a prefabricated building presenting a glazed façade on the southern side and preserving several faunal paleontological remains. The method is applied here since it is fundamental to know in advance the effect of a retrofit in buildings with conservation purposes to avoid and reduce the occurrence of degradation of artefacts. The potential solution will be adopted only if it benefits both the conservation environment and the thermal comfort requirements of visitors and staff. In case of conflict, the priority should be given to conservation [8].

2. Methodology

The proposed methodology combines both the search for a Combination Optimized to Meet Building Objectives (COMBO) for BIPV system and whole-building dynamic simulation software (schematically shown in Figure 1) with the dual purpose to suggest an innovative approach in retrofitting solution and to test it in a peculiar case study.

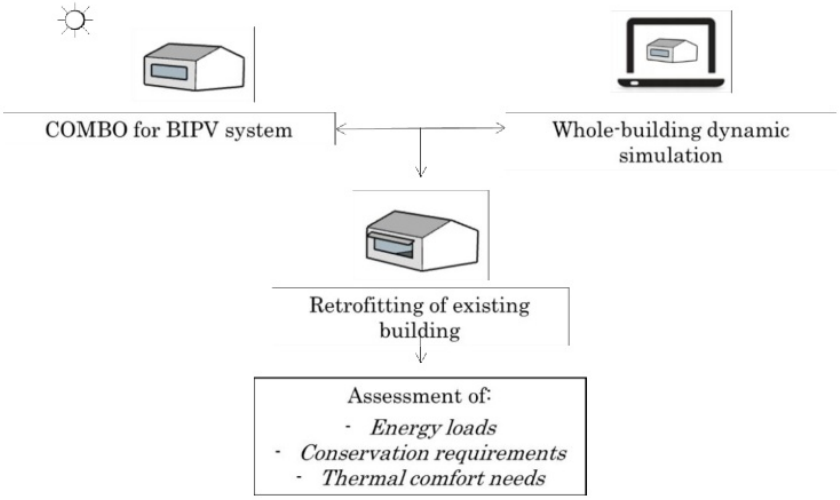

Figure 1: Schematic workflow of methodology proposed in this study.

As a first step, the building model is calibrated using hourly indoor temperature measured on-site and then energy demand is simulated. After that, an array of photovoltaic (PV) modules along the glazed façade is set and optimized arranging the tilt angle and distance between PVs in a parametric design environment (i.e. a design framework in which the attributes are described by means of variables instead of constants). Then, a further energy load is run with the optimized arrangement in order to assess the energy performance of the retrofit and the impact on indoor climate for conservation requirements.

The methodology presents two main innovations which improve speed and versatility in the identification of the best solution. The optimization method does not require running simulation for each parametric combination of photovoltaic modules, because it is based on the incoming irradiance on the glazed surface, greatly boosting the speed of the optimization. Given the load profile provided by the simulation of building model with the use of ideal heating and cooling systems, the algorithm searches a COMBO to minimize the solar irradiance during cooling hours and to maximize it during heating hours. The versatility of methodology relies on a ray-tracing procedure (using Radiance based Daysim [9]) to generate the hourly irradiance profiles on the glass. The computational resources required by ray-tracing do not increase much for complex geometries and are therefore a good candidate for BIPV simulation applications.

The case study is “La Polledrara di Cecanibbio” (Figure 2), located at NW of Rome (Lat. 41.93° N, Long. 12.30° E) in a rural area. The building was built in 2000 with the main purpose to preserve fossils from meteorological events and to make it a public museum. The remains exhibited in the north side suffer from biological degradation due to hygrometric conditions of the deposit (RH>90%) and both staff and visitors complain of thermal discomfort. The building envelope covers an excavated area of 900 m^2 (30-by-30 m per side) and is placed directly on the soil. The maximum height of the building is 8 m (east side), while the minimum is 6.5 m (west side).

The monitoring campaign of indoor climate parameters in the site under study started on June 2008 and it is still in operation. Measurements of indoor air temperature (T) and relative humidity (RH) were used for the calibration of the building model and together with the measurements of cracks (FO) parameters for the risk analysis of mechanical degradation of faunal remains. Finally, the air mixing ratio (MR) has been calculated using T and RH in the equation reported in the European Standard EN 16242:2012 [10].

Figure 2 “La Polledrara di Cecanibbio” southern façade, Rome (Italy). Picture by courtesy of the “Soprintendenza Speciale per i Beni Archeologici di Roma”.

2.1 Dynamic Simulation environment

Dynamic building simulation for indoor climate analysis was performed using the software tool IDA Indoor Climate and Energy (IDA ICE) 4.7.1 developed and distributed by EQUA simulation AB.

After the calibration and validation of the building model, the simulation was run with regards to the energy load due to ideal heater and cooler for a whole year.

2.1.1 IDA ICE setting

The geometry of the building of "La Polledrara di Cecanibbio" was created in the model working out information from the architectural survey provided by the "Soprintendenza Speciale per i Beni Archeologici di Roma".

The first guess of the building model was represented as directly placed on soil taking into account only the impact of external climate. The external walls are double skin panels insulated by polyurethane with a nominal thickness of 6 cm, whereas the roof is a trapezoidal sheet for concrete slabs with a nominal thickness of 12 cm. The windows (i.e. double-pane clear glazing with aluminium frame without thermal-break) are along the north and south walls covering an area of about 1900 m^2 and are shadowed in the inner side by white PVC roller blinds which have been never opened. The properties of opaque and transparent components are reported in Table 1 and Table 2, respectively.

Table 1: Thickness and overall heat transfer coefficient (U-value) of opaque components.

Component		Thickness (m)	U-value (W/m^2*K)
External walls	double insulated panel	0.07	0.27
Roof	concrete slab	0.15	1.13
Floor	clay silt soil	1.85	0.25

Table 2: Glazing heat transfer coefficient (U-value), Solar Heat Gain Coefficient (SHGC) and solar Transmittance (T) of transparent component

Component		U-value (W/m^2*K)	SHGC	τ
Window	Double clear pane (4-12-4)	3.05	0.769	0.692

The soil layer was modelled using the version ICE 3, which computes the soil temperature as the mean air temperature given by the climate file without 2D or 3D modelled effects. The air infiltrations were modelled considering air tightness at 2.9 ACH (Air Change per Hour) and at pressure difference of 50 Pa. The thermal bridges were considered among external walls and roof. Lightning, equipment and visitors are not included because only reserved visits are possible.

Ideal heater and cooler were used to condition the area since no detailed information about the actual air conditioning systems were available. They have no given physical location on any room surface and are not connected to the plant of the building. The capacity parameters of both ideal heater and cooler were set up at a large enough value to always cover any foreseen need, 150kW and 20 kW respectively.

The temperatures of the air conditioning system were set up 16°C and 26°C for cool and warm conditions, respectively. These limits have been chosen for a first assessment of the indoor climate with the aim not to widely modify the historical climate [11], at which faunal remains have adopted after unearthing, but to eventually provide an improvement of thermal comfort. However, further studies will be carried out to find adequate dynamic control limits of air conditioning system.

A climate file was created to run the model for the calibration using outdoor T and RH measured at La Polledrara. Wind direction and speed intensity, global radiation on a horizontal surface, measured at Fiumicino Testa di Lepre station (Lat. 41.95°, Lon. 12.28° far from the site about 2.7 km) belonging to ARSIAL (Regional Agency for Development and Innovation of Agriculture in Lazio), were also included in the climate file.

2.1.2 Calibration and validation

The calibration was carried out using hourly indoor temperature (T) data collected from January 1st 2016 to February 29th 2016 (for more details about the calibration procedure [12]). The model was initialized at the start-up period from December 18th 2015 to December 31st 2015. The validation was performed using data collecting in July 2016.

Two statistical parameters were calculated: root-mean-square-error (RMSE) and Coefficient of Variation of the RMSE (CV-RMSE). RMSE is used to measure the difference between modelled and measured indoor T. CV-RMSE describes the model fit in terms of the relative sizes of the squared residuals and outcome values assessing the similarity of the modelled to the actual values.

2.2 Optimization of the BIPV system

The aesthetical or technological details of BIPV system are not the core of this study. Indeed, the adjective "integrated" refers to the analysis of the PV interaction with the building energy system. The PV modules are used as static shading devices or "brise soleil" therefore including the function of reducing the excess solar gain during cooling hours. Alongside the passive purpose the PV modules should produce electrical energy, so they are evaluated as multifunctional elements. The system is optimized by means of multi target genetic algorithm [13], that uses the slope angle of the static shadings and the distance between the blades of static shadings as parameters of optimization (Figure 3). Instead of generating a model specific for this application, an essential and general purpose layout of the problem was employed as shown in (Figure 4).

The hourly solar irradiance [kW/m^2] was evaluated using the Radiance based Daysim software [14]. The climate file used as input was generated using data collected by ARSIAL (see par 2.1.2). The irradiance was calculated in eight reference planes: three reference planes were positioned along the surface of the photovoltaic module, five were positioned between two blades and parallel to the façade of the building (i.e. vertical and 20.6° West of South). The model also included two blades: the lower one hosted the reference planes and the upper one served to cast shadows and so to assess the self-shading of a particular solution. The irradiance on the three planes along the surface were used to simulate a PV module formed by three strings connected in series and equipped with a bypass diode. Given the geometry of the array, the nearby modules were assumed to be in an identical shading condition. The instantaneous power of the module was assessed as the power of the least irradiated cell multiplied by the number of strings that are not bypassed. This approach is a strong approximation [15], but served the purpose to estimate, for each hour, the number of bypassed strings. An ideal maximum power point tracking (MPPT) device was assumed. The power in a specific hour of year (HOY) of the simulated module is therefore described as:

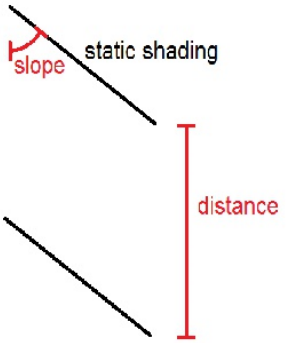

Figure 3 : stylized representation of the cross section of the static shadings. The variable parameters of the system are shown in red.

$$P(HOY) = Max_{c=1}^{3}(G(HOY,c)\cdot\eta\cdot A\cdot N(c)\cdot PR)\cdot N_{modules}, \qquad (1)$$

where P(HOY) is the power in a specific hour of the year. Max is an operator that indicates the configuration "c" generating more power, it works as an ideal MPPT device. G(HOY,c) is the irradiance of the least irradiated string in a given HOY and "c", it is lower in the configuration where no string is bypassed. η is the efficiency at a module level and A is the active area of one string. N(c) is simply the number of strings that are not bypassed in the configuration "c". PR is a static Performance Ratio of the system (a value that takes into account losses at system level) and $N_{modules}$ is the number of modules in the solution (is higher when the blades are closer).

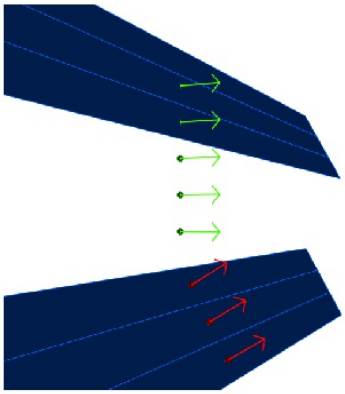

Figure 4: tridimensional representation of the model used in the optimization, the arrows represents the perpendiculars to the measuring planes.

The irradiance filtering through the shading blades during heating and cooling period was evaluated to ensure the performance of the system from a passive perspective. This calculation does not take into account the G value of the windows or the transmitted radiation through the wall but only the quantity of radiation that filters through the shading system in each hour of the year. The hourly ideal heating and cooling demand of the building was retrieved from the calibrated IDA ICE model and each HOY was defined as a heating or cooling hour based on the most prominent load. An index called "gain index" was defined as:

$$Gain = \sum_{CHOY}\frac{1}{5}\sum_{p=1}^{5}G(HOY,p) - \sum_{HHOY}\frac{1}{5}\sum_{p=1}^{5}G(HOY,p), \qquad (2)$$

where CHOY are the heating hours of the year, p are the measuring planes, G(HOY,p) the relative irradiance in a specific hour and HHOY the cooling hours of the year.

This index is therefore a purely geometrical performance index for the shadings and takes into account the radiation energy going through the system during the cooling hours minus that going through it during the heating hours. A lower gain index is preferred to a higher one in terms of passive performance.

The two quantities extrapolated from (1) and (2) are used as objective functions in the GA optimization. Being a multi target optimization the result consists into a Pareto front, or the group of non dominated solutions.

3. Results

The main results of the proposed methodology are shown in the three subsections. In the last subsection (3.3), the retrofitting solution chosen by COMBO is assessed analysing separately the impact of passive and active control of the indoor climate both on the risk analysis of faunal remains (passive and active control) and on the energy demands of the building (only active control).

3.1 Calibration and validation of building model

Table 3 summarizes the outcomes of the calibration and validation procedure of the building model using hourly indoor temperature (T). RMSE and CV-RMSE of the calibrated model are 0.5°C and 4.0%, respectively. As for the validation, the simulation has been run in July: RMSE=0.6°C and CV-RMSE=2.3%. The RMSE values are higher than instrumental accuracy (0.2°C).

Table 3: the RMSE and the CV-RMSE for the first guess model, the calibration and validation are reported.

	RMSE	CV-RMSE
First Guess model	1.0°C	7.8%
Calibration	0.5°C	4.0%
Validation	0.6°C	2.3%

Concerning relative humidity (RH), the modelled values show a larger deviation from measured values (RMSE=15.1% and CV-RMSE=20.0%), since the wall model only calculates the moisture transport due to infiltration without considering the moisture transport through components (in this case only the soil).

3.2 COMBO

The optimization produced a Pareto front comprising a number of non dominated solutions (i.e. those whose objective function cannot be further improved altogether without compromising another one) as shown in Figure 5. Among these, one was chosen in a balance point between low gain index and high system output. The solutions with high output were characterized by a small distance between blades to increase the active area and a vertical angle to reduce self-shading, the solutions with low gain index (highly negative) indeed had the minimum number of blades to increase the Winter solar radiation. This result indicates that for a better passive strategy, if both heating and cooling load is accounted for, no shading is required. This result is confirmed by the dynamic simulation in which the cumulative annual consumption increased for the retrofitted solution. Clearly the algorithm would be different in case only the cooling system is installed. The parameter of array power does not take into account the yield [kWh/kWp], the yield decrease with increasing array power due to self-shading of the blades until approaching the solutions in the rightmost part of the chart, this is due to the fact that the highest array power solutions are characterized by an almost vertical angle.

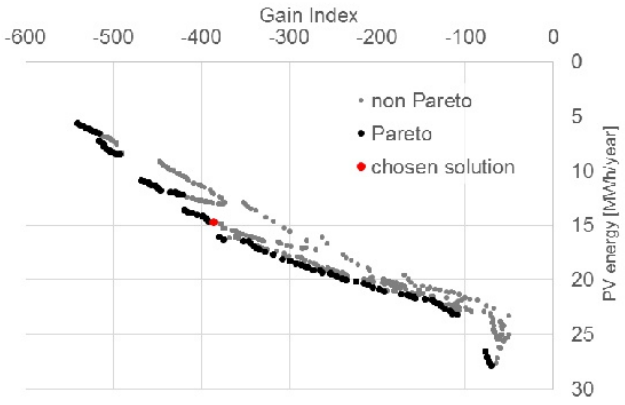

Figure 5: performance chart of all the combination investigated by the genetic algorithm.

3.3 Retrofitting solution

The design solution of BIPV system, chosen by COMBO, consists in four blades, with a slope of 80° and a distance of 2.15 m, which are set in the southern façade of the building model as fixed shadows with a high shortwave reflectance (Rs=0.861). The blades correspond to an installed capacity of 14.04 kW peak.

In this section, the retrofitting solution as passive and active control of the indoor climate is separately assessed.

Passive control

If a passive control of indoor climate is considered (free floating), the effect of the shading provokes a decrease in temperature on average of 0.4°C with a maximum of 0.5°C on September, as shown in Figure 6. Moreover, the shading contributes to reduce the mean maximum daily fluctuations from 4.5°C to 4.0°C. The use of shading as passive control seems not to widely affect the indoor thermal conditions. Anyway, a risk analysis of mechanical degradation of faunal remains has been performed taking into account their daily crack evolution.

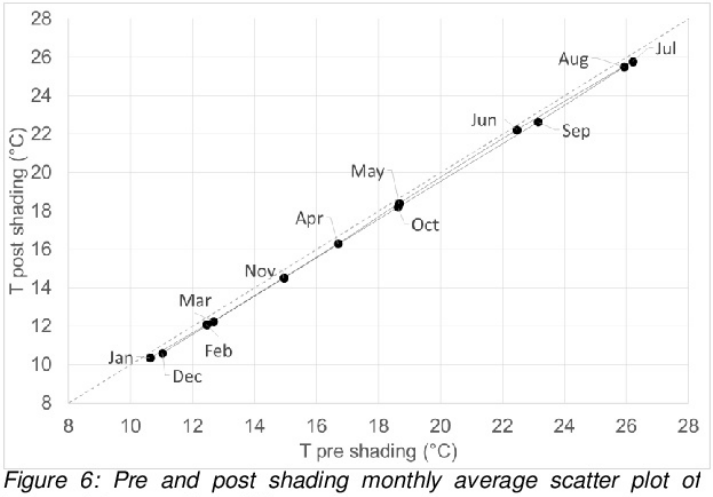

Figure 6: Pre and post shading monthly average scatter plot of indoor air temperature (°C).

Indeed, a study of daily crack evolution of faunal remains, carried out with available data collected from July to December 2016, has allowed to define an empirical relationship among T-RH parameters and crack thickness (FO), given by the following equation (3):

$$FO = a * RH^b * T^c, \qquad (3)$$

where a, b and c are coefficients (Table 4). Modelled FO differs from measured with a RMSE=0.04 mm which is less than instrumental accuracy.

Table 4: Equation coefficients calculated by a non-linear multiple regression.

a	b	c
7.4534	-0.1000	0.0202

Since the shading, used as a passive control, does not affect the mixing ratio of humidity in air (MR) but only the temperature, the relative humidity was computed in the estimated indoor thermal conditions and eq. 3 was applied. Figure 7 shows the scatter plot of FO pre and post shading. The values of FO post shading are mainly below the bisectrix, showing that, over the selected period, a reduction of indoor T (mean value from 17.8°C to 17.4°C) and, consequently, an increase of RH (mean value from 77.1% to 79.0%) provoke the shrinking of FO.

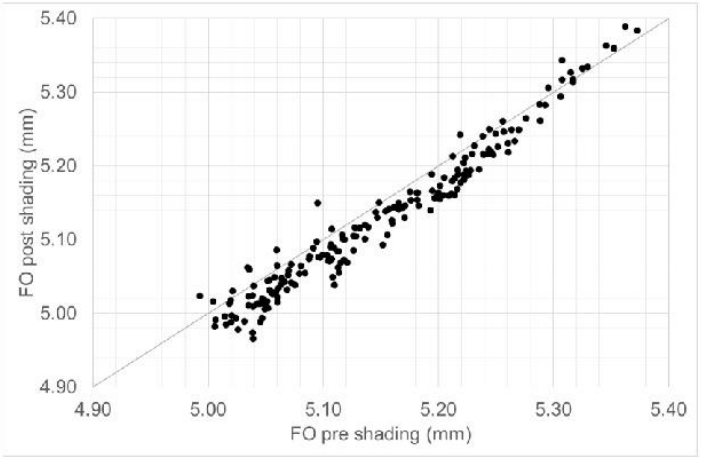

Figure 7: Scatter of crack thickness (FO) post shading vs FO pre shading calculated from eq. 3. Active control

If an active control of indoor climate is considered, the indoor temperature increases up to 10.4°C in cold season and decreases up to 5.0°C in warm season with respect to the control actions set up for heater and cooler system, respectively.

From the assumption that, when room units are switched on, they do not affect the MR inside the building, the evolution of crack thickness has been assessed using eq. 3.

As shown in Figure 8, in cold period (from 120 to 180) when heating system is in operation (Tair<16°C), the crack thickness increases. In fact, since the evolution of cracks is related to both T and RH parameters, when T is kept constant, RH values tend to decrease with respect to values at lower Ts. This means that in drier conditions and at constant temperature the crack thickness increases (up to 0.34 mm).

In warmer period (from 0 to 60), the crack thickness tends to decrease when cooling system is switched on and T is constant, which provokes an increase of RH values.

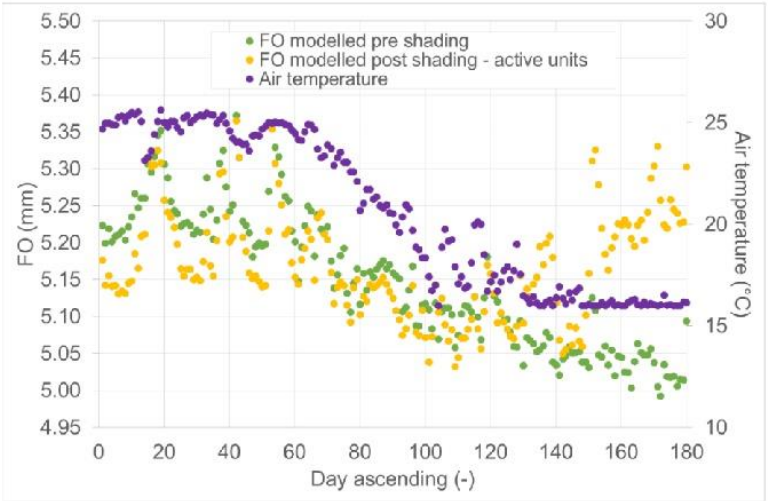

Figure 8: Evolution of crack thickness (FO) calculated from eq. 3 pre (green dots) and post (yellow dots) shading with room units and air temperature (purple dots).

The proposed design allows reducing the use of cooling energy demand of 27.6%. However, during heating hours, an increase of consumption of 6.5% occurs. This means that the total delivery energy increases of 1.18 kWh/m2 which corresponds to 2.5%. Table 5 summarizes the delivery energy in kWh/m^2 occurring in pre and post shading. This result is encouraging in the case only a cooling system is installed. Apart from the energy related aspects, the preservation of remains would be worsened by the use of an heating system. Installing the blades and a cooling system would improve the comfort situation compared to the baseline (no heating nor cooling devices), reduce the energy demand compared to an only cooling condition that doesn't have shading devices and leaving unaltered the heating demand and preservation of remains. If the contemporary electricity production from PV (i.e. the production that happens during cooling hours) is taken into account, the remaining cooling demand is almost zero as shown in Figure 9.

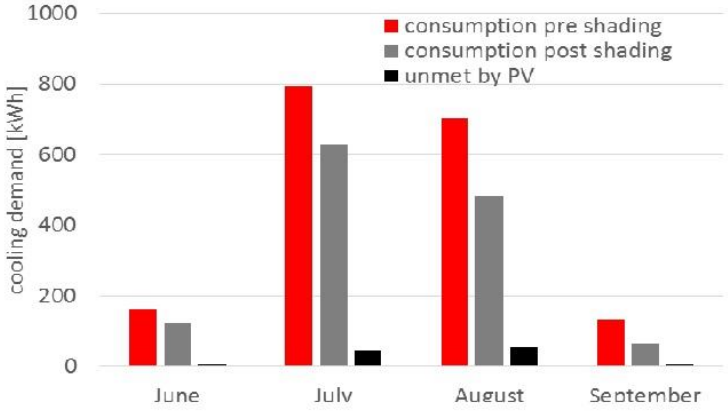

Figure 9: Monthly cumulative energy consumption: using the electricity produced (contemporary to the demand) by the shading blades the electric energy demand is almost completely met.

Table 5: Delivered energy in kWh/m^2 per month and total for pre and post shading retrofitting solution.

	Pre shading		**Post shading**	
Month	*Heating*	*Cooling*	*Heating*	*Cooling*
Jan	10.72	0	11.18	0
Feb	6.59	0	7.04	0
Mar	7.02	0	7.51	0
Apr	1.04	0	1.26	0
May	0.23	0	0.28	0
Jun	0	0.54	0	0.41
Jul	0	2.64	0	2.09
Aug	0	2.34	0	1.60
Sep	0	0.44	0	0.21
Oct	0.39	0	0.51	0
Nov	4.25	0	4.67	0
Dec	10.42	0	11.05	0
Total	**40.67**	**5.96**	**43.49**	**4.31**

4. Conclusion

The proposed methodology provides an improvement for the retrofit of existing buildings combining BIPV optimization and whole-building dynamic simulation. This is particularly true in sites where the solar radiation plays a key role in the indoor climate behaviour. The methodology has been applied to a peculiar case study, “La Polledrara di Cecanibbio”, in which faunal remains from Middle Pleistocene are preserved.

The retrofitting solution was optimized by considering four blades set along southern façade. The study has analysed the impact of the shading with and without air conditioning system, taking into account both a risk analysis of mechanical degradation of the objects and the energy load pre and post shading.

The retrofitting solution without AC system does not induce a significant change in indoor air temperature (a reduction of 0.4°C on yearly basis). However, the novel condition slightly seems to determine a reduction of crack thickness as shown in Figure 5. Instead, when the ideal heater is switched on and indoor air temperatures never fall below 16°C, drops in RH values, i.e. drier conditions, are responsible of a widening of crack thickness with respect to the initial conditions. Since low RH values tend to increase the crack thickness of faunal remains, it would seem that an optimal retrofitting solution should consider only a cooling system in summer. However, further studies should be conducted to estimate how much the increase of RH values can simultaneously affect the biological degradation.

The retrofitting solution has shown to reduce the ideal cooling load of 27.6% while increasing the heating load of only 6.5%. The method has proven to be effective in finding a configuration that selectively blocks most of the radiation in the warm season. Nevertheless, given that the heating load predominates, the solutions prove slightly disadvantageous on an annual cumulative basis. Despite this effect, the method should be applied to other case study where the heating-cooling loads are more equilibrated. Furthermore, work will be carried out analysing the same building with different set points for the HVAC or even in absence of any heating load.

5. Acknowledgement

The authors wish to acknowledge “ARSIAL” (Regional Agency for Development and Innovation of Agriculture in Lazio) for wind and radiation data and “Tecno.El S.r.l.” for indoor and outdoor thermo-hygrometric data.

6. References

[1] Sun, Liangliang, Lin Lu, and Hongxing Yang. Optimum design of shading-type building-integrated photovoltaic claddings with different surface azimuth angles. Applied Energy 90.1 (2012): 233-240.

[2] Sun, L. L., and H. X. Yang. Impacts of the shading-type building-integrated photovoltaic claddings on electricity generation and cooling load component through shaded windows. Energy and buildings 42.4 (2010): 455-460.

[3] Yoo, Seung-Ho. Simulation for an optimal application of BIPV through parameter variation. Solar Energy 85.7 (2011): 1291-1301.

[4] Yoo, Seung-Ho, and Eun-Tack Lee. Efficiency characteristic of building integrated photovoltaics as a shading device. Building and Environment 37.6 (2002): 615-623.

[5] E. P. B. D. "Directive 2010/31/EU of the European Parliament and of the Council of 19 May 2010 on the energy performance of buildings (recast)." Official Journal of the European Union 18.06 (2010): 2010.

[6] Cornaro C., Puggioni V.A. and Strollo R.M. Dynamic simulation and on-site measurements for energy retrofit of complex historic buildings: Villa Mondragone case study. Journal of Building Engineering 6 (2016):17-28.

[7] Tagliabue L.C., Leonforte F., Compostella J. Renovation of an UNESCO heritage settlement in southern Italy: ASHP and BIPV for a “Spread Hotel” project. Energy Procedia 30 (2012): 1060-1068.

[8] Camuffo Dario. Microclimate for cultural heritage (second edition) conservation, restoration, and maintenance of indoor and outdoor monuments. Elsevier, Amsterdam (2012).

[9] Ward Greg. The Radiance 3.1 Synthetic Imaging System. Radiance Reference Manual (1997).

[10] EN 16242:2012. Conservation of cultural property—procedures and instruments for measuring humidity in the air and moisture exchanges between air and cultural property. European Committee for Standardization, Brussels.

[11] Camuffo D., Bertolin C., Bonazzi A., Campana F., and Merlo C. Past, present and future effects of climate change on a wooden inlay bookcase cabinet: a new methodology inspired by the novel European Standard EN 15757: 2010. Journal of Cultural Heritage 15.1 (2014):26–35.

[12] Frasca F., Cornaro C., Siani A.M. On-site measurements and whole-building thermal dynamic simulation of a semi-confined prefabricated building for heritage conservation. Paper presented at “Building Simulation Applications (BSA) 2017”, 8-10 February 2017, Bolzano, Italy.

[13] Vierlinger R., and Hofmann A.. A Framework for flexible search and optimization in parametric design. Proceedings of the Design Modeling Symposium Berlin. 2013.

[14] Reinhart C., and Breton P.F.. Experimental validation of Autodesk® 3ds Max® Design 2009 and DAYSIM 3.0." Leukos 6.1 (2009): 7-35.

[15] Martínez-Moreno F., Muñoz J., and Lorenzo E.. Experimental model to estimate shading losses on PV arrays. Solar Energy Materials and Solar Cells 94.12 (2010): 2298-2303.

Appendix D

Performance assessment of a heat and moisture dynamic simulation model in IDA ICE by comparison with WUFI Plus

Frasca F., Cornaro C. and Siani A. M.

In IOP Conference Series: Materials Science and Engineering (Vol. 364, No. 1, p. 012024). IOP Publishing. (2018).

Appendix D

IOP Conf. Series: Materials Science and Engineering **364** (2018) 012024 doi:10.1088/1757-899X/364/1/012024

Performance assessment of a heat and moisture dynamic simulation model in IDA ICE by the comparison with WUFI Plus

F Frasca[1*], C Cornaro[2] and AM Siani[3]

[1] Sapienza Università di Roma, Department of Earth Sciences, P.le A. Moro 2, 00185 Rome, Italy.
[2] Università degli Studi di Roma "Tor Vergata", Department of Enterprise Engineering, Via del Politecnico 1, 00133 Rome, Italy
[3] Sapienza Università di Roma, Department of Physics, P.le A. Moro 2, 00185 Rome, Italy.

* Corrisponding author: f.frasca@uniroma1.it

Abstract. Recently, in the field of preventive conservation, the use of accurate whole-building dynamic simulation models is becoming an effective approach for preventing degradation phenomena due to changes in indoor historic climate. Among microclimate parameters, the moisture plays a key role in the degradation of organic-hygroscopic artworks as well as in the durability of building components. Some simulation codes combine both heat and moisture transfer calculations, however their capability to accurately model the moisture transport is limited. The HMWall model coupled with IDA Indoor Climate and Energy (IDA ICE) software is one of those models.
This study aims at comparing the performance of the HMWall model with respect to WUFI Plus, developed by Fraunhofer Institute for Building Physics (IBP). Temperature (T) and relative humidity (RH) provided by both codes in the case of a building envelope with no infiltration, windows and incoming solar radiation, are compared. This allows to assess whether both models calculate the moisture transport throughout walls in the same way. *Dynamic simulations have been run over a year by using different T-RH outdoor conditions.* Even if both models are based on the same heat and moisture transport equations, RH behaviour simulated by HMWall is significantly different from that by WUFI Plus. This mainly depends on the calculation of saturated vapour pressure (p_{sat}) inside the material. Then, the Common Exercise 3 has been applied to test if HMWall were capable to affect indoor RH when cladding materials with different sorption behaviour are used.
The new HMWall implemented model is resulted more effective than the previous one, and in the case of simplified building, RHs modelled by both programs are highly correlated.

1. Introduction

In the last years, a commensurable interest on the use of accurate whole-building dynamic simulation models has been shown in preventive conservation studies, even though up to now this modelling approach has been extensively applied to determine energy efficiency of buildings [1-3] and thermal comfort optimization [4]. At the present time, the whole-building dynamic simulation model is also becoming an effective methodology to assess the microclimate risk on artworks when changes in indoor

historic climate occur due to refurbishment or climate change [5]. Physical measurements and simulation provide a complete evaluation of the indoor climate and interactions among object-environment and building-environment.

Both temperature (T) and relative humidity (RH) can induce degradation phenomena [6]. Specifically, RH is the main responsible of the deterioration in organic-hygroscopic artworks as well as in the durability of building components. For this reason, an accurate simulation and control of RH behaviour in these sites is of significant importance.

Most of simulation codes has been developed to model moisture exchanges between indoor and outdoor environments setting a specific moisture storage capacity to the interior of the building [7] and not to model the moisture flow between the air and porous surfaces, such as walls [8]. Some of them use two simulations distinctly but running together: one for building energy or envelope simulation and one for modelling the heat and moisture transport between the air and porous surfaces. The HMWall model coupled with IDA Indoor Climate and Energy (IDA ICE) and WUFI® Plus (hereafter called WUFI) belong to the latter group [9], and their performance will be compared in this paper.

WUFI® Plus is a holistic model based on the hygrothermal envelope calculation model developed by H.M. Kunzel's at Fraunhofer Institute for Building Physics (IBP) [10]. It takes into account sources and sinks of moisture inside a component, liquid water transport, diffusion and vapour ab - and de-sorption as well as the thermal parameters [11].Field and laboratory validation are performed for WUFI® Plus more than for other hygrothermal simulation tools [12]. Moreover, it has been widely compared with other hygrothermal software [13-15] and used within the European project Climate for Culture (CfC) [16].

The HMWall model coupled with IDA ICE has been developed in 1999 [17] and, then, updated in 2011. In the first version, the moisture transfer was modelled by one moisture-transfer potential (the humidity by volume), whereas the liquid water transport and the hysteresis of moisture transport were not taken into account. This version, coupled with IDA ICE 3.0, was used within the IEA Annex 41 [18] and to model the hygrothermal behaviour inside historical buildings [19-20]. In 2011, the code has been edited according to the same balance heat and moisture equations of WUFI [10] (section 1.1), mainly due to the lack of the hygrometric data of materials required to run the code. The latter has been validated to conform with the EN 15026:2007 standard validation test; however, no study about this HMWall model has been published yet.

Currently, the HMWall code differs from WUFI for the following features: the percentage of material porosity is not taken into account and hygrometric properties of materials, not available in the software library, have to be extracted from available database and time-by-time compiled in the model object. Hygrothermal curves can only be derived by mathematical relations and not built by using experimental data. Finally, heat or moisture sources (e.g. fraction of driving rain, pipe failures, etc.) cannot be added by the users within the wall component.

This paper aims at investigating for the first time the capability of the HMWall model, updated in 2011 and coupled with IDA ICE 4.7.1 released in 2015, to calculate the moisture transport across walls at increasing complexity of the building structures and boundary conditions. First, a simplified building envelope was modelled in IDA ICE and WUFI and, then, a comparison of time series of RH modelled by both models, was carried out. This has allowed to assess only the moisture transfer across walls, which is the main focus of this exercise. Then, the Common Exercise 3 (CE3) developed by the Fraunhofer IBP in the framework of IEA Annex 41 and also used within the CfC was applied to evaluate the capability of HMWall to simulate the influence of different cladding material in the rooms on the RH.

A successful performance of HMWall model coupled with IDA ICE will provide a validated improvement of IDA ICE packages to both users and experts of preventive conservation of historical buildings and artworks.

1.1. Basic governing equations

Appendix D

Both models are based on the following balance equations for heat (eq. 1) and moisture (eq. 2) transfers [10]:

$$\frac{dH}{dT}\cdot\frac{\delta T}{\delta t}=\nabla\cdot\left(\lambda\cdot\nabla\vartheta\right)-h_v\cdot\nabla g_v \qquad 1)$$

where dH/dT is the heat capacity of the wet material (J/m³·K); $\delta T/\delta t$ is the change of temperature (T) in time (K/s),; λ is the thermal conductivity of the wet material (W/m·K); $h_v\cdot\nabla g_v$ is the latent heat source, h_v is the evaporation enthalpy of water (J/kg) and g_v is the vapour diffusion flux (kg/m²·s).

$$\frac{dw}{d\varphi}\cdot\frac{\delta\varphi}{\delta t}=\nabla\cdot\left(g_w+g_v\right) \qquad 2)$$

where w is the equilibrium water content (w) and φ is the relative humidity; $dw/d\varphi$ is the moisture storage capacity of the material (kg/m³); $\delta\varphi/\delta t$ is the change of relative humidity (φ or RH) in time (1/s); g_w is the capillary moisture flux (kg/m²·s), i.e. $D\varphi\cdot\nabla\varphi$ with $D\varphi$ as the liquid conduction coefficient of water (kg·m/s); g_v as above, i.e. $\delta_p\cdot\nabla(RH\cdot p_{sat})$ with δ_p as the water vapour permeability of material (kg/m·s·Pa) and p_{sat} as the saturated vapour pressure of water (Pa).
In both codes, δ_p is calculated as the ratio between δ_a (the water vapour permeability of air given by Schirmer's equation) and μ (the dimensionless vapour resistance factor of the material).
Concerning $D\varphi$, the codes use two different equations both reported in [10]. In WUFI, $D\varphi$ is the product between the capillary transport coefficient (Dw), once the water absorption coefficient of the material (A_w) is known, and dw/dRH. In HMWall, $D\varphi$ is calculated taking into account both wet (μ_w) and dry (μ_d) cup vapour diffusion resistance factor. One of the main issues is that μ_w is not available in database and, if any, only for few materials.
The sorption curves are calculating as a function of RH and not dependent on T, since the equilibrium water content (w) is assumed to be little sensitive to T changes [10].
Equations 1) and 2) are strongly related when the number of variables in both equations are limited to T and RH. In fact, it follows that: λ in eq.1 is moisture-dependent; the enthalpy flux is related to g_v so that heat transfer considers the contribution of water vapour phase change; and g_v is dependent on T through p_{sat}.

2. Material and method

In this paper, the examination of the performance of the HMWall model coupled with IDA ICE 4.7.1 has been carried out as shown in the schematic workflow in Figure 1. The workflow consists of test cases at increasing complexity of the building envelope. In this way, it has been possible to assess: a) the capability of HMWall to calculate the heat and moisture transport across walls when the only difference between indoor and outdoor climate is given by RH (first test case); b) *the capability of HMWall to simulate the influence of different cladding material on the indoor RH (second test case). All simulations have been run in transient conditions using hourly step over a year.*

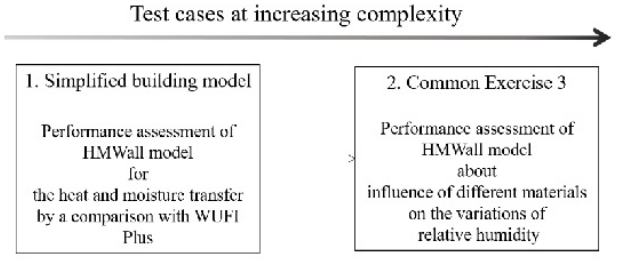

Figure 1. Schematic workflow of methodology applied in this study.

2.1. A simplified building model

The first test case is to perform the simulation considering a simplified building having the following characteristics: an envelope of a parallelepiped with a volume of 26.0 m³, with height of 2.6 m and a

length of 2.5 m oriented in east-west direction and of 4.0 m in north-south. It was designed without windows and with a flat ceiling. All opaque components are built by a monolayer of lime silica brick of 0.2 m, whose hygrothermal properties are reported in Table 1. Air changes by infiltration are set to 0.0 h^{-1} and no thermal bridges are taken into account. The initial values of indoor T and RH are 10°C and 50%, respectively. *The file of the external environmental conditions consists of T and RH values taken at 1-hour time slot, so that no contribution from solar radiation and ventilation can affect the heat and moisture transfer calculations. This is very important to avoid misleading with input parameters, such as wind, infiltration or radiation, whose setting varies from a code to another code. Two simulations are run with outdoor temperature T_{out}=10°C and relative humidity RH_{out}=60% (the first simulation) and T_{out}=10°C and RH_{out}=40% (the second simulation). A third simulation is run setting T_{out}=10°C and RH_{out} as a sinusoidal curve (RH_{min}=42.0% and RH_{max}=58.0%), in order to assess the response of both models when there is a seasonal variation of RH over a year. The simulations are performed over the period from January, 1st to December 31st at 1-hour step.* In this test case, variations of RH are mainly driven by water vapour partial pressure (p_v) transferred across walls and by the moisture storage capacity of envelope, since the heat transfer is constant and, consequently, the p_{sat} which is a function of T is constant.

Table 1. Hygrothermal properties of lime silica brick as provided by *MASEA Datenbank - Materialdatensammlung für die energetische Altbausanierung*

Hygrothermal properties	**Value**
Density (ρ)	1830.0 kg/m³
Heat capacity (c_p)	850.0 J/(kg·K)
Thermal conductivity (λ)	1.0 W/(m·K)
Wet cup vapour diffusion resistance factor (μ_w)	18.0
Dry cup vapour diffusion resistance factor (μ_d)	27.0
Free water saturation (W_f)	257.1 kg/m³
Equilibrium water content at 80% rel hum (W_{80})	27.5 kg/m³
Water absorption coefficient (A_w)	0.059 kg/(m²·s$^{1/2}$)

2.2. The Common Exercise 3 (CE3)

The Common Exercise 3 (CE3) consists of a double climatic chamber (test room and reference room) [7]. A detailed description of this exercise can be found in [18]. The CE3 aims at simulating the indoor climate of two rooms in order to assess the influence of the sorption of different material on the RH in the rooms. *Four boundary conditions around the rooms are set, so that internal walls are surrounded by controlled T and RH areas, whereas external walls are exposed to weather data of Holzkirchen, i.e. its TRY (Test Reference Year-type) weather data*. Indoor T is controlled by a small radiator (with maximum heat dissipation of 1000 W) at 20±2°C and the moisture production corresponds to 2.4 kg/day. Natural air changes by infiltration correspond to 0.09 h^{-1} for the reference room and 0.07 h^{-1} for the test room, whereas mechanical ventilations are 0.63 h^{-1} and 0.66 h^{-1}, respectively. The exercise consists in 3 steps, in which simulations are run with different cladding materials in the test room: 1) test room only with aluminium foil; 2) test room with gypsum boards on the walls and 3) test room with gypsum boards on the walls and roof. This paper will show the results from HMWall coupled with IDA ICE 4.7.1, to assess the influence of different materials on RH peaks [18], in the case of test room.

3. Results and discussion

3.1. A simplified building model

Figure 2 shows the scatter diagram (HMWall *vs* WUFI Plus) of indoor modelled RH values driven only by the moisture transport across walls. The initial indoor RH is 50% and the boundary RH is 60%. The WUFI RHs tend to increase towards the RH boundary value, whereas the HMWall RHs remain quite

Appendix D

constant around initial condition (RH_{max}=50.3%). The slope of linear regression (red line in Figure 1) is 0.03%, demonstrating that the two codes have modelled indoor RH with significant differences. In fact, the RHs modelled by HMWall seem not be affected by the moisture transport across walls, suggesting that no difference between indoor and boundaries RH has been detected.

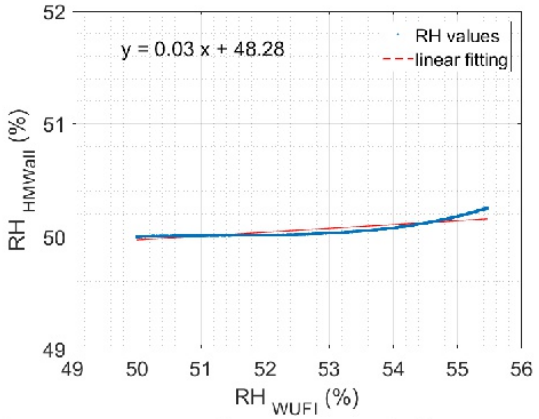

Figure 2. Scatter diagram of simulated RH values (HMWall *vs* WUFI Plus) over a year. The hygrometric boundary condition is set to 60%. Temperature is 10°C, constant inside and outside the envelope.

Since T was constant ($T_{in} = T_{out} = 10°C$), the p_{sat} was expected to be constant and equals to 12.30 hPa according to Magnus formula [21] for the pressure of water vapour at the saturation. It was observed that the p_{sat} calculated by HMWall was 13.08 hPa.

Moreover, it was found that the codes used a different calculation of the water vapour transfer (g_v) between the wall surface and the boundary air layer close to it. In WUFI Plus, g_v is determined in analogy to that used for the heat transfer, and water vapour transfer coefficient (β_p) is derived from the convective heat transfer coefficient. In HMWall, the calculation of moisture transfer at the boundaries of the building component is different from that in WUFI, since g_v is calculated as the discretized derivative of the vapour pressure between the last layer of wall material and the boundary air layer.

For the above reasons, we have modified this HMWall model (hereafter called HMWall_old) and in order to verify the sensibility of the code at g_v calculated as described by [10] and used in the WUFI Plus, two HMWall codes have been implemented as follows:

- HMWall (A), where only p_{sat} has been updated;
- HMWall (B), where p_{sat} is the same of HMWall (A) and g_v is also calculated as in the same as that in WUFI.

Figure 3 shows the scatter diagrams of the modelled RH values when the boundary conditions are set to RH_{out}=60%. RHs modelled by HMWall (A) and HMWall (B) tend to increase over time towards the equilibrium with the boundary condition in accordance with WUFI. Both HMWall (A) and (B) codes underestimate the maximum RH value modelled by WUFI, as if they buffer the moisture transport towards indoor over time. However, the coefficient of determination (R^2) is 0.994 for HMWall (A) and 0.996 for HMWall (B) (Table 2), showing a visible improvement of both codes with respect to the HMWall_old (R^2=0.771).

When the boundary conditions are drier (RH_{out}=40%) than the indoor climate (Figure 4), RHs modelled by HMWall (A) and HMWall (B) tend to decrease in accordance with WUFI. However, HMWall (A) (left panel in Figure 4) shows a better behaviour with respect to HMWall (B) with a slope of linear fitting close to unity. HMWall (B) (right panel of Figure 4) seems to go in equilibrium with boundaries more rapidly than the other two. The R^2 (Table 2) is 0.998 for HMWall (A) and 0.993 for HMWall (B).

Figure 5 shows the scatter diagrams of the modelled RH values when the hygrometric boundary conditions are defined as a sinusoidal curve. RH values modelled by both HMWall (A) and HMWall (B) are highly correlated with those modelled by WUFI. The slope of both linear fittings is 0.78, showing that both HMWall codes are in accordance to each other, when the hygrometric boundary conditions are more complex than the previous cases whose boundary conditions are constant.

Florence Heri-Tech – The Future of Heritage Science and Technologies IOP Publishing
IOP Conf. Series: Materials Science and Engineering **364** (2018) 012024 doi:10.1088/1757-899X/364/1/012024

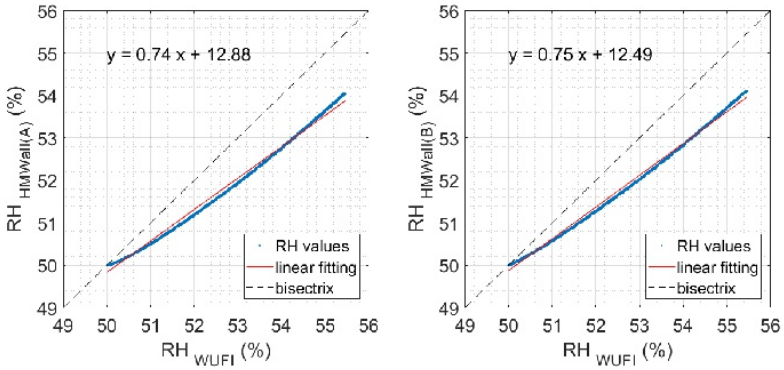

Figure 3. Scatter diagram of modelled RH values (HMWall *vs* WUFI Plus) over a year. The hygrometric boundary condition is set to 60%. T was constant (T_{in} = T_{out} = 10°C).

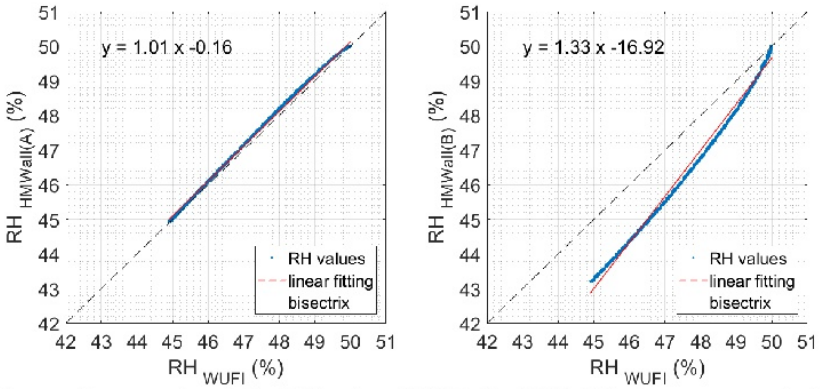

Figure 4. Scatter diagram of modelled RH values (HMWall *vs* WUFI Plus) over a year. The hygrometric boundary condition is set to 40%. T was constant (T_{in} = T_{out} = 10°C).

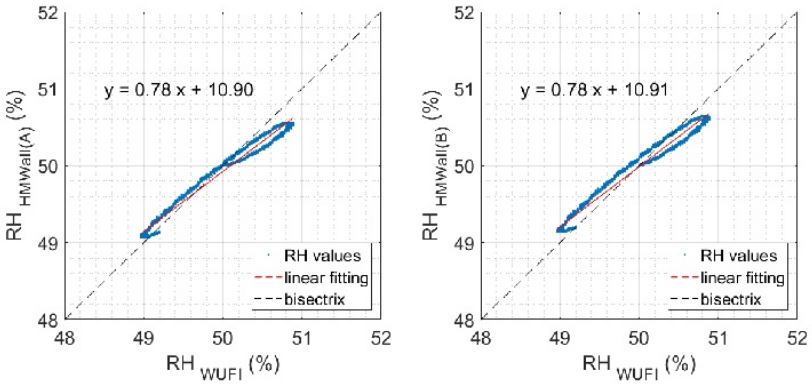

Figure 5. Scatter diagram of modelled RH values (HMWall *vs* WUFI Plus) over a year. The hygrometric boundary condition is a sinusoidal curve with a RH decrease in summer. T was constant (T_{in} = T_{out} = 10°C).

Appendix D

Table 2 summarizes the R^2, MBE (Mean Biased Error) and RMSE (Root Mean Squared Error) calculated for each case. Differences between HMWall (A) and HMWall (B) are at the third decimal place, demonstrating that both codes calculate the moisture transport in similar way. Especially, the HMWall (A) seems to be more in accordance with WUFI when boundaries are drier than indoors, since both the MBE and the RMSE are close to zero. Concerning the HMWall (B), it usually underestimates the RH modelled by WUFI except for the case 3 (MBE = 0.0%). For both the HMWall (A) and (B), the RMSE is close to the unity in the case 1 and close to zero in the case 3, whereas a significant difference is in the case 2 when RMSE is 0.1% and 1.2%, respectively.

Table 2. The coefficient of determination (R^2), the mean biased error (MBE) and the root mean squared error (RMSE) calculated for HMWall (A) and HMWall (B) in three different hygrometric boundary conditions.

Parameter	Case 1		Case 2		Case 3	
	A	B	A	B	A	B
R^2 (%)	0.994	0.996	0.998	0.993	0.979	0.977
MBE (%)	-0.8	-0.8	0.1	-1.1	-0.1	0.0
RMSE (%)	1.0	0.9	0.1	1.2	0.2	0.2

3.2. The Common Exercise 3

Three simulations have been run according to the three steps defined in the common exercise: 1) test room only with aluminium foil; 2) test room with gypsum boards on the walls and 3) test room with gypsum boards on the walls and roof. For this exercise, the maximum daily variations of RH modelled by HMWall (A) and HMWall (B) have been calculated in order to assess the influence of different cladding materials on the indoor RH.

Figure 6 shows that the HMWall (B) generally model higher daily span of RH values with respect to HMWall (A) in both rooms, which result to be very similar each other even though walls and ceiling of the test room were coated by aluminium foils, which means no sorption.

Scatter diagrams of the maximum daily RH variations computed for test2 are in Figure 7. In test room (right panel), the daily RH variations modelled by HMWall (A) are affected by gypsum boards covering walls provoking their reduction up to 6% with respect to HMWall (B). Results from test3 are not shown since no significant differences have been detected with respect to test2.

Generally, the maximum daily variations of RH modelled by HMWall (A) are lower than those modelled by HMWall (B).

4. Conclusion

A preliminary comparison between the HMWall model and WUFI Plus has been carried out in the test case of a simplified building. The difference between the two codes mainly depended on the calculation of saturated vapour pressure (p_{sat}) inside the layer material. This bug has been found and solved thank to the accessibility and adjustability of the HMWall code by the users. Moreover, it has been found that HMWall model did not calculate the water vapour transfer (g_v) between the wall surface and the boundary air layer close to it considering the effect of convection. For this reason, two HMWall codes, called HMWall (A) and HMWall (B), have been derived in order to verify the sensibility of the code at g_v calculated as that in WUFI. Both HMWall (A) and (B) show a visible improvement with respect to the previous HMWall code when RH_{out}=60%. The HMWall (A) seems more compatible with WUFI, especially when the hygrometric boundary condition is drier than indoor. In the case of a sinusoidal RH behaviour of boundaries, both HMWall (A) and (B) are quite similar with WUFI.

The main difference between codes can be related to the calculation of the liquid conduction coefficient of water ($D\varphi$). In HMWall, $D\varphi$ only varies as function of the saturated pressure (p_{sat}) and the water vapour permeability of material (δ_p), since μ_w and μ_d do not change over the calculation, whereas, in WUFI, $D\varphi$ varies according to the water content (w) and hence with RH inside the material.

Florence Heri-Tech – The Future of Heritage Science and Technologies IOP Publishing
IOP Conf. Series: Materials Science and Engineering **364** (2018) 012024 doi:10.1088/1757-899X/364/1/012024

From the Common Exercise 3, a comparison between HMWall (A) and (B) has been carried out. For both HMWall models, aluminium foils seem not to affect the indoor RH, whereas gypsum boards tend to reduce the maximum daily variations of RHs. However, the effect of gypsum boards is more effective in HMWall (A), suggesting that this model would allow a better simulation of sorption given by gypsum.

Further studies will be addressed in order to compare the results, modelled by modified HMWall models, with respect to the measured indoor data (not available at current state). The future goal is to validate the HMWall model coupled with IDA ICE, that better simulates indoor climate, in order to be definitively implemented in the software.

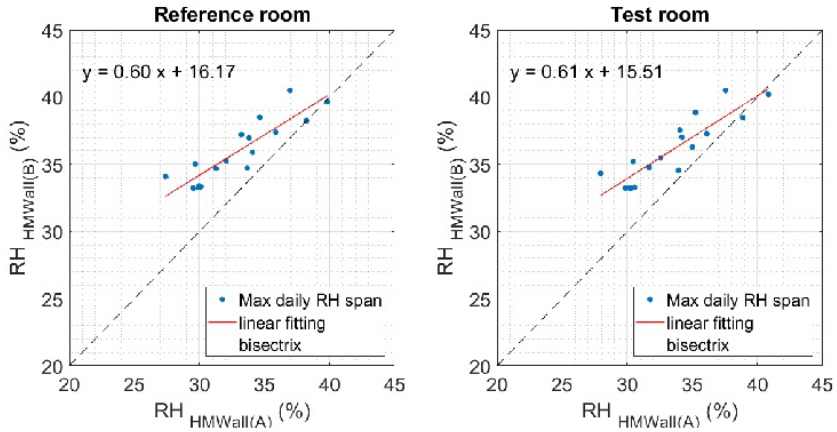

Figure 6. Scatter diagram HMWall (B) *vs* HMWall (A) of maximum daily RH variations modelled in reference room (left panel) and test room (right panel) when walls and ceiling are covered only with aluminium foil (test1). Simulation has been run from January 17th to February 2nd 2005.

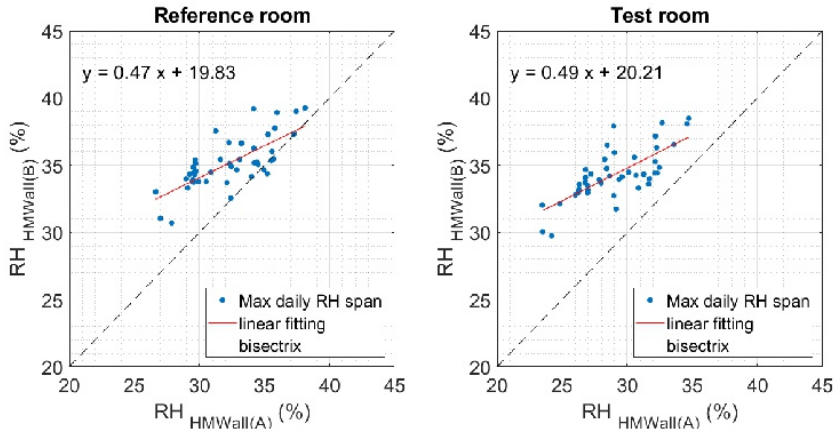

Figure 7. Scatter diagram HMWall (B) *vs* HMWall (A) of maximum daily RH variations modelled in reference room (left panel) and test room (right panel) when walls and ceiling are covered with gypsum boards (test2). Simulation has been run from February 14th to March 30th 2005.

Acknowledgements
Ph.D. student Francesca Frasca thanks Dr. Florian Antretter, Chief Group of Hygrothermic Department of Fraunhofer Institute for Building Physics (IBP), for supporting in simulations by WUFI® Plus.

Appendix D

References

[1] Gigliarelli E, Calcerano F and Cessari L 2016 *EuroMed Conf 2016, Part I, LNCS* Vol **10058** eds Ioannides M et al. (Springer, Cham) pp 91–103
[2] Tronchin L and Fabbri K 2017 Energy and Microclimate Simulation in a Heritage Building: Further Studies on the Malatestiana Library *Energies* **10** 1621
[3] Lucchi E 2016 Multidisciplinary risk-based analysis for supporting the decision making process on conservation, energy efficiency, and human comfort in museum buildings *J. Cult. Herit.* **22** 1079-89.
[4] Roberti F, Oberegger UF, Lucchi E and Troi A 2017 Energy retrofit and conservation of a historic building using multi-objective optimization and an analytic hierarchy process *Energ. Buildings* **138** 1-10.
[5] Leissner J, Kilian R, Kotova L, Jacob D, Mikolajewicz U, Broström T, Ashley-Smith J, Schellen H L, Martens M, Van Schijndel J, Antretter F, Winkler M, Bertolin C, Camuffo D, Simeunovic G and Vyhlídal T 2015 Climate for culture: Assessing the impact of climate change on the future indoor climate in historic buildings using simulations *Herit. Sci.* **3** 1–15
[6] Camuffo D 2014 *Microclimate for Cultural Heritage- Conservation, Restoration, and Maintenance of Indoor and Outdoor Monuments* (Amsterdam: Elsevier) pp 557
[7] Holm A, Kuenzel H M and Sedlbauer K 2003 The hygrothermal behaviour of rooms : combining thermal building simulation and hygrothermal envelope calculation *Build. Simul.* 499–506
[8] Rode C and Woloszyn M 2007 Whole-building hygrothermal modeling in IEA Annex 41. Thermal Performance of Exterior Envelopes of Whole Buildings, *ASHRAE*, Atlanta, 2007, pp. 1–15
[9] Delgado JMPQ, Barreira E, Ramos NMM and de Freitas VP 2013 *Hygrothermal Numerical Simulation Tools Applied to Building Physics* (Springer-Verlag Berlin & Heidelberg) pp 66
[10] Künzel H M 1995 Simultaneous Heat and Moisture Transport in Building Components One- and two-dimensional calculation using simple parameters. Doctoral dissertation. (Stuttgart: University of Stuttgart, IRB-Verlag) pp 65
[11] Antretter F, Sauer F, Schöpfer T and Holm A 2011 Validation of a hygrothermal whole building simulation software. Fraunhofer-Institut für Bauphysik, Holzkirchen , Germany *Ashrae Stand.* 14–6
[12] Corcoran L, Duffy A and Rouholamin S 2013 *2nd Central European Symp for Building Physics,* eds Mahdavi A and B Martens (Vienna: University of Technology - Faculty of Architecture and Regional Planning) pp 305–12
[13] Schmidt S, Lindauer M and Hoppe M 2012 *Proc 5th Int Building Physics Conf (IBPC).* (Kyoto: Kyoto University) pp 1143–48
[14] Ozolins A, Jakovics A and Ratnieks A 2013 *Comsol Conf.* (Comsol Incorporated). 1–6
[15] Barclay M, Holcroft N and Shea A D 2014 Methods to determine whole building hygrothermal performance of hemp-lime buildings *Build. Environ.* **80** 204–12
[16] Bichlmair S, Raffler S and Kilian R 2015 The temperierung heating systems as a retrofitting tool for the preventive conservation of historic museums buildings and exhibits *Energy Build.* **95** 80–5
[17] Kurnitski J and Vuolle M 2000 Simultaneous Calculation of Heat, Moisture and Air Transport in an Modular Simulation Environment *Est. Acad. Publ.* 25–47
[18] Woloszyn M and Rode C 2008 Tools for performance simulation of heat, air and moisture conditions of whole buildings *Build. Simul.* **1** 5–24
[19] Napp M and Kalamees T 2015 Energy use and indoor climate of conservation heating, dehumidification and adaptive ventilation for the climate control of a mediaeval church in a cold climate *Energy Build.* **108** 61–71
[20] Napp M, Wessberg M, Kalamees T and Broström T 2016 Adaptive ventilation for climate control in a medieval church in cold climate *Int. J. Vent.* **15** 1–14
[21] Parish OO and Putnam TW 1977 Equations for the determination of humidity from dewpoint and psychrometric data. *Nasa Technical Note, NASA TN D-8401* 1–24

Appendix E

Performance assessment of a heat and moisture dynamic simulation model as an extension of IDA ICE

Frasca F., Cornaro C. and Siani A.M.

PRE-SUBMITTED. (2018).

Appendix E

Performance assessment of a heat and moisture dynamic simulation model as an extension of IDA ICE

F. Frasca[1], C. Cornaro[2] and A.M. Siani[3]

[1] Department of Earth Sciences, Sapienza Università di Roma, P.le Aldo Moro 5, 00185, Rome, Italy
[2] Department of Enterprise Engineering, University of Rome, Tor Vergata, Via del Politecnico, 1, 00133 Rome, Italy
[3] Department of Physics, Sapienza Università di Roma, P.le Aldo Moro 5, 00185, Rome, Italy

Abstract

In the last years, a commensurable interest has been shown in the use of the hygrothermal assessment by means of the analysis of temperature, relative humidity and moisture content within buildings. It provides valuable information needed for decision-making, since it helps to understand the enclosure behaviour and the building performance issues. For this reason, numerical models of the heat air and moisture transfer through porous have been developed to extend or combine existing building dynamic simulation tools. The HMWall model is a one-dimensional hygrothermal model. This study aims at validating the IDA ICE software extended with the HMWall object by means of four exercises at increasing complexity. The validation is performed using HMWall as an independent object (exercise 1) and as a component of a larger system (exercises 2-4). The validation considers analytical verification, empirical validation and comparative test. All exercises demonstrate the efficacy of the HMWall object for hygrothermal assessment. Especially, the last exercise confirms that IDA ICE extended with HMWall provides more accurate RH time series with respect to the default one.

Introduction

In the last years, a commensurable interest has been shown in the use of the hygrothermal assessment by the analysis of temperature, relative humidity and moisture content within buildings. It provides valuable information needed for decision-making, since it helps not only to the understanding of enclosure behaviour but also to the identification of building performance issues in terms of energy consumptions and human comfort.

Almost all building materials are porous in nature and are completely dry when water is only chemically bounded. Otherwise, they can contain water as solid (ice), liquid (water) and gas (vapour) state (Straube and Burnett 1991). The moisture can migrate by three modes of transports: vapour transport, liquid transport and phase changes (evaporation/condensation and freeze/thawing). These processes strongly affect the building behaviour and are an important aspect of the overall performance of the building (Holm et al. 2004), as the inside moisture may change the envelope's durability or the thermal performance and affect the indoor air quality, becoming a driving potential for mould and dust infection (Hens 2009). The above issues show the

importance of measuring and modelling the heat and moisture transfer through hygroscopic materials with an accurate and reliable way.

The aim of the study

The aim of this paper is to investigate the performance of the IDA Indoor Climate and Energy (ICE) software extended with the HMWall model in four exercises: 1) a semi-infinite wall as stated in the EN 15026:2007; 2) an adiabatic building envelope; 3) the Common Exercise 3 (CE3) from the International Energy Agency – Annex 41; and 4) an historical building. The exercises were set up so that various combinations of climatic loads and materials were modelled. The four exercises are separately presented. More attention is paid to the second and the fourth exercise, since they were set up by the authors. The code validation was based on the three requirements suggested by Judkoff and Neymark (1995), i.e. analytical verification, empirical validation and comparative test. An appendix is added with the equation of statistics using in the analysis.

State of art

The hygrothermal analysis is a valuable tool for design, assessment and study. For example, Martinez (2017) demonstrated by means of thermal transmittance (U-value) measurements how a pre-fabricated hemp-based timber-frame envelope system, i.e. a new building made of low impact materials, has large capability to achieve high insulation levels combining with a good moisture buffering for the indoor environment. Kraus (2017), instead, showed that the complex health problems connected with the Sick Building Syndrome (SBS), such as tearing eyes, nose irritation, wheezing, coughs and frequent respiratory infections, can be strictly related to the hygrothermal performance of the building envelope with respect to the use of HVAC system or as a function of season variability. In Litti et al. (2015), non-invasive techniques were used to investigate the thermal performance of a heritage building and its alteration due to the moisture distribution variation. They demonstrated how water can locally or globally modify the thermal behaviour of the envelope, since it has higher specific heat and thermal conductivity with respect to the traditional dry materials.

Although the hygrothermal assessment using measurements of T and RH gives important information of the current state of the building, a powerful tool for prevention and prediction of building performance and for research and development of novel materials or systems is the whole building dynamic simulation. At the end of fifties, the research was focused on the simulation of the heat, air and moisture transport through the opaque components (Hens 2009). One of the first simple evaluation was the Glaser method (Glaser 1958), that aimed at scaling the interstitial condensation using two steady state transports: the heat flow by conduction and the water vapour flow by diffusion. The method was standardized in the EN ISO 13788:2002 and assumes that the built-in water has dried out and no effect of moisture content occurs on material intrinsic properties. This means that it can be applied only in those cases where the previous effects are negligible (Hagentoft 2004). The Glaser method is mainly used when an approximation of reality is enough for understanding the building issues, as

demonstrated in Ramos et al. (2009) and Magrini et al. (2017). Since the heat and moisture flows are transient, more sophisticated one- and two-dimensional dynamic models can give more detailed and accurate information. Most of simulation codes were developed to model moisture exchanges between indoor and outdoor environments setting a specific moisture storage capacity to the interior of the building (Holm et al. 2003) and not to model the moisture flow between the air and porous surfaces (Rode and Woloszyn 2007). The latter modelling has been generally implemented with the so-called HAM model, i.e. Heat Air and Moisture model, and combines the heat and moisture flow equations with the mass and energy balances. In the case of the moisture transfer, which includes both liquid and vapour flow, it was established that the driving factors were the capillary pressure (p_k) and the vapour partial pressure (p_v), (Janssen 2014). The whole moisture exchange in a building can be mainly modelled using the co-simulation or extending the building simulation software architecture. The co-simulation is one of the most advanced and versatile method (Nicolai et al. 2007; Steeman et al. 2010; Tariku et al. 2010; Djedjig et al. 2012; Spitz et al. 2013; Ferroukhi et al. 2016). It consists in combining two existing software (Gomes et al. 2018), one for whole building dynamic simulation and the other one for the hygrothermal transfer modelling (Ferroukhi et al. 2015). A review of hygrothermal tools available in literature identified 57 models, however only 14 are available to the public (Delgado et al. 2012). Nine belong to commercial programs (1D-HAM, BSim2000, Delphin, GLASTA, hygIRC-1D, IDA-ICE coupled with HAMWall, MATCH, MOISTURE-EXPERT and WUFI) and five are freeware programs (EMPITIED, HAMLab, HAM-Tools, MOIST and HUMIDUS), all briefly described in Delgado et al. (2012). In some of them, such as WUFI and IDA ICE, the hygrothermal transfer modelling is included within the software architecture. This is a very important feature, because the hygrothermal assessment can be performed by using only one simulation tool. The WUFI family tools were extensively used for testing the building material performance (Allison and Hall 2010; Antretter et al. 2012; Pasztory et al. 2012; Barclay et al. 2014; Hamid and Wallestein 2017) and the occupants' health (Hall et al. 2013), or as a predictive tool for retrofitting solutions in historical buildings (Antretter et al. 2011; Antretter et al. 2013; Bichlmair et al. 2015; O'Leary et al. 2015; Kupczak et al. 2018).

In any case, many validation examples are necessary to test the accuracy and enhance the performance of a hygrothermal model. In fact, the building model response can be strongly affected by the behaviour of materials, whose properties are defined in laboratory test at steady-state conditions. This means that the materials might react differently when they are, instead, exposed to transient conditions (Holm et al. 2004).

The validation of dynamic building simulation models is particularly difficult, since drawbacks are mainly due to the definition of general equations which simultaneously and accurately describe both heat and moisture transport over time. However, the European standard EN 15026:2007 is the first attempt to define an international norm for the validation procedure of dynamic simulation model, since it provides: a) the description of the physical model and its possible equations; b) the necessary input parameters; and c) a benchmark example with an analytical solution. Except for the EN

15026:2007, there is no standard for the validation of a hygrothermal whole building simulation software at the European level.

In the last 30 years, international projects were developed in order to create platforms useful at assessing the performance of HAM transport in building physics. These projects were important for updating standards and certifications for existing HAM models or for new calculation tools.

In 1991-1997, the International Energy Agency (IEA) Energy Conservation in Buildings and Community Systems program (ECBCS) issued the Annex 24 – Heat, Air and Moisture Transfer in Highly Insulated New and Retrofitted Envelopes – with the aim of studying the physics of heat, air and moisture transfer related to the insulation requirements and analysing the consequences for energy use, hygric response and durability of building components (Hens 1996). The Annex, joined by fourteen countries, consisted of five subtasks: 1) modelling; 2) environmental conditions; 3) materials properties; 4) experimental verification and 5) practice. The first subtask included both the state-of-the-art review and the model validation by means of six common exercises restricted to one-dimensional problems: concrete flat roof, timber-framed wall, cavity wall, industrial metallic roof, timber flat roof cassette and crawl space. In the final report, further intermodal comparisons were claimed to be necessary (Hens 1996).

In 2000-2002, the European Committee funded the HAMSTAD project, whose aim was to support the use the HAM models instead of the Glaser method. It represented one of the first attempt to create a platform for the control of the HAM models' accuracy. The project had two Work Packages (WP). WP1 focused on standards and methodologies for determination of moisture transfer coefficients and moisture properties of building materials. WP2 dealt with HAM models and assessment methods for the validation of one-dimensional hygrothermal simulations. Five benchmarks were developed which included at least two transfer mechanisms: insulated roof, analytical case, lightweight wall, response analysis and capillary active inside insulation. Reasonable consensus solutions were found (Hagentoft 2004).

In 2004-2007, the IEA – ECBCS issued the Annex 41 which was a cooperative project on "Whole-Building Heat, Air, and Moisture Response" (MOIST-ENG), joined by seventeen countries. The project was structured in four subtasks: 1) modelling principles and common exercises; 2) experimental investigation; 3) boundary conditions and 4) applications. In the subtask 1, modelling principles and common exercises (CEs) were dealt with to gauge the HAM model performance and to stimulate the participants in the development of new model or in the advanced use of the existing ones (Rode and Woloszyn 2007). The CEs were developed so that the validation of simulation codes was done by analytical verification, empirical validation by means of experimental data and comparative tests. The project concluded that more validation cases should be executed in order to achieve a reasonable consensus solution among models for a more accurate simulation of reality.

The above literature review shows the fundamental issue to accurately simulate the indoor relative humidity and the difficulties in validating heat and moisture transfer modelling tools. Indeed, these tools should be able to integrate several factors, such as moisture sources, airflows and moisture exchange with materials, that are strongly dependent on each other. This research gives a further contribution to improve the whole building dynamic simulation, especially for those buildings, such as historical buildings, in which the indoor relative humidity plays a key role on the durability of building components, the energy consumption and the perceived air quality.

Materials and methods

In this paper, the validation of the HMWall model as an independent object and as a component of a larger system in IDA ICE 4.7.1 was carried out as shown in the schematic workflow in Figure 1. The workflow consisted of four exercises at increasing complexity of the building model, briefly reported in Table 1 The exercises were selected in order to use various combinations of climatic loads and materials. The modelled data were validated with the measurements in the exercises coded as 1, 3 and 4; whereas they were compared with the results achieved by using WUFI Plus in the exercise coded as 2. In this way, the validation was conducted taking into account analytical verification, empirical validation and comparative test.

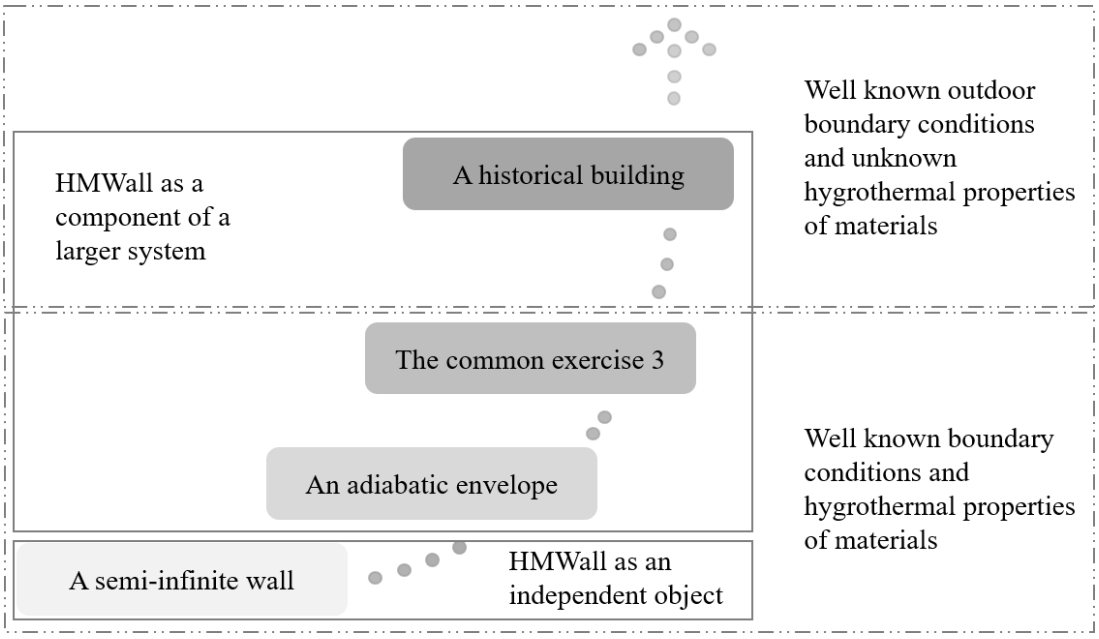

Figure 1 Schematic workflow of the validation procedure. Each exercise is coloured by grades of saturation and they are connected by an arrow to show the increasing complexity of the procedure. The exercises bordered by dot-dashed line have in common the knowledge about boundary conditions and hygrothermal properties of materials. The exercises bordered by continuous line use HMWall as an independent object (lower box) and as a component of a larger system (upper box).

Table 1 Summary of the four exercises used in this paper. Every exercise is briefly defined taking into account the model complexity, the climate loads, the wall stratigraphy, the duration and the validation.

		Model complexity	Climate loads		Stratigraphy	Duration	Validation
			Indoor	Outdoor			
Exercise	1	Semi-infinite wall	n.a. Layer conditions T = 20°C RH = 50%	T = 30°C RH = 95%	Mono-layered wall Thickness = 19m	a. 168 h b. 720 h c. 8760 h	Standard
	2	Adiabatic building envelope	T = 10°C RH = 50%	T = 10°C a. RH = 60% b. RH = 40% c. RH = 42-57%	Mono-layered walls Thickness = 0.2m	8760 h	Comparison with other simulation model
	3	Two real identical rooms (CE3)	Controlled: T = 20°C Scheduled moisture loads	EW(1) TRY of Holzkirchen IW(2) controlled	Insulated walls coated by: a. Aluminium foils b. Gypsum board on walls c. Gypsum wall on walls and ceiling	a. 408 h b. 816 h c. 624 h	Indoor climate experimental validation
	4	Historical building	Uncontrolled	EW(1) Weather file IW(2) Adiabatic conditions	Multi-layered walls suffered by degradation phenomena	2160 h	Indoor climate experimental validation

(1) External Wall; (2) Internal Wall

The HMWall model

The IDA Indoor Climate and Energy (IDA ICE) software, distributed by EQUA simulation AB, was chosen in this study as it has a modular architecture. It allows to extend his features at advanced level with an object that implements a one-dimensional heat and moisture transfer model, i.e. the HMWall model. This can be used either as a single independent wall-object or as a component of a larger system, by simply replacing the default thermal wall selected by the program. The HMWall model belongs to the family of HAM tools and, in this paper, it has been called HMWall with the aim to distinguish it from the first version documented in Kurnistki and Voulle (2000). The HMWall object is not available in the release of IDA ICE, but it can be integrated on request.

The HAMWall model was firstly developed in 1999 by Kurnistki and Voulle (2000). The moisture transfer was modelled by one moisture-transfer potential, i.e. the humidity by

volume (ν), neglecting the temperature dependence; whereas the liquid water transport and the hysteresis of moisture transport were not considered. This version, coupled with IDA ICE 3.0, was used within the IEA Annex 41 (Kalamees, report meeting) and reported in the review of the whole building dynamic simulation software given by Woloszyn and Rode (2008). It was also used to model the hygrothermal behaviour inside three historical buildings located in Estonia after the refurbishment of the HVAC system (Napp et al. 2015; Napp et al. 2016a; Napp et al. 2016b).

In 2011, the HMWall code was edited according to the balance heat and moisture equations and the driving potentials given by Hartwing Künzel and used in WUFI family tools (Künzel 1995). This hygrothermal model was chosen because WUFI was validated by means of comparative test and analytical verification more than other hygrothermal simulation tools demonstrating its quality and robustness (Holm 2003; Holm 2005; Karagiozis 2010). The transfer potentials for liquid and vapour transfers are the relative humidity (φ or RH) and the vapour partial pressure (p_v), respectively. The relative humidity can be used as driving potential for liquid transfer because it is related to the capillary pressure by the Kelvin's equation (Skinner and Sambles 1972). The main differences between the IDA ICE extended with the HMWall object and WUFI as well as the basic governing equations are reported in Frasca et al. (2018). Currently, a correct implementation of wind driven rain and its impact on the building envelope remains a weakness as well as any moisture source within the wall layer.

In the HMWall model, the moisture storage curve is calculated as a function of relative humidity as follows (eq. 1):

$$w = w_f \cdot \frac{(b-1)\cdot\varphi}{b-\varphi} \qquad (1)$$

where w is the water content, w_f is the free water saturation, φ is the relative humidity and b is the approximation factor. b must always be greater than one and it is calculated from the equilibrium water content at 80% of relative humidity (w_{80}) (Künzel 1995).

The HMWall model used in this research was updated with respect to the versions shown in Frasca et al. (2018). In this version, the calculation of liquid conduction coefficient (Dφ) is executed starting from the liquid transport coefficient for suction (Dws) (eq. 2) and assuming no difference between suction and redistribution processes.

$$\mathrm{Dws}(\mathrm{w}) = 3.8 \cdot \left(\frac{\mathrm{A_w}}{\mathrm{w_f}}\right)^2 \cdot 1000^{\frac{\mathrm{w}}{\mathrm{w_f}}-1} \qquad (2)$$

where A_w is the water penetration coefficient. Dφ and Dws are related each other as reported in Künzel (1995) as follows (eq. 3):

$$\mathrm{D\varphi} = \mathrm{Dws} \cdot \frac{\mathrm{dw}}{\mathrm{d\varphi}} \qquad (3)$$

where dw/dφ is the derivative of moisture storage function and φ is a further notation for relative humidity.

The effect of the heat transfer on the water vapour transfer (g_v) between the wall surface and the boundary air layer close to it is not considered, since its contribution is negligible as demonstrated in Frasca et al. (2018).

The upgrading of the HMWall model was mainly due to the lack of hygrometric properties of materials required to run the previous code. In this version of the HMWall model, the hygrothermal properties are listed below:

- heat conductivity (λ)
- density (ρ)
- specific heat (c)
- free water saturation (w_f)
- equilibrium water content at 80% of relative humidity (w_{80})
- thermal conductivity supplement (b)
- vapour diffusion resistance factor (μ)
- water absorption coefficient (A_w)

All these properties, collected by seven research institutes, are available in the MASEA geprüfte DatenBank web site for most of building materials (https://www.masea-ensan.de/). The web site is written in German.

The semi-infinite wall

The European standard EN 15026:2007 provides a minimum criterion for simulation software used to predict one-dimensional transient heat and moisture transfer in multi-layer building components exposed to transient climate conditions in both sides. Moreover, it specifies the equations to be used in a dynamic simulation model for calculating heat and moisture transfer through building structures. These equations consider one-dimensional transport phenomena and should not be applied in case of: convection in pores, two-dimensional effects, hydraulic or osmotic or electrophoretic forces and when the daily mean temperature in component is more than 50°C.

In this exercise, a semi-infinite wall is modelled using the HMWall as a single independent object and setting four layers with the same hygrothermal properties for a total thickness of 25 m. This is needed for taking the temperature (T) and water content (w) loads at the thickness specified by the standard, since the HMWall allows only a linear spacing of the layer. Figure 2 shows the layer structure and connection how they should appear at the advanced level of the IDA ICE software. The boundary conditions were fixed on both side and set to T = 30°C and RH = 95% on external side and T = 20°C and RH = 50% as initial values inside the material. The wall was perfectly airtight and no boundary resistance or rain impact were considered.

The exercise aimed at testing T and w profile loads in the material after a period in which the wall experienced the outdoor T-RH conditions. The three periods were 7, 30 and 365

days. The modelled distribution of T and w inside the material were compared with the limits of validity for results provided by the norm in the Annex A.

The thermal properties of the material were provided by the norm, whereas the hygric properties were set by minimizing the errors between the hygrothermal curves computed by our code and those given by the norm. This was necessary because it is not possible to enter the values of curves calculated according to the norm also as a table of discrete function values that can be linearly interpolated. This feature was implemented in the WUFI family tools. In the case of HMWall, we used the percentage bias (PB) to estimate whether the HMWall curves consistently under- or overestimated those of the norm taken as the reference.

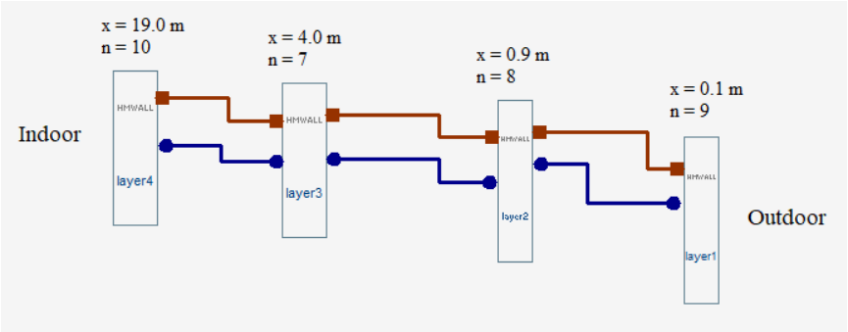

Figure 2 Sketch of the schematic model built in advanced level of IDA Indoor Climate and Energy: x is the thickness of layer and n is the number of nodes. Red lines are the thermal flow connections whereas blue lines are the moisture flow connections. The HMWall is used as an independent model.

Figure 3 shows the moisture storage curve for both calculation methods. The two curves tended to significantly deviate when RH is lower than 70%. The PB between the two curves was minimized at -3.8% in the RH range 50-95%, i.e. the humidities occurring in the exercise, which meant that the w calculated by HMWall underestimated w given by the norm.

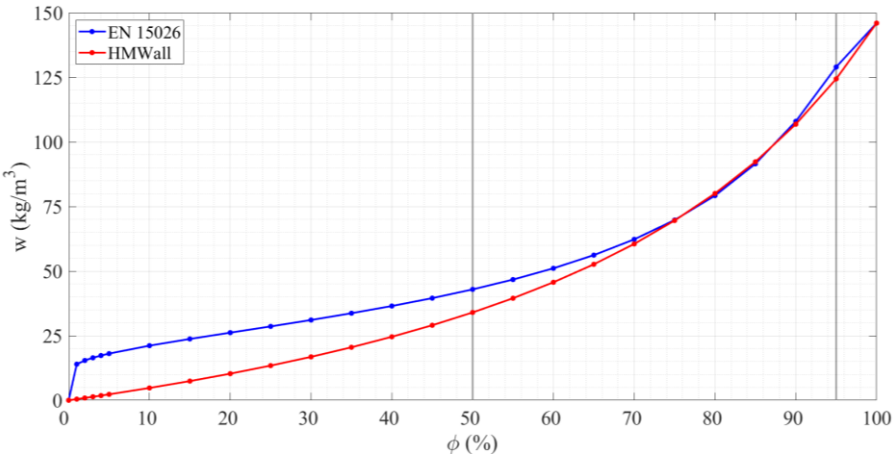

Figure 3 The moisture storage curves, water content (w) versus relative humidity (φ), calculated according to the EN 15026:2007 (blue line) and HMWall (red line). The vertical lines indicate the φ range occurring in the exercise.

In the norm, the vapour diffusion coefficient (δ_0) is a function of w as well as the vapour diffusion resistance factor (μ), which is the ratio between the vapour diffusion in still air

(δ) and δ_0. In the case of the HMWall, since only a value of ⌾ can be used, the δ_0 is solved as a single value for the whole w range. In this way, δ_0 changes only with T, since δ is calculated by means of the Schmirer's equation (Slanina and Šilarová 2009). For this reason, we selected a δ so that the $\delta_0 = 5.97 \cdot 10^{-13}$ was the average of the δ_0 computed by the norm and occurred in the RH range 50-95%. As above, we selected A_w = 0.0012 ($kg/(m^2 \cdot s^{0.5})$) as the average of the Aw derived from the Dws calculated from the norm. The PB of the logarithm of Dws is 0.5% in the RH range 50-95%.

The hygrothermal properties used in this exercise are listed in Table 2.

Table 2 List of hygrothermal properties needed in HMWall tab according to the minimization of hygrothermal curves calculated according to the European Standard EN 15026:2007.

Exercise	Parameters							
	λ	ρ	c	w_f	w_{80}	b	μ	A_w
	$\frac{W}{m \cdot K}$	$\frac{kg}{m^3}$	$\frac{J}{kg \cdot K}$	$\frac{kg}{m^3}$	$\frac{kg}{m^3}$	–	–	$\frac{kg}{m^2 \cdot s^{0.5}}$
1	1.5	1000	1842	146.00	80.06	10.534	324	0.0012

The adiabatic building envelope

The exercise 2 consisted of the dynamic simulation of an adiabatic building envelope, that appears as in Figure 4 in the IDA ICE advanced level. The building had a volume of 26.0 m^3 with a height of 2.6 m, a length of 2.5 m oriented in the east-west direction and of 4.0 m in the north-south. It was designed without windows and with a flat ceiling. The walls were a mono-layer of lime silica brick of 0.2 m, whose hygrothermal properties are reported in Table 3. The wall thickness was chosen as a limit for detecting a significant transport of relative humidity through a wall. Air changes by infiltration were set to 0.0 h^{-1} and no thermal bridges were taken into account. Solar radiation and ventilation were not included in the climate file to avoid any misleading with input parameters, such as wind, infiltration or radiation, whose setting might vary from a simulation code to another code. The indoor T and RH were 10°C and 50%, respectively. The climate file had only T and RH values taken at 1-hour time slot. Two simulations were run with outdoor temperature T_{out} = 10°C and relative humidity RH_{out} = 60% (the first simulation) and RH_{out} = 40% (the second simulation). A third simulation was run setting RH_{out} as a sinusoidal curve ($RH_{out,min}$ =42.0% and $RH_{out,max}$ = 58.0%), in order to assess the indoor climate response when there was a seasonal variation of RH over a year. It is worth to notice that, considering the definition of RH given by the WMO (World Meteorological Organization), in this exercise the variations of RH_{in} depended only on the water vapour partial pressure (p_v) gained by walls, since the saturated pressure (p_{sat}) was constant ($T_{in} = T_{out}$ = 10°C). The simulations were performed over 365 days at 1-hour step.

The exercise aimed at investigating the capability of IDA ICE extended with the HMWall to model the amount of indoor air RH (RH_{in}) depending only on the moisture transfer

across the walls. The validation was based on a comparative test with the well know simulation tool, WUFI Plus, because it is one of the most validated simulation tools and because the HMWall model uses the same one-dimensional heat and moisture balance equations. The response of the indoor RH_{in} was assessed by a comparison of the modelled RH data.

Table 3 List of hygrothermal properties used in the HMWall tab and in WUFI Plus as provided by MASEA Datenbank - Materialdatensammlung für die energetische Altbausanierung.

Exercise	**Parameters**							
	λ $\frac{W}{m \cdot K}$	ρ $\frac{kg}{m^3}$	c $\frac{J}{kg \cdot K}$	w_f $\frac{kg}{m^3}$	w_{80} $\frac{kg}{m^3}$	b –	μ –	A_w $\frac{kg}{m^2 \cdot s^{0.5}}$
2	1	1830	850	257.12	27.47	4.000	27	0.0590

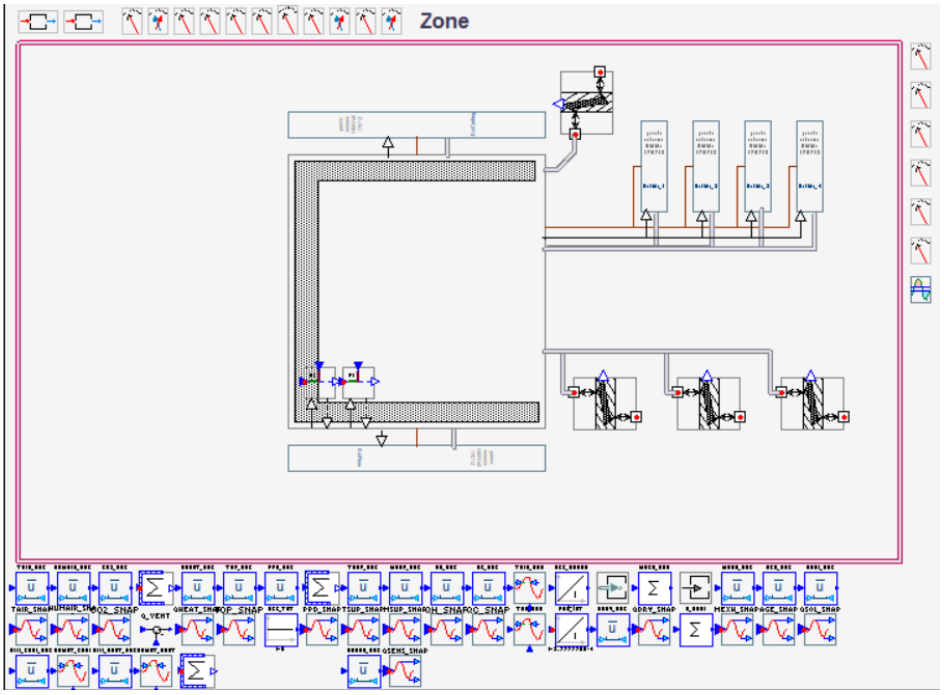

Figure 4 Sketch of the schematic model of the adiabatic building envelope in advanced level of IDA Indoor Climate and Energy. The HMWall is used as an extension of a complex system.

The Common Exercise 3

The Common Exercise 3 (heareafter called CE3) belongs to one of the six Common Exercises developed in the framework of the IEA Annex 41. This exercise was used in Ferroukhi et al. (2016) for validating TRNSYS–COMSOL co-simulation tool and in the European project Climate for Culture (2011-2014) for validating different dynamic simulation tools of choice (Leissner et al. 2015). The CE3 was an experimental exercise, that was developed by the Fraunhofer Institute for Building Physics. It consisted of two identical and insulated rooms: the test room and the reference room (Holm et al. 2003). A detailed description of this exercise can be found in Woloszyn and Rode (2008). Four

boundary conditions around the rooms were set, so that internal walls were surrounded by controlled T and RH areas, whereas external walls were exposed to weather data of Holzkirchen (Germany, Lat. 47.9° and Lon. 11.7°), i.e. its TRY (Test Reference Year-type) weather data. The indoor T was controlled by a small radiator (with maximum heat dissipation of 1000 W) at 20±2°C. The moisture production was scheduled by means of an ultrasonic evaporator at 2.4 kg/day with two peaks at 400 g/h during 6-8 h and 200 g/h during 16-22 h, which corresponded to the equivalent amount for a household of three persons (Woloszyn and Rode 2008). Natural air changes by infiltration corresponded to 0.09 h^{-1} for the reference room and 0.07 h^{-1} for the test room, whereas the mechanical ventilation was set to 0.63 h^{-1} and 0.66 h^{-1}, respectively. The CE3 allowed investigating the moisture buffering capacity of the test room with respect to the reference room that kept the same wall stratigraphy over the experiments. The exercise consisted in three steps, in which the cladding material of the wall stratigraphy of the test room was modified: 1) test room only with aluminium foil (from January 17th till February 2nd); 2) test room with gypsum boards on the walls (from February 14th till March 20th); and 3) test room with gypsum boards on the walls and roof (from March 27th till April 22nd).

The aim of this exercise was to investigate the indoor RH response modelled by IDA ICE 4.7.1 extended with HMWall, when RH_{in} was governed by the moisture buffering effect of different materials for a controlled indoor climate. It was conducted by a comparison with the measurements. Moreover, a further comparison was made with the available data modelled by WUFI Plus and those by IDA ICE 3.0 extended with HAMWall (version 1999), with the aim to achieve more confidence with results. All these data were shown in the final report of the IEA ECBCS Annex 41.

The box-and-whisker plot was used for a synthetic visualization of all data without any assumption of data distribution. The Wilcoxon-Mann-Whitney test was used to establish if any significant difference was among each pair measured RH and RH data modelled by the simulation tools. The null hypothesis is that two independent data are samples from continuous distributions with equal medians and are not normally distributed. The significance level was set to 5%. Moreover, the mean absolute error (MAE), the root mean square error (RMSE), the Coefficient of Variation of the RMSE (CV-RMSE) and the Spearman's correlation coefficient (rho) were performed to assess the agreement between the modelled and measured data. Finally, we analysed the discrepancies between the models and the measurements considering the RH span at 6-8 h (eq. 4) and 16-22 h (eq. 5) to evaluate the sorption effect of cladding material when the production of moisture reached 400 g/h and 200 g/h, respectively.

$$\Delta RH_{6-8} = RH_{8:00} - RH_{6:00} \qquad (4)$$

$$\Delta RH_{16-22} = RH_{22:00} - RH_{16:00} \qquad (5)$$

The historic building

In the case of historic building, the achievement of robust simulation is hard due to the complexity of establishing accurate hygrothermal properties of materials. This is mainly due to the way a material was manufactured, which generally concerned local skills, and how it was damaged along its life, for example because of uncontrolled condensation (O'Leary et al. 2015).

The HMWall model was applied to a building previously studied, the Chiesa of Santa Rosalia (hereafter called the church). The church, located in the central Italy close to Rome (Palestrina, Lat. 41.8° and Lon. 12.9°), was built in the 17th Century on the Francesco Contini's project by Maffeo Barberini (Figure 5). Most of internal side of walls are cladded by decorative marble slabs. The water infiltration from the north side of the church, due to rocky front behind the wall, is causing chromatic alteration of marble slabs and their detachment from calcareous mortar. For this reason, a hygrothermal analysis was conducted coupling on-site indoor climate measurements with whole building dynamic simulation in order to have a comprehensive assessment of the above issues. A monitoring campaign of indoor and outdoor climate parameters (T and RH with an accuracy of 0.3°C and 1.5%, respectively), was performed from January 1st till March 31st, 2015. The building model was created starting from the architectural survey provided by LAREA (LAboratorio di Rilievo E Architettura belonging to University of Rome Tor Vergata) and using the hygrothermal properties reported in MASEA Datenbank for opaque components. Since the calculations were based on idealised homogeneous walls, the wall in contact with the rocky front was split in order to accurately simulate the area with the altarpiece, also close to the rocky front. The weather file was compiled with outdoor measured T and RH, whereas wind and radiation data belonged to the weather station ESTER – Università degli Studi di Roma "Tor Vergata" (Italy, Lat. 41.8° and Lon. 12.6°), which is very close to Palestrina. Even though HMWall does not allow implementing a source of water inside a wall component or on one side of the wall, the issue is overpassed setting the RH loads to 100%.

Figure 5 The Chiesa di Santa Rosalia in Palestrina (Italy): outside (left panel) and inside (right side).

The exercise aimed at assessing the performance of IDA ICE extended with HMWall, when one side of a historical building is wetted due to water infiltration mainly driven by rain. The church was modelled using IDA ICE as it is, and IDA ICE extended with HMWall, in order to stand out the differences when a hygrothermal model is inserted in the simulation. The building was modelled using IDA ICE, as it is, and IDA ICE

extended with the HMWall object. Both T and RH modelled data were compared with the measurements in order to point out which building model was more accurate. The boxplot was performed to visualize the distributions of measured and modelled RH data. The MAE, the RMSE and the CV-RMSE were calculated to evaluate the discrepancies between modelled and measured data.

Results

The semi-infinite wall

Figure 6 shows the thermal profiles of the semi-infinite wall modelled by HMWall (blue dots) and the limits of validity (red area) defined by the European standard EN 15026:2007. In all three step changes, the modelled Ts are within the limits along the whole wall thickness.

In Figure 7, the w distribution modelled by HMWall (blue dots) shows an acceptable agreement only in the third step change, i.e. when the wall experienced RH = 95% for 365 days (right panel). That area corresponds to the range of relative humidity in which the discrepancy between the moisture storage curves is small. When the perturbation of the initial conditions inside the wall is short (left and mid panels), the moisture profiles differ from the limits of validity (red areas) up to 14 kg/m^3. This depends on the range of RH within the first 0.01 m of thickness, which suddenly passes from 95% to 60%, i.e. in the range in which the moisture storage curves are different.

It is worth to notice that in Figure 8 the RH profile (blue dots) modelled by HMWall at 7 days is within the limits of validity (red area), calculated as the inverse function of the moisture storage function.

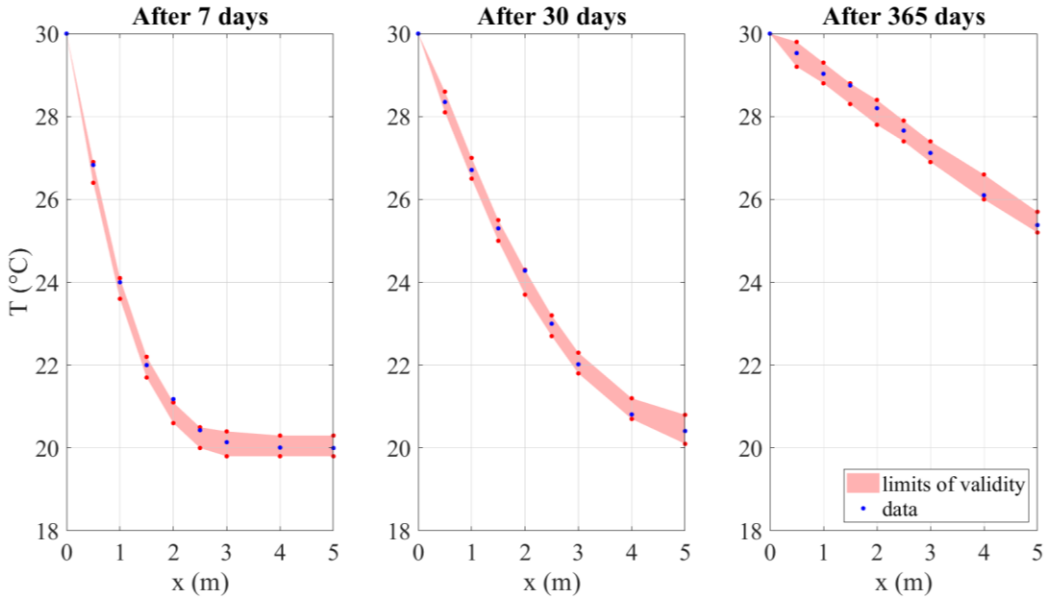

Figure 6 The temperature (T) distributions along layer thickness (x) at 7 days, 30 days and 365 days: HMWall results (blue dots) and the analytical results from EN 15026:2007 (red area) that represents the permissible error range.

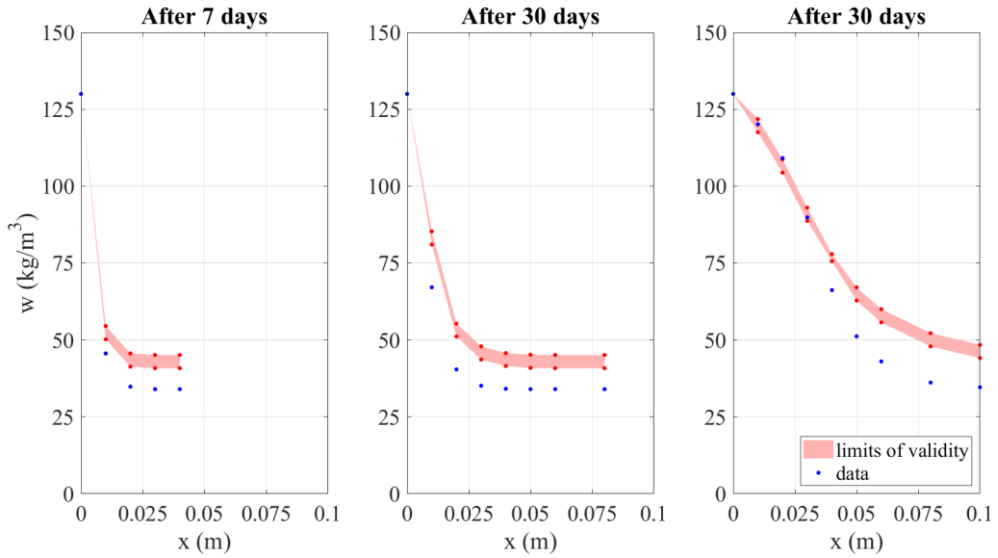

Figure 7 The water content (w) distributions along layer thickness (x) at 7 days, 30 days and 365 days: HMWall results (blue dots) and the analytical results from EN 15026:2007 (red area) that represents the permissible error range.

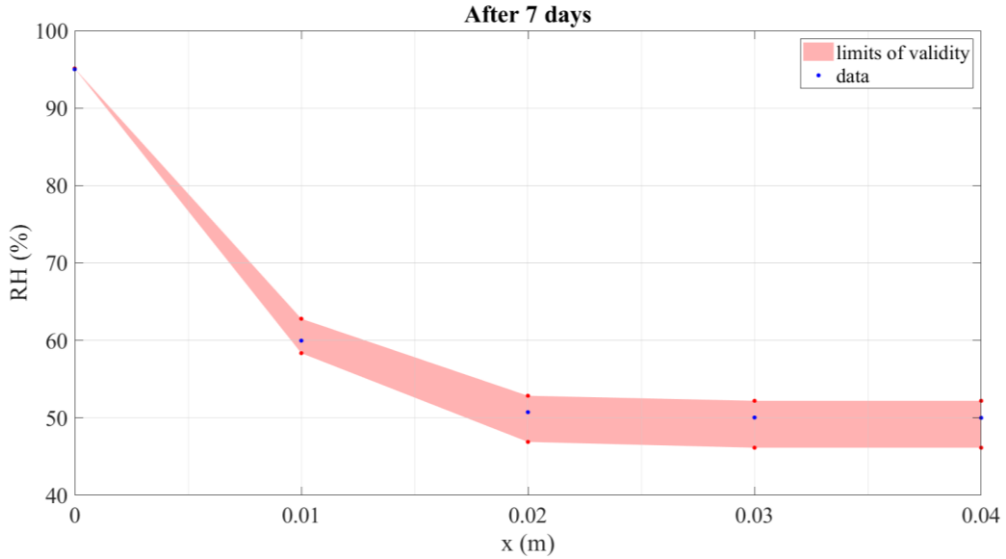

Figure 8 The relative humidity (RH) distributions along layer thickness (x) at 7 days: HMWall results (blue dots) and the analytical results from EN 15026:2007 (red area) that represents the permissible error range calculated as the inverse function of the moisture storage curve.

The adiabatic building envelope

Figure 9 shows the scatter diagrams of modelled RH values (IDA ICE – HMWall *vs* WUFI Plus) over a year for all three cases. There is a high agreement between the two codes with the linear fitting very close to the bisector. The slope, indeed, is always close to the unity. However, when RH_{out} = 40% (mid panel), IDA ICE tends to reach the equilibrium with the outdoor condition more quickly than WUFI. This is probably due to the way in which WUFI generates the estimated table with the liquid transport coefficients for redistribution (Dww). Indeed, in WUFI, Dww is equal to Dws (eq. 2) except when w = w_f and Dww is one-tenth of Dws; whereas in HMWall, Dww is always equal to Dws. The error between the simulation tools is within the accuracy of relative

humidity sensors used for indoor monitoring campaign in the RH range 20% - 80% for all three cases.

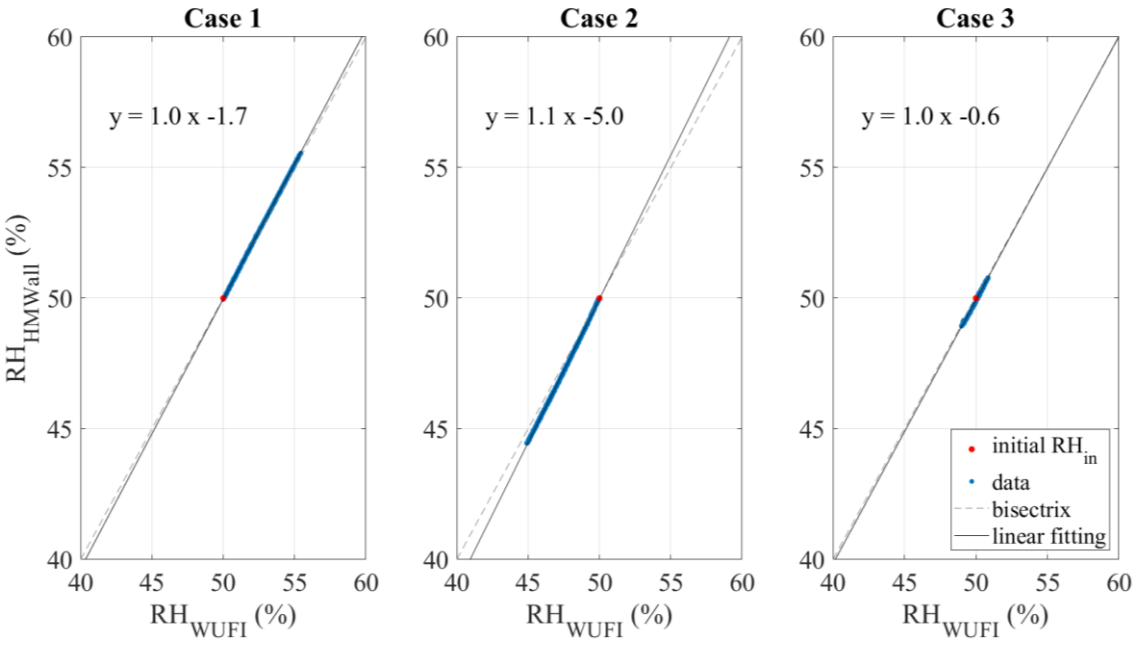

Figure 9 Scatter diagram of modelled RH values (HMWall versus WUFI) over a year. The indoor RH starts from 50% (red dot). The linear fitting (grey line) and its equation are reported for each case. The hygrometric boundary conditions are set to: RH = 60% (case 1), RH = 40% (case 2) and RH as a sinusoidal curve. T was constant (Tin = Tout = 10°C).

The common exercise 3

To simplify the readability of results, Wufi Plus, IDE ICE 3.0 extended with HAMWall and IDA ICE 4.7.1 extended with HMWall are hereafter called WUFI, HMWallM and HMWall, respectively.

The summary of statistics for calculating the agreement between each simulation with respect to the measurements is reported in Table 4 for each case test.

Test 1

In test 1, the walls of the test room are coated by aluminium foils, which are characterized by no sorption effect, i.e. the walls do not absorb or desorb water vapour from the air. In Table 4 (Test 1), WUFI has the lowest errors with MAE and RMSE lower than 2.0%. The correlation between modelled RHs and measured RH is close to the unity for the three simulation tools in both rooms. It is worth to notice that HMWall has, on average, a better agreement with the measurements than HMWallM, where the values, instead, are generally doubled.

Figure 10a shows the box-and-whisker plots of reference (right panel) and test room (left panel). This graph seems to suggest that the two rooms are very similar each other. In both panels, the box plots totally overlap, showing that no difference is among the modelled and measured indoor RH data. In reference room (left panel), the median of measured RH is 31.9%, whereas the 25th and the 75th percentile are 25.8 and 41.8%,

respectively. Considering the simulation tools in order of appearance in plot, the boxes of modelled RHs have these values: the median at 32.5% between 26.3 and 42.5%, 29.9% between 22.9% and 41.9% and, finally, 32.4% between 24.7% and 41.9%, respectively. In test room (right panel), the median of measured RH is 31.9%, whereas the 25th and the 75th percentile are 23.2% and 42.9%, respectively. As for the simulation tools, the boxes of modelled RHs have these values: the median at 31.8% between 23.0% and 44.3%, 27.2% between 19.6% and 41.0% and, finally, 31.8% between 24.3% and 42.1%, respectively for each simulation tool.

The Wilcoxon-Mann-Whitney test demonstrates that in both rooms the median value of RH modelled by HMWall has the highest agreement ($p > 0.5$) with the median of measurements. On opposite, the median of RH distribution modelled by HMWallM is slightly different from the median of measurements with $p < 0.03$.

Figure 11a shows the median of RH fluctuations and minimum – maximum deviations for $\Delta RH_{6\text{-}8}$ (left panel) and $\Delta RH_{16\text{-}22}$ (right panel), which are related to the daily moisture production peaks at 400 g/h and 200 g/h, respectively. Both measurements and WUFI and HMWallM show that the fluctuations in the test room (red bars) are higher than those in the reference room. This is due to the effect of aluminium foils, that is not able to absorb or desorb the RH from indoor air. HMWall, instead, seems to not properly model the no-sorption effect of aluminium especially during the moisture production at 200 g/h (right panel), so that the differences in ΔRH between rooms, if any, are mainly due to the infiltrations. At this step, HMWall shows a weakness since it is not possible to build a moisture storage curve equal to zero in whole range of RH: w_f (free saturation water) and w_{80} (equilibrium water content at RH = 80%) have to be always higher than zero.

Test 2

In test 2, the walls of the test room are coated by gypsum boards. The aim is to test the capabilities of simulation tools to detect the moisture buffering effect of gypsum on the indoor RH. In Table 4 (Test 2), it can be noticed that in both rooms the RH modelled by HMWall has the lowest values of RMSE, i.e. 3.5% in reference room and 2.6% in test room, and CV-RMSE, i.e. 10.5 in reference room and 7.8% in test room, showing a better agreement with the measured RH data with respect to the other simulation tools. In general, HMWallM is the worst among the simulation tools, especially in the reference room. The correlation between modelled RHs and measured RH is still high in both rooms and close to the unity.

Figure 10b shows the box-and-whiskers plots for the RH data in reference room (left panel) and test room (right panel), respectively. The box plots for both rooms overlap each other. Moreover, the inter-quartile-range (IQR), i.e. the distance between the 25th percentile and the 75th percentile of the boxes, of the test room are less than those of the reference room, clearly showing the sorption effect of gypsum on indoor RH. The suspected outliers (black dots), i.e. the values either 1.5×IQR or more above the 75th percentile, or 1.5×IQR or more below the 25th percentile, are considered in the analysis,

because they correspond to the maximum indoor RH reached after every moisture production.

If we compare the median values by the Wilcoxon-Mann-Whitney test, the RH data modelled by HMWallM and HMWall do not have a statistical difference with the measured RH data ($p > 0.3$) instead of WUFI ($p < 0.02$) in both rooms.

For a better interpretation of moisture buffering capacity of gypsum boards, Figure 11b shows the median values and their maximum deviation of $\Delta RH_{6\text{-}8}$ (left panel) and $\Delta RH_{16\text{-}22}$ (right panel). If we consider the measurements, in test room (red bars), the gypsum boards reduce, on average, the fluctuations in RH of 12.0% during the peak at 6-8 h and of 5.0% at 16-22 h. If we consider the modelled ΔRHs, WUFI shows a reduction of 13% in reference room and 6% in test room, HMWallM of 15% and 4% and finally, HMWall of 10% and 6%, respectively.

All simulation tools can estimate the effect of gypsum boards on indoor RH with different accuracy.

Test 3

In test 3, both walls and ceiling of the test room are coated by gypsum boards. In this step, the moisture buffering effect of the gypsum boards is again put in evidence. This step has been renamed Test 3*, because, as shown in Figure 12, from April 17th an anomalous behaviour of measured RH has been detected. This might be due to an erroneous operation of the ultrasonic evaporator, since the time plot does not show any peak corresponding to the moisture production hours.

Table 4 (Test 3*) summarises the statistics of modelled vs measured RH data taking into account the period from March 27th till April 16th. In this step, HMWall has, on average, the minimum values in statistics with respect to the other simulation tools. Especially, in test room, the CV-RMSE calculated for HMWall is 8.8%, indicating less residual variance with respect to those calculated for WUFI and HMWallM, which correspond to 10.7% and 9.5%, respectively. The modelled RHs by all simulation tools are highly correlated with measurements ($0.72 \leq rho \leq 0.89$) in both rooms.

Figure 10c shows the box-and-whiskers plots for the RH data in reference room (left panel) and test room (right panel), respectively. In reference room, the box plots overlap each other. However, there is no significant differences among medians only in the reference room ($p > 0.1$). Looking at the box plots of test room, the median of measured RH is 46.4%, whereas the 25th and the 75th percentile are 41.6 and 51.5%, respectively. Considering the simulation tools in order of appearing in plot, the boxes of modelled RHs have these values: median of 50.5% between 46.4 and 54.3%, 49.6% between 43.7 and 55.7% and, finally, 49.9% between 43.8 and 55.2%, respectively. The IQR of WUFI is 2.1% less than the IQR of measurements, showing that the simulation overestimates the moisture buffering effect of gypsum; whereas the IQR of HMWall is only 1.4% higher than measurements. In general, the values of modelled RHs are higher than the measurements and, at the same time, they are very similar each other. This can suggest

that the simulation tools have been set correctly with respect to the instructions, but the reality in the room changed over time with respect to the initial conditions.

Figure 11c shows the medians and their maximum deviation of $\Delta RH_{6\text{-}8}$ (left panel) and $\Delta RH_{16\text{-}22}$ (right panel), respectively. The ΔRH in test room (red bars) is usually less that ΔRH in reference room (blue bars) due to the moisture buffering effect of gypsum. HMWall is the simulation tool which more precisely simulate the ΔRH, especially in the test room. In the reference room, the $\Delta RH_{6\text{-}8}$ are 30.6% and 31.9% and the $\Delta RH_{16\text{-}22}$ are 21.5% and 24.2% for measurements and HMWall, respectively. In the test room, the $\Delta RH_{6\text{-}8}$ are 19.2% and 17.3% and the $\Delta RH_{16\text{-}22}$ are 15.7% and 15.8% for measurements and HMWall, respectively.

Table 4 Summary of the statistics of modelled vs. measured RH data for three whole-building dynamic simulation software: WUFI Plus, IDA ICE 3.0 extended with HMWallM (version 1999) and IDA ICE 4.7.1 extended with HMWall (version 2018). Four statistics are considered: MAE = mean absolute error; RMSE = root mean square error; CV-RMSE = coefficient of variation of RMSE; rho = Spearman correlation). Test 3* concerns a reduced time interval from March 27th, 2005 till April 16th, 2005, since measurements show an anomalous behaviour.

		Reference room			**Test room**		
		WUFI	*HMWallM*	*HMWall*	*WUFI*	*HMWallM*	*HMWall*
Test 1	MAE	1.0	2.7	1.5	1.4	3.3	1.8
	RMSE	1.6	3.5	1.9	2.0	4.2	2.5
	CV-RMSE	4.5	10.2	5.6	6.0	12.5	7.5
	rho	0.99	0.97	0.99	0.99	0.97	0.98
Test 2	MAE	2.2	3.2	2.3	1.9	1.9	1.8
	RMSE	3.8	4.8	3.5	2.8	2.8	2.6
	CV-RMSE	11.4	14.3	10.6	8.3	8.4	7.9
	rho	0.95	0.93	0.96	0.97	0.96	0.96
Test 3*	MAE	1.7	3.0	1.9	4.1	3.4	3.0
	RMSE	2.9	4.2	2.5	5.0	4.4	4.1
	CV-RMSE	5.8	8.7	5.1	10.7	9.5	8.8
	rho	0.87	0.86	0.89	0.72	0.82	0.82

* From March 27th, 2005 till April 16th, 2005

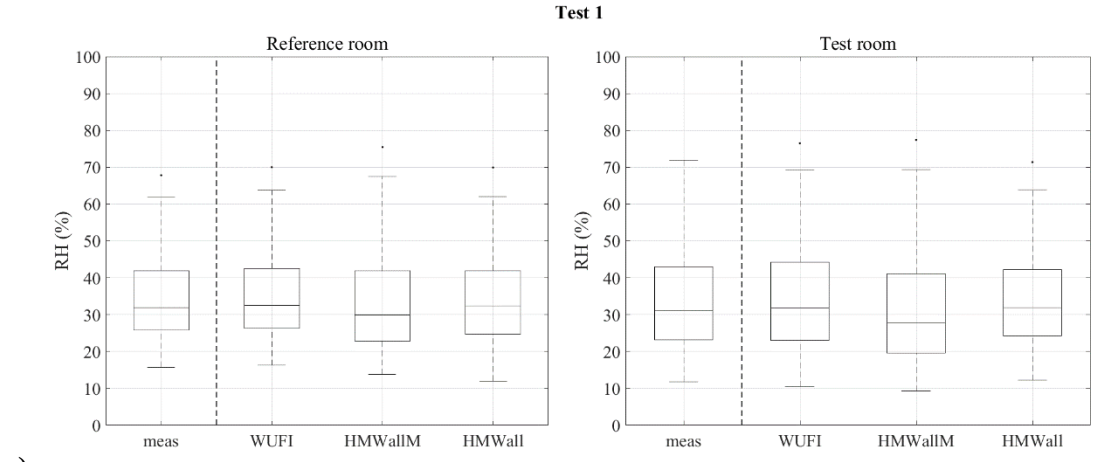

a)

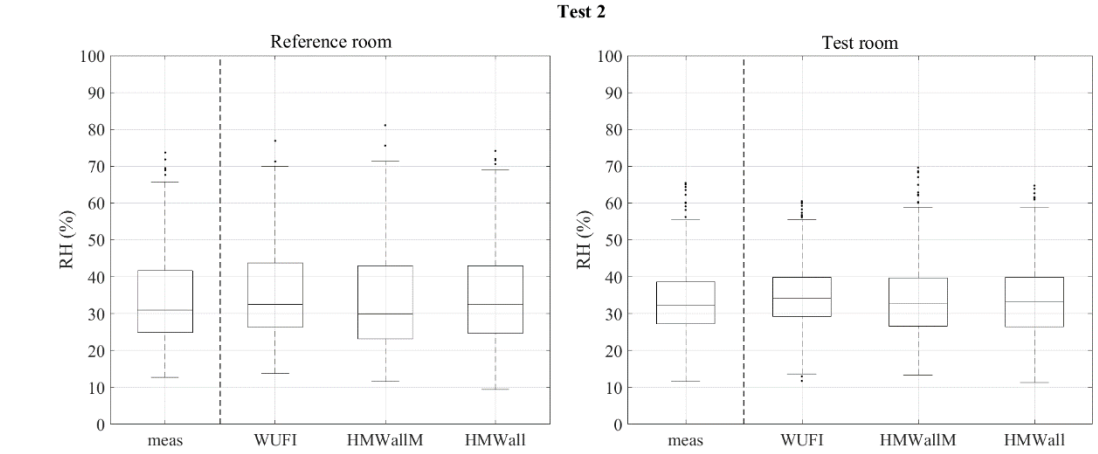

b)

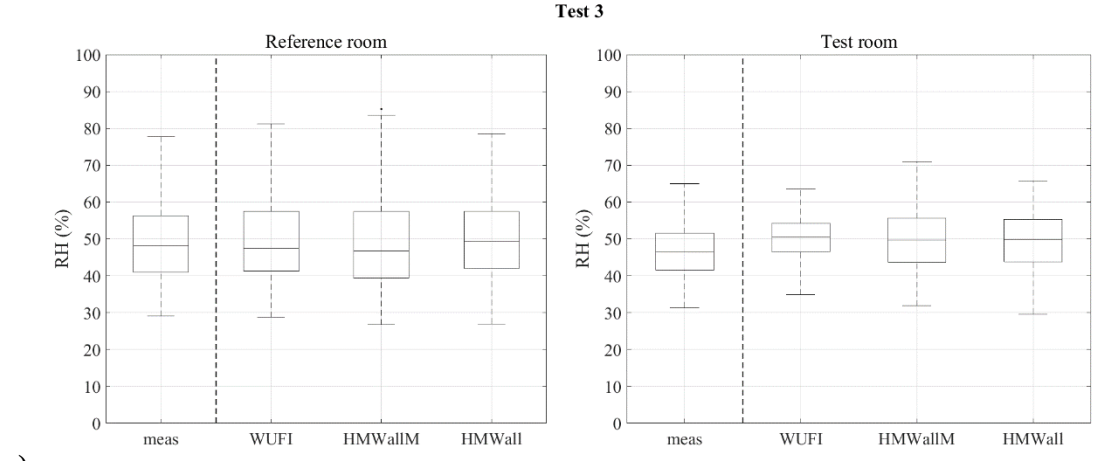

c)

Figure 10 Box-and-whisker plots of relative humidity (RH) in reference room (left panels) and test room (right panels) for each case test: a) Test 1 – test room with aluminium foils on walls; b) Test 2 – test room with gypsum boards on walls; and c) Test 3 – test room with gypsum boards on walls and ceiling. The line inside the box is the median value, with the 25th and 75th percentiles as lower and upper sides of the box, respectively. The lowest and the highest value of the data set are plotted as whiskers when they are not outliers, indicated as the circle (i.e., above or below 1.5*IQR, IQR interquartile range).

Appendix E

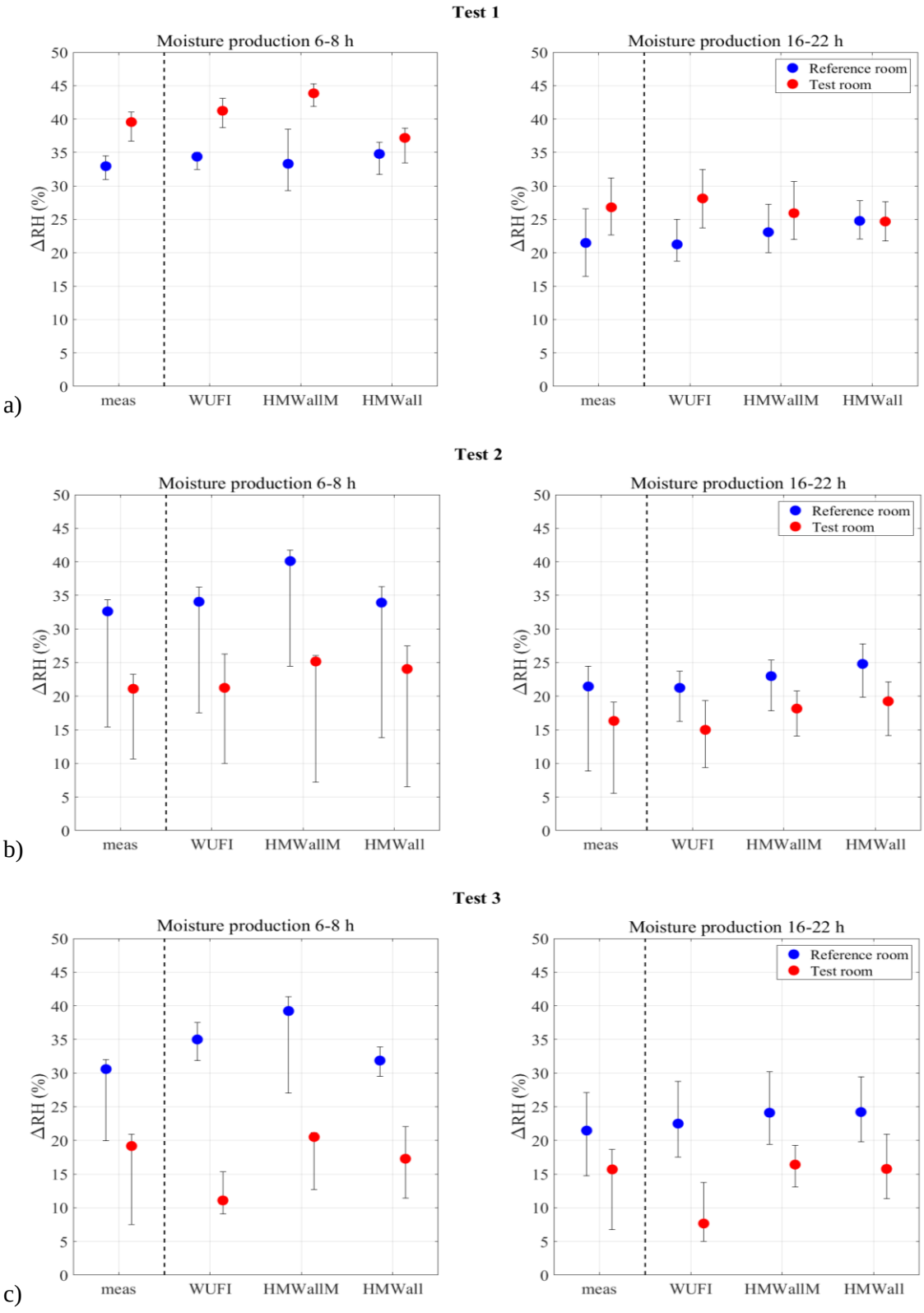

Figure 11 Plots of relative humidity span (ΔRH) at moisture production peak of 400g/h at 6-8 h (left panels) and of 200 g/h at 16-22 h (right panels) for each case test: a) Test 1 – test room with aluminium foils on walls; b) Test 2 – test room with gypsum boards on walls; and c) Test 3 – test room with gypsum boards on walls and ceiling. The reference room is depicted as blue dot; whereas the test room is depicted as red dot.

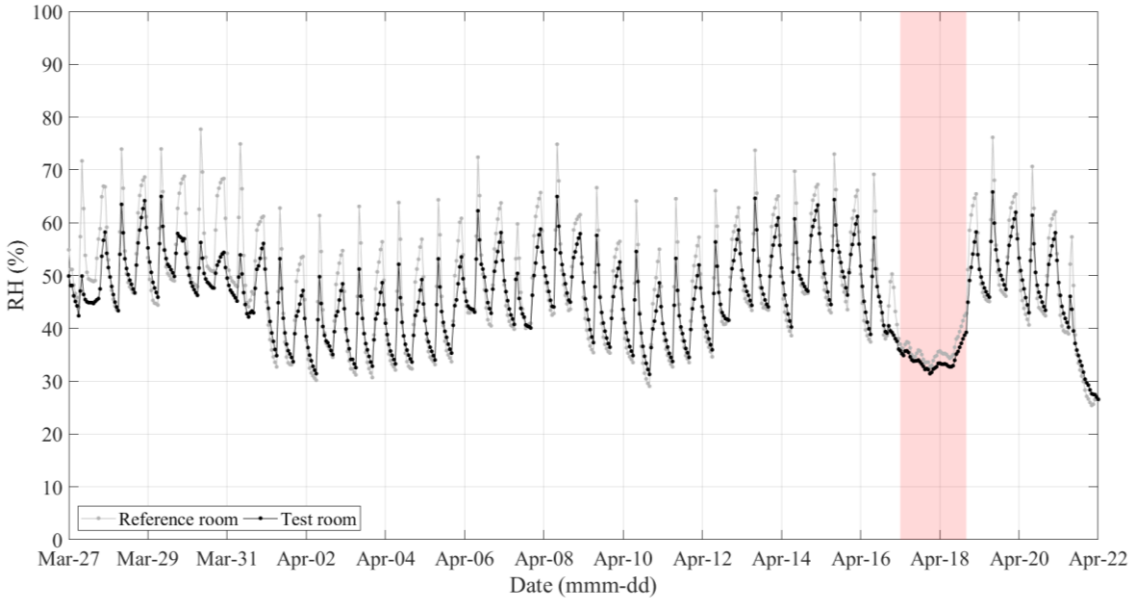

Figure 12 Time evolution of relative humidity (RH) in reference room (grey line) and test room (black line) when walls and ceiling of test room are coated by gypsum boards. The red band individuates the anomaly.

A historical building

In this step, the thermal model of wall is replaced by the HMWall model and no change of the other parameters are done. Table 5 summarises the statistics of modelled vs measured T and RH data taking into account IDA ICE 4.7.1 with the default thermal model (hereafter called thermal model) and IDA ICE 4.7.1 extended with the HMWall (hereafter called HMWall).

Table 5 Summary of the statistics of modelled vs. measured T and RH data taking into account both the IDA ICE as it is and IDA ICE extended with the HMWall object (MAE = mean absolute error; RMSE = root mean square error; CV-RMSE = coefficient of variation of RMSE; rho = Spearman correlation).

	IDA ICE		**IDA ICE & HMWall**	
	T	**RH**	**T**	**RH**
MAE	0.2 °C	7.4 %	0.2 °C	3.6 %
RMSE	0.2 °C	8.9 %	0.2 °C	4.7 %
CV-RMSE	2.0 %	14.8 %	1.8 %	7.8 %
rho	0.95	0.92	0.95	0.88

If we consider the temperature, there is no significant difference between the values modelled by the thermal model and the HMWall. Both simulation tools are highly correlated (rho = 0.95) with measurements, and both MAE and RMSE are 0.2°C and are statistically consistent with the instrumental accuracy. However, the CV-RMSE of the HMWall is 1.8% and indicates a less residual variance than that of the thermal model (2.0%).

Appendix E

The HMWall-performance errors for RH data are MAE = 3.6%, RMSE = 4.7% and CV-RMSE = 7.8%. These values are, on average, the half of those calculated for the thermal model. This means that the HMWall can give a more accurate representation of the indoor climate with respect to the thermal model. Looking at Figure 13, it is clear that the box of RH distribution modelled by HMWall overlaps that of measurements. The medians are 58.7% and 60.8%, respectively; whereas the IQRs are 10.0% and 12.5%, respectively. The RH values modelled by the thermal model, instead, underestimate the measurements with the median at 55.1% and show a higher variability with IQR = 15.4%.

Figure 14 shows the time evolution of modelled and measured RH in the church. The RH modelled by HMWall (black line) well estimates peaks and drops of measured RH (grey line) over time with respect to the thermal model (dark grey line), that underestimates the drops in correspondence of high ex/infiltration (red areas). This means that the thermal model is not able to well represent the indoor climate because it does not take into account the effect of walls on the moisture equilibrium in the ambient air. From March 6th, both modelled RHs are slightly moved forward with respect to the measured data. It might depend on the weather data used for the creation of the climate file. Indeed, it was found that the same low-pressure area was delayed of 3 hours between the two sites, Palestrina and ESTER station.

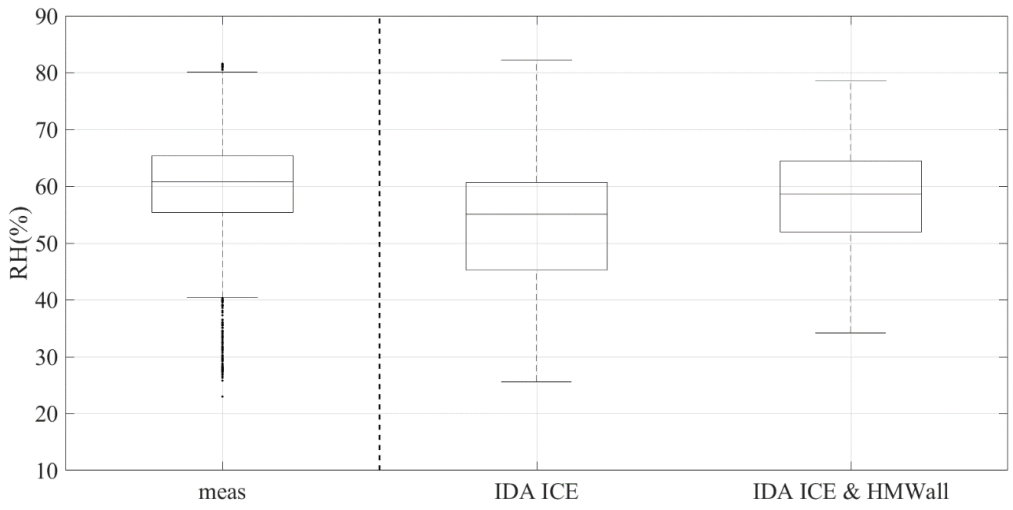

Figure 13 Box-and-whisker plots of relative humidity (RH) measured in the church and modelled by IDA ICE and IDA ICE extended with the HMWall object. The line inside the box is the median value, with the 25th and 75th percentiles as lower and upper sides of the box, respectively. The lowest and the highest value of the data set are plotted as whiskers when they are not outliers, indicated as the circle (i.e., above or below 1.5×IQR, IQR interquartile range).

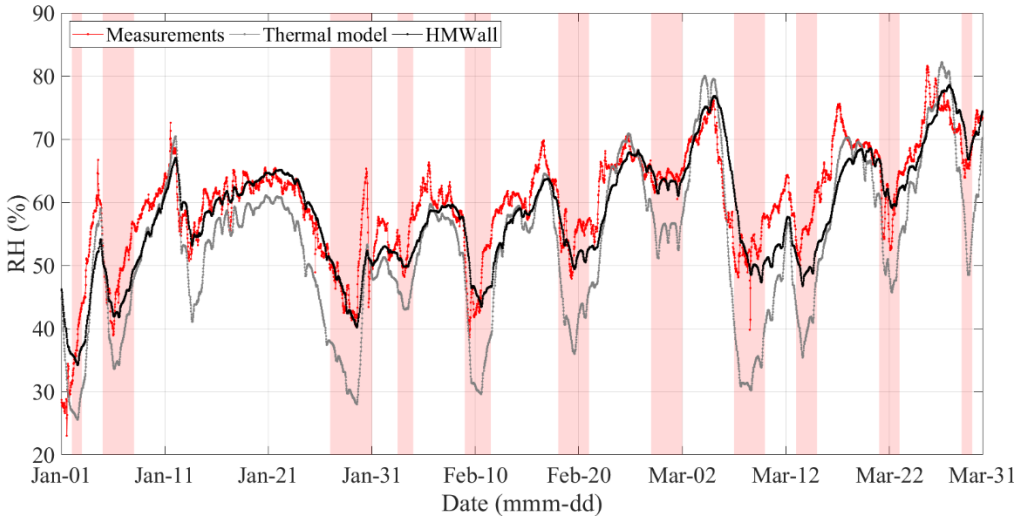

Figure 14 Time evolution of relative humidity (RH) measured (red line) and modelled by IDA ICE (grey line) and IDA ICE extended with HMWall (black line). The occurrences of high ex/infiltrations are depicted as red area.

Conclusion

This study analysed the performance of the HMWall model as an independent object and as a component of a larger system in IDA ICE 4.7.1 using four exercises at increasing complexity of climatic loads and envelope structures. The exercises were performed so that the performance of HMWall was assessed by means of analytical verification, empirical validation and comparative test. This study allowed to point out the advantages and limitations of HMWall so to encourage its application, as an extension of IDA ICE for the hygrothermal analysis, and its further implementation.

In the first exercise, the analytical benchmark described in the European standard EN 15026:2007 was carried out, in which the HMWall model was used as an independent object. It well modelled the temperature uptake within the specimen for the three step changes, since the retrievals were within the permissible error range given by the standard. However, the moisture distribution agreed with the permissible error range only when the specimen experienced a step change of 365 days. This was due to the difference in the calculation of the moisture storage function in the standard and in HMWall, that resulted as a good approximation only when RH ranged between 70 and 95%. This pointed out that an implementation of the code is necessary, since the HMWall does not allow to enter the hygrothermal function as discrete values that can be linearly interpolated. This might be very useful when a more accuracy is demanded and experimental data, especially moisture dependent properties, are measurable and available.

In the second exercise, a comparative test was performed using two simulation tools (IDA ICE extended with HMWall and WUFI Plus) that had in common the governing equations for the one-dimensional heat and moisture transfer through walls. The results perfectly agreed in two of three test cases. In fact, when the indoor relative humidity was higher than the outdoor, IDA ICE extended with HMWall tended to reach the

equilibrium more quickly than WUFI Plus. This difference was probably due to the calculation of the liquid transport coefficients for redistribution, that, in WUFI, is one tenth of the free water saturation when RH = 100%. However, this feature will not be taken into account in further implementation of HMWall code, since the difference in modelled RH values did not overcome the accuracy of RH sensor used monitoring of the indoor climate.

In the third exercise, the Common Exercise 3, developed by the Fraunhofer Institute for Building Physics within the IEA ECBCS Annex 41, was used to test the capability of IDA ICE extended with HMWall to model the moisture buffering effect of different cladding material on the indoor relative humidity. The validation was carried out comparing the modelled relative humidity values with the measurements for an empirical validation and with the values modelled by WUFI Plus and IDA ICE 3.0 extended with the first version of HAMWall for a comparative validation. For the three test cases, HMWall had a better agreement with the measurements in comparison with the HMWallM. However, when the walls were coated by aluminium foils, HMWall did not properly simulate the effect of no sorption on the indoor relative humidity. This means that the HMWall needs for a further implementation which might be specific for materials that behave as vapour barrier. When the walls were coated by gypsum boards, HMWall was able to gather both the overall evolution of measured RH and the RH span occurring during the two-daily peaks of moisture productions. It showed a better agreement with measurements with respect to the other two simulation tools.

In the fourth exercise, an historical building with a wall exposed to a wet rocky front, the Church of Santa Rosalia in Palestrina, was modelled and the indoor climate variables were compared with the measurements performed during a winter monitoring campaign. The exercise pointed out that even though it was not possible to add a moisture source to the HMWall object, the simulation tool was able to detect the moisture uptake from walls setting the wet front as RH = 100% load. Moreover, it emerges that for a comprehensive hygrothermal assessment the IDA ICE should be extended with HMWall since it allows to model the moisture equilibrium in the ambient air as the sum of the moisture buffering and the moisture uptake from the walls (HMWall) together with the moisture exchange due to the infiltration and the moisture capacity of the building (IDA ICE). Since both MAE and RMSE for RH data are less than 5.0%, we assumed that the building model was a very good representation of the church. This exercise represents a typical situation in the hygrothermal assessment of unknown structures, whose materials cannot be sampled for investigating their hygrothermal properties due to their cultural and/or historic worth.

We concluded that the simulation tool IDA ICE + HMWall can be used for hygrothermal assessment and, also, in the case of historical buildings which are characterised by high uncertainty related to hygrothermal properties of materials and other envelope features. The HMWall object is easy to handle with both as independent object and as a component of a larger system. It can well model the one-dimensional heat and moisture transfer for hygroscopic materials, even if it is not possible to enter the hygrothermal curves as discrete values and the liquid conduction coefficient is calculated taking into

account the same moisture storage curve both for suction and redistribution. Finally, when IDA ICE is extended with HMWall does not change the duration of simulation and lasts a few seconds when HMWall is used as independent object.

Acknowledgement

The authors are grateful to Dr. Florian Antretter (Fraunhofer Institute for Building Physics) for the availability in using the software WUFI Plus for executing the benchmark 2 within this research. The authors also thank Dr. Targo Kalamees (Tallinn University of Technology) for the modelled data by means of IDA ICE 3.0 extended with the HAMWall model (version 1999), Dr. Kristin Lengsfeld (Fraunhofer Institute for Building Physics) for simulated data by means of WUFI Plus and Dr. Carsten Rode (Technical University of Denmark) for measurements, with which the analysis within the benchmark 3 were performed. Finally, Dr Francesca Frasca thanks Sapienza Università di Roma for funding her visit at the Fraunhofer Institute for Building Physics in 2017.

Appendix

The formulas of the statistical parameters mentioned in the paper are reported below.

$$PB = \left(\frac{\sum_{i=1}^{N} (y_i - x_i)}{\sum_{i=1}^{N} (x_i)} \right) \cdot 100$$

$$MAE = \frac{\sum_{i=1}^{N} |y_i - x_i|}{N}$$

$$RMSE = \sqrt{\frac{\sum_{i=1}^{N} (y_i - x_i)^2}{N}}$$

$$CV - RMSE = \frac{RMSE}{\langle x \rangle}$$

where y_i is the *i*th modelled data, x_i is the *i*th measured data, N is the number of all the possible data pairs analysed and <x> is the average of measured data.

Appendix E

$$\mathrm{rho} = \frac{\sum_i \left(r_i - \bar{r}\right)\left(s_i - \bar{s}\right)}{\sqrt{\sum_i \left(r_i - \bar{r}\right)^2}\sqrt{\sum_i \left(s_i - \bar{s}\right)^2}}$$

where r_i is the *i*th rank of measured data and r its average, s_i is the *i*th modelled data and s its average.

References

Allinson, D., & Hall, M. (2010). Hygrothermal analysis of a stabilised rammed earth test building in the UK. Energy and Buildings, 42(6), 845-852.

Antretter, F., Schöpfer, T., & Kilian, R. (2011). An approach to assess future climate change effects on indoor climate of a historic stone church. In 9th Nordic Symposium on Building Physics.

Antretter, F., Mitterer, C., & Young, S. M. (2012). Use of moisture-buffering tiles for indoor climate stability under different climatic requirements. HVAC&R Research, 18(1-2), 275-282.

Antretter, F., Kosmann, S., Kilian, R., Holm, A., Ritter, F., & Wehle, B. (2013). Controlled Ventilation of Historic Buildings: Assessment of Impact on the Indoor Environment via Hygrothermal Building Simulation. In Hygrothermal Behavior, Building Pathology and Durability (pp. 93-111). Springer, Berlin, Heidelberg.

Barclay, M., Holcroft, N., & Shea, A. D. (2014). Methods to determine whole building hygrothermal performance of hemp–lime buildings. Building and environment, 80, 204-212.

Bichlmair, S., Raffler, S., & Kilian, R. (2015). The Temperierung heating systems as a retrofitting tool for the preventive conservation of historic museums buildings and exhibits. Energy and Buildings, 95, 80-85.

Delgado, J. M., Barreira, E., Ramos, N. M., & de Freitas, V. P. (2012). Hygrothermal numerical simulation tools applied to building physics. Springer Science & Business Media.

Djedjig R, Ouldboukhitine SE, Belarbi R, Bozonnet E (2012). Development and validation of a coupled heat and mass transfer model for green roofs. International Communication of Heat and Mass Transfer, 39: 752–761.

EN ISO 13788 (2002) Hygrothermal performance of building components and building elements—internal surface temperature to avoid critical surface humidity and interstitial condensation—calculation methods. International Standards Organization, Geneva.

EN 15026 (2007) Hygrothermal performance of building components and building elements – Assessment of moisture transfer by numerical simulation. European Committee for Standardization, Brussels.

Ferroukhi, M. Y., Djedjig, R., Belarbi, R., Limam, K., & Abahri, K. (2015). Effect of coupled heat, air and moisture transfers modeling in the wall on the hygrothermal behavior of buildings. Energy Procedia, 78, 2584-2589.

Ferroukhi, M. Y., Djedjig, R., Limam, K., & Belarbi, R. (2016). Hygrothermal behavior modeling of the hygroscopic envelopes of buildings: A dynamic co-simulation approach. Building Simulation, 9:5, 501-512.

Frasca, F., Cornaro, C., & Siani, A. M. (2018). Performance assessment of a heat and moisture dynamic simulation model in IDA ICE by the comparison with WUFI Plus. IOP Conference Series: Materials Science and Engineering 364:1, 012024.

Gomes, C., Thule, C., Broman, D., Larsen, P. G., & Vangheluwe, H. (2018). Co-Simulation: A Survey. ACM Computing Surveys (CSUR), 51(3), 49.

Glaser, H. (1958). Temperatur und Dampfdruckverlauf in einer homogene Wand bei Feuchteausscheidung. Kältetechnik, 6, 174-181.

Hagentoft, C. E., Kalagasidis, A. S., Adl-Zarrabi, B., Roels, S., Carmeliet, J., Hens, H., and Adan, O. (2004). Assessment method of numerical prediction models for combined heat, air and moisture transfer in building components: benchmarks for one-dimensional cases. Journal of thermal envelope and building science, 27(4), 327-352.

Hall, M. R., Casey, S. P., Loveday, D. L., & Gillott, M. (2013). Analysis of UK domestic building retrofit scenarios based on the E. ON Retrofit Research House using energetic hygrothermics simulation–Energy efficiency, indoor air quality, occupant comfort, and mould growth potential. Building and Environment, 70, 48-59.

Hamid, A. A., & Wallentén, P. (2017). Hygrothermal assessment of internally added thermal insulation on external brick walls in Swedish multifamily buildings. Building and Environment, 123, 351-362.

Hens, H. 1996. Final report Task 1. Modeling Common Exercises. Summary reports. International Energy Agency, Energy Conservation in Buildings and Community Systems, Annex 24 Heat, Air and Moisture Transport in New and Retrofitted Building Envelope Parts (HAMTIE).

Hens, H. (2009). IEA-ECBCS Annex 41 Whole building heat, air and moisture response. In Nordic Building Physics Conference Copenhagen, June 19, 2008 (p. 1).

Holm, A., Künzel, H. M., & Sedlbauer, K. (2003). The hygrothermal behaviour of rooms: combining thermal building simulation and hygrothermal envelope calculation. IBPSA Proceedings Building Simulation Einhoven.

Janssen, H. (2014). Simulation efficiency and accuracy of different moisture transfer potentials. Journal of Building Performance Simulation, 7(5), 379-389.

Judkoff, R., & Neymark, J. (1995). International Energy Agency building energy simulation test (BESTEST) and diagnostic method (No. NREL/TP-472-6231). National Renewable Energy Lab., Golden, CO (US). doi:10.2172/90674.

Karagiozis, A., Desjarlais, A., Künzel, H. M., & Holm, A. (2010). „The evolution of hygrothermal design: WUFI to WUFI Plus. Journal of Building Enclosure Design, 24-9.

Kraus, M. (2017, October). Hygrothermal Analysis of Indoor Environment of Residential Prefabricated Buildings. In IOP Conference Series: Materials Science and Engineering (Vol. 245, No. 4, p. 042071). IOP Publishing.

Künzel, H. M. (1995). Simultaneous heat and moisture transport in building components. One-and two-dimensional calculation using simple parameters. IRB-Verlag Stuttgart.

Künzel H.M., Holm A., Zirkelbach D. and Karagiozis, A. N. (2005). Simulation of indoor temperature and humidity conditions including hygrothermal interactions with the building envelope. Solar Energy, 78(4), 554-561.

Kupczak, A., Sadłowska-Sałęga, A., Krzemień, L., Sobczyk, J., Radoń, J., & Kozłowski, R. (2018). Impact of paper and wooden collections on humidity stability and energy consumption in museums and libraries. Energy and Buildings, 158, 77-85.

Kurnitski, J., & Vuolle, M. (2000, March). Simultaneous calculation of heat, moisture, and air transport in a modular simulation environment. In Proceedings of the Estonian academy of sciences engineering (Vol. 6, No. 1, pp. 25-47).

Leissner, J., Kilian, R., Kotova, L., Jacob, D., Mikolajewicz, U., Broström, T., ... and Antretter, F. (2015). Climate for Culture: assessing the impact of climate change on the future indoor climate in historic buildings using simulations. Heritage Science, 3(1), 38.

Litti, G., Khoshdel, S., Audenaert, A., & Braet, J. (2015). Hygrothermal performance evaluation of traditional brick masonry in historic buildings. Energy and Buildings, 105, 393-411.

Magrini, A., Lazzari, S., & Marenco, L. (2017). Energy retrofitting of buildings and hygrothermal performance of building components: Application of the assessment methodology to a case study of social housing. International Journal of Heat and Technology, 35(S1), S205-13.

Martinez, R. G. (2017). Hygrothermal Assessment of a Prefabricated Timber-frame Construction Based in Hemp. Procedia environmental sciences, 38, 729-736.

Napp, M., & Kalamees, T. (2015). Energy use and indoor climate of conservation heating, dehumidification and adaptive ventilation for the climate control of a mediaeval church in a cold climate. Energy and Buildings, 108, 61-71.

Napp, M., Kalamees, T., Tark, T., & Arumägi, E. (2016a). Integrated Design of Museum's Indoor Climate in Medieval Episcopal Castle of Haapsalu. Energy Procedia, 96, 592-600.

Napp, M., Wessberg, M., Kalamees, T., & Broström, T. (2016b). Adaptive ventilation for climate control in a medieval church in cold climate. International Journal of Ventilation, 15(1), 1-14.

Nicolai, A., Zhang, J., & Grunewald, J. (2007). Coupling strategies for combined simulation using multizone and building envelope models. In Proc. of Building Simulation.

O'Leary, T. P., Menzies, G., & Duffy, A. (2015). The Design of a Modelling, Monitoring and Validation Method for a Solid Wall Structure. Energy procedia, 78, 243-248.

Parish OO and Putnam TW 1977 Equations for the determination of humidity from dewpoint and psychrometric data. Nasa Technical Note, NASA TN D-8401 1–24.

Pasztory, Z., Peralta, P. N., Molnar, S., & Peszlen, I. (2012). Modeling the hygrothermal performance of selected North American and comparable European wood-frame house walls. Energy and Buildings, 49, 142-147.

Ramos, N. M., Delgado, J. Q., Barreira, E., & De Freitas, V. P. (2009). Hygrothermal properties applied in numerical simulation: Interstitial condensation analysis. Journal of Building Appraisal, 5(2), 161-170.

Rode, C., & Woloszyn, M. (2007). Whole-building hygrothermal modeling in IEA Annex 41. In Thermal Performance of the Exterior Envelopes of Whole Buildings: Buildings X (pp. 1-15). American Society of Heating, Refrigerating and Air-Conditioning Engineers.

Slanina, P., & Šilarová, Š. (2009). Moisture transport through perforated vapour retarders. Building and Environment, 44(8), 1617-1626.

Spitz C, Woloszyn M, Buhe C, Labat M (2013). Simulating combined heat and moisture transfer with EnergyPlus: An uncertainty study and comparison with experimental data. In: Proceedings of International IBPSA Building Simulation Conference, Chambery, France.

Steeman M, Janssens A, Steeman HJ, Van Belleghem M, De Paepe M (2010). On coupling 1D non-isothermal heat and mass transfer in porous materials with a multizone building energy simulation model. Building and. Environment, 45: 865–877.

Tariku F, Kumaran K, Fazio P (2010). Integrated analysis of whole building heat, air and moisture transfer. International Journal of Heat and Mass Transfer, 53: 3111–3120.

Skinner L.M., and Sambles J.R. (1972). The Kelvin equation - a review. Journal of Aerosol Science, 3(3), 199-210.

Straube, J. and Burnett E.F.P. (1991). Overview of hygrothermal (HAM) analysis methods, HR Trechsel, editor. ASTM manual 40-moisture analysis and condensation control in building envelopes.

Woloszyn, M. and Rode, C. (2008, March). Tools for performance simulation of heat, air and moisture conditions of whole buildings. In Building Simulation (Vol. 1, No. 1, pp. 5-24). Springer-Verlag.

Appendix F

On-site measurements and whole-building thermal dynamic simulation of a semi-confined prefabricated building for heritage conservation

Frasca F., Siani A.M. and Cornaro C.

In BSA 2017–Building Simulation Applications 3rd IBPSA-Italy Conference, 8.2. 2017–10.2. 2017. BU, press. Proceedings book ISBN 9788860461360 pp 185.-192. (2017).

On-site measurements and whole-building thermal dynamic simulation of a semi-confined prefabricated building for heritage conservation

Francesca Frasca – Sapienza Università di Roma, Department of Earth Sciences, P.le A. Moro 2, 00185 Rome, Italy – f.frasca@uniroma1.it
Anna Maria Siani – Sapienza Università di Roma, Department of Physics, P.le A. Moro 2, 00185 Rome, Italy – annamaria.siani@uniroma1.it
Cristina Cornaro – Università degli Studi di Roma "Tor Vergata", Department of Enterprise Engineering, Via del Politecnico 1, 00133 Rome, Italy – cornaro@uniroma2.it

Abstract

In this study the capability of BDFWall model (IDA Indoor Climate and Energy software) is assessed in a semi-confined site for conservation of works of art. The case under study is the paleontological deposit of "La Polledrara di Cecanibbio" (Rome, Italy), where many valuable faunal remains from Middle Pleistocene are preserved. Thermo-hygrometric data collected over the period 2009 – 2013 allowed thoroughly investigating the environmental conditions of the site. The calibration of the simulation building model was performed in two phases. First, a sensitivity analysis was conducted to identify which input parameters significantly affect the discrepancy, if any, between measured and modelled hourly indoor temperature (T) data (from September to December 2013). Second, the calibration of the model was carried out taking into account the most effective parameters. The dual approach, given by both experimental and simulation data, can support preventive measures about risk analysis for artworks in the case of retrofit solutions of a building used for the conservation purpose.

1. Introduction

Recently, the whole-building dynamic simulation has become a useful tool in preventive climate control actions in buildings which preserve cultural artefacts. However, the existing software has been developed to model the indoor climate of modern buildings having regular geometries and for which the thermo-physical properties of building materials are well known.

In historical and archaeological buildings, the libraries of the simulation codes do not include materials of these structures and, in the case of semi-confined sites, strongly affected by the external and/or boundaries forcing, the performance of these codes has not been thoroughly investigated.

The possibility to know in advance the effect of a retrofit in buildings with conservation purposes is fundamental in order to assess the optimal solutions taking into account both conservation needs and people thermal comfort requirements.

This paper describes how the performance of dynamic simulation software, IDA Indoor Climate and Energy, applied to a semi-confined site such as the paleontological deposit of "La Polledrara di Cecanibbio" at Rome (Italy) has been used.

The aim is to investigate the thermal behaviour of the case under study using both on-site measurements and simulated values. This allows better understanding the interaction object/environment and building/environment. This study pays particular attention to the calibration of the whole-building dynamic model using only the features of the building envelope, since variations of geometry and thermo-physical properties of building components and boundaries do not affect the model in the same way.

2. The case study

"La Polledrara di Cecanibbio" (Lat. 41.9°, Long. 12.3°)

is a paleontological deposit located about 15 km NW of Rome (Italy) in a rural area. Several valuable faunal remains from Middle Pleistocene are preserved, such as large mammals (*Palaeoloxodon antiquus* and *Bos primigenius*). The largest faunal remains are held by cineritic tuffite fluvial sediments (Fig. 1). The faunal remains placed in the north side of the site suffer from biological degradation because they are directly exposed to soil hygrometric conditions.

Fig. 1 – La Polledrara di Cecanibbio, Rome (Italy).

The deposit was discovered in 1984 within a survey supported by "Soprintendenza Speciale per i Beni Archeologici di Roma" (SSBAR) and was kept unearthed in the following years. In 2000, a prefabricated building was built with the main purpose to preserve fossils from meteorological events and to make it a public museum.

The building covers an excavated area of 900 m² (30x30 m per side) and is placed directly on the soil. The maximum height of the building is 8 m (east side), while the minimum is 6.5 m (west side).

The windows (i.e. double-pane clear glazing with aluminium frame without thermal-break) are along the north and south walls covering an area of about 1900 m² with a solar factor of 0.79 and heat transmittance (U-value) of 5.80 W/(m² K). There are internal white PVC roller blinds which usually are never opened.

The external walls are double skin panels insulated by polyurethane with a nominal thickness of 6 cm and a U-value=0.60 W/(m² K).

The roof is a trapezoidal sheet for concrete slabs with a nominal thickness of 12 cm, a slope of 30 cm and a U-value=1.09 W/(m²K).

3. Measurement and simulation

On-site monitoring campaign and whole-building dynamic simulation software were used with the double purpose to investigate the thermal behaviour of La Polledrara di Cecanibbio and to optimize a semi-automatic calibration of the simulation model in the case of a semi-confined site.

3.1 On-site monitoring campaign

Sensors for measurements of indoor temperature (T), relative humidity (RH) and cracks (FO) parameters were installed in June 2008. The analysis was carried out taking into account data from January 2009 till December 2013. The outdoor T and RH sensors were installed in June 2013 in the south corner of the building accurately shaded from direct solar radiation and protected from meteorological events. T sensor is a platinum resistance thermometer Pt100 1/3 DIN (accuracy = 0.3°C), whereas RH sensor is a film capacitor "Rotronic" C94 (accuracy = 1.5%). The metrological features of T and RH sensors are in accordance with the European Standards EN 15758:2010 and EN 16242:2012, respectively.

FO sensor is a capacitor (accuracy = 0.25%) and is installed on a crack of a cinerite that holds a fang of a *Palaeloxodon antiquus*.

All the sensors were connected to a datalogger CR 1000 distributed by Tecno.el S.r.l. (Italy), with an acquisition and recording time set to 30 minutes.

The monitoring campaign is still in operation.

3.2 Analysis of microclimatic data series

Before performing the exploratory data analysis (EDA), the quality of the T-RH data series was assessed using the Continuity Index (CI) and the Completeness Index (CoI) (Frasca et al., 2016). Both indexes range between 0 (poor quality) and unity (high quality, i.e. no missing values).

Assuming any distribution of the data, the Spearman's rank correlation coefficient (ϱ) was computed to assess whether there was a monotonic

relationship between the T-RH parameters and the cracks, so that an empirical relationship among parameters could be defined. This relationship will be useful, in combination with simulation results, to support preventive measures about risk analysis for artworks in the case of retrofit solutions of a building used for conservation purposes.

3.3 Simulation environment

3.3.1 IDA ICE setting

Dynamic building simulation for indoor climate analysis was performed using the software tool IDA Indoor Climate and Energy (IDA ICE) 4.7.1 developed and distributed by EQUA simulation AB. The BDFWall model (finite differences model of a multilayer component) was used to carry out the simulation of the thermal behaviour of the building.

The geometry of the building model of La Polledrara di Cecanibbio was created starting from the architectural survey provided by the SSBAR and using the thermo-physical properties reported in UNI 10351:2015 for opaque components and in EN 673:2011 and EN 410:2011 for glass components. The first guess building model was assumed as an unconditioned large area, only affected by external climate and directly placed on soil.

The soil layer was modelled according to model ICE 3, which computes the soil temperature as the mean of T of the selected climate file without 2D or 3D modelled effects.

The air infiltrations were modelled according to wind driven flow and considering air tightness at 0.5 ACH (Air Change per Hour) at pressure difference of 50 Pa.

Lightning, equipment and people were not included, since the site has a limited number of visitors in the selected period.

A climate file was built to run the model for calibration using outdoor T and RH measured at La Polledrara. Wind direction and speed intensity, direct and diffuse (sky) radiation on a horizontal surface, measured at ESTER station (Energia Solare TEst e Ricerca), belonging to the Università degli Studi di Roma "Tor Vergata" (Lat. 41.9°, Long. 12.6°), were also included in the climate file.

3.3.2 Method

In this study, MatLab 2014a was used to set the configuration parameters of the building model to carry out the Sensitivity Analysis (SA) and the calibration of the simulation model, based only on the parameters which describe the building envelope.

First, the SA was carried out for identifying the most effective parameters of the model. Then, the calibration based on these selected parameters was performed to minimize the difference between modelled and measured data. The aim was to identify the most proper settings of thermal-physical properties of building components and boundaries.

After that, the model was validated in a different period (January 2016) given the availability of measured indoor and outdoor temperature data.

3.3.3 Sensitivity analysis

In this study, the Elementary Effects method (EEs) was applied using modelled hourly indoor T from September till December 2013 and based on the Morris random sampling method of the set of parameters (Morris 1991) which defined the building model. The experimental plan is built taking into account the number of EEs (r) for each parameter and the number of levels (p) in which parameters range. In this study, we computed r=10 for each parameter using only p=4 discretized levels in the experimental plan. We selected 24 parameters (k) for screening and defined ranges according to a fixed uncertainty at ±10% from initial value, as listed in Table 1.

In this way, the resulting computational effort was 250 runs (N) which corresponds to:

$$N = r*(k+1) \quad (1)$$

The input set parameter matrix given by Morris sampling is *N-by-k*. The N-models were run in batch mode in IDA ICE. The error between simulated T and T from the first guess model was expressed in term of the mean absolute error (MAE), that was used as a target function for the calculation of the EEs.

The EEs ascribed to each parameter are defined as the difference in the output between two following simulations divided by the variation of the input parameter (Saltelli et al., 2004). The EEs were

Appendix F

computed according to eq. 2:

$$EEs(x) = \frac{y(x_1, x_2, \ldots, x_i + \Delta x_i, \ldots, x_k) - y(x)}{\Delta x} \quad (2)$$

where x is the set of parameters, y is the target function and Δx is the variation of the input parameter.

Finally, the mean (μ^*) of the absolute values of the EEs associated with each parameter, the standard deviation (σ) and the ratio σ/μ^* were calculated. μ^* provides a measure of the parameter relevance (Campolongo et al., 2011), in the rank order. The ratio σ/μ^* is an indicator of linearity of each parameter effect ($\sigma/\mu^*<0.1$) with respect to other parameters and to whole modelled building (Garcia Sanchez et al., 2014). In EEs scatter plot (σ *vs* μ^*) four areas delimited by $\sigma/\mu^*<0.1$, $0.1\leq\sigma/\mu^*<0.5$, $0.5\leq\sigma/\mu^*<1$ and $\sigma/\mu^*\geq1$, allows highlighting if outcomes from SA are physically consistent.

3.3.4 Calibration

The simulation model was calibrated using hourly indoor T measurements from September till December 2013. The model was initialized at a

Table 1 Modelling parameter values used in the first guess model (initial value) and parameter ranges value used in Morris sampling for SA.

Component	Parameter	Initial Value	Range for SA
External Wall - Steel	λ [W/(m K)]	52	47-57
	s [m]	0.001	0.001-0.005
	d [kg/m³]	7800	7000-8600
	c [J/(kg K)]	550	490-600
External Wall - Polyurethane	λ [W/(m K)]	0.034	0.029-0.040
	s [m]	0.15	0.13-0.17
	d [kg/m³]	25	22-28
	c [J/(kg K)]	1.464	1.320-1.610
Roof - Concrete	λ [W/(m K)]	0.21	0.18-0.25
	s [m]	0.15	0.14-0.17
	d [kg/m³]	700	630-770
	c [J/(kg K)]	1050	1000-1150
Soil	λ [W/(m K)]	1.5	1.3-1.7
	s [m]	1	0.9-1.1
	d [kg/m³]	1200	1080-1320
	c [J/(kg K)]	840	765-925
Window	U [W/(m² K)]	3.052	2.950-3.500
Thermal Bridges	ExtW-Slab [W/(m K)]	0.05	0.04-0.06
	ExtW-IntW [W/(m K)]	0.03	0.02-0.04
	ExtW- ExtW [W/(m K)]	0.08	0.07-0.09
	WinPerim [W/(m K)]	0.03	0.02-0.04
	DoorPerim [W/(m K)]	0.03	0.02-0.04
	Roof [W/(m K)]	0.09	0.08-0.10
	Slab [W/(m K)]	0.14	0.13-0.15

Note: λ=thermal conductance; s=thickness; d=density; c=specific heat; U=heat transmittance; ExtW-Slab=external wall-internal slab; ExtW-IntW=external wall-internal wall; ExtW-ExtW= external wall-external wall; WinPerim = external window perimeter; DoorPerim = external door perimeter; Roof=roof-external wall; Slab=external slab-external wall.

start-up period from August 18th 2013 till August 31st 2013.

The calibration was carried out taking into account only the most effective parameters with the aim to minimize the root-mean-square-difference (RMSD) and the CV-RMSD (Coefficient of Variation of the RMSD) between modelled and measured indoor T. They were used to assess the goodness of the modifications to calibrate the building model (Cornaro et al., 2016). The most effective parameters were ranged within the interval reported in Table 1, using a major number of levels with respect to the Morris sampling.

The modelled and measured indoor T were compared using Taylor Diagram (Taylor K.E. 2001). It summarizes the agreement between observed data (a) and modelled data (b) using three statistical quantities: standard deviation (SD), correlation coefficient (R) and the centred RMSD (E′), whose relation is given by the following equation:

$$E' = \sqrt{SD_a^2 + SD_b^2 - 2\cos(SD_a SD_b R)} \quad (3)$$

4. Results and discussion

4.1 Microclimate analysis

Both the T and RH data series are of high quality (CI=1.00 and CoI=0.96) and hence suitable for exploratory data analysis.

Fig. 2 shows the box-and-whiskers plots of RH data. Several outliers (indicated as circles in the figure) are observed in winter, spring and fall. A detailed study of RH outliers has shown that they occurred mainly in the hourly intervals between 13:00 UTC and 20:00 UTC, i.e. after the maximum solar exposure of the building.

Box plots for T (figure not shown), do not show any anomalous values and there is no significant difference among seasons over the selected period. The mean yearly value is 17.7°C ranging between 12.4°C (25th percentile) and 23.1°C (75th percentile).

In summer, it was found that the indoor environmental conditions resulted too warm and too humid, while, in winter, they were too cold and humid especially in morning. These conditions provoked thermal discomfort, as communicated by staff and visitors, and might have favoured the biological degradation in north side of building.

The behaviour of T and RH daily span (difference between the maximum and minimum values) allows studying their short-term variability. A similar behaviour among season (except in summer) was observed: ΔT_{daily}=1-7°C and ΔRH_{daily}=3-40%. In summer, the daily span of T and RH range as follows: ΔT_{daily}=5-6°C and ΔRH_{daily}=20-40%, showing that the period is mostly characterized by large fluctuations.

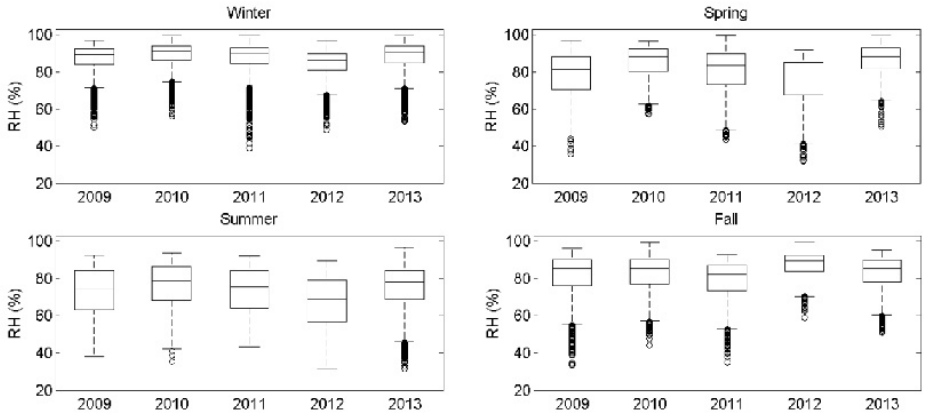

Fig. 2 Box-and-whiskers plots of indoor relative humidity (RH) for each seasons over the period 2009-2013. The line inside the box is the median value, with the 25th and 75th percentiles as lower and upper sides of the box, respectively. The lowest and the highest value of the data set are plotted as whiskers when they are not outliers, indicated as the circle (i.e. above or below 1.5*IQR, IQR interquartile range).

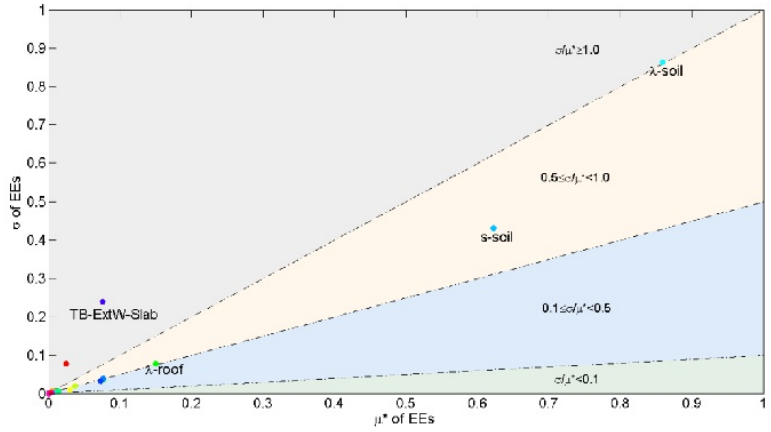

Fig. 3 Scatter plot (σ *vs* μ^*) of Elementary Effects method for 250 runs taking into account 24 input parameters (indicated as colored dots) of building envelope. Four areas delimited by the ratio σ/μ^* indicate the effect of parameter on model: light green (σ/μ^*<0.1, linear effect), light blue (0.1≤σ/μ^*<0.5, monotonic effect), pink (0.5≤σ/μ^*<1, almost monotonic effect) and grey (σ/μ^*≥1, non-linear and/or non-monotonic effect).

Finally, T-RH parameters affect the evolution cracks measured on cinerite which holds a fang: the correlation with T is ϱ=0.62 whereas with UR is ϱ=-0.68.

An empirical relationship was found:

$$FO = b_1 * RH^{b2} * T^{b3} \quad (4)$$

where b_1 = 6.76, b_2 = -0.09 and b_3 = 0.01. Modelled FO data deviate from measured FO of at most 5%.

4.2 Simulation

Fig. 3 shows the results of EEs computed taking into account 24 parameters (see Table 1). The most effective parameters corresponding with high values of μ^* and σ are: the thermal conductance (λ_s) and thickness (s_s) of soil, the thermal conductance of roof (λ_r) and the thermal bridge related to external walls and slab ($TD_{ExtW\text{-}Slab}$).

The scatter plot shows that the effects of λ_s and $TD_{ExtW\text{-}Slab}$ are non-linear and/or non-monotonic (indicated as grey area in figure ($\sigma/\mu^*\geq1$)), while the effects of λ_r and s_s are almost monotonic (indicated as pink area in figure ($0.5\leq\sigma/\mu^*<1$)).

The significant influence of the soil on indoor T is due to its low resistance at the heat transfer. This is controlled by several factors such as the porosity and the soil temperature. Further studies will be carried out taking into account the actual temperature of the soil.

The other parameters form a cluster with low μ^* and σ, which means that they have a limited influence on the model and could be neglected in the model calibration.

Fig. 4 shows the Taylor Diagram for the comparison among modelled hourly indoor T (indicated as coloured dots) and measured hourly indoor T (indicated as A) running several simulations varying the first two effective parameters as described above (subsection 3.3.4).

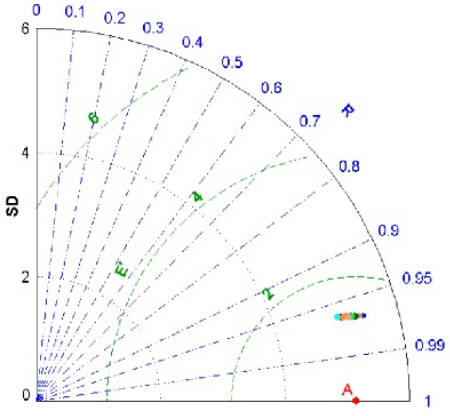

Fig. 4 Taylor Diagram displaying a statistical comparison among observations (A) and 15 run models (clustered coloured dots). Black dotted circles are standard deviation (SD), green dashed circles are the centred root-mean-square-difference (E') and, finally, blue dash-dotted lines are the correlation coefficient (R).

Modelled indoor T data are strongly clustered showing that, even though λ_s and s_s result the most

effective parameters, their variation does not play a key role in minimizing the error among modelled and measured T. Data series are highly correlated (R>0.95), the E′ ranges within 1.32°C and 1.39°C and the SD is between 5.0°C and 5.5°C.

In Table 2, the RMSD and the CV-RMSD of the indoor T over the calibration period for the first guess model and the calibrated model are reported with respect to the observations. The RMSD and the CV-RMSD of the calibrated model are quite lower than in the first guess model. Even though the most effective parameters were identified, the calibration procedure did not improve the capability of the model to well simulate the building. This would confirm that an accurate monitoring of the soil temperature should be performed and included in the analysis.

Table 2 The RMSD and the CV-RMSD for the first guess model and the calibrated model are reported.

	First Guess Model	Calibrated Model
RMSD	1.38°C	1.32°C
CV-RMSD	8.0%	7.8%

Fig. 5 shows the temporal behaviour of bias (%) calculated between measured and calibrated modelled indoor T. The mean bias is 0.6% (indicated as dashed blue line), while the 7th and 93rd percentile are -9.0% and 14.5%, respectively (indicated as dashed red lines). The calibrated modelled T usually overcomes the measured T, mainly from the end of November, when a sudden drop of outdoor T occurred.

The RMSD and the CV-RMSD of the indoor air T over the validation period (January 2016) are 1.92°C and 20.0%, respectively. In general, the modelled T overestimates the measured T.

The increase in RMSD and CV-RMSD can be due to a different behaviour in heat transfer of the soil during the meteorological events. Over the validation period, the amount of precipitation was about 18 mm/day, while in the calibration period heavy rainfall (about 230 mm/day), although sporadic, occurred.

5. Conclusion

The temporal behaviour of indoor thermo-hygrometric parameters seems to be related to the solar exposure of the building and its capability to transfer the heat thorough external walls (i.e. thin double skin insulated panels). This has favoured an indoor environment not suitable for the conservation purpose of faunal remains. The empirical relationship between cracks and T-RH (eq. 4) will be used for preventive measures after an accurate calibration of the building dynamic simulation model.

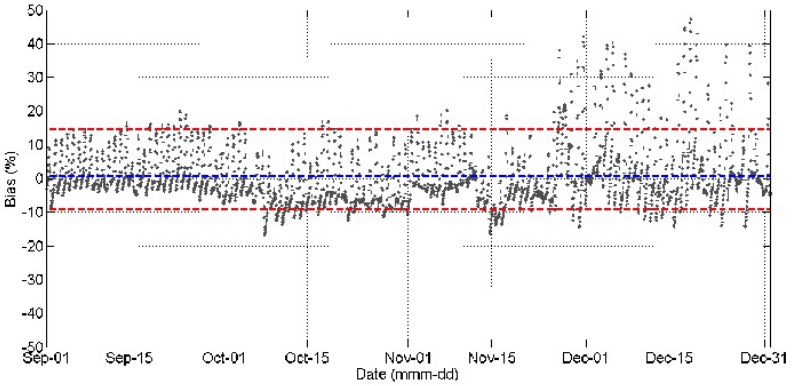

Fig. 5 Time plot of bias (%) computed between measured indoor T and calibrated modelled indoor T data from September till December 2013. Blue line is the mean of bias (0.6%), while red lines are 7th (-9.0%) and 93rd (14.5%) percentile of bias respectively.

The Elementary Effects (EEs) method allowed identifying the most effective parameters, then used in the calibration. In this case study, the most effective parameters are the thermal conductance and the thickness of the soil. Nevertheless, the use of these parameters do not allow minimizing the error between calibrated modelled and measured indoor temperature, suggesting that other parameters such as air infiltration rate should be taken into account.

Further studies will be conducted considering measured soil temperature and humidity and using the HAMWall model implemented into IDA ICE environment. The HAMWall allows simultaneously simulating the transfer of heat, air mass and moisture. In this way, it will be possible to find the most adequate thermo-hygrometric conditions to consider in the building retrofit for the conservation of faunal remains.

6. Acknowledgement

The authors wish to acknowledge Arch. Carmelo La Micela for plant and section of *La Polledrara di Cecanibbio* and Tecno.El S.r.l. for microclimate data.

The authors thank all the anonymous reviewers for their precious suggestions to improve the contribution.

References

Campolongo F., A. Saltelli and J. Cariboni. 2011. From screening to quantitative sensitivity analysis. A unified approach. *Computer Physics Communications* 182(4):978-988.

Cornaro C., V.A. Puggioni and R.M Strollo. 2016. Dynamic simulation and on-site measurements for energy retrofit of complex historic buildings: Villa Mondragone case study. *Journal of Building Engineering* 6:17-28.

EN 410:2011. Glass in building - Determination of luminous and solar characteristics of glazing. European Committee for Standardization, Brussels.

EN 673:2011. Glass in building - Determination of thermal transmittance (U value) - Calculation method. European Committee for Standardization, Brussels.

EN 15758:2010. Conservation of cultural property—procedures and instruments for measuring temperatures of the air and the surfaces of objects. European Committee for Standardization, Brussels.

EN 16242:2012. Conservation of cultural property—procedures and instruments for measuring humidity in the air and moisture exchanges between air and cultural property. European Committee for Standardization, Brussels.

Frasca F., A.M. Siani, G.R. Casale, M. Pedone, Ł. Bratasz, M. Strojecki and A. Mleczkowska. 2016. Assessment of indoor climate of Mogiła Abbey in Kraków (Poland) and the application of the analogues method to predict microclimate indoor conditions. *Environmental Science and Pollution Research*, 1-13. doi:10.1007/s11356-016-6504-9.

Garcia Sanchez, D., B. Lacarrière, M. Musy, and B. Bourges. 2014. Application of sensitivity analysis in building energy simulations: Combining first-and second-order elementary effects methods. *Energy and Buildings* 68:741-750.

Hani, A., and T. A. Koiv. 2012. Optimization of office building façades in a warm summer continental climate. *Smart Grid and Renewable Energy* 3(3):222-230.

Morris, M. D. 1991. Factorial sampling plans for preliminary computational experiments. *Technometrics* 33(2):161-174.

Saltelli A., S. Tarantola, F. Campolongo and M. Ratto. 2004. *Sensitivity analysis in practice: a guide to assessing scientific models*. John Wiley & Sons.

Taylor K.E. 2001. Summarizing multiple aspects of model performance in a single diagram. *Journal of Geophysical Research: Atmospheres* 106(D7):7183-7192.

UNI 10351:2015. Materiali e prodotti per edilizia - Proprietà termo-igrometriche - Procedura per la scelta dei valori di progetto. Ente nazionale italiano di unificazione.

Appendix G

A method based on environmental monitoring and building dynamic simulation to assess indoor climate control strategies in the preventive conservation within historical buildings

Frasca F., Cornaro C. and Siani A.M.

Submitted in:

Science and Technology for the Built Environment (STBE) "IBPC Topical Issue". (2019)

Appendix G

A method based on environmental monitoring and building dynamic simulation to assess indoor climate control strategies in the preventive conservation within historical buildings

F. Frasca[1], C. Cornaro[2] and A.M. Siani[3]

[1] Department of Earth Sciences, Sapienza Università di Roma, P.le Aldo Moro 5, 00185, Rome, Italy
[2] Department of Enterprise Engineering, University of Rome, Tor Vergata, Via del Politecnico, 1, 00133 Rome, Italy
[3] Department of Physics, Sapienza Università di Roma, P.le Aldo Moro 5, 00185, Rome, Italy

Abstract

This paper proposes a multidisciplinary method to assess a strategy for a better conservation and thermal comfort of visitors in historical buildings. The method combines microclimate observations along with the dynamic simulation of the building and an empirical evaluation of the degradation of hygrosocopic artifacts. It was applied to a historic building in Priverno (Italy) where cracks along the tangential direction in valuable wooden ceilings have been observed. The method has allowed to identify a strategy of temperature control that, if applied, would reduce the total spread of cracks from 0.25 mm to 0.10 mm.

Introduction

The refurbishment of existing buildings to reach the decarbonisation of the construction sector is one of the most crucial issues that Europe and the world are now facing.

In this framework, the Italian situation shows a peculiarity. It was estimated that about 30% of public building stock was built before 1945, i.e. they are historical buildings, and that a 2% of these belongs to the cultural heritage i.e. they are historic buildings (Mazzarella 2015). In addition, the Italian Legislative Decree No 192 of 19 August 2005 (D. Lgs. 192/2005) establishes that historic buildings should not be retrofitted in order to accomplish the priority of conservation requirements. For this reason, researches were focused on the use of simulation as an effective tool to know in advance the impact of the refurbishment on the esthetical and architectural features of such buildings. Thus, several approaches were proposed with the aim to balance architectural conservation and energy efficiency (to cite but the few: Cornaro et al., 2016; Roberti et al., 2017; Tronchin and Fabbri 2017).

Generally, the whole building dynamic simulation has been mainly used for the energy performance evaluation in the refurbishment of existing buildings. However, it can be exploited as a diagnostic tool to achieve a comprehensive assessment of the current indoor climate (Janssen and Christensen 2013). Another potential use is related to the assessment of the impact of climate changes on the indoor climate. This is important since any change in the heat and moisture exchange between indoor and outdoor has a direct influence not only on the energy performance of the building but also on the

conservation of artworks (Cassar and Pender 2003). Indeed, indoor climate and its fluctuations, directly and indirectly, activate and control the ageing of an artefact and the alteration of its chemical-physical properties (Camuffo 2014). Some recent publications demonstrated the potentiality of the dynamic simulation as a tool for conservation risk assessment (e.g. Kompatscher et al., 2017; Schito et al., 2018;).

This issue was the main topic of the European project *Climate for Culture* (CfC – 2009-2014) funded within the 7th Framework Programme (EU FP7). The project was based on a multidisciplinary research team with the aim to identify the damage potential of the cultural heritage at risk and to encourage the development of strategies to mitigate the effects of climate change (Leissner et al., 2015). However, the prediction capability of such a method is particularly complex, since it should consider at least the uncertainty related to (1) the future outdoor climate, (2) the building model and (3) the damage functions (Leijonhufvud et al., 2012). The efficacy of the dynamic simulation strongly depends on the accuracy of the building model, that should be able to detect short- and long-term fluctuations of the indoor climate variables, especially the relative humidity (Bilchmair et al., 2012; Antretter et al., 2013; Kupczak et al., 2018). This variable is particularly complex to simulate, since many factors, such as infiltrations and moisture exchanges with hygroscopic materials, should be simultaneously considered. Most of simulation codes were developed to model moisture exchanges between indoor and outdoor environments setting a specific moisture storage capacity to the interior of the building (Holm et al., 2003) and not to model the moisture flow between the air and porous surfaces (Rode and Woloszyn 2007). For this reason, in the last 30 years, some dynamic simulation tools were developed to model moisture exchanges also through porous materials (Delgado et al., 2012), allowing to study issues related to uncontrolled condensation typical of old masonries (O'Leary et al., 2015). Furthermore, in the case of old buildings, the complexity in geometry and the heterogeneity in materials make extremely complicated and time consuming the model building setting (Coakley et al., 2014; Coelho et al., 2018). Yet, the calibration of the building model is also of relevant importance and it requires a particular attention. However, most of the calibration procedures is based on matching of energy data (Ascione et al., 2011) or indoor air/surface temperature at hourly scale (Pernetti et al., 2013; Roberti et al., 2015) rather than the relative humidity data (Napp and Kalamees 2015). The calibration of relative humidity plays, indeed, a key role in the historic building modelling and in the risk degradation assessment.

To our knolwdge few investigations are available regarding the risk assessment of cultural heritage involving environmental monitoring and building dynamic simulation, especially with regard to the relative humidity modelling. In particular, only few simulation tools provide the combined transport of heat and moisture through the building walls. Moreover, as far as the authors know, the use of degradation response functions, which input variables are provided by building dynamic simulation to predict the degradation behaviour, is still not thoroughly explored. On the contrary, this approach can be of relevance for the conservators, since it allows to test various strategies of climate management evaluating those most suitable for the specific case.

Appendix G

This paper proposes a methodological approach which uses indoor microclimate measurements along with simulations for a complete characterization of the indoor climate conditions. The method also includes an analytical relationship of mechanical degradation response function of an artifact with the objective to test a new strategy for the climate and/or occupancy control and retrofitting interventions, taking into account comfort conditions of the occupants and reducing to a minimum the artefact degradation risk. The vapour migration across the building walls has been investigated through one simulation tool, i.e. IDA Indoor Climate and Energy (IDA ICE), provided with a custom module accurately evaluated and tested, i.e. the HMWall model.

Materials and methods

The case study

The "Museo Archeologico di Priverno" (hereafter called Museum) is housed in the Palazzo Valeriani-Guarini-Antonelli (Figure 1a), in the central Italy at about 70 km SE far away from Rome (Lat. 41.5° and Long. 13.2°). It is a three-storey building, built between 13th and 16th century and restored in 1924-1926. During this restoration, the wooden ceilings at the second floor were finely decorated by Pietro Campeggi with oil paintings characterised by typical geometric patterns of the *Viennese* school. In 2012, the building was restored in order to house the museum.

The palace is oriented in the SW-NE direction with respect to the main entrance and has an internal courtyard and a terrace in the north-west side. The west-side of the palace is contiguous with another historical building, whereas the east-side overlooks a narrow street.

The thirteen rooms of the museum are deployed between the first (from room 1 to room 7) and the second floor (from room 8 to room 13) following a historical theme, from the Bronze Age to the Roman Age of the ancient Priverno. The collection mainly consists of sculptures, architectural elements, ceramics, inscriptions, etc (Figure 1a). In room 9 at the second floor, there is the most important piece of the museum - the *Nilotic sill* or *Soglia Nilotica* - that is often loaned for temporary exhibition around the world. All rooms are adjoining and, except for the west-side ones, have one or more wooden-framed windows shaded by wooden shutters and/or black-roller blinds.

A HVAC system connected to fan coils for the temperature control is turned on during the opening hours by staff both in cold season (from November to mid April) and in warm season (from June to August). All fan coils are installed under the windows and some devices are covered by black drilled-metallic panels. The temperature set-point of the system is set to 18°C and 26°C during the cold and warm seasons, respectively. Nevertheless the rigid temperatures in winter and the warm temperatures in summer affect the indoor climate which becomes unpleasant to visitors.

The conservation staff carries out periodical surveys to check the conservation state of the collections and of the wooden ceilings at the second floor. The wooden ceilings were

restored in 2012, after that painted-layer detachments, panels' deformations and cracks along the tangential section of wood (Figure 1b) occurred. After the restoration, no further damages was observed at the surface layer of the ceiling by the restorer.

Figure 15 a) The "Museo Archeologico di Priverno": outside (left panel) and inside (right panel). b) Details of the wooden ceilings decorated with oil paintings by Pietro Campeggi at the second floor. Cracks are visible along the tangential sections of wood.

Methodology

A flow chart of the methodology proposed in this study is shown in Figure 2 for a better description on how the different tasks are interrelated.

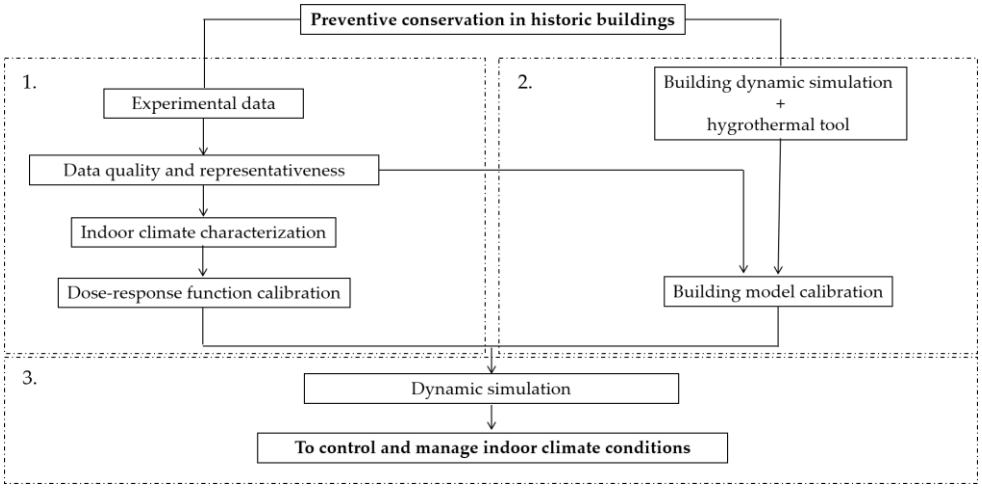

Figure 16 **Schematic workflow methodology. Dashed boxes correspond to the main three steps of the procedure.**

The first step of the methodology consists in collecting experimental data of the main indoor climate parameters, i.e. temperature (T) and relative humidity (RH) in the room under study, the surface temperature (Ts) and the crack-width (C) close to objects if needed to monitor the mechanical degradation (i.e. swelling and shrinkage) of hygroscopic materials (in this case study close to the wooden ceiling). The monitoring

should last one year in order to significantly record short- and long-term variability of indoor climate over seasons. Then, the quality and representativeness of collected data are evaluated before conducting any further investigation on the indoor climate and on the degradation risk assessment. Thereafter, climate and crack-width data are investigated to find whether a strong relation exists between them. In such a case, an empirical evaluation of the dose-response function related to the degradation can be derived and validated with the crack-width measurements. It is specific for the observed degradation, since it depends on the features of the material and the environmental conditions at which object has been kept over a whole year.

In parallel, a building model is created based on geometric and stratigraphy features of the building envelope. The whole-building dynamic simulation software should be integrated with a heat and moisture transfer model in order to include the sorption and desorption effect of hygroscopic building materials. The above task is of crucial importance to accurately and thoroughly model the indoor moisture dynamics. The building model calibration is carried out using hourly T and RH data. This is a further reason for the assessment of high-quality T-RH data.

Finally, after the validation of the dose-response function and after the calibration of the building model, climate control strategies and/or retrofitting interventions can be modelled in the simulation environment and assessed with respect to the current conservation state of the object.

Microclimate observations

On-site monitoring system

Four indoor temperature (T) and relative humidity (RH) sensors were installed in three of the most representative rooms of the Museum and indicated by colours in Figure 3a. Each site allowed the characterization of a different area typology of the building. In room 9, indicated as yellow room in Figure 3a, the two T-RH probes were positioned at 1m and 2m in order to study whether the air mass is stable or unstable. In the same room, a surface temperature sensor (Ts) and a crack-width meter (C) were installed on a crack of a wooden panel ceiling. C can be reasonably conceived as a marker-tracking of microdamage of wood structure at the crack tip due to the stress concentration, i.e. the environmental conditions at the interface between air and surface layer, through the mechanism related to the fatigue process. The Ts sensor was installed on the wood via paraloid and lied on the crack-width meter support, that was fixed on the wood with an epoxy on a substrate of gauze and paraloid.

A probe with T-RH sensor, coded as out, was also installed at the terrace to record the outdoor hygrothermal conditions (blue circle in Figure 3a). The external probe was shaded from solar radiation and protected from ventilation.

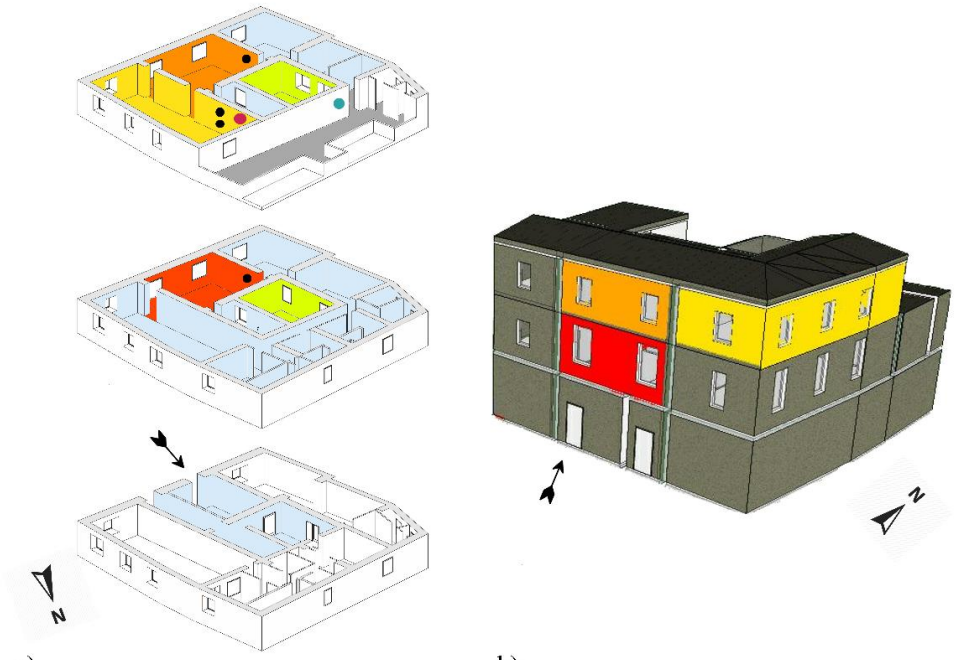

Figure 17 a) Exploded view of the "Valeriani-Guarini-Antonelli Palace". All colored rooms belong to the Archaeological Museum of Priverno. The green area indicates the internal courtyard. Probes were installed in room 4 (red), 9 (yellow) and 10 (orange). Circles indicate the indoor T-RH probe (as black), the Ts and C sensors (as purple) and the external T-RH probe (as blue). b) 3D model of the building obtained with the dynamic building simulation (DBS) software. Rooms 4, 9 and 10 are indicated with different colors, i.e. red, orange and yellow, respectively. The black arrow indicates the main entrance of the building.

The list of sensors and their technical features are reported in Table 1. The metrological features of T and RH sensors are in accordance with the accuracies suggested by the European standards EN 15758:2010 and EN 16242:2012, respectively. All the sensors were connected to four dataloggers "Grillo Bee", each corresponding to the three rooms and the outdoor spot, developed and distributed by Tecno.El S.r.l. (Italy), with a remote data transmission by GSM/GPRS technology. The acquisition time was set to 5 minutes and the processing time was set to 30 minutes, providing the average, minimum and maximum of the recorded parameters.

Table 6 The technical features of sensors used within the monitoring campaign.

	T	**RH**	**T_s**	**C**
sensor	Pt100 1/3 DIN	film capacitor "Rotronic" C94	thermistor NTC	potentiometer in conductive plastic
operating range	-40°C to +60°C	0 – 100%	-30°C to +150°C	10 mm
accuracy	±0.3°C	+1.5%	±0.1°C	+0.025 mm

Moreover, the mixing ratio of moist air (MR), both indoors and outdoors, was calculated from T and RH readings, using the equation reported in the European standard EN

16242:2012 and taking into account the standard value of the atmospheric pressure (p=1013 hPa). The uncertainty related to MR was 0.3 g/kg.

The monitoring campaign was conducted over the period from August 2016 till November 2017; whereas the analysis concerned the period from September 2016 till August 2017.

Microclimate analysis

First, the quality of the T-RH data series was assessed using the Completeness Index (CoI) and the Continuity Index (CI) (Frasca et al., 2016). The indexes range between 0 (poor quality) and unity (high quality, i.e. no missing values).

Thereafter, the ASHRAE 2011 was applied in order to couple a climate type, defined as Class of Climate Control, to the risks that this climate may affect the collections. The Museum would belong to the class V within the controlled climate. It means that the climate classes of control AA, A, As and B would be sustainable in relation to the energy usage. Since no degradation phenomena of artworks have occurred over the last years and the HVAC system does not allow the RH control, a higher class of control, such as AA and A, would imply an excessive energy cost for the Museum. Thus, the classes of control As and B were chosen in accordance with the characteristic of the building envelope (heavy masonries and double glazing), the typical building use (walk-through visitors only and education groups) and the HVAC system (simple fan coils for heating and cooling). Thus, T-MR data were plotted into a psychrometric chart in order to provide a synthetic visualization of data with respect to the short-term fluctuations' limits as defined by the class of climate control. The psychrometric chart also includes a 3-by-3 matrix that reports, on yearly and seasonal basis, the percentage of time that indoor conditions are within the guidelines (second row and column), above the T and RH maxima (first row (too warm) and third column (too humid), respectively) and below the T and RH minima (third row (too cold) and first column (too dry), respectively).

Thereafter, the short-term variability of the indoor climate was investigated as daily spans, i.e. the difference between the maximum and minimum value observed during each day. The analysis allowed to study both the variability of the hygrothermal parameters and the short-term stresses of environmental conditions experienced by the material.

The wood, as a hygroscopic material, responds to variations in relative humidity (RH) by absorbing and desorbing moisture. Since the interaction between climate and object is dynamic and cumulative, the highest risk for the conservation of organic and hygroscopic material strongly depends on the extent and rapidity at which environmental conditions change. For this reason, the relationship between the crack width (C) and hygrothermal data at the surface-air interface (Ts-RHs) was assessed by using Spearman's rank-order correlation (r_s) with a confident level (α) of 5%. RHs was derived from Ts and MR using the inverse formula in the EN 16242:2012 and assuming that the water vapour gradient (ΔMR) was constant from air ambient to the interface

between air and wooden surface. The RHs propagation within the material, i.e. the approximation of the hygrometric gradient from superficial layer to the inner layers of panel (Camuffo personal communication, 2016), was investigated as the central moving average of RHs (smoothed-RHs) at 3h, 24h, 48h and 1 week. The deviation of RHs from smoothed-RHs values, i.e. the internal stresses of material, was computed to extract the short-term fluctuations and a safe band variability was defined as the 7th and the 93rd percentiles of the short-term fluctuations.

Simulation environment

Empirical evaluation of the dose-response function

A dose-response function between crack width (C) in wooden panel and T_s – RH_s data was derived as a non-linear multiple regression:

$$C_m = a \times RH_s^{\,b} \times T_s^{\,c} \qquad (1)$$

where a, b, and c were coefficients. The coefficients were calibrated using daily values of Ts and RHs over a whole year in order to detect the long-term response of the crack evolution. In this way, the coefficients are specific to the material type and the hygrothermal conditions at which it has been kept over the last years. In this way, C_m can allow to know in advance if a new control strategy of the indoor climate is capable to reduce the mechanical degradation risk in the wooden panel.

Building modelling

The dynamic building simulation (DBS) for indoor climate analysis was performed using the IDA Indoor Climate and Energy (IDA ICE) 4.8 developed and distributed by EQUA simulation AB.

The geometry of the building model was created starting from the architectural survey. The building model, shown in Figure 3b, consisted of sixteen zones. It was oriented in the SW-NE direction with respect to the main entrance (indicated as a black arrow in figure) at a height of 150 m of m.s.l. The thermal model (BDFWall), used by the DBS for the modelling of walls, was replaced by the HMWall model only in the case of room 9. This room, indeed, was chosen as the pilot study room for testing the new climate control strategy within the Museum.

The stratigraphy of the wall was retrieved from literature and referred to construction techniques in lower Latium in the Middle Age. It was assumed to be unchanged over time except for ceilings, which were rebuilt after the restoration in 1924-26. The hygrothermal properties of opaque components were extracted from the MASEA Datenbank (https://www.masea-ensan.de/) and reported in Table 2. These values were used to initialize the building model. It is worth to notice that only the first three columns of Table 2 were needed for the BDFWall. In Table 3, the stratigraphy of opaque components is reported as discretised layers in the HMWall model.

Appendix G

The glazing system consisted of low-emitted double pane glazing filled with air (6 mm – 12 mm – 6 mm) with wooden frames. Its internal and external emissivity was 0.04 and 0.84, respectively. The thermal parameters of glazing system were set with a trasmittance (U-value) of 1.59 W m^{-2} K^{-1} and a solar heat gain coefficient (SHGC) value of 0.38 for the glazing and U-value of 1.0 W m^{-2} K^{-1} for the frame. All windows were shaded with black interior roller shades in PVC. The infiltrations were set at 0.09 ACH and the wind profile was taken as that of a urban site. The properties of the ground floor were taken those reported in the standard ISO 13370:2007.

Table 7 The hygrothermal properties of building materials for opaque components extracted from MASEA Datenbank both for the BDFWall model and for the HMWall model. For the BDFWall model, only the first three columns were needed. List of properties: ρ = density; c_P = specific heat; λ = thermal conductivity; μ = vapour diffusion resistance factor; w_{80} = equilibrium water content at 80% of relative humidity; wf = free water saturation; A_w = water absorption coefficient.

	Hygrothermal properties						
Material	**ρ**	**c_P**	**λ**	**μ**	**w_{80}**	**w_f**	**A_w**
	kg/m^3	J/(kg·K)	W/(m·K)	-	kg/m^3	kg/m^3	kg/(m^2·$h^{0.5}$)
brick	1900.0	1000.0	1.07	28.0	24.9	250.0	2.70
concrete	2104.0	776.0	1.94	76.1	101.0	144.0	0.75
lime plaster	1600.0	850.0	0.70	7.0	30.0	250.0	3.00
lime-cement render	1900.0	850.0	0.90	19.0	45.0	210.0	2.00
restoration plaster	590.0	1000.0	0.17	8.6	11.9	500.0	0.24
floor brick	1952.0	863.0	0.96	19.4	123.0	161.0	8.51
light mortar	830.0	1000.0	0.21	13.2	26.3	423.0	1.63
wood	740.0	1400.0	0.81	223.0	104.0	349.0	0.10

Table 8 Stratigraphy of opaque components used in the HMWall model. Cell numbers and thickness of each layer of the material (m) are summarized; the internal surface is at the left side (+ in, - out).

external wall																				
Cell №	+	1	2	3	4	5	6	7	8	9	10	11	12	13	14	15	16	17	18	-
Thickness (cm)	+	1.0	1.0	1.0	3.0	3.0	4.0	5.0	5.0	6.0	7.0	5.0	5.0	4.0	3.0	3.0	1.0	1.0	2.0	-

internal wall																				
Cell №	+	1	2	3	4	5	6	7	8	9	10	11	12	13	14	15	16	17	18	-
Thickness (cm)	+	1.5	1.0	1.0	3.0	3.0	4.0	5.0	5.0	6.0	7.0	5.0	5.0	4.0	3.0	3.0	1.0	1.0	1.5	-

floor											
Cell №	+	1	2	3	4	5	6	7	8	9	-
Thickness (cm)	+	2.0	2.0	2.0	2.0	3.0	3.0	2.0	1.0	3.0	-

wooden slab				
Cell №	+	1	2-9	-
Thickness (cm)	+	3.0	5.0	-

External climate conditions (Tout and RHout) used to run the climate file were provided by outdoor measurements. Wind variables (direction and speed) and global horizontal solar irradiance, measured at Maenza station (Lat. 41.5° and Long. 13.2°) belonging to the ARSIAL (Agenzia Regionale per lo Sviluppo e l'Innovazione dell'Agricoltura del Lazio), were also included in the climate file. The global horizontal solar irradiance was divided in the direct and diffuse solar irradiance components using the Maxwell model (Ineichen et al., 1992).

Our purpose was to calibrate the building envelope when the HVAC system, both for heating and for cooling, was not in operation. Thus, the calibration and validation procedures were run in May and September/October, respectively.

The calibration procedure comprises a first automatic step and a second manual step. It was carried out using data collected from May 15th, 2017 till May 31st, 2017. To take into account the high inertia of historic buildings, the initialization period started from February 1st, 2017.

The first step consists of the calibration of the building model with the T-RH measurements taken in all the three monitored rooms. The calibration was carried out by searching the best hour T and RH match. Thus, the Sensitivity Analysis (SA), based on the Elementary Effects method (EEs), was conducted to identify the most effective input parameters of the building model, such as thermal bridges and infiltrations, which were mostly unknown. The SA was performed in order to achieve 10 EEs for each of 18 input parameters, that were discretized into 4 ranges of values. The EEs were calculated using hourly indoor T and RH as reported in Roberti et al. (2015). Then, the Particle Swarm Optimization – General Pattern Search of Hooke-Jeeves (PSO-GPSHJ) genetic algorithm, implemented in GenOpt®, was used to minimise the discrepency between modelled and measured T-RH data. The root mean square error (RMSE) and the coefficient of variation of RMSE (CV-RMSE) with respect to the average of measured data (Fabrizio and Monetti 2015) were used using as target functions. Since the thresholds of the above statistical parameters for the calibration with hourly T-RH data were not available in the literature, the accuracy of T-RH sensors was assumed as rejection criteria. More the targets were close to the sensor accuracy, more the building model reproduced the actual building.

The second step consists of replacing the BDFWall model of opaque components in room 9 with the HMWall model in order to consider the heat and moisture transfer through porous building materials. It is worth to notice that the HMWall model calibration is currently manual and further implementations will be developed. For this reason, the room 9 model and the above crawl space of the roof were included in a new file and manually calibrated. The internal wall and the floor were defined as adiabatic components and connected to a RH value of 50% experienced by room 10 (close to the internal wall) and room 4 (close to the internal floor). The internal wooden ceiling was thermally connected to the crawl space and to a RH value of 55%, assumed as a compromised value between internal and external hygrometric conditions.

After that, the validation of the whole building model and of the room 9 model was performed using data collected from September 24th, 2017 till October 8th, 2017 with an initialization period from June 1st, 2017 till September 23rd, 2017. In the case of room 9, the RH above the ceiling was set to 50%, since the validation was performed after a warm period where RH was, on average, less than 50% in the other rooms of the building.

Climate control strategy

The improvement of the indoor climate control strategy in the room 9 was aimed at a new set-point of temperature in the existing HVAC system taking into account both the conservation of wooden ceilings and the thermal comfort of users. The HVAC was designed in the simulation environment as simple fan coils, set to a maximum heating power of 3500 W and a maximum cooling power of 3000 W.

The new control strategy of the indoor climate was tested using a dynamic set-point for temperature (Kramer et al., 2017). The indoor relative humidity was assumed as free-floating and evaluated a-posteriori with respect to the conservation requirements suggested by ASHRAE 2011. The workflow consists of three steps:

Temperature safe-band for the conservation. The class of climate control As (ASHRAE 2011) was chosen because it is associated with less mechanical degradation risks than the class of climate control B. The T safe-band was calculated starting from the 90-days centred moving average of recorded T data, seasonally adjusted according to As class (+5/-10°C with respect to the annual average) and taking into account the upper and lower limits of proofed short-term fluctuations (±2°C) (Figure 4a).

Temperature safe-band for the thermal comfort. The Adaptive Temperature Limits (ATL) were chosen as T safe-band for the thermal comfort (Nicol and Humphreys, 2002). The ATL is calculated on the basis of the procedure reported by Kramer et al. (2018) for temperate climates (Figure 4b).

Temperature safe-band for both conservation needs and thermal comfort. T safe-band was determined comparing for each hour the T safe-band for the conservation with that for the thermal comfort, and choosing the less wide safe-band among the allowable thresholds. After that, T safe-band were seasonally smoothed out (Figure 4c).

Finally, the estimated indoor variables were replaced in the equation 1 to analyse the effect of the new control strategy on the crack width with respect to the current indoor climate conditions and to no control strategy, i.e. the free-floating indoor climate.

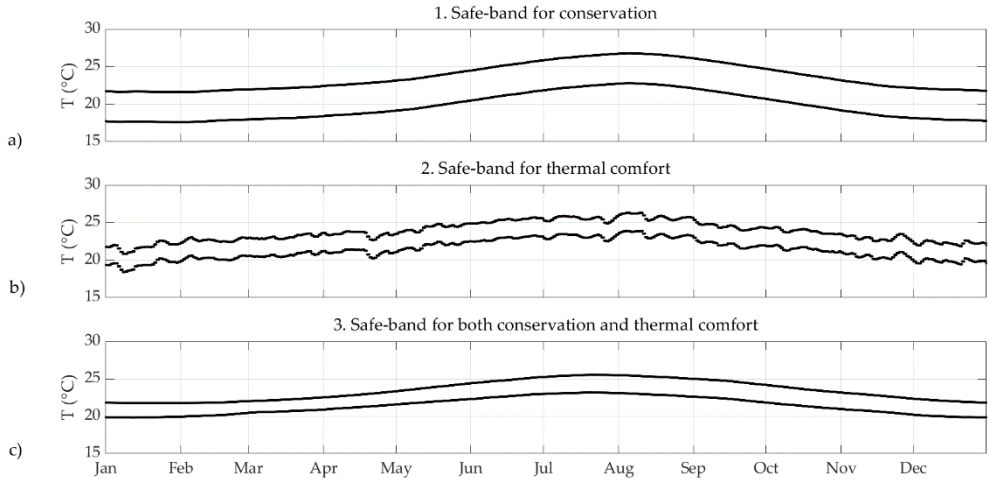

Figure 18 The three steps for the dynamic temperature safe-band: 1) Temperature safe-band for the conservation; 2) Temperature safe-band for the thermal comfort; 3) Temperature safe-band for both conservation needs and thermal comfort.

Results

Microclimate analysis

The quality assessment of the variables recorded in room 9 has revealed that the time series are continuous and complete, since CoI is 0.94 and CI is 0.99. This means that the whole data set can be used to thoroughly characterize the microclimate in room 9 and that T-RH time series can be also exploited for the calibration of the building model.

Taking into account both the seasonal behaviour of hygrothermal parameters and their short-term fluctuations, it was found that T-RH data fit the class of climate control As in 60.0% of time. This means that a small risk of mechanical damage may occur to highly vulnerable artworks in less than 40% of time.

The psychrometric chart (Figure 5) shows the distribution of T and RH data collected in room 9 over the whole year. Data are seasonally grouped by different colours. The blue horizontal lines is determined as the T short-term fluctuations (±2°C) added to the annual average (21.3°C); the same is for the blue RH lines (±5%) added to the annual average (52.3%). It follows that more data are scattered and more indoor climate is fluctuating. In this case, T ranges between 8.5°C and 33.4°C whereas RH ranges between 35.3% and 71.6% over the whole year. The percentage of T-RH data within the As class is 13.1%. It was found that: in Winter (blue data), T values are lower than limit in 98% of time and January is the coldest month; in Spring (green data), T limits show that the environment is too cold in March (41% of time) and too warm in May (20% of time); in Summer (red data), the environment is always too warm and also too dry in 81% of time; in Autumn (orange data), the environment is too warm in September in 20% of time and too humid in 57% of time between October and November.

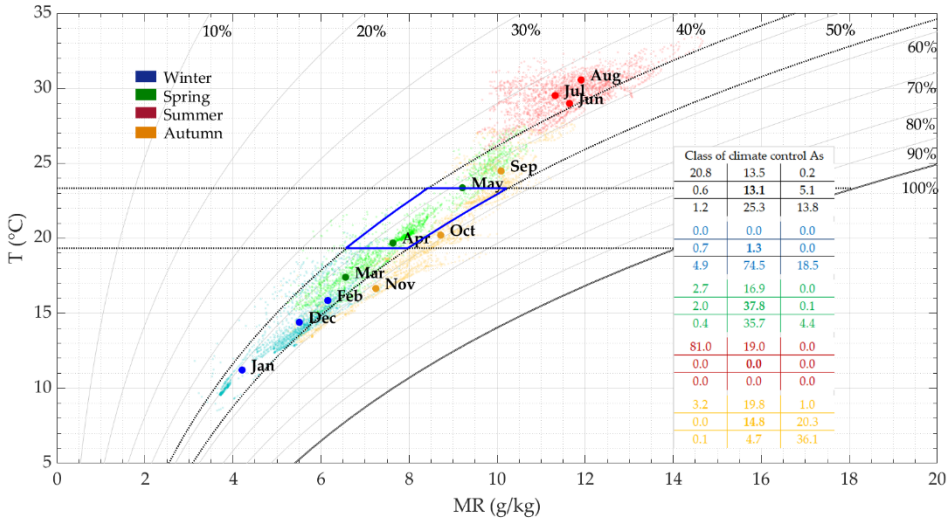

Figure 19 Psychrometric chart. Indoor climate within room 9 is seasonally grouped: blue (winter), green (spring), red (summer), and orange (autumn). Seasonal monthly averages are also displayed. The class of climate control As area is delimited by two horizontal blue lines (T = 21.3 ± 2°C) and two blue curves (RH = 52.3 ± 5%). The T and RH limits divide the chart into nine parts and the percentage of data within limits is reported by the 3-by-3 matrixes on the right.

Figure 6 shows the RH daily span (ΔRH) *versus* the T daily span (ΔT). ΔRH is always lower than 20%, whereas ΔT overcomes 6°C in few days. In Winter data (blue dots) are assembled in a distinguishable area with respect to the other seasons, standing out the combined effects of the intermittent use of the heating system on the indoor climate with the too low outdoor temperatures. On the contrary, in Summer, the effect of the cooling system is not visible.

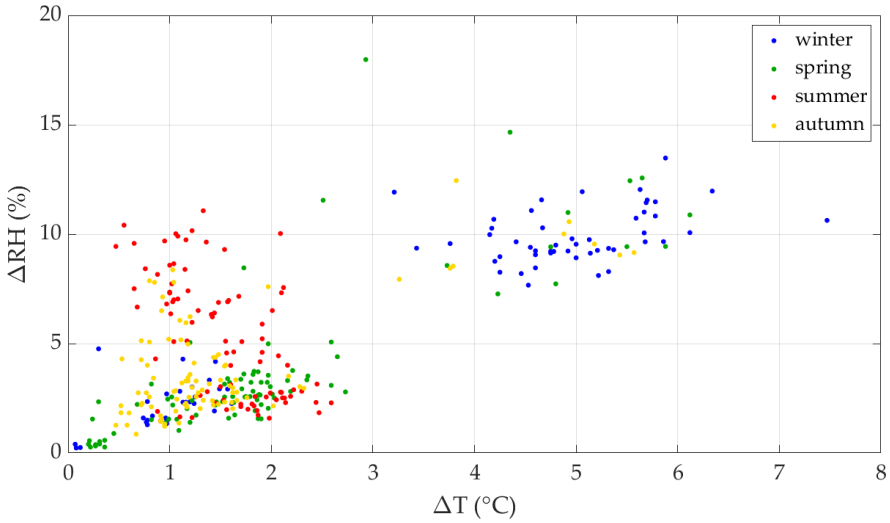

Figure 20 Scatter diagram of daily RH span (ΔRH) *vs* daily T span (ΔT). The daily span is calculated as the difference between the maximum and minimum values per each day. Blue, green, red and orange dots indicate winter, spring, summer and autumn, respectively.

The temperature and relative humidity at the interface air-surface (named Ts and RHs) were related with the crack-width (C), as shown in Figure 7. It was found that an increase of ΔTs=10.0°C and a decrease of ΔRHs=10.0% over the year with respect to the annual averages (Figure 7a) can cause an increase of C equal to 0.12mm (Figure 7b). This

confirms that too dry environmental conditions mainly related to too warm thermal conditions, could be responsible for C widening (i.e strain in the material) and, hence, risky conditions for the conservation of the material. Besides, the Spearman's rank correlation coefficient resulted 0.67 (C, Ts) and -0.91 (C, RHs), showing that C is highly correlated with both hygrothermal variables. The most critical periods for the conservation of wooden ceilings seem to be connected when the heating system was on and during Summer.

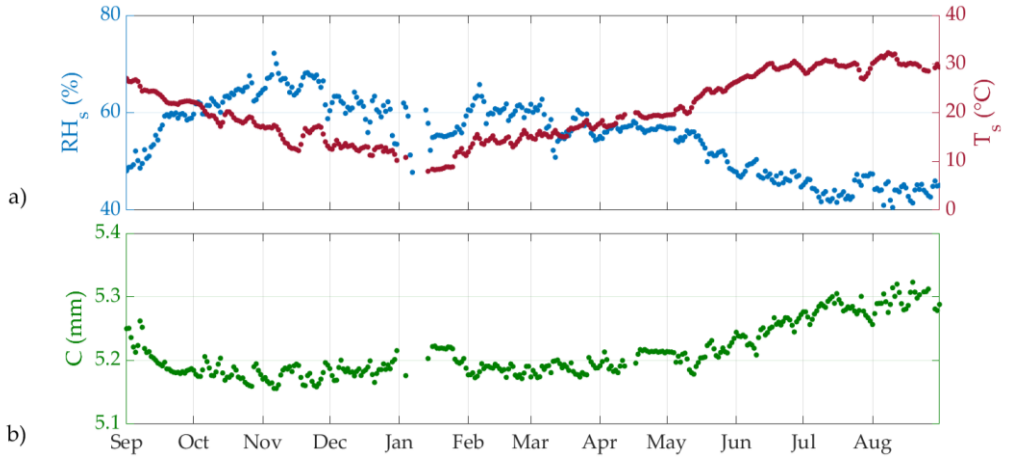

Figure 21 a) Relative humidity (blues dots) and temperature (red dots) temporal behavior at the interface air-surface (RHs – Ts) over the whole year. b) Crack width (C) temporal behavior over the whole year.

Moreover, Figure 8 shows the ΔRHs calculated with a time lag of one-week and the crack width temporal behaviour over the whole year. It can be noticed that, when the heating system is on, the moisture-induced strain is closely related to the daily fluctuations of RHs and of Ts (not shown); in Summer time, the moisture-induced strain is strongly affected by the RHs gradient within the material, since the inner layers are moister than the surface layer. On the other hand, when ΔRHs is within the safe band, C is stable and this occurred in September-October and in April-May.

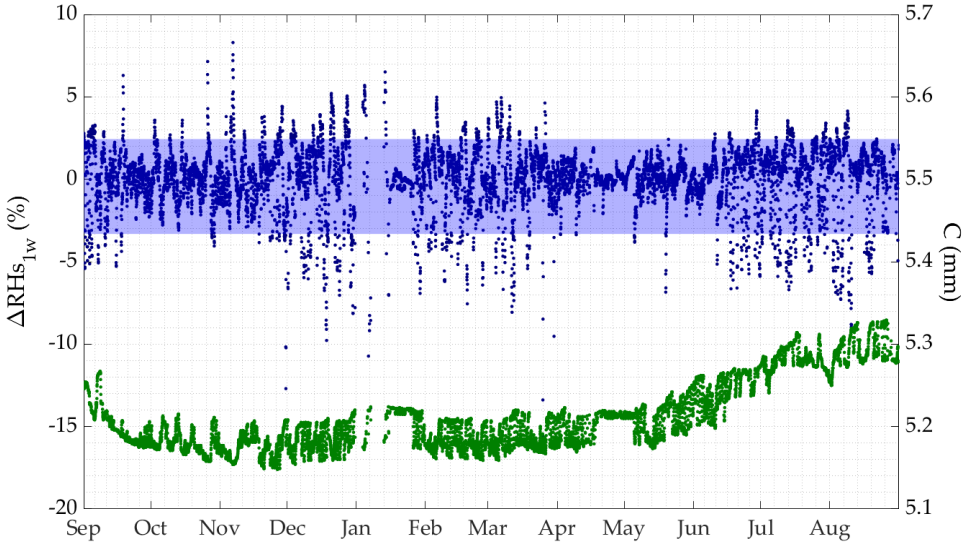

Figure 22 ΔRHs$_{1w}$ calculated as the difference between RHs and RHs smoothed at 1week (inner layer of wooden panel) and crack width evolution.

Dynamic simulation analysis

Empirical evaluation of the dose-response function

The relation between C and Ts-RHs allowed to derive an analytical relationship for the dose-response function by minimising the coefficients of the equation (1). The coefficients found are: a = 0.6479 (mm/(100^{b}·°C^{c})); b = -0.0542 and c = -0.0004. It can be noticed that RHs has the highest effect on the crack behaviour, since the coefficient b is two orders of magnitude greater than c. The RMSE is 0.014 mm, i.e. lower than the crack-width meter's accuracy (Table 1).

Building modelling

The results from the Sensitivity Analysis (SA) have demonstrated that the indoor RH of the building model is strongly affected by the rate of infiltration, whereas the indoor T by the thermal bridges. The whole building model was automatically calibrated starting from these two parameters with the aim to minimize the RMSE between modelled and measured hourly T-RH data. Then, the room 9 model was further manually fine-tuned after having included the HMWall model. Table 4 reports the main statistic parameters about the calibration performed to model room 9 without the HMWall model and with the HMWall model. It can be noticed that the use of the HMWall model has allowed to better simulate the relative humidity inside the room, halving the error between modelled and measured RH and increasing their correlation from 0.7 to 0.9. Table 4 shows that the indoor temperature is also better modelled. This outcome encourages the use of the HMWall model in the historic building modelling. Figure 9 shows measured and modelled T (Figure 9a) and RH (Figure 9b) temporal behaviour and displays the instrumental uncertainty of T-RH sensors as shaded areas.

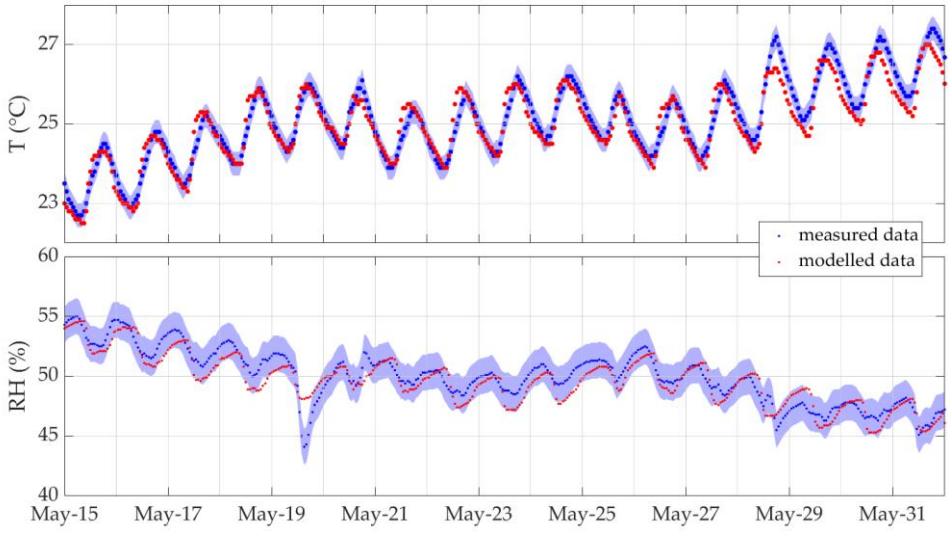

Figure 23 Measured (blue dots) and modelled (red dots) temperature (T) and relative humidity (RH) trends inside room 9. The shaded areas are the measurement uncertainties: ±0.3°C and ±1.5%, respectively.

Finally, the validation phase of room 9 was conducted and it was found that the discrepancy between modelled and measured T does not change (Table 4). In this case the statistic parameters calculated on modelled RH are: MAE=1.0%, RMSE=1.2%, CV-RMSE=2.4% and r_s=0.7.

Table 9 Summary of the calibration statistics of air temperature (T), relative humidity (RH) and the surface temperature (Ts) in room 9 modelled with IDA ICE (no HMWall) and extended IDA ICE with the HMWall model (HMWall). List of parameters: MAE = mean absolute error; RMSE = root mean square error; CV-RMSE = coefficient of variation of RMSE; r_s = Spearman's rank correlation coefficient.

Room 9		MAE	RMSE	CV-RMSE	r_s
T	no HMWall	0.4°C	0.4°C	1.7%	1.0
	HMWall	0.2°C	0.3°C	1.2%	1.0
RH	no HMWall	1.6%	2.0%	3.9%	0.7
	HMWall	0.8%	1.0%	2.0%	0.9

In conclusion, the building model was characterised by an infiltration rate of 0.02 ACH and poor thermal bridges. Besides, the calibrated room 9 was also characterised by the hygrothermal properties reported in Table 5.

Table 10. The list of building materials and the changed hygrothermal properties (as bold) obtained from the calibration of room 9.

Material	**Hygrothermal properties**						
	ρ, kg m^{-3}	**c_p,** J kg^{-1} K^{-1}	**λ,** W m^{-1} K^{-1}	**μ,** -	**w_{80},** kg m^{-3}	**w_f,** kg m^{-3}	**A_w,** kg m^{-2} h$^{-0.5}$)
brick	1900.0	1000.0	**1.06**	28.0	24.9	250.0	2.70
concrete	2104.0	776.0	**1.81**	76.1	101.0	144.0	0.75
lime plaster	1600.0	850.0	**0.65**	7.0	30.0	250.0	3.00
light mortar	830.0	1000.0	**1.20**	13.2	26.3	423.0	1.63
wood	740.0	**740.0**	0.81	223.0	**155.0**	349.0	**15.00**

Climate control strategy

The calibrated room model was used to estimate the effect of the dynamic temperature control strategy on the conservation of wooden ceilings, by replacing the estimated T-RH into equation 1. The conservation needs and the thermal comfort requirements were both considered.

For the above control strategies inside room 9, the peak demand is 2.6 kW during heating hours and 1.6 kW during cooling hours; whereas the annual energy consumption is 4532 kWh and 1877 kWh, respectively.

Figure 10 shows the psychrometric chart of the estimated T-RH data related to the new climate control configuration. The annual averages of T and RH are 22.3°C and 54.9%, respectively. The hygrothermal data are less scattered with respect to the actual

environmental conditions (T ranges between 19.8°C and 25.8°C and RH ranges between 47.7% and 65.4%). T-RH data are within the allowable limits in 41.5% of time. Specifically, in Winter, T is 91% of time below the lower T limit (20.3°C); whereas RH is 56% of time above the RH upper limit (59.9%), never exceeding the value of 64.5%. In Spring, T-RH data are within the allowable area in more than 85% of time, even though RH is below the lower limit and above the upper limit in 5% and 8% of time, respectively. In Summer, T is always above the upper limit (24.3°C), however it never exceeds 25.8°C; whereas RH is below the lower limit (49.9%) in 18% of time. Finally, in Autumn, warmer episodes than the upper T limit (on average 15%) are related to September; whereas RH is lower than 49.9% in 5% of time. Moreover, the daily spans are less than 2.5°C for T and less than 4.0% for RH.

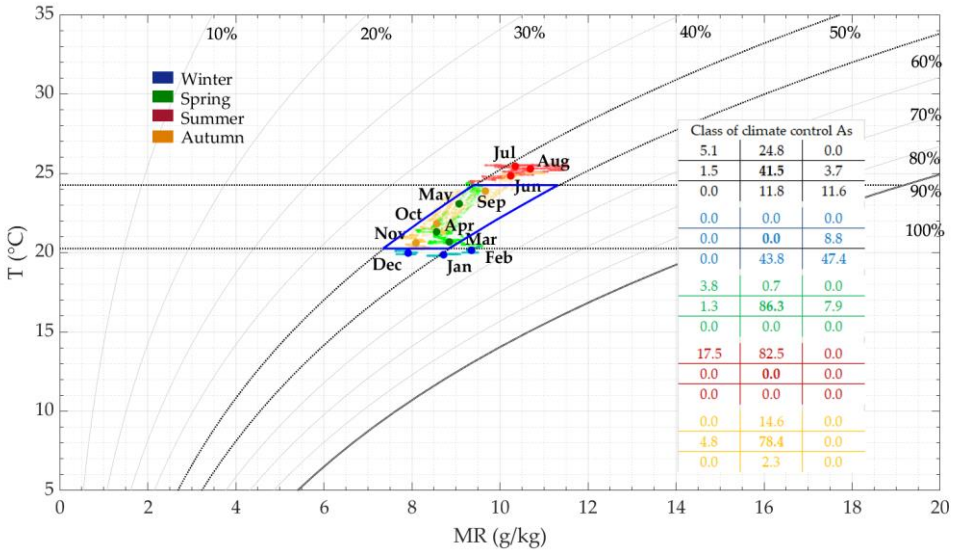

Figure 24 Psychrometric chart. Indoor climate within room 9 with the new climate control strategy is seasonally grouped: blue (winter), green (spring), red (summer), and orange (autumn). Seasonal monthly averages are also displayed. The class of climate control As area is delimited by two horizontal blue lines (T = 22.3 ± 2°C) and two blue curves (RH = 54.9 ± 5%). The T and RH limits divide the chart into nine parts and the percentage of data within limits is represented by the 3-by-3 matrixes on the right.

Figure 11a shows the histogram with the percentage of occurrences of C in: i) current climate conditions (black-white bins); ii) the free-floating (red bins) and iii) the new climate control strategy (blue bins). C_m is calculated from the equation 1 in ii) and iii) by replacing Ts and RHs with those retrieved as output from the simulation file.

In i) case, the observed cracks range between 5.15 mm and 5.35 mm and, among those, about 20% is above 5.25 mm, corresponding to the Summer.

In ii) case, the T-RH conditions allow to meet the conservation requirements in 22% of time, since T is below the lower limit in 47% of time and above the upper limit in 32% of time. The thermal comfort requirement of visitors, instead, is reached only in 10% of time, since T is below the ATL lower limit in 58% of time in cold season and above the ATL upper limit in 32% of time in warm season. Finally, RH is about 51% of time below the RH lower limit in the warm season. In these climate conditions, as shown in Figure 11a, about 15% of data is within the range of 5.00-5.05 mm, when, in cold period, T is

<15°C and RH is >60%. Instead, about 27% of data is within the range of 5.25-5.35 mm, when, in warm period, T increases up to 31°C and RH decreases below 40%.

On the contrary, in iii) case, the new control of the indoor climate determines a reduced annual variation between minimum and maximum width of wooden cracks, since it is 0.10 mm instead of 0.20 mm in current conditions and 0.25 mm in free-floating. This means that, when both thermal comfort and conservation needs are satisfied, wooden panels would experience less stresses and, consequently, less strains.

Looking at Figure 11b, i.e. the histograms of daily span of C_m (ΔC_m), the current conditions is characterised by daily stresses up to 0.06 mm. On the contrary, the free-floating strategy might induce daily stress up to 0.03 mm per day. If a control of indoor climate is considered, the daily span is less than 0.01 mm in more than 80% of the occurrences.

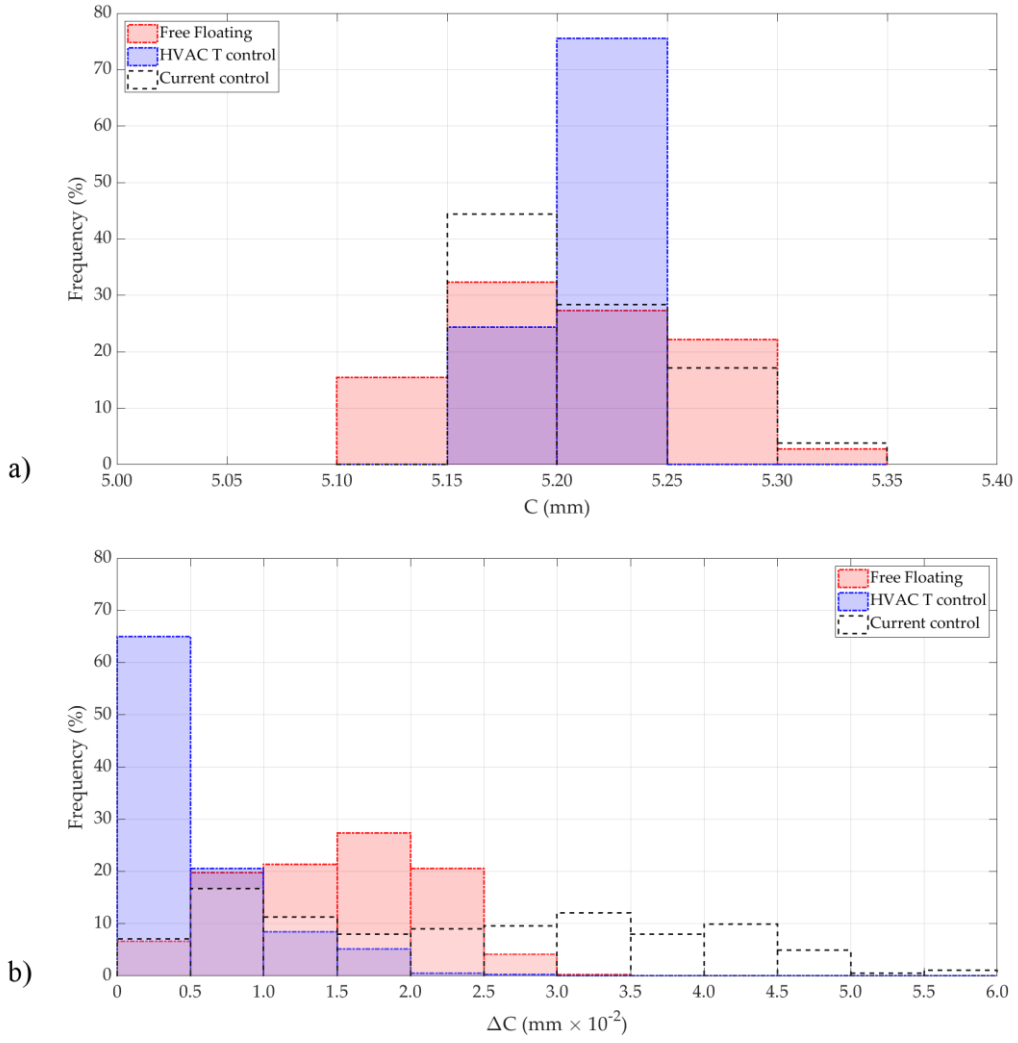

Figure 25 **a) Histogram plot with the percentage of occurrences (%) of crack width (C) observations (black-and-white bins), when the indoor climate is free-floating (red bins) and when it is controlled by a dynamic T safe-band (blue bins). b) Daily span (ΔC) of crack width observations (black-and-white bins), when the indoor climate is free-floating (red bins) and when it is controlled by a dynamic T safe-band (blue bins).**

It results that a dynamic temperature control is more effective to reduce the stress-and-strain cycle in wooden ceilings, since it reduces both the annual spread of cracks and, especially, their daily spans. It is worth to notice that the T control, so as that designed, can guarantee the control of RH as recommended by the class of climate control As in more then 70% of time. Nevertheless, this implies that a new climate control strategy cannot be designed only with the temperature control, because the HVAC system should be integrated with a de/humidifying device in order to guarantee the RH control, as well.

Conclusions

The management of historic buildings in Italy is strongly related to the priority of preservation of architectural components. So, the control of the indoor climate should mainly concern the optimization of the current climate control system with respect to the degradation of artifacts. This paper proposed a method that allows to assess strategies for better conservation and thermal comfort of the visitors, by coupling the climate monitoring and the building dynmic simulation. The method can be generally applied to historic buildings that need for refurbishment or new control strategies and where the conservation of artworks has the priority.

The application of the method to the case study of "Museo Archeologico di Priverno" has proved that the building model which more accurately simulates the indoor temperature and relative humidity dynamics is that in which a hygrothermal transfer model of opaque building components is included in the dynamic simulation software. Furthermore, the semi-automatization of calibration method using hourly measurements of climate variables is effective to design a building model as representative as possible of the actual case.

In addition, the study has demonstrated that long-term indoor climate observations coupled with the monitoring of the crack width of wood can be effectively used to investigate on the indoor climate aimed at reducing the stress-and-strain cycle of valuable wooden ceilings, and improving the thermal comfort. The new climate control strategy has the main advantage to consider the historical climate at which wooden ceilings have been kept over the last years. This means that the application of the dynamic temperature safe-band does not imply any abrupt changes in the indoors, highly reducing further triggers of degradation.

It is worth to notice that this methodology takes advantages only if a thorough knowledge of the indoor climate and its interaction with the objects is reached. Even if the method has been applied to a particular case study, the "Museo Archeologico di Priverno" (Italy), it can be potentially exploited for other cases in which also other types of degradation are present, providing that a degradation response function or its empirical evaluation of object is available.

Acknowledgement

We thank Sapienza University of Rome for funding the multidisciplinary project "Preservation, conservation and valorisation of archaeological sites: The case of the ancient site Privernum". This research has been carried out within the *"Renovation of existing buildings in NZEB vision (nearly Zero Energy Buildings)"* Project of National Interest (Progetto di Ricerca di Interesse Nazionale - PRIN) funded by the Italian Ministry of Education, Universities and Research (MIUR).

References

Antretter, F., Kosmann, S., Kilian, R., Holm, A., Ritter, F., and Wehle, B. 2013. Controlled Ventilation of Historic Buildings: Assessment of Impact on the Indoor Environment via Hygrothermal Building Simulation. In Hygrothermal Behavior, Building Pathology and Durability (pp. 93-111). Springer, Berlin, Heidelberg.

Ascione, F., De Rossi, F., and Vanoli, G.P. 2011. Energy retrofit of historical buildings: theoretical and experimental investigations for the modelling of reliable performance scenarios. Energy and Buildings 43(8):1925-1936.

Bichlmair, S., Krus, M., Kilan, R., and Sedlbauer, K. 2012. Building simulation modelling of the historic building Linderhof Palace taking account visitors. In 7th IBPSA Conference (pp. 296-309).

Camuffo D. 2014. Microclimate for cultural heritage (second edition) conservation, restoration, and maintenance of indoor and outdoor monuments. Amsterdam: Elsevier.

Cassar, M. and Pender, R. 2003. Climate change and the historic environment. London: Centre for Sustainable Heritage University College London.

Coakley, D., Raftery, P., and Keane, M. (2014). A review of methods to match building energy simulation models to measured data. Renewable and sustainable energy reviews 37:123-141.

Coelho, G.A., Silva, H., and Henriques, F.A. 2018. Hygrothermal simulation models optimization for historic buildings. Building and Environment 142:439-450.

Cornaro, C., Puggioni, V.A., and Strollo, R.M. 2016. Dynamic simulation and on-site measurements for energy retrofit of complex historic buildings: Villa Mondragone case study. Journal of Building Engineering 6:17-28.

Decreto Legislativo 19 agosto 2005, n. 192. "Attuazione della direttiva 2002/91/CE relativa al rendimento energetico nell'edilizia" pubblicato nella Gazzetta Ufficiale n. 222 del 23 settembre 2005 - Supplemento Ordinario n. 158.

Delgado, J.M., Barreira, E., Ramos, N.M.M., and de Freitas, V.P. 2012. Hygrothermal numerical simulation tools applied to building physics. Springer-Verlag Berlin Heidelberg.

EN 16242:2012. Conservation of cultural property—Procedures and instruments for measuring humidity in the air and moisture exchanges between air and cultural property. European Committee for Standardization, Brussels.

EN 15758:2010. Conservation of cultural property—Procedures and instruments for measuring temperatures of the air and the surfaces of objects. European Committee for Standardization, Brussels.

Frasca, F., Siani, A.M., Casale, G.R., Pedone, M., Strojecki, M., and Mleczkowska, A. 2017. Assessment of indoor climate of Mogiła Abbey in Kraków (Poland) and the application of the analogues method to predict microclimate indoor conditions. Environmental Science and Pollution Research 24(16):13895-13907.

Holm, A., Kuenzel, H.M., and Sedlbauer, K. 2003. The hygrothermal behaviour of rooms: combining thermal building simulation and hygrothermal envelope calculation. IBPSA Proceedings Building Simulation Einhoven.

Ineichen, P., Perez, R.R., Seal, R.D., Maxwell, E.L., and Zalenka, A. 1992. Dynamic global-to-direct irradiance conversion models. Ashrae Transactions 98(1):354-369.

Janssen, H., and Christensen, J.E. 2013. Hygrothermal optimisation of museum storage spaces. Energy and Buildings 56:169-178.

Kompatscher, K., Seuren, S., Kramer, R., van Schijndel, J., and Schellen, H. 2017. Energy efficient HVAC control in historical buildings: a case study for the Amsterdam Museum. Energy Procedia 132:891-896.

Kramer, R., van Schijndel, J., and Schellen, H. 2017. Dynamic setpoint control for museum indoor climate conditioning integrating collection and comfort requirements: Development and energy impact for Europe. Building and Environment 118:14-31.

Kramer, R., Schellen, L., and Schellen, H. 2018. Adaptive temperature limits for air-conditioned museums in temperate climates. Building Research and Information 46(6):686-697.

Kupczak, A., Sadłowska-Sałęga, A., Krzemień, L., Sobczyk, J., Radoń, J., and Kozłowski, R. 2018. Impact of paper and wooden collections on humidity stability and energy consumption in museums and libraries. Energy and Buildings 158:77-85.

Leijonhufvud, G., Kjellstrom, E., Brostom T., Ashley-Smith J. and Camuffo D. Uncentainties in damage assessment of future indoor climates. In: J. Ashley-Smith, A. Burmester, M. Eibl (Eds.), Climate for Collections—Standards and Uncertainties, Postprints of the Munich Climate Conference, London, 2012, pp. 11–19.

Leissner, J., Kilian, R., Kotova, L., Jacob, D., Mikolajewicz, U., Broström, T., ... and Antretter, F. 2015. Climate for Culture: assessing the impact of climate change on the future indoor climate in historic buildings using simulations. Heritage Science 3(1):38.

Mazzarella, L. 2015. Energy retrofit of historic and existing buildings. The legislative and regulatory point of view. Energy and Buildings 95:23-31.

Napp, M., and Kalamees, T. 2015. Energy use and indoor climate of conservation heating, dehumidification and adaptive ventilation for the climate control of a mediaeval church in a cold climate. Energy and Buildings 108:61-71.

Nicol, J.F., and Humphreys, M.A. 2002. Adaptive thermal comfort and sustainable thermal standards for buildings. Energy and buildings 34(6):563-572.

O'Leary, T.P., Menzies, G., and Duffy, A. 2015. The design of a modelling, monitoring and validation method for a solid wall structure. Energy Procedia 78:243-248.

Pernetti, R., Prada, A., and Biggio, P. 2013. On the influence of several parameters in energy model calibration: the case of a historical building. In 1st IBPSA Italy conference BSA.

Roberti, F., Oberegger, U. F., and Gasparella, A. 2015. Calibrating historic building energy models to hourly indoor air and surface temperatures: Methodology and case study. Energy and Buildings 108:236-243.

Roberti, F., Oberegger, U.F., Lucchi, E., and Troi, A. 2017. Energy retrofit and conservation of a historic building using multi-objective optimization and an analytic hierarchy process. Energy and Buildings 138:1-10.

Rode, C., and Woloszyn, M. 2007. Whole-building hygrothermal modeling in IEA Annex 41. In Thermal Performance of the Exterior Envelopes of Whole Buildings: Buildings X (pp. 1-15). American Society of Heating, Refrigerating and Air-Conditioning Engineers.

Schito, E., and Testi, D. 2017. Integrated maps of risk assessment and minimization of multiple risks for artworks in museum environments based on microclimate control. Building and Environment 123:585-600.

Tronchin, L., and Fabbri, K. 2017. Energy and microclimate simulation in a heritage building: further studies on the malatestiana library. Energies 10(10):1621.

To my grandparents